UNIVERSITY OF SOUTHAMPTON

Faculty of Engineering and Physical Sciences

DROPLET MICROFLUIDICS BASED PLATFORM TECHNOLOGY FOR CONTINUOUS CHEMICAL SENSING

By

Wahida Taskin Bhuiyan

Thesis for the degree of Doctor of Philosophy

2021

Abstract

Continuous monitoring of biomarkers such as metabolites and hormones can be extremely useful in understanding physiological processes, for drug development, personalised therapy, and many other applications. In environmental analysis, continuous monitoring can help generate nutrient profiles necessary for identifying short-term events, cyclic variations, thereby has potential in expanding our knowledge of aquatic ecosystems and guiding us in taking appropriate remedial actions. Droplet microfluidics, which is the compartmentalization of liquids into nano-litre droplets, provides advantages such as small volumes of sample and reagents consumption, improved sensitivity and temporal resolution, short analysis time, high throughput and parallelisation compared with conventional laboratory assays. In recent times, continuous measurement of analytes in droplets indicates it as a potential new sensor platform in continuous biochemical analysis resulting in a new class of dataset for dynamics to be captured. The most up-to-date systems however address mostly homogenous, single step “mix-and-read” assays. This thesis presents the technology development of advanced droplet platforms for multiple step assays and autonomous analysis for continuous monitoring.

Heterogeneous assays such as enzyme-linked immunosorbent assays (ELISA) are commonly used to measure antibodies, antigens, proteins and glycoproteins in biological samples, and with wide applications in disease diagnostics and treatment. ELISA normally requires multiple assay steps to be carried out with complex laboratory equipment. This thesis presents a miniaturised magnetic bead-based platform, where a multitude of assays can be implemented using a versatile droplet generation method. The platform incorporates a phased peristaltic micropump and microfluidic chip for droplet generation, a pair of ‘electromagnetic tweezers’ for manipulation of magnetic beads and a spectrophotometer for colorimetric detection. This platform automates the entire process from sample collection to detection. As a proof-of-concept, the platform was used to carry out a heterogeneous assay and analysis of cortisol, a stress related hormone implicated in many diseases including dementia and Cushing’s syndrome. The prototype device is able to analyse sample containing free bioactive cortisol every 10 seconds and has an initial sample-to-signal time of 10 minutes. It is able to measure in the analytical range of 3.175-100 ng/mL with less variability than the well plate-based assay.

Ammonium is one of the most important macronutrients and intermediates of the nitrogen cycle. Increased concentrations of ammonium could lead to nutrient enrichment, oxygen depletion and toxicity to aquatic ecosystems. This thesis reports the first of its kind droplet microfluidics ammonium sensor. The sensor miniaturizes the widely adopted indophenol blue assay and can perform high-frequency measurement and long-term monitoring with low sample consumption. The sensor has been implemented for two separate applications, which displays its versatility, with the first measuring ammonium in river water samples. Another application of this sensor prototype has been in a sequential batch bioreactor enriched with PHA accumulating bacteria. The sensor can autonomously collect samples (via filter) from the bioreactor, produce droplet trains, regulate temperature for completion of reaction and provide colorimetric measurements (5 per minute) via an in-line spectrophotometer, thus removing human intervention. The preliminary data obtained over a four-day period demonstrates high resolution monitoring, and reveals the fast-feeding behaviour of the bacteria. This kind of monitoring data could lead to feedback-controlled bioprocessing and the development of more efficient bioreactors.

This thesis further presents the development of a multiple micropump platform for the robust generation of droplet trains, based on phased droplet generation technology. The multiple micropump platform can generate droplet trains containing different sizes, compositions, and sequences on-demand. This setup does not require any change in pump hardware for different assays, therefore making the platform truly versatile. The 3D printed micropumps are robust with low footprint and the platform can be taken to point of care. Latest design can generate droplets from 120 nL upwards with a coefficient of variation of less than 0.7%.

Overall, the developments and research findings in this thesis paves the way for a new generation of droplet microfluidic sensors for continuous monitoring.

Table of contents

Acknowledgements

First and foremost, I would like to thank my supervisor, Prof Xize Niu for giving me the opportunity to do this studentship under his supervision. Without his rightful guidance, valuable advice, and encouragement, this work would not have been possible. I would also like to thank my second supervisor, Prof Hywel Morgan for his support and valuable advice. I could not have done it without the support of Dr. Adrian Nightingale who has been a brilliant mentor. I would like to express my gratitude to Dr. Gareth Evans for all the collaborative work. I would also like to thank Kyriacos Makris, Brett Warren, Dr. Sharon Coleman, Dr. Evanthia Papadoupoulou, Carla Ruggiero, Dr. Bingyuan Lu, Dr. Sammer-Ul Hassan, and Dr. Susan Pang for collaboration and support during different stages of the development of the project.

I would also like to thank my amazing friends and relatives for always being there and motivating me throughout. Finally, I would like to thank my wonderful parents Kabir and Tokon for their constant motivation, guidance, and support in this journey.

List of Figures

Research activities and achievements

Publications:

1. "A portable droplet microfluidic device for cortisol measurements using a competitive heterogeneous assay" Gareth W.H. Evans, **Wahida T. Bhuiyan**, Susan Pang, Brett Warren, Kyriacos Makris, Sharon Coleman, Sammer-ul Hassan and Xize Niu, *Analyst (2021).*
2. "Easily fabricated monolithic fluoropolymer chips for sensitive long-term absorbance measurement in droplet microfluidics", Adrian M. Nightingale, Sammer-ul Hassan, Kyriacos Makris, **Wahida T. Bhuiyan**, Terry J. Harvey, and Xize Niu, *RSC Advances.*

Conference presentations:

1. "An *in situ* droplet microfluidics based ammonium sensor and its application to a sequential batch bioreactor", **Wahida T. Bhuiyan**, Carla Ruggiero, Seongbong Heo, Akash Srivastava, Brett Warren, Yongqiang Liu, Adrian Nightingale, Xize Niu, 25th International Conference on Miniaturized Systems for Chemistry and Life Sciences , 2021.
2. "An *in-situ* droplet microfluidics based ammonium sensor and its application to a sequential batch bioreactor", **Wahida T. Bhuiyan**, Carla Ruggiero, Seongbong Heo, Akash Srivastava, Brett Warren, Yongqiang Liu, Adrian Nightingale, Xize Niu, Emerging Investigators in Microfluidics (July 20th-21st, 2021)
3. "Monitoring of ammonia in natural waters using a versatile, programmable droplet microfluidic platform", **Wahida Bhuiyan**, Evanthia Papadopoulou, Sharon Coleman, Matthew Pearson, Adrian Nightingale, Gareth Evans, Xize Niu, Poster Presentation, 24th International Conference on Miniaturized Systems for Chemistry and Life Sciences (Virtual conference), 2020.
4. "Easily-fabricated fluoropolymer chips for sensitive longterm absorbance measurement in droplet microfluidics", Adrian M. Nightingale, Sammer-ul Hassan, Kyriacos Makris, **Wahida T. Bhuiyan**, Terry J. Harvey and Xize Niu, Poster Presentation, 24th International Conference on Miniaturized Systems for Chemistry and Life Sciences (Virtual conference), 2020.

5. “Droplet microlfuidic based method for in-situ calibration and determination of recovery rate of microdialysis”, Gareth W H Evans, Jameelah Salahuddin, **Wahida T Bhuiyan**, Brett Warren, Xize Niu, Poster Presentation, 24th International Conference on Miniaturized Systems for Chemistry and Life Sciences (Virtual conference), 2020.
6. “Micro peristaltic pump system for the generation of arbitrary droplet sequence and multiple-step biochemical assays”, **Wahida Bhuiyan**, Gareth Evans and Xize Niu, Poster Presentation, 23rd International Conference on Miniaturized Systems for Chemistry and Life Sciences, 2019, Basel, Switzerland.
7. “Droplet Microfluidics for the Continuous Chemical Sensing of Cortisol”, Gareth W.H. Evans, **Wahida T. Bhuiyan**, Sammer-Ul Hassan, Susan Pang (LGC) and Xize Niu, Poster presentation at Microfluidics for Analytical Chemistry conference by Royal Society of Chemistry, 2018, Southampton, UK.
8. “Droplet microfluidics platform for continuous monitoring of cortisol”, **W. T. Bhuiyan**, G. Evans, S. Pang, S. Hassan, S. Coleman, B. Warren, X. Niu, Oral presentation at PGR Conference 2019, Department of Mechanical Engineering, University of Southampton.
9. “Droplet microfluidics for continuous chemical sensing of cortisol”, Gareth Evans, **Wahida Bhuiyan**, Sammer-Ul Hassan, Brett Warren, Sharon Coleman and Xize Niu, Oral presentation at BioMedEng18, 2018, London, UK.
10. “C.H.A.D.: CONTINUOUS HETEROGENOUS ASSAY IN DROPLETS FOR THE MEASUREMENT OF CORTISOL”, Gareth Evans, **Wahida Bhuiyan**, Sammer-Ul Hassan, Brett Warren, Sharon Coleman and Xize Niu, Oral Presentation, 22nd International Conference on Miniaturized Systems for Chemistry and Life Sciences, 2018, Kaohsiung, Taiwan.

Declaration of Authorship

I, Wahida Taskin Bhuiyan, declare that this thesis entitled '**Droplets Microfluidics based platform technology for Continuous Chemical Sensing'** and the work presented in it are my own and has been generated by me as the result of my own original research.

I confirm that:

1. This work was done wholly or mainly while in candidature for a research degree at this University;
2. Where any part of this thesis has previously been submitted for a degree or any other qualification at this University or any other institution, this has been clearly stated;
3. Where I have consulted the published work of others, this is always clearly attributed;
4. Where I have quoted from the work of others, the source is always given. With the exception of such quotations, this thesis is entirely my own work;
5. I have acknowledged all main sources of help;
6. Where the thesis is based on work done by myself jointly with others, I have made clear exactly what was done by others and what I have contributed myself;

Signed: ....

Date: ....

Symbols and Abbreviations

Aβ 1-42 and Aβ 1-40	Amyloid-β peptide-based biomarkers
AC	Alternating current
AM EWOD	Active matrix electrowetting-on-dielectric
ATP	Adenosine triphosphate
B	Magnetic field density
BSA	Bovine serum albumin
Ca	Capillary number
CE	Capillary electrophoresis
CH	Congenital hyperthyroidism
Cortisol-HRP	Cortisol-3-carboxymethyloxime horseradish peroxidase conjugate
COVID-19	Corona virus disease 2019
DC	Direct current
DEP	Dielectrophoresis
DMF	Digital microfluidics
DMV	Droplet Morphometry and Velocimetry
DNA	Deoxyribonucleic acid
ELISA	Enzyme-linked immunosorbent assay
EWOD	Electrowetting-on-dielectric
ESI	Electrospray ionization
F	Force on magnetic particle
FDM	Fused deposition modelling
GUI	Graphical user interface
h	Microfluidic channel height
ICU	Intensive care unit
ID	Inner diameter
IPB	Indophenol blue
L	Characteristic length of microfluidic device
LED	Light emitting diode
LFA	Lateral flow assay
LOC	Lab-on-a-chip
μ_0	Permeability of free space

MALDI	Matrix-assisted laser desorption ionization
MEGA	microfluidic emulsion generator array
MB	Magnetic bead
MBS	Magnetic bead shifter
MUG	4-Methylumbelliferyl β-D-glucuronide
MS	Mass spectrometry
OD	Outer diameter
OPA	O-phthaldialdehyde
O/W/O	Oil-in-water-in-oil
PBS	Phosphate buffered solution
PCB	Printed circuit board
PDMS	Polydimethylsiloxane
PFPE-PEG	Perfluoropolyether- Poly (ethylene glycol)
PLA	Polylactic Acid
PMMA	Polymethylmethacrylate
POC	Point-of-care
POCT	Point-of-care testing
PTFE	Polytetrafluoroethylene
PCR	Polymerase Chain Reaction
Q	Flow rate
Q_c	Continuous phase flowrate
Q_d	Dispersed phase flowrate
R	Gas constant
Re	Reynolds number
RNA	Ribonucleic acid
SLA	Stereolithography
T	Temperature
TBI	Traumatic brain injury
TSH	Thyroid stimulating hormone
TBS	Tris Buffered Saline
TMB	Tetramethylbenzidine
T_{50}	Magnetic tweezer with 50 windings
T_{100}	Magnetic tweezer with 100 windings
T_{200}	Magnetic tweezer with 200 windings
V	Volume of magnetic particle

V	Droplet volume
V_{fill}	Volume of droplet filling microfluidic channel
w_c	Channel width
We	Weber number
W/O/W	water-in-oil-in-water
α	Fitting parameter which are
λ	Viscosity ratio
$\emptyset$	Flow rate ratio
γ	Interfacial tension
g	Gravity
t	Time
o	Channel outlet
or	Orifice
ρ	Density
p	Pressure
η	Dynamic viscosity
f	force of body per unit volume
Γ	Surface concentration
c	Surfactant concentration
Δx	Magnetic susceptibility

CHAPTER 1

INTRODUCTION

This chapter introduces the background and significance of the research area, and the aims and objectives of this study.

1.1. Motivation

1.1a. The latest progress and challenges of continuous monitoring in healthcare applications

Monitoring biomarkers continuously could provide opportunities such as better understanding of physiological processes and improved management of diseases. *In situ* analysis is key to quicker decision-making benefited from short turnaround time compared to conventional offline laboratory procedures. For example, recent research has shown the importance of continuous monitoring of glucose and lactate in the area of critical care. Lactate is an important indicator of oxygen deficiency due to shock, surgery, respiratory failure or heart attack, therefore monitoring of lactate has been recommended to determine the condition of the patient and to understand if therapy is working (Smart, 2004). Real-time monitoring can be beneficial in guiding treatment for patients experiencing traumatic brain injury (TBI) (Booth et al., 2018), organ transplantation, or cardiovascular diseases by tracking biomarkers such as thrombin which is related to blood coagulation (Yu et al., 2014) or troponin which can indicate heart attack (Wettersten and Maisel, 2015).

However, continuous analysis of biomolecules poses many challenges to current technologies. Not only are the fluid mixtures complex, but also the working volumes are usually very small. The measurement devices need to be sensitive to dynamic changes and be robust, autonomous, and efficient. Point-of-care technologies (POCT) provide benefits like bringing healthcare at the site of patient with low-cost, easy to use and portable devices (Vashist, 2017). Unfortunately, most of the POCT can provide only single sample analysis and are not optimized for continuous monitoring. Electrochemical sensors which have been developed over decades still have limitations such as surface fouling due to continuous exposure to biofluids, electrical interference, non-specific adsorption on sensor surface, degradation of electrodes and the need for frequent re-calibration (Heikenfeld et al., 2018). Therefore, there is a need for developing robust, low power, low footprint POCT for continuous monitoring of biomarkers.

1.1a.1. Current technologies and challenges for monitoring cortisol

Cortisol is a stress-related hormone and is the end product of the Hypothalamus Pituitary Adrenal (HPA) axis (Lee et al., 2015). Cortisol secretion is initiated by the hypothalamus which releases corticotrophin releasing hormone (CRH) after receiving an environmental stimulus. CRH stimulates the production of adrenocorticotrophic releasing hormone (ACTH) from the pituitary gland which then triggers the release of corticosteroids from the adrenal cortex (Lee et al., 2015). Cortisol secretion follows a 24-hour circadian rhythm with increased levels just after a person wakes up and it decreases throughout the day. Diseases like Addison’s disease and Cushing ’s syndrome can perturb these levels (Kaushik et al., 2014).

Cortisol can be detected in various bio-fluids like blood, interstitial fluid, saliva, sweat, and urine. Cortisol is usually measured by traditional blood sampling via trained medical personnel and sterile equipment. Cortisol levels in the blood vary nominally from about 25 µg/dL to 2 µg/dL from morning to midnight (Levine et al., 2007). Blood can be sampled at different times of the day, but is not ideal for monitoring purposes as prior knowledge to having veins punctured can trigger stress among patients thus altering the cortisol level. Moreover, cortisol is a molecule that is unstable at room temperature and needs handling with care. To determine cortisol levels in urine, a 24 hr urinary free cortisol (UFC) test (cortisol range 10-100 µg/24 hr) is performed which is one of the non-invasive forms of measurement (Brossaud et al., 2012). However, sample collection usually proves to be inconvenient, as patients require carrying a urine collection container for 24 hr and this technique is not suitable for real-time analysis at POC. Saliva and sweat are two other non-invasive methods but tend to be unreliable for real-time analysis (Russell et al., 2014). In saliva, cortisol varies cyclically from 0.5 µg/dL to 0.005 µg/dL, detecting which demands highly sensitive assays (Price et al., 1983). Russell and co-workers have managed to detect cortisol in sweat in the range of 8.16 to 147.7 ng/mL post-exercise (Russell et al., 2014). However, the collection of sweat requires sweat patches and has high variability among patients. Cortisol levels in the interstitial fluid can be 3-4 times higher than saliva which makes it quite suitable for detecting cortisol (Venugopal et al., 2011). Different techniques have been implemented to obtain interstitial fluid in a minimally invasive and painless manner. Venugopal *et al.* have developed a low-energy laser system to create micro-pores about the diameter of human hair on the skin to draw interstitial fluid using vacuum pressure (Venugopal et al., 2011). For higher sampling rates, transdermal microneedles have also been fabricated which can be very compatible with biosensors (Mukerjee et al., 2004, Ahmed El-Laboudi, 2013).

Cortisol detection techniques include chromatography as one of the older forms, immunoassays, and electrochemical immunosensing. Liquid chromatography method has been used to measure serum cortisol in 1 mL samples and detect up to 2 ng/mL (Kabra et al., 1979). High-performance liquid chromatography (HPLC) techniques have also been used to detect cortisol in plasma and saliva (Funk et al., 1981). Electrochemical sensing has emerged as a great technology for point of care monitoring due to its high sensitivity and ease of fabrication (Wan et al., 2013). Sun and co-workers have fabricated Au electrodes coated with cortisol antibody and used alkaline phosphate enzyme to detect cortisol up to 0.27 ng/mL in saliva (Sun et al., 2008). Saliva samples were taken at five different time points from patients during the entire day and frozen to be analysed later. For POC measurement of cortisol from saliva, carbon nanotube chemiresistive sensor functionalised with cortisol analog and anti-cortisol antibody has been developed to detect down to 1 pg/mL (Tlili et al., 2011). Immunoassays have also seen widespread usage for cortisol detection with radioimmunoassay (RIA) in the early 1970s and now shifting more towards using florescent tags due to the adverse effects of dealing with radioisotopes (Abraham et al., 1972, Appel et al., 2005). Enzyme linked immunosorbent assay (ELISA) has turned out to be one of the most sensitive assays among the labelled immunoassays and is used as a gold standard to compare newer methods to it (Shimada et al., 1995).

Most of the current sensing systems and methods are restricted to laboratories and come with limitations like cost, portability, long turnaround time, inconvenience of sampling, and the need for skilled personnel for performing the procedures. Immunosensors suffer from short shelf-life and denaturisation of antibodies due to changes in temperature, humidity, pH, and other environmental influences (Kaushik et al., 2014). Therefore, technologies are required, which would be able to capture the dynamic changes in cortisol taking into consideration the challenges that have been mentioned above.

1.1b. The latest progress and challenges of continuous monitoring in Environmental applications

Aquatic ecosystems such as oceans, coastal water and estuaries are dynamic, and concentration of dissolved nutrients and biological parameters vary in high spatial and temporal scales. These parameters are critical indicators of the health of the aquatic ecosystems and the biogeochemical cycles. The key chemical parameters commonly analysed are nitrate, nitrite, ammonium, phosphate, carbonate system parameters, dissolved gases, other trace elements and other biological parameters such as DNA, RNA (Nightingale et al., 2015, Fukuba and Fujii, 2021, Bastos et al., 2016).

Traditionally spot sampling and following laboratory analysis is carried out for quantifying dissolved nutrients in water. It is a labour-intensive process and also limits the sampling frequency, thereby missing to identify short-lived events. *In situ* analysers overcome these problems and prevent sample degradation and contamination during transport. The majority of current environmental analysers are based on ion-selective electrodes (Denuault, 2009), which are user-friendly and feature high measurement frequencies. However, as is commonly found for electrochemical-based sensors, their calibration drift over time requiring frequent manual recalibration and they have also been shown to be highly susceptible to interference from changes in ionic concentration (Mills and Fones, 2012). Flow through wet chemical analysers have been a popular choice in for *in situ* analysis but requires complex valve and pumping systems (Xu et al., 2005). Microfluidics sensors have shown great potential in recent years for *in situ* analysis and analysers for nitrate/nitrite (Beaton et al., 2011, Nightingale et al., 2019a), phosphate (Grand et al., 2017), etc. have demonstrated good monitoring capabilities. Therefore, designing more robust and efficient microfluidics analysers seems to be a way forward in environmental monitoring.

1.1c. Droplet microfluidics for continuous monitoring

Droplet microfluidics (discrete nano litre droplets carried by an immiscible oil) has emerged as a powerful tool in biochemical-analysis. Integrating droplet microfluidics in POC testing and into environmental analysers could mitigate the aforementioned challenges. Droplet microfluidics is capable of scaling down many of the available chemical assays into a microfluidic device; thus providing numerous benefits such as decreased consumption of expensive sample and reagents, high-throughput analysis and high temporal resolution (Teh et al., 2008, Shang et al., 2017). Droplet microfluidics also provides other advantages like removal of Taylor dispersion (Song et al., 2003), enhanced mixing due to chaotic advection (Wang et al., 2015a) and prevents contamination between samples due to having individual reactor units (Belder, 2005).

1.2. Aims and objectives

The aim of this PhD thesis is to develop a droplet microfluidics-based platform technology, capable of miniaturising and automating complex bioassay procedures such as multiple-step immunoassays, which are otherwise labour intensive and require expensive laboratory equipment. The device could incorporate most steps of testing protocol including liquid sampling, droplet generation and handling, reaction and optical detection, and most importantly, run repeated analysis, thereby giving a real-time measurement of the biomarker or environmental parameters, which is unique to any of today's technology.

For healthcare applications, the platform will be used to monitor biomarkers continuously and as a proof-of-concept a steroid hormone Cortisol will be measured. Cortisol plays a major role in various physiological processes such as glycolysis, management of blood pressure, etc. of the body and is a stress-biomarker (Lee et al., 2015, Gracie et al., 2017). Droplet microfluidics will be developed to miniaturise ELISA into a train of droplets for continuous monitoring of cortisol. Once the ELISA protocol is successfully implemented, the platform could be customised for other bead-based assays.

On the environmental monitoring side, the focus will be on monitoring of ammonium for river water and wastewater facilities. The indophenol blue assay based on modified Berthelot's reaction will be optimised and miniaturised into droplets.

The main objectives of this project are as follows:

1. Design and fabrication of a robust pumping system capable of generation of monodisperse droplets.
2. Development of modular peristaltic micropumps to decentralize the droplet generation process and equip the microfluidic platform with the ability to generate droplets on-demand with variable size and composition.
3. Development of microfluidic chips for droplet train generation.
4. Development of optical flow cells for colorimetric identification of analytes in droplets.
5. Design and fabrication of automated magnetic bead tweezers for manipulating magnetic microbeads for heterogeneous, multiple-step assays.
6. Optimising and miniaturising mix-and-read, multiple-step and multiplexed assays from lab to droplets.
7. Calibrating the device in the laboratory.
8. Validating the droplet platform by implementing in clinical setting and in the field.

1.3. Thesis layout

This thesis is divided into six chapters and the layout is as follows:

Chapter 1 illustrates the motivation and significance of the work, the aims of the PhD project and provides an overview of thesis.

Chapter 2 is the literature review which highlights the different aspects of microfluidics and showcases the power of using droplet microfluidics as an analytical tool for continuous monitoring.

Chapter 3 covers the development and implementation of the microfluidic platform for performing heterogeneous assays. An automatic magnetic tweezer has been designed to give us the capability of magnetic bead manipulation. The stress hormone cortisol has been measured as a proof of principle.

Chapter 4 highlights the benefits of using our platform for environmental analysis. This chapter describes the optimisation of the indophenol blue assay for measuring ammonium and its translation to droplets.

Chapter 5 describes the development of a novel 3D printed peristaltic multi-pump platform which is versatile in nature and is able to generate different sequence, composition and size of droplets autonomously. Some applications have been demonstrated using the platform.

Chapter 6 summarises the work presented in the thesis and discusses the limitations and future research directions.

CHAPTER 2

LITERATURE REVIEW

This literature review aims to provide background knowledge on the importance and necessity of continuous monitoring in tracking biomarkers and environmental parameters, and to review the challenges presented to the current technologies. In particular, I review state-of-the-art Point-of-Care (POC) technologies and various portable and wearable sensors, demonstrating their capabilities for disease diagnostics and monitoring. I also study *in situ* sensors for environmental monitoring. The science and technology of microfluidics developed in the recent years has provided new potential in addressing these challenges, especially droplet microfluidics has emerged as the new tool of bio-chemical assays for continuous monitoring of analytes and environmental parameters.

2.1. Point-of-care diagnostics and monitoring

"Point-of-Care Testing (POCT) is defined as laboratory testing conducted close to the site of patient care, typically by clinical personnel whose primary training is not in the clinical laboratory sciences, or by patients (self-testing)" (Wild, 2013). POCT brings detection of analytes to the location of a patient, providing benefits like instantaneous access to test results, improved diagnosis, and better management of disease. POC technologies reduce or simplify testing steps, decrease manual intervention and hence, facilitate faster clinical decision making and increase overall workflow efficiency (St-Louis, 2000, Chin et al., 2012). Due to the numerous advantages and future potentials, the POCT industrial sector has grown rapidly in recent years (Vashist, 2017) and is projected to grow at a compound annual growth rate (CAGR) of 3.25% from 27.66 billion USD valued at 2020.

POCT can be categorised into small handheld, portable devices such as lateral flow strips with antibodies for pathogen detection, or simplified laboratory benchtop equipment which includes analysers for critical care, haematology and devices performing Polymerase Chain Reaction (PCR) for testing infectious diseases *in situ*. The POCT devices can also be classified into 'over the counter' products and the 'professional product', with the former consisting of blood glucose monitoring or pregnancy tests which do not require professionals for operating and the latter including products for molecular testing such as ELISA or PCR requiring healthcare professionals (St John and Price, 2014). The major share in POCT market is occupied by glucose testing followed by pregnancy tests; infectious disease testing projects the fastest growth rate (St John and Price, 2014), as can be seen with lateral flow rapid antigen tests playing critical roles in the test and tracing in recent COVID-19 pandemic (Dinnes et al., 2021).

Mobile healthcare devices are extremely useful in low-resource areas, where setting up advanced healthcare facilities can be very challenging. In developed countries, these devices are particularly useful for remote sensing, thus decreasing hospital time and cost for patients with chronic illnesses. Therefore, faster and precise diagnosis through POCT can lead to intervention in early stages of disease and better outcome for patient (Chan et al., 2013). St John *et al*. have mentioned some key requirements that should be in all POC devices (Price et al., 2010, St John and Price, 2014):

1. They should be simple to use.
2. Consumables and reagents should be stored and used in a robust manner.
3. The results provided should be in accordance to conventional laboratory methods.

4. The device and included reagents and consumables should be safe for usage.

Figure 1 illustrates numerous patient-centred mobile health monitoring and diagnosis technology currently available, indicating the flourishing of POCT market. Modern smartphones are equipped with higher resolution cameras, faster processers, better apps and improved wireless connectivity than previous versions and are widely used; it is no surprise that smartphones have found more applications as various diagnostic platforms for monitoring biomolecules and physical activities (Zarei, 2017). Kadlec *et al.* developed a portable cell phone-based diagnostic system consisting of an iPhone, microwell array and optical instruments in a 3D printed housing, for fast testing of antimicrobial susceptibility (Kadlec et al., 2014). Likewise, other smartphone-based platforms have been demonstrated such as surface plasmon resonance imaging for high-throughput biomolecule detection (Guner et al., 2017), immunosensor for colorimetric detection of Cancer Antigen 125 (Hosu et al., 2017) and many of such examples have been reviewed by Zhang and Liu *(Zhang and Liu, 2016).*

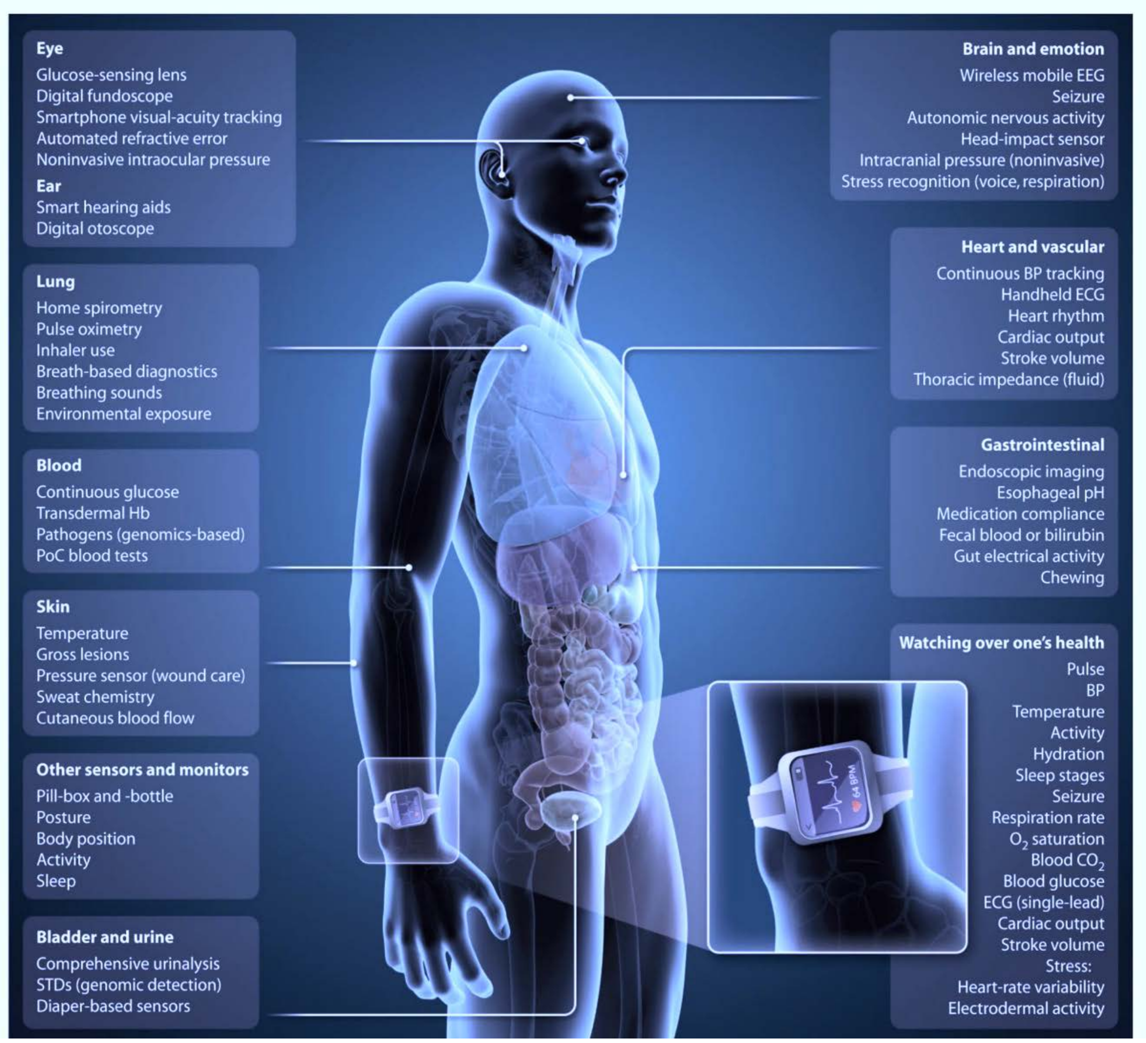

Figure 1. *Different bodily measurements performed by mobile health technologies for monitoring, diagnosis and management of disease and other physiological processes (Steinhubl et al., 2015).*

Lateral flow assay (LFA) based POC are among the fastest growing platforms for qualitative and quantitative investigation. LFA platforms are used for monitoring disease epidemics, checking pregnancy, sensing biomarkers, etc. (Sajid et al., 2015). Lab-on-a-chip (LOC) technologies and microfluidics have also been widely used in POC due to their advantages like higher sensitivity, better integration, automation, high-throughput analysis, less sample requirement, cost-effectiveness, etc. (Zarei, 2017, Su et al., 2015).

2.2. Continuous monitoring for biomedical applications

Chemical signals in biology vary constantly. The signals work in a broad range of time scales starting from merely milliseconds to over several days. Diseases or injuries disturb the pattern of these signals and clinicians can use these traces for diagnosis and treatment. However, continuous monitoring to provide a clear, representative picture has been limited by current laboratory protocols and technology (Michelle L. Rogers, 2013). In traditional analysis, a clinician draws venous blood (few mLs) from the patient which is then sent to a central laboratory for analysis of the biomarker of interest, which can take up days to a week, yielding delayed results and hindering rapid diagnosis.

POC testing shortens the analysis timescale by using LFAs but the majority of POCT offers single time measurements and therefore cannot provide trends of variations in biomarkers levels or the rate at which they are changing. Continuous monitoring of biomarkers could guide in making quick and informed decisions and providing immediate treatment (Hassan et al., 2016). Monitoring vital signs and biomarkers can be extremely useful for patient treatment in intensive care units (ICUs) and tracking deterioration in their early occurrence. Monitoring of glucose, lactate and pyruvate can be beneficial for diagnosis and prognosis of patients suffering from traumatic brain injury (TBI) (Samper et al., 2019). Tracking of biomarkers such as thrombin could reveal blood coagulation resulting in cardiovascular diseases (Yu et al., 2014) or troponin indicating heart attack (Wettersten and Maisel, 2015). Drug dosage can be tailored to an individual’s needs by measuring its concentration in tissue in real-time (Booth et al., 2018), which could lead to personalised medicine.

2.2.1. Approaches for continuous monitoring

Different strategies exist for continuous monitoring, such as electrochemical techniques and sampling procedures by microdialysis or ultrafiltration (Michelle L. Rogers, 2013).

2.2.1.1. Electrochemical sensing

Electrochemical sensors consist of a recognition element for analyte detection and an electrochemical transducer for conversion of the interaction between the electrode and analyte of interest to an electrical signal (Stoytcheva and Zlatev, 2014). Advantages of electrochemical sensors include economic viability for mass production, miniaturisation, low detection limits, usage of small sample volumes, high specificity, applicability to turbid bio fluids and easy electrical data processing, etc. (Grieshaber et al., 2008).

Electrochemical sensors can be categorised into potentiometric, amperometric and conductometric sensors (Ronkainen et al., 2010). Potentiometric sensors provide information about the analyte of interest and ion (charged ion reacts selectively) by measuring the difference in potential between two electrodes. Glass pH electrodes and ion selective electrodes (ISEs) for ions like K^+, Na^+, Cl^-, etc. are some common potentiometric sensors. Amperometric sensors measure the current (proportional to concentration of analyte) due to electrolysis at the working electrode when a potential is applied between a working and a reference electrode. Conductometric sensors exploit the changes in electrical conductivity of a sample due to the presence of the analyte.

One of the earliest forms of continuous electrochemical sensing was pioneered by Clark *et al*., where they used a platinum electrode covered by cellophane film to measure blood oxygen levels (Leland C. Clark et al., 1953). Bio-recognition elements such as enzymes can be immobilized on electrodes for catalysing reactions and generating ions to be detected by the electrode. The most common example and commercially successful category is that of continuous monitoring glucose sensors (Ronkainen et al., 2010, Koncki, 2007). The rapid progress in the development of electrochemical sensing has resulted in commercialization of several hand-held analyzers like ACCU-CHEK (Roche Diagnostics, Inc.), Lactate Scout (Sports Resource Group, Inc.), etc. for monitoring electrolytes and metabolites (Windmiller and Wang, 2013). Antibodies, bio-membranes, organisms have also be used for sensing, resulting in a range of electrochemical immunosensors for clinical analysis, environmental monitoring, etc. (Sadik and Van Emon, 1996). Sensor arrays have also been for detecting multiple analytes (Koncki, 2007). Electrochemical sensors provide the ability to miniaturise laboratory protocols to wearable devices. Hence, screen printed electrodes, flexible electrodes and textile based thick film-sensors have garnered interest recently (Windmiller and Wang, 2013).

However, electrochemical sensors still have limitations such as surface fouling due to continuous exposure to biofluids, interference from other analytes and electrical interference, non-specific adsorption on sensor surface, degradation of electrodes and the need for frequent re-calibration (Heikenfeld et al., 2018).

2.2.1.2. Microdialysis and ultrafiltration

Sampling methods like microdialysis and ultrafiltration employ size-controlled porous membranes to extract target analytes from a heterogeneous environment (containing similar analytes, organisms, etc. of varying size) into a carrier solution. Microdialysis is extensively used for passive sampling of neuropeptides, neurotransmitters and complex proteins by a concentration gradient, to a perfused solution that does not contain the analytes of interest. Diffusion can occur in both directions, with analytes diffusing into perfusate or drugs and other substances diffusing from the perfusate to the tissue (Fig. 2) (Hersini et al., 2014).

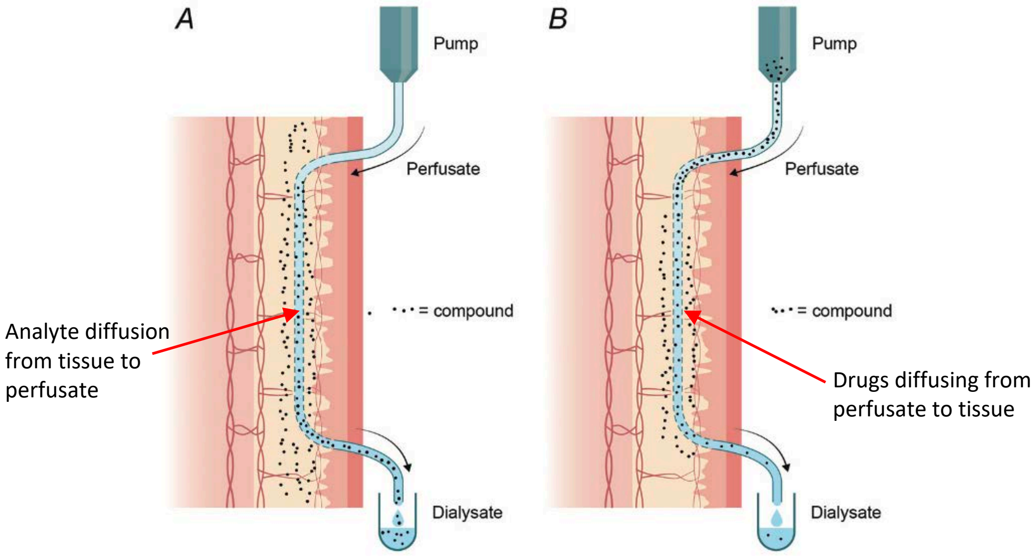

Figure 2. *Basic principle of microdialysis. (A) Analyte diffusion from tissue to perfusate. (B) Diffusion of drugs or substances from perfusate to tissue (Hersini et al., 2014).*

Microdialysis sampling has many advantages. The small probe size is less invasive, the membrane creates a barrier between tissue and perfusate which protects the tissue from large molecules, bacteria and turbulent flow of the perfusate. The Boutelle group have demonstrated online microdialysis and electrochemical detection of glucose and lactate in dialysate in neurointensive care head trauma patients (Jones et al., 2002). The dialysate stream was split into two using a custom valve system leading to an enzyme bed followed by an electrode sensor for glucose and lactate assay each thus allowing simultaneous detection (Jones et al., 2002). Niu group have also demonstrated (Nightingale et al., 2019b) the monitoring of glucose and lactate from dermal tissue with a much smaller handheld droplet microfluidic sensor. They used a microdialysis probe to draw interstitial fluid and peristaltic pumping technology to generate droplets to perform colorimetric detection. Ultrafiltration is an alternative to microdialysis, which involves suction of analytes to a tube covered with a dialysis membrane. Compared to microdialysis, the principal advantage of ultrafiltration is that it does not depend on the flow rate and the extraction efficiency is 100%, (Shippenberg and Thompson, 2001, Moscone et al., 1996, Michelle L. Rogers, 2013) however, it may lead to a fluidic imbalance in sampling site. Non-invasive methods (Bandodkar and Wang, 2014) have obvious desirability for the patient, but analytes taken from fluids such as sweat are generally present in lower concentrations compared to blood and have higher variation between subjects; requiring analytical methods with greater sensitivity and precision.

2.2.2. Bodily samples for analysis

Real-time monitoring of various analytes or biomarkers can be performed from different areas in the body. These body fluids supply ample information and can be collected by invasive or non-invasive methods.

2.2.2.1. Body fluids, tissue and internal organs

Blood, interstitial fluid, sweat, tears, saliva, breath, urine and stool, all can be analysed to extract vital physiological information. Up to now blood is no doubt the mostly collected body fluid. The pH of blood, gases in blood, glucose, lactate and electrolytes (Na^{+}, K^{+}, Cl^{-}) can change drastically in patients in critical care and real-time analysis could be of utmost importance (Frost and Meyerhoff, 2015). Due to its non-invasive nature for analysis, sweat is a good alternative sample as the concentrations of many analytes in sweat are proportional to that in blood (Brasier and Eckstein, 2019). Sempionatta and co-workers have designed eye glasses with microsensor and electrodes integrated in the nose pad, for continuous monitoring of lactate and potassium (Sempionatto et al., 2017). Koh *et al.* have developed a flexible microfluidics sensor patch (Fig. 3) for colorimetric detection of water, lactate, glucose and pH by a smartphone camera (Koh et al., 2016). However, the desired amount of sweat might not always be present and techniques have been used to induce sweat (Booth et al., 2018). Monitoring saliva also falls under an attractive, non-invasive method and a mouth guard with embedded wireless sensor for measuring uric acid has been demonstrated (Kim et al., 2015).

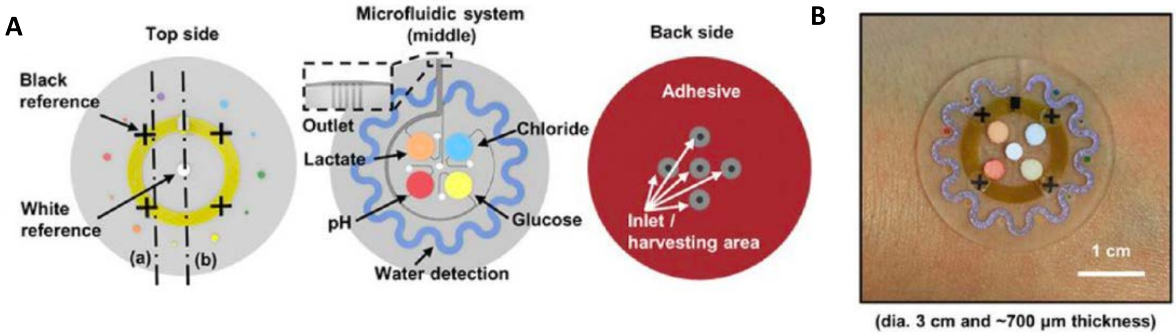

Figure 3. *Microfluidic sensor patch. (A) Schematic of top, middle and bottom layers of microfluidics set sensor patch designed by Koh et al. for detecting water, lactate, glucose and pH. (B) Picture of actual sensor on arm (Koh et al., 2016).*

Monitoring interstitial fluid provides an abundance of opportunities and huge attention has been given on the real-time monitoring of glucose (Gómez et al., 2017). Lactate is an important indicator of oxygenation of tissue and is commonly linked with impaired functioning of body (Smart, 2004), and it can be measured using subcutaneous microdialysis (Nightingale et al., 2019b). Continuous measurements can also be taken from muscle fluids, but they prove to be more difficult due to muscle fibre movement during contraction. Assessing the condition of organs during transplant is essential and recently a 3D printed microfluidic device has been attached to a porcine kidney to sample biomolecules (Singh et al., 2017) as shown in Fig. 4.

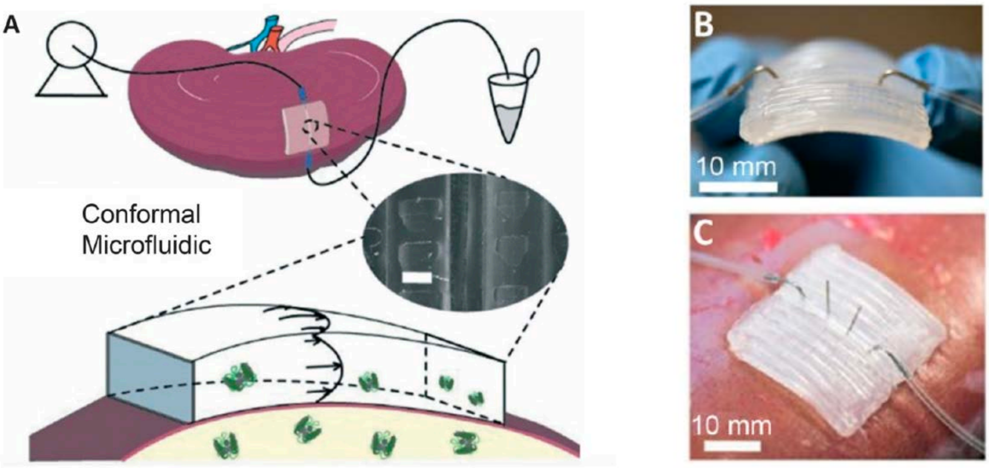

Figure 4. *(A) Microfluidic device schematic for sampling biomarkers from organ surface. (B) Photo of the device and (C) the device planted on the porcine kidney (Singh et al., 2017).*

Therefore, there are various technologies which have been already used or are at different stages of development for real-time monitoring. As most of the bodily fluids are present in small volumes, excess sampling should be avoided to prevent imbalance of chemical distribution and skewed measurement. Microfluidics is a technology capable of handling minute amount of samples from micro litre to nano litre, and could be an enabling technology in the analysis of bodily fluids (Michelle L. Rogers, 2013).

2.3. *In situ* sensors for monitoring natural waters

Understanding the biogeochemical cycles and changes in aquatic ecosystems that take place due to natural and anthropogenic processes is crucial for the preservation and sustainability of global aquatic environments and biodiversity (Nightingale et al., 2015, Wang et al., 2019b). For better characterisation and study of aquatic systems, and patterns in biogeochemical cycles, it is essential to measure nutrients such as nitrate, nitrite, ammonium, phosphate, carbonate system parameters, dissolved gases, other trace elements and biological components (Nightingale et al., 2015, Fukuba and Fujii, 2021). Usually, water samples are manually collected or via auto samplers and then transported to on-board survey vessels or laboratories for analysis. This may result in sample degradation, contamination and a long lag between sample collection and results. One of the key challenges for water monitoring is the high spatial and temporal changes of signals. Samples collected manually or via auto samplers are unable to provide continuous data for tracking varying trends and conclusively identifying pollution events (Nightingale et al., 2019a).

In order to obtain high frequency, valuable data and track events in real time, *in situ* sensor technologies have been identified as powerful tools for generating rich nutrient profiles and characterizing 'episodic and transient' events such as algal blooms, agricultural run-off, effluent discharges, storms, etc. (Daniel et al., 2020). The Biogeochemical-Argo, – a network of battery-powered floats that measure oxygen, pH, nitrate, suspended particles, chlorophyll a, and downwelling irradiance in the oceans – represents a powerful implementation of these new tools (Claustre et al., 2020). The floats perform a cycle of descending to 2000 m depth and then resurfacing every 10 days, transmitting the data continuously via an iridium satellite data system to be accessed freely within 24 hrs.

In situ nutrient sensors can be broadly divided into three categories based on their method of analysis: wet chemical analyzers, ultraviolet optical sensors, and electrochemical sensors (Daniel et al., 2020). Wet chemical sensors utilise colorimetric analytical procedures where reagents and analytes react to produce a coloured product, which is eventually detected spectroscopically or by fluorescence. UV optical sensors do not require chemical reagents as they depend on the absorption characteristics of marine or river water parameters (such as dissolved organic carbon and nitrite) to be measured. They can measure wider concentration ranges, have faster response time but can display lower sensitivity than their wet chemical analyser counterparts due to particulate or dissolved matter interference during detection. Electrochemical sensors, with most common ones being Ion-Selective Electrodes (ISEs) also do not require reagents and are easily miniaturised however, they may produce signal drift, are susceptible to ionic interferences and require frequent recalibration(Mills and Fones, 2012). Colorimetry usually provides higher precision than ISEs but usually have a smaller detection range, are mostly temperature dependant and the response time is generally limited by reaction completion and complete colour development (Mills and Fones, 2012, Daniel et al., 2020, Blaen et al., 2016). Therefore, a sensor type should be chosen and the system should be designed depending on the monitoring objectives and the aquatic conditions. For instance, the deployment platform such as AUVs, gliders, and floats, and water characteristics such as temperature, depth, and salinity and concentration would all influence the choice of sensor device (Daniel et al., 2020).

For underwater analyzers, especially those to be used in marine environments, special challenges exist including waterproofing for electrical insulation, low power consumption, withstanding high hydrostatic pressure and sea water corrosion, resistance to biofouling, enough reagents for long-term deployment, and high degree of automation to reduce frequent calibration or intervention (Fukuba and Fujii, 2021). *In situ* sensors usually remove the logistical problems of sample transport and could provide rich, high frequency data for tracking and mapping spatial and temporal variability. Pollution events can be identified quicker and lead to effective intervention and appropriate remedial action. Lab on a Chip (LOC) technologies based on microfluidics devices are therefore the way forward for miniaturising *in situ* analysers (Fukuba and Fujii, 2021, Nightingale et al., 2015) for monitoring natural waters. Beaton and co-workers have miniaturised a Griess assay for detection of nitrite using an *in situ* microfluidic colorimetric sensor (Beaton et al., 2011). Their fluid handling consists of seven micro-inert valves and syringe pumps. A more sophisticated peristaltic pumping system has been implemented in their droplet microfluidic sensor by Niu group for the colorimetric detection of both nitrate and nitrite (Nightingale et al., 2019a). A LOC phosphate analyser (Grand et al., 2017) utilizing optimised phosphomolybdenum blue method has been developed by Grand *et al.*. Deployment in both hypernutrified estuarine and oligotrophic tropical waters demonstrated the capabilities of the sensor for tracking small dynamic changes in phosphate levels and stochastic events. Some other examples of *in situ* LOC analyzers include ones for determining dissolved manganese in sea water (Geißler et al., 2021) and measuring adenosine triphosphate (ATP) for detecting microbial biomass in deep sea (Fukuba et al., 2018). Therefore, LOC microfluidic analyzers are undoubtedly useful for continuous environmental monitoring as can be seen from the aforementioned examples.

2.4. Microfluidics

Microfluidics involves the manipulation of minute amounts of liquid through micro channels measuring from a few to hundreds of micrometres. Since its initial studies in 1990s, microfluidics research has grown rapidly and is transforming bio-chemical analysis by offering advantages like utilizing less sample and reagents, reducing diagnosis time by giving rapid responses, miniaturizing complex laboratory protocols, allowing portability, producing higher sensitivity, decreasing the footprint of diagnostic devices and in turn lowering costs (Whitesides, 2006). These advantages have led to a huge interest in commercialization and employment of microfluidics devices for various applications (Chin et al., 2012). Some examples can be seen in Fig 5.

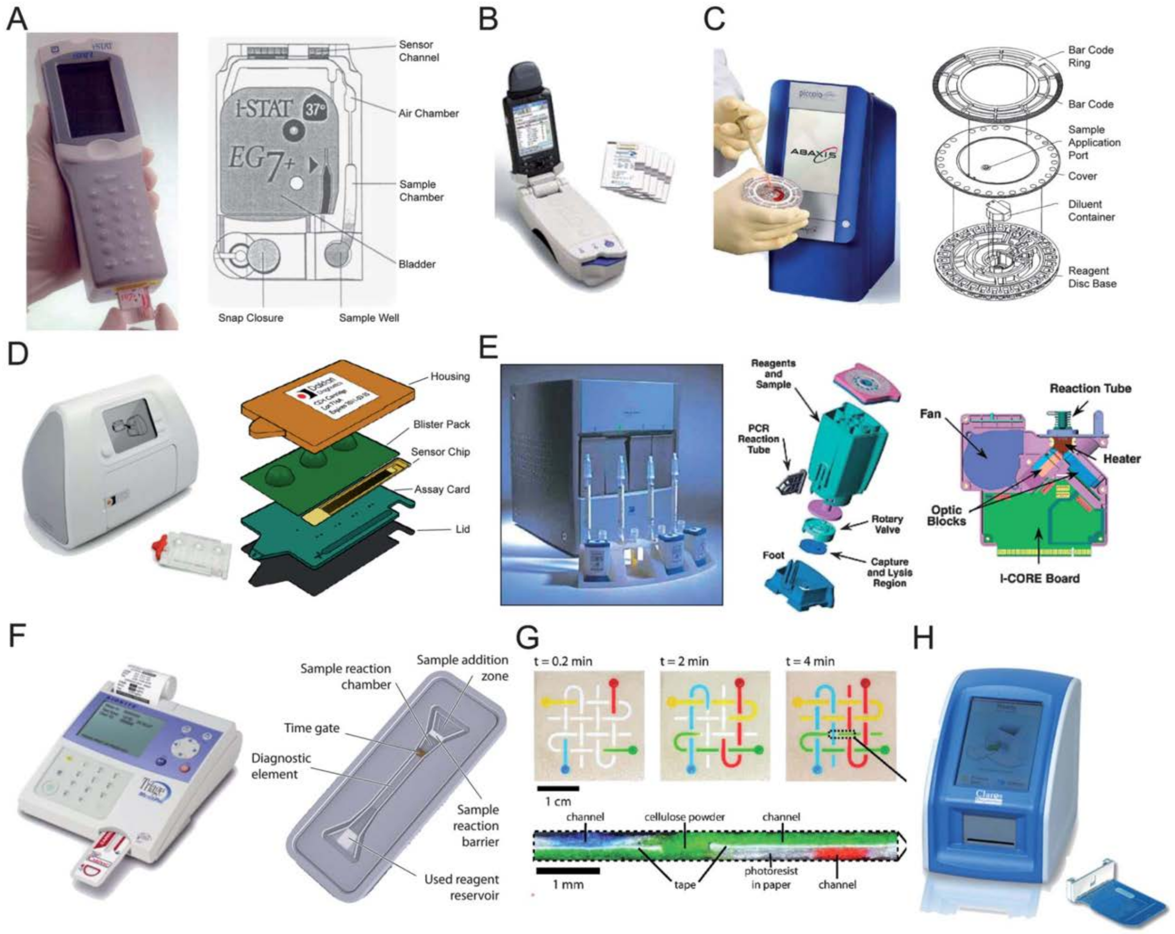

Figure 5. Various commercialized microfluidics-based POC tests (Chin et al., 2012).

2.5. Pumping technology for microfluidic systems

One of the most important components for microfluidic systems are micropumps, as fluid transport is essential for these systems. Micropumps contribute significantly to the reliability, robustness, power and size of the overall system.

There are various pumps available to cater to the requirements of microfluidic systems such as syringe pumps, osmotic pumps, peristaltic pumps and solenoid pumps (Fig. 6). Syringe pumps (Fig. 6 (a)) are the most commonly used pumps for microfluidic applications as they are cost effective, readily available and can be computer controlled for automating systems. Although syringe pumps can introduce a range of different flow rates, they take time to stabilise in between flowrates. When moving from benchtop applications to *in situ* portable sensors or POC applications, syringe pumps introduce some drawbacks due to the relatively small reservoirs or syringes which might need replacing and also the overall size might be hard to incorporate in sensor systems requiring a small footprint. Miniaturising syringe pumps lead to miniaturising the fluid reservoir hence decreasing the fluid that could be supplied (Yokokawa et al., 2006).

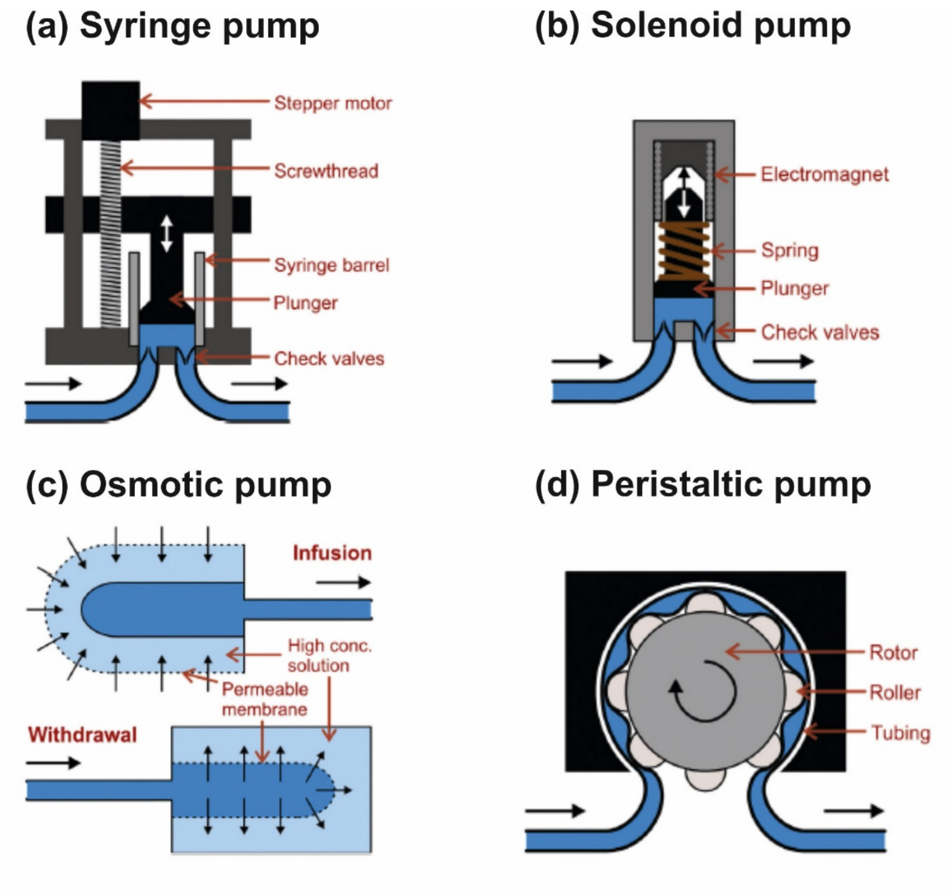

Figure 6. *Schematic diagrams showing the different types of pumping technology for microfluidic systems: (a) syringe pumping (b) solenoid pumping (c) osmotic pumping and (d) peristaltic pumping (Nightingale et al., 2015).*

Solenoid pumps (Fig. 6 (b)) provide low power solutions to microfluidic applications. It was first proposed in 1996 by Weeks *et al.* (Weeks and Johnson, 1996) and has been implemented widely since (Thouron et al., 2003, Chapin et al., 2004, Plant et al., 2009). Solenoid pumps utilise an electromagnetically actuated piston and a pair of check valves to propagate fluid in discrete pulses. Although solenoid pumps are low power (around 0.5 W shown by Weeks *et al.* (Weeks and Johnson, 1996)), they are usually incapable of handling large backpressures and flow rates may drift over time (Thouron et al., 2003). Another low power alternative are osmotic pumps (Fig. 6 (c)) (Rose and Nelson, 1955) which do not require any electrical input and depend on the osmotic flow between low and high salinity reservoirs separated by a semi permeable membrane. This makes them suitable for long term deployment applications. However, they still require mechanical pumps to introduce blank and standard solutions for calibration. Osmotic pumps also operate at very slow flow rates (1 litre/hr) and suffer from problems such as flow rate drift over time, very long calibration time, and variation or reversal of flow due to temperature and pressure changes (Chapin et al., 2002, Jannasch et al., 1994).

Peristaltic pumps (Fig. 6 (d)) utilize a rotary motor to drive a series of rollers to propagate fluids in elastic tubing. They are a popular choice for microfluidic systems (Chin et al., 1992, Nightingale et al., 2018, Evans et al., 2021) due to their wide commercial availability, self-priming design and user friendliness. W. Rhie and T. Higuchi have developed a portable peristaltic pump (Fig. 7 (a)) whose main components are a screw shaft (3D printed) and a disposable pumping channel unit (made of PDMS) in a transparent PMMA housing (Rhie and Higuchi, 2010). The eight pumping channels “occluded by a screw shaft”, are deformed and closed as the shaft rotates. The cross-sectional view of the pump displaying the pinching off of a channel at a given moment can be seen in Fig. 7 (b). Niu group have also developed a phased-peristaltic pumping technology (Nightingale et al., 2017, Evans et al., 2021) for continuous monitoring applications.

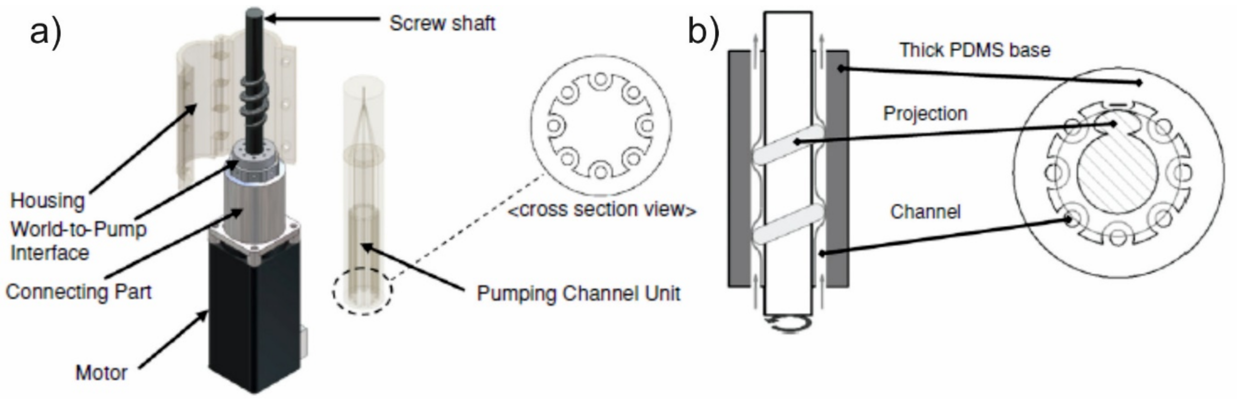

Figure 7. *(a) 3D CAD model showing the screw pump parts. (b) Cross sectional view of the screw shaft and pumping channels. (Rhie and Higuchi, 2010).*

The Quake group first introduced on-off valves which they fabricated using soft lithography techniques (Unger et al., 2000). It is a three-layered structure in poly(dimethyl siloxane) (PDMS) with one microchannel orthogonally positioned on top of another separated by an elastomer membrane. When pressure is applied to the control channel (upper channel), the membrane deviates and closes the flow channel (lower channel). By using the same design principle, the Quake group have fabricated peristaltic pumps, switching valves, grid on-off valves and others multi-layered structures as can be seen in Fig. 8. Derived from the ‘Quake valve’ design, Lee *et al.* have also fabricated 3D printed micro valves from biocompatible resin using stereolithographic printer removing the requirement of elastomer moulding and bonding (Lee et al., 2018). They have demonstrated the reproducibility and scalability of the technique by printing an 8x8 valve array and actuating them over 500000 times. Some of the many applications in which quake valves have been applied are polymerase chain reaction (Liu et al., 2002), cell sorting (Fu et al., 2002) and protein separation (Wang et al., 2004).

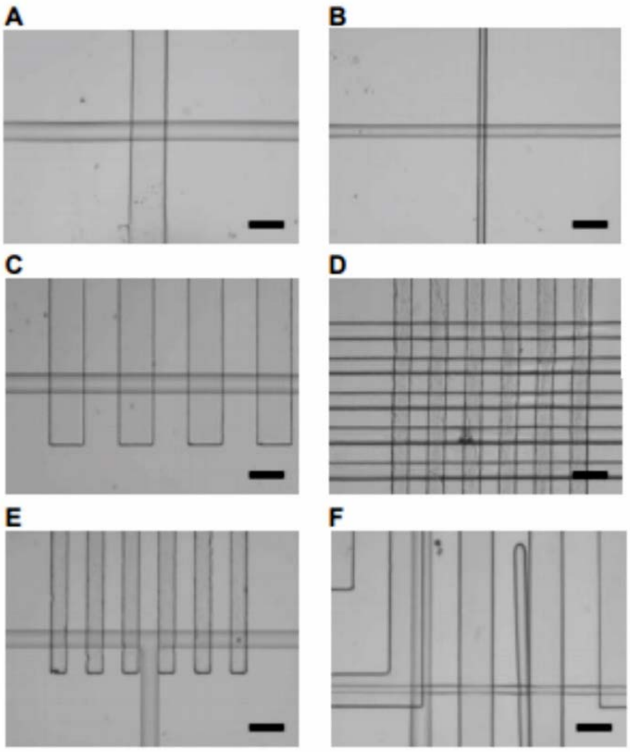

__Figure 8.__ Quake valves (Unger et al., 2000). (A) 200 µm x 100 µm on-off valve. (B) 30 µm x 50 µm on-off valve. (C) Peristaltic pump with one flow channel and four control channels. (D) Grid of on-off valves. (E) A switching valve. (F) A multi-layered structure. Scale bars are 200 µm.

2.6. Droplet Microfluidics

Droplet microfluidics, a subcategory of microfluidics, is the compartmentalization or digitalization of liquid into femto (fL) to nano (nL) litre droplets by the interaction of two immiscible liquids (Teh et al., 2008). Droplet microfluidic systems produce monodispersed, controllable and scalable droplets making them very robust for measurement and monitoring purposes. There are numerous benefits of this tool such as the usage of minute amounts of samples and reagents, decreased reaction time due to high surface-to-volume ratio, repeatability, higher analytical throughput, etc. These “micro-reactors” provide advantages by making the sample and reagent less prone to surface interaction with the micro channels and also prevents contamination by encapsulating the reaction volume (Teh et al., 2008, Baroud et al., 2010, Huebner et al., 2008, Zhu and Wang, 2017, Kaminski and Garstecki, 2017).

One of the main challenges faced in single-phase microfluidics (continuous microfluidics) is the effect of Taylor dispersion (Song et al., 2003). Generally, shear forces are applied to the channel walls resulting in a parabolic velocity profile of the fluid. This causes different elements in the fluid to spend different lengths of time in the chip and thereby dispersion of samples (Fig. 9 (a)). Droplet microfluidics overcomes this problem by compartmentalizing the mixture within a droplet and providing a single, well-defined incubation time (Fig. 9 (b)).

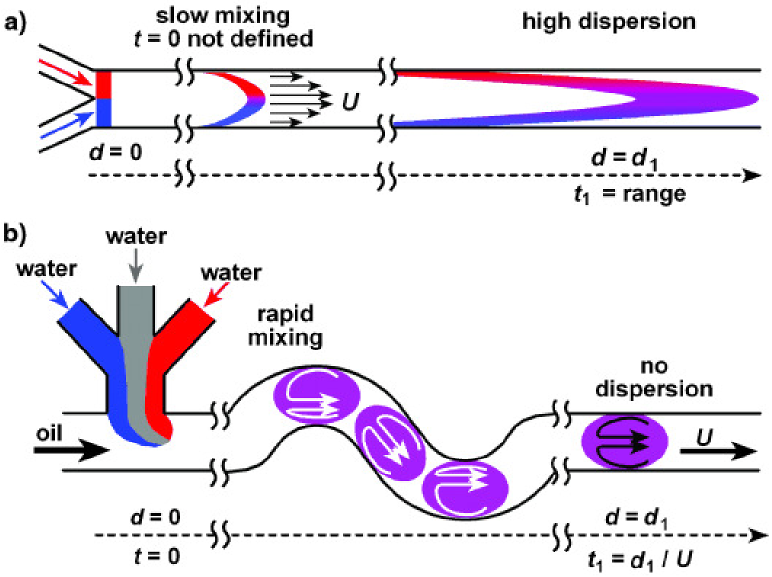

Figure 9. *Demonstrating the effect of Taylor dispersion (a) in single phase microfluidics channel compared to droplet microfluidics (b) (Song et al., 2003).*

Kaminski *et al.* classifited droplet microfluidics into different categories including ultrahigh throughput droplet microfluidics, digital microfluidics, and controlled droplet microfluidics (Fig. 10). Ultrahigh throughput droplet microfluidics (Guo et al., 2012) involves continuous, high-frequency passive generation of femto to nano-litre droplets for single-step processes, where off chip incubation of droplets and re-injection is carried out. Though extraction and re-injection can be challenging with loss of volume of droplets and stability, it can avoid on-chip problems such as formation of bubbles during heating or the requirement of large storage chambers. Electrowetting-on-dielectric (EWOD) microfluidics systems, also referred to as digital microfluidics (DMF) (Choi et al., 2012) uses electrowetting effect to control generation, motion, splitting or merging of droplets by the aid of electrodes arranged in 2D arrays. DMF technology provides individual and simultaneous control of droplets and implementation of complex procedures, however, the rate of operation in DMF is slower than in ultrahigh throughput. Controlled droplet microfluidics falls in between DMF and ultrahigh throughput droplet microfluidics (Kaminski and Garstecki, 2017). Controlled droplet microfluidic approaches depend on automation and passive flow control and address droplets in series. It encompasses passive systems like Slipchips (Du et al., 2009), hydrodynamic traps (Niu et al., 2011), droplet trains on-demand (Churski et al., 2012, Leung et al., 2012) and oscillatory and iterative droplet systems (Jakiela et al., 2013).

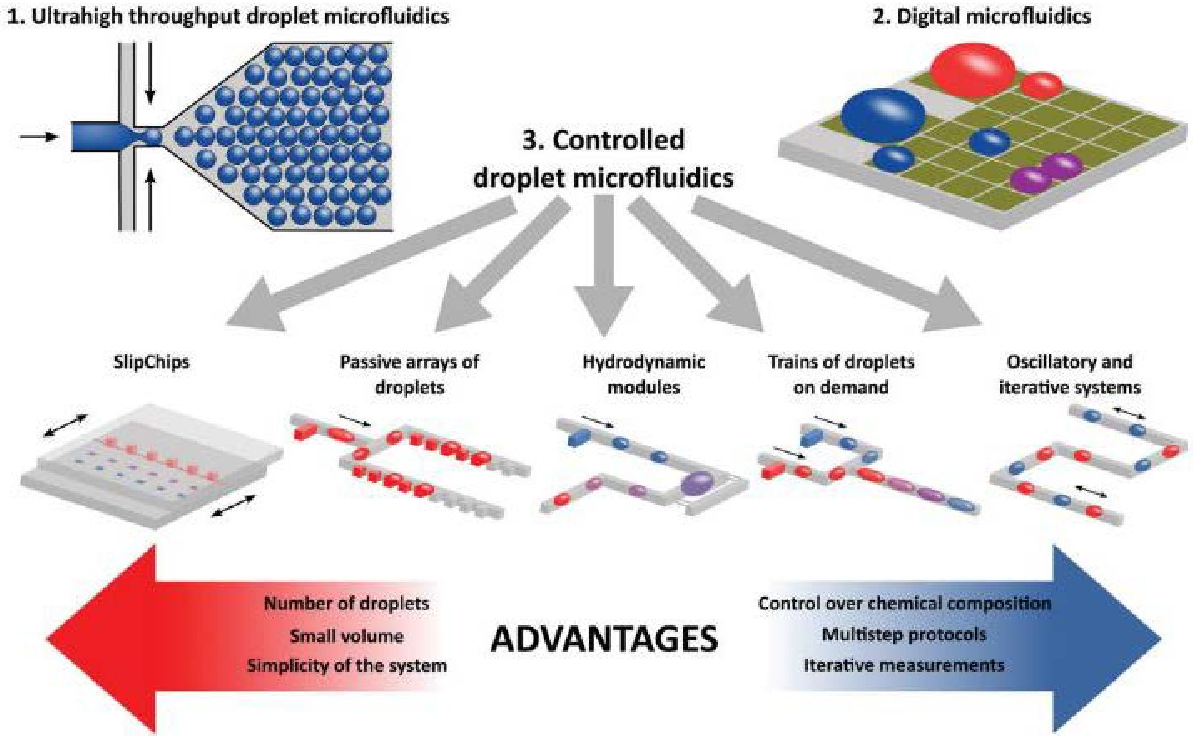

Figure 10. *Different categories of droplet microfluidics, namely ultrahigh throughput droplet microfluidics, digital microfluidics and controlled droplet microfluidics (Kaminski and Garstecki, 2017) and their advantages.*

2.6.1. Dimensionless parameters in droplet microfluidics

When analysing droplet microfluidics containing carrier phase (phase carrying the droplets) and the dispersed phase (which are the droplets), there are four forces, inertia, viscous shear, buoyancy and interfacial tension that come into play (Zhu and Wang, 2017, Glawdel et al., 2013). The behaviour of the liquids can be characterised by several dimensionless numbers such as Reynolds number, capillary number, bond number and weber number as displayed in Table 1 (Glawdel et al., 2013, Gu et al., 2011, Anna, 2016). These dimensionless numbers originate from the Navier-Stokes equation of incompressible Newtonian fluids (Zhu and Wang, 2017):

$$\rho_s \frac{\partial u_s}{\partial t} + \rho_s u_s . \nabla u_s = -\nabla P_s + \eta_s \nabla^2 u_s + f_s \qquad (1)$$

where t denotes time, ρ is density of fluid, pressure is P, η is the shear dynamic viscosity, u is the velocity vector of the fluid and f denotes the force of body per unit volume. The subscript 's' refers to either *'c'* or *'d'* for either the continuous or the dispersed phase of the fluid. The terms on the left side of the equation refers to inertial acceleration with $\rho_s \frac{\partial u_s}{\partial t}$ showing the time-dependence of acceleration and $\rho_s u_s . \nabla u_s$ showing the acceleration due to convection. The terms on the right side of the equation denote the force densities.

Table 1. Dimensionless parameters used to characterize droplet generation (Zhu and Wang, 2017).

Symbol	Name	Formula		Physical meaning
Re	Reynolds number	$Re = \frac{\rho u L}{\eta}$	(2)	Inertial force/ viscous force
Ca	Capillary number	$Ca = \frac{\eta u}{\gamma}$	(3)	Viscous force/ interfacial tension
We	Weber number	$We = \frac{\rho u^2 L}{\gamma}$	(4)	Inertial force/ interfacial tension
Bo	Bond number	$Bo = \frac{\Delta \rho g L^2}{\gamma}$	(5)	Buoyancy/ interfacial tension
λ	Viscosity ratio	$\lambda = \frac{\eta_d}{\eta_c}$	(6)	Dispersed viscosity/ continuous viscosity
∅	Flow rate ratio	$\emptyset = \frac{Q_d}{Q_c}$	(7)	Dispersed flow rate/ continuous flow rate

Effects of inertia and gravity become negligible in microfluidics systems and interfacial tension and viscous forces are dominant. This is due to the high surface-to-volume ratio in microfluidics channels and lower flow velocities (Garstecki et al., 2006b). The ratio between viscous and interfacial tension is the capillary number (Ca) which is equal to $Ca = \frac{\eta u}{\gamma}$, an important parameter in understanding droplet formation, merging splitting, mixing, etc. (Glawdel et al., 2013). In the equation 3, η is the viscosity, u is the velocity and γ is the interfacial tension. Interfacial tension plays a vital role in formation of droplet and stabilizing because interfacial tension works in reducing the interfacial area. Viscous force on the other hand, works to elongate the interface. When the capillary number (Ca) is low (less than 1), interfacial tension is prominent, and we get more uniform and round droplets. When viscous force is dominant, indicated by a higher Ca (>>1) it may lead to distortion of droplets (Gu et al., 2011). Therefore, a fine balance of the parameters is required for formation of stable, monodisperse droplets.

2.6.2. Droplet Formation

2.2.2. 1. Channel geometry and break-up regimes for droplet generation

There are various channel geometries used to form droplets; cross-flow (Garstecki et al., 2006b), co-flow and flow-focusing (Garstecki et al., 2004, Anna et al., 2003) geometries are the ones most widely used (Fig. 11).

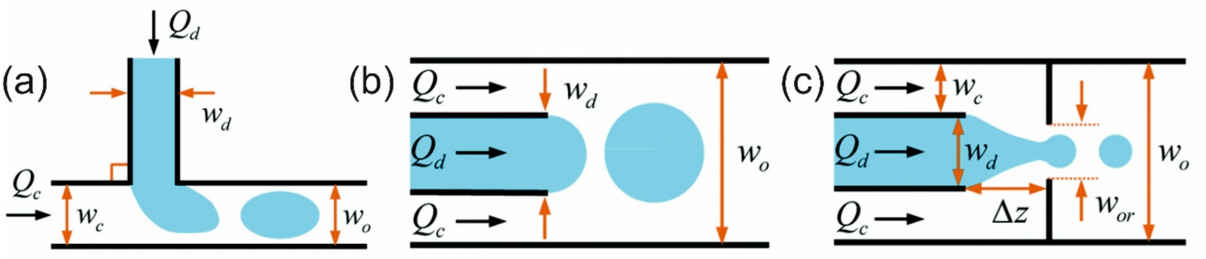

Figure 11. *Droplet formation in (a) cross-flow, (b) co-flow and (c) flow focusing geometry. Q denotes the volumetric flow rate, w is the channel width and Δz is the horizontal distance between the end of the microchannel containing the dispersed phase and the orifice entrance. The subscripts c, d, o and or denote continuous phase, dispersed phase, channel outlet and orifice respectively (Basova and Foret, 2015, Zhu and Wang, 2017).*

In cross-flow (Fig. 11 (a)) the continuous and dispersed flows meet at an angle between 0° and 180°. This geometry, which was first demonstrated by Thorsen *et al.* is usually implemented by a T-junction which causes the two phases to meet orthogonally (Thorsen et al., 2001). Different flow regimes can be depicted such as squeezing, dripping and jetting for different flow rates (Fig. 12), different viscosity of fluids and also for various ratio of channel width and height and the breakup regime can be predicted by the capillary number (Shang et al., 2017, Gu et al., 2011).

At low values of capillary number ($C_a < 10^{-2}$) for microchannels in the order of 100 µm and with flow rates of 10^{-2} to 1 µL/s (Garstecki et al., 2006a), confinement of fluid in microchannel and interfacial dynamics dominate viscous, inertial and gravitational forces, the droplets are produced using the 'squeezing' regime. The droplet formation cycle starts with a 'filling' period where the dispersed phase from the side channel completely fills the main channel, narrowing the flow of the continuous phase into a thin film. This marks the beginning of the 'squeezing' phase, where due to the build-up of pressure upstream, the continuous phase squeezes the neck of the dispersed phase and ultimately 'pinch-off' occurs (Garstecki et al., 2006a, van Steijn et al., 2010).

In the 'squeezing' regime, the droplet/ slug length can be characterized by the scaling law (Garstecki et al., 2006a)

$$\frac{L}{w_c} = 1 + \frac{\alpha Q_d}{Q_c} \tag{8}$$

where, L denotes the length of the slug, w_c is the channel width, $Q_{c/d}$ are the carrier and dispersed fluid flow rates and α which is a constant of order and with its value depending on the T-junction geometry. Size of the droplet is determined solely by the volumetric flow rate ratios of the dispersed and continuous phases and the scaling equation is independent of fluid properties such as viscosities and interfacial tension (van Steijn et al., 2010).

The droplet volume (V) generated is

$$\frac{V}{hw^2} = \frac{V_{fill}}{hw^2} + \frac{\alpha Q_d}{Q_c} \tag{9}$$

linearly proportional to the flow rate ratios and V_{fill} and α are 'fitting parameters' which are microfluidic device specific. The height and width of channel has been denoted by h and w respectively.

As the capillary number (Ca) increases, the droplet generation regime shifts from 'squeezing' to 'dripping' (De Menech et al., 2008). Viscous forces govern over interfacial tension (which stabilises the droplet) and cause droplet break up at the dispersed phase nozzle. Constant viscous stress can generate highly monodisperse droplets in this regime. A transition from the 'dripping' to the 'jetting' regime is caused either by increasing the continuous (Q_c) or dispersed flow rates (Q_c). In the 'jetting' mode, the dispersed phase emits an extended jet and breaks up into droplets at the end of the jet due to Rayleigh-plateau instability (Utada et al., 2007, De Menech et al., 2008, Zhu and Wang, 2017).

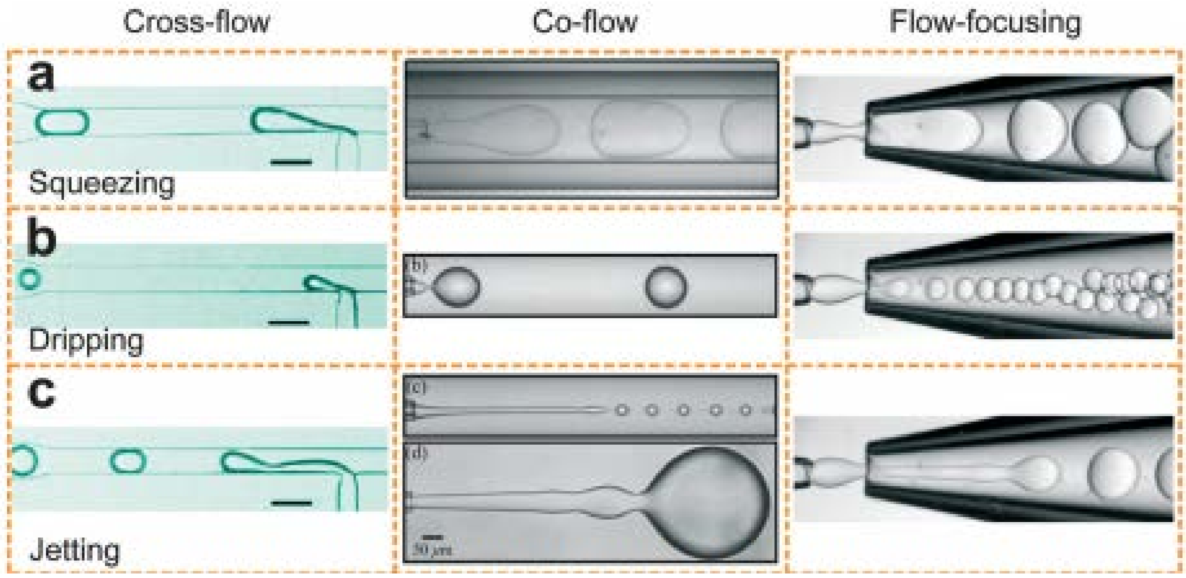

Figure 12. *Images of cross-flow, co-flow and flow-focusing geometries showing (a) squeezing, (b) dripping and (c) jetting regimes for droplet break up.*

As the name implies, in co-flow geometry (Fig. 11, 12), the dispersed and continuous phases flow in parallel through coaxial channels (Shang et al., 2017). The continuous phase flows through the outer concentric channel and the dispersed phase is introduced through the inner one. The droplet size increases with increase in dispersed phase flow rate and similarly decreases with continuous phase flow rate, as it allows lower volume of dispersed phase to enter the channel (Shang et al., 2017). This geometry was first implemented by Cramer *et al.* and ‘dripping’ and ‘jetting’ regimes were studied (Cramer et al., 2004).

Flow focusing geometry (Fig. 11, 12) (Garstecki et al., 2004, Anna et al., 2003, Dreyfus et al., 2003) is similar to co-flow geometry but both the phases flow through a contraction downstream. This causes elongation of the flow and ultimate ‘pinching- off’ due to shearing force leading to the formation of small, monodisperse droplets either inside or downstream of the contraction. At high flow rates, this geometry can cause jetting and result in polydisperse droplets (Tran et al., 2013).

Double emulsions (Utada et al., 2005) such as oil-in-water-in-oil (O/W/O) or water-in-oil-in-water (W/O/W) can be produced using double T-junctions, double cross microchannels or other 3D microchannels (Chong et al., 2015). Emulsions with multiple droplets inside (Utada et al., 2005) and multiple emulsions (Abate and Weitz, 2009) with precise control on size can be achieved by different geometries and flow control. Figure 13 shows a 3D micro capillary device implemented by Utada *et al.*

to produce double emulsions with varying shell thickness and internal droplets by independently controlling the flow of the immiscible inner, middle and outer fluids (Utada et al., 2005). Hydrodynamic focusing of the co-axial flow results in the formation of the double emulsions. Double emulsions are very useful tools for drug delivery and controlled release of drug (Rajian et al., 2011), cell studies (Brower et al., 2020) and synthetic biology (Zhao et al., 2018).

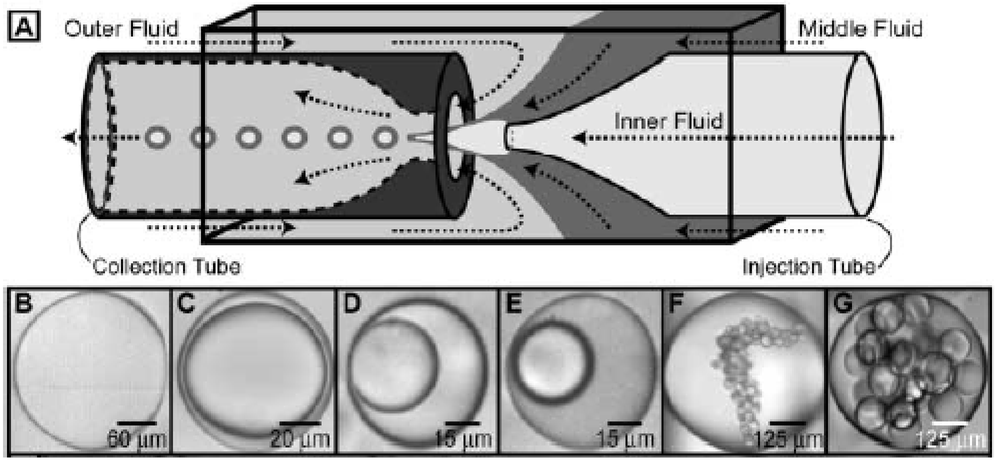

Figure 13. Generation of double emulsion droplets (Utada et al., 2005). (A) 3D micro capillary device implemented by Utada et al. to produce double emulsions. (B-G) Different number and sizes double emulsions with varying number of inner droplets.

2.6.3. Active droplet generation

Active droplet generation involves introducing external energy input that can be either “electrical, magnetic, centrifugal, optical, thermal” or “mechanical” to produce droplets (Zhu and Wang, 2017). The external inputs work by influencing the dynamic velocity of droplets thereby manipulating the inertial, viscous and capillary forces. External inputs could also alter intrinsic material properties such as interfacial tension, viscosity, density of fluid and wettability of channels (Zhu and Wang, 2017). Active droplet generation provides certain benefits like independent control of droplet size and frequency unlike passive control and the time required to stabilise droplet production is also much shorter than passive methods (Chong et al., 2016).

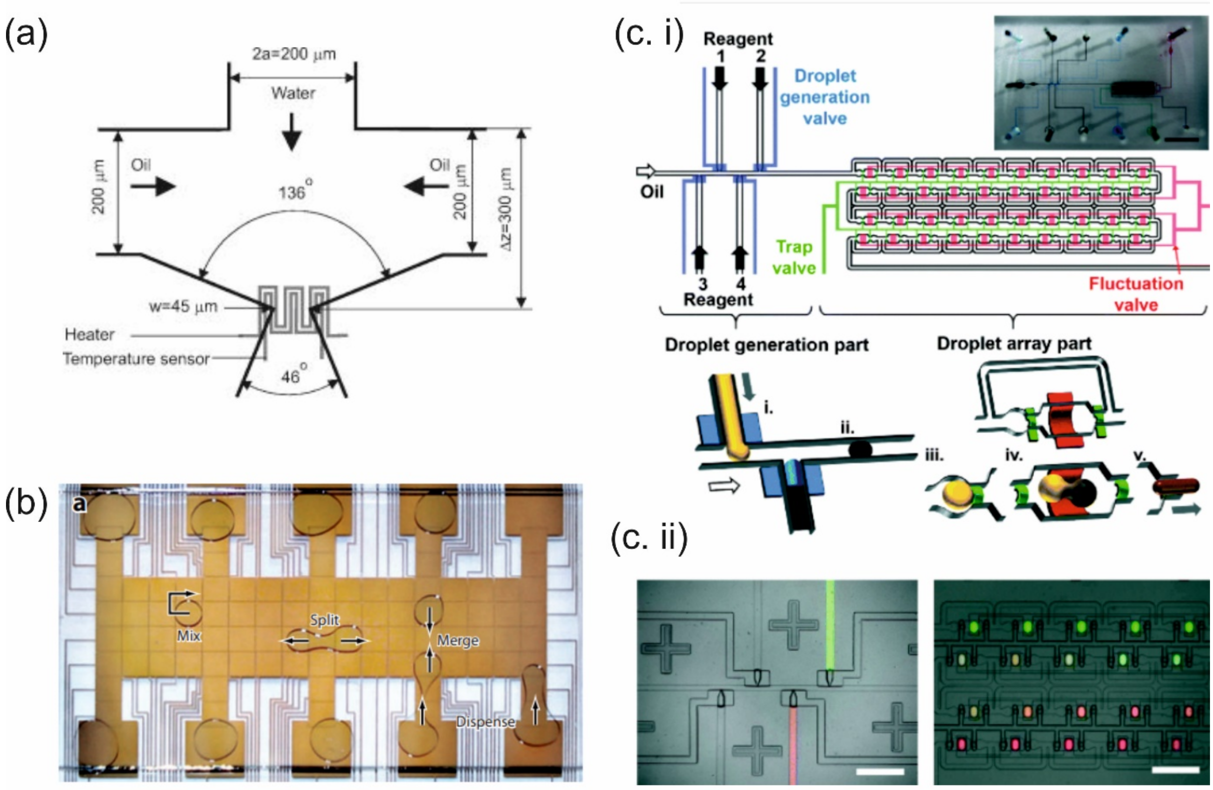

Figure 14. Examples of active droplet generation methods. (a) Schematic of micro heater for thermally controlled droplet generation (Nguyen et al., 2007). (b) EWOD device displaying droplet dispensing, mixing, splitting and merging (Choi et al., 2012). (c) Pneumatically actuated valves for droplet generation and trapping (Jin et al., 2015). (i) Schematic of device showing droplet formation valves, trap valves and fluctuation valves. (ii) Actual picture of droplet generation area and trapping area.

Droplets can be generated using electrical methods such as Dielectrophoresis (DEP) (Pit et al., 2015) and ElectroWetting-On-Dielectric (EWOD) (Mugele and Baret, 2005). EWOD (Mugele and Baret, 2005) utilizes an array of insulated electrodes (coated with thin dielectric and hydrophobic layers) to manipulate conductive droplets by varying the interfacial tension between the droplets and the electrodes using electric potential. This provides independent control over individual droplets to perform on-demand generation, merging, mixing, splitting and transport as can be seen in Fig. 14 (b) (Choi et al., 2012). One of the main advantages of EWOD is the vast number of droplets that can be controlled on-demand and has been demonstrated by Hadwen *et al.* (Hadwen et al., 2012). They have implemented a feedback controlled active matrix electrowetting-on-dielectric (AM EWOD) device consisting of 64 x 64 thin film transistor array which can be programmed to carry out multiple parallel operations. EWOD has also been shown in applications such as enzymatic and immunoassays (Bogojevic et al., 2012), DNA analysis (Chang et al., 2006) and cell culture (Srigunapalan et al., 2012). Dielectrophoresis (DEP) is defined as the motion of polarizable particles/ droplets in a non-uniform electric field. Devices utilize DEP by applying a voltage across two or more electrodes outside the microfluidic channels (Pit et al., 2015). One way to obtain an electric field gradient is by implementing a pointed electrode at one end where the field lines would converge. In one of the recent works, Wang and co-workers have developed a micro droplet generator based on DEP (Wang et al., 2019a). They used liquid metal electrodes to create an electric gradient which acted as 'invisible scissors' to chop off aqueous droplets in silicone oil. The droplet size could be varied by designing different sized electrodes or by deciding which electrode to switch on in the electrode array.

Mechanical control involves the utilizing hydraulic (Unger et al., 2000, Abate et al., 2009), pneumatic (Zeng et al., 2009) or piezoelectric actuation (Xu and Attinger, 2008) to distort or pinch-off the liquid interface. Pneumatic micro valves have been implemented by Zeng and co-workers to generate on-demand droplets of different size (by controlling the valve switching time) and composition (increasing channel numbers) (Zeng et al., 2009). An interesting application shown by Jin *et al.* is of a static droplet array 'combinatorial matrix' by pneumatically actuated valves (Jin et al., 2015). Their device (Fig. 14 (c)) is able to generate on-demand droplets with different sizes and distance between them, hydro-dynamically trap the droplets and store them in order to carry out multiple parallel reactions.

Various groups have implemented thermal control (Khater et al., 2019, Miralles et al., 2015, Stan et al., 2009) for droplets, exploiting the dependence of fluid viscosity and interfacial tension on temperature. Microheaters (Fig. 14 (a)) (Nguyen et al., 2007, Fang et al., 2015), heat exchangers (Stan et al., 2009) and laser heating (Baroud et al., 2007) have been applied to manipulate droplets. Baroud *et al*. have shown that localised heating with a laser can block formation of droplets therefore acting as a 'tunable valve' for two phase microfluidics (Baroud et al., 2007).

2.6.4. Droplet generation using phased peristaltic pump

Niu group has developed a screw pump (Nightingale et al., 2019b) based on the technology first demonstrated by Rhie *et al.* (Rhie and Higuchi, 2010), for a handheld microfluidic system for the continuous monitoring of biomolecules such as glucose and lactate (system schematic can be seen in Fig. 15). The pump uses a screw thread to propagate fluid through the pumplines and the flowrate can be controlled by changing the motor speed, the inner diameter of the pumpline or the screw pitch. In order to produce aqueous droplets in oil at a T-junction, the screw thread engages and disengages in a way that antiphase aqueous and oil pulses are produced. As there is continuous compression of the pumplines, backflow of liquid is prevented (Nightingale et al., 2019b).

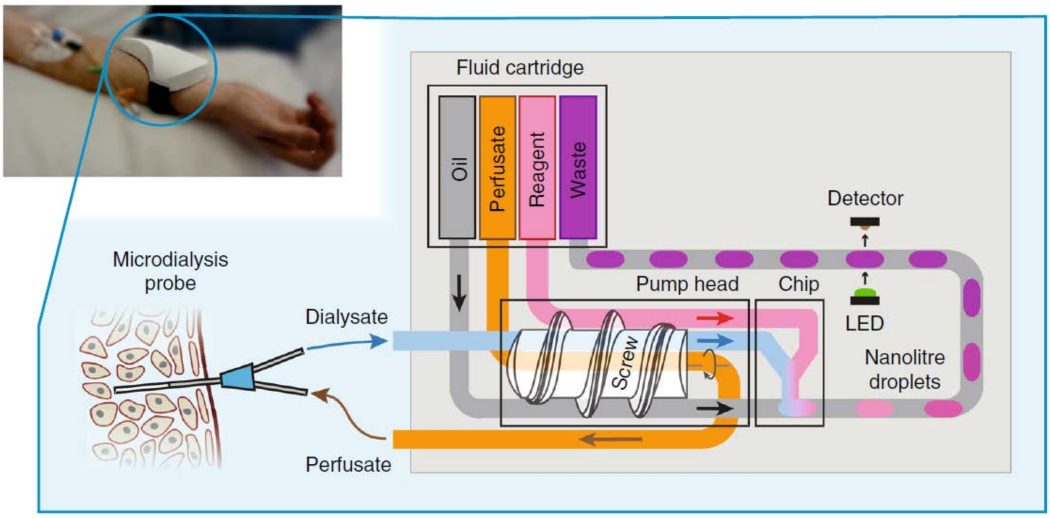

Figure 15. *Microfluidic system schematic demonstrating the operation of a miniature peristaltic screw pump utilised in a handheld sensor device for continuously monitoring biomolecules like glucose and lactate. The screw pump propagates dialysate from a micro dialysis probe, reagent and oil into a T-junction chip in anti-phase pulses to produce reaction droplets. Perfusate is also introduced into the microdialysis probe in order to replace the dialysate. The droplets are then driven downstream to a detection flow cell for colorimetric analysis (Nightingale et al., 2019b).*

Although the screw pump developed in the group miniaturises the pumping system to be incorporated in a handheld device and reliably generates droplets of fixed volume, it does have some limitations. As the pumplines need to be around the screw, there is a constraint on the number of pumplines that can be positioned, reducing the number of droplets that can be generated and limiting the scope for multiplexed assays. It is also hard to time the phases due to the continuous rotation of the screw.

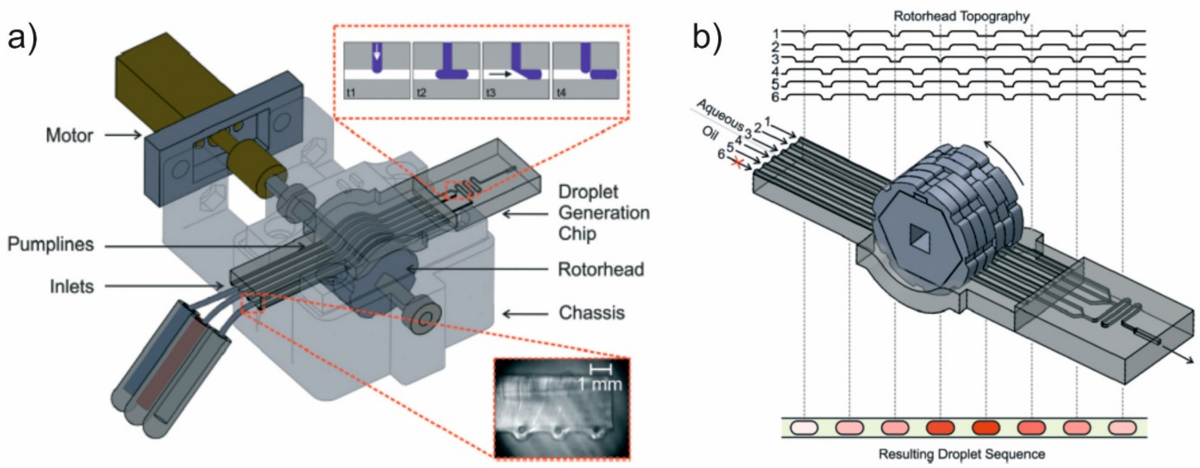

Figure 16. *Phased peristaltic pump designed by Niu group. (a) 3D Solidworks CAD file showing the peristaltic micropump in operation. The pump unit consists of a motor, chassis, rotorhead with features and a monolithic*

PDMS droplet generation chip with attached pump lines. The top inset shows the generation of droplets per turn of the pump. The bottom inlet shows a cross sectional view of the pump lines. (b) Solidworks CAD file demonstration of dilution series being generated by 'pre-specified' rotorhead and chip design. The oil and aqueous lines are in antiphase and the aqueous lines 1 and 3 vary to generate the dilution series with keeping the droplet volume consistent throughout (Nightingale et al., 2017).

In order to overcome the limitations of the screw based peristaltic pump, another version of the phased peristaltic pump was developed by the Niu group (Nightingale et al., 2017) consisting of a rotor head with features around it to propagate liquid in antiphase pulses onto a microfluidic chip for robust droplet generation (Fig. 16 (a)). The droplets generated are stable, invariant to the properties of the liquid being introduced and the volumes are determined by the 'hardcoded' rotor features. It requires much less time for stable fluidic control compared with syringe pumps. Comparison of droplet generation between anti-phased peristaltic pump developed by our group and a traditional syringe pump is shown in Fig. 17. By changing the rotorhead topography and the number of channels, it is possible to perform chemical protocols such as dilutions and titrations. Figure 16 (b) shows the Solidworks CAD file designs for the rotorhead and chip to perform continuous serial dilutions. The topography of the roller is such that the oil and aqueous lines are in antiphase and the aqueous lines 1 and 3 vary to generate the dilution series with keeping the droplet volume consistent throughout (Nightingale et al., 2017).

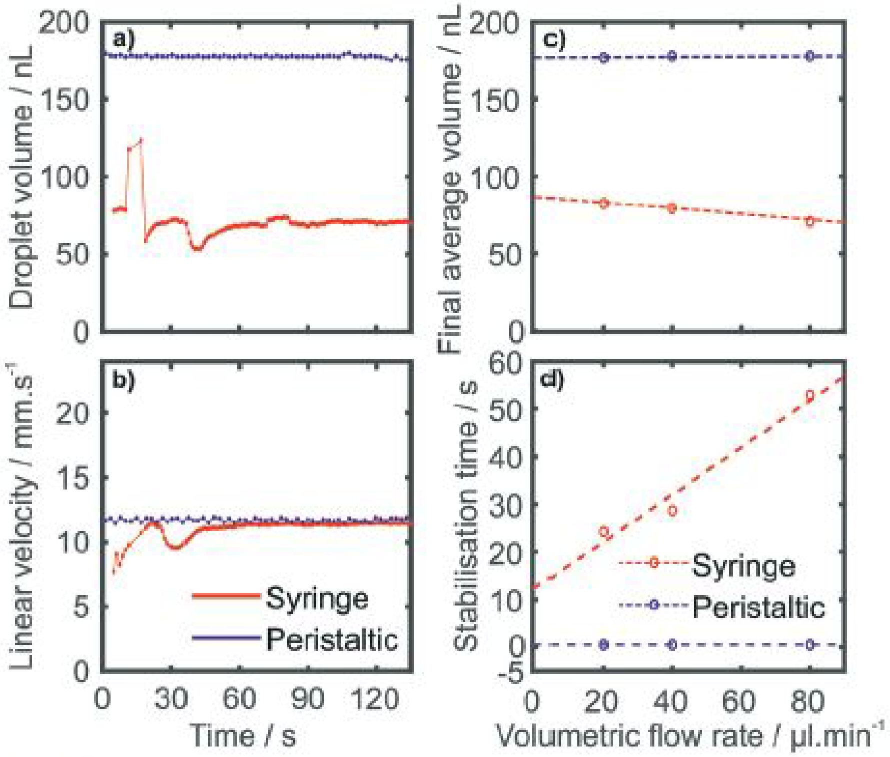

Figure 17. *Comparison of droplet generation between peristaltic micropump and traditional syringe pump: (a) droplet volume with change in time, (b) linear velocity as a function of time, (c) stabilised droplet volume vs volumetric flow rate and (d) time taken for flow stabilisation vs volumetric flow rate (Nightingale et al., 2017)*

2.6.5. Microfluidic chip fabrication and channel wettability

The primary requirement and an essential step for droplet formation is the fabrication of chip with appropriate geometry and surface properties. To fabricate a microfluidic chip, there are various techniques (Gale et al., 2018) like lithography (McDonald and Whitesides, 2002), glass/silicon etching, laser micromachining (Shiu et al., 2008), milling (Guckenberger et al., 2015), replica moulding (Kim and Meng, 2015), hot embossing (Lee et al., 2001), 3D printing (Yazdi et al., 2016), etc. which can be chosen depending on the material and application (Shang et al., 2017). Materials are generally chosen based on function of the chip, compatibility with the reagents and samples being used or biocompatibilities (Ren et al., 2013).

Lithography based microfabrication is one of the prime methods of chip fabrication on glass/ silicon and a standard process involves three steps namely lithography, etching and bonding. There are certain advantages of using silicon and glass such as their thermal stability and their resistance to solvents when organic reactions are taking place. However, their impermeability to gas and their structural rigidness can make them unsuitable for many applications. The requirement for disposable and cheap chips have led to an increased demand for replica moulding using polymer. Soft lithography technique usually using poly(dimethylsiloxane) (PDMS) (McDonald et al., 2000) to transfer patterns from a master was first introduced by Whitesides *et al.* PDMS is a silicone based elastomer with desirable properties such as biocompatibility, optical transparency, oxygen-permeability, thermal stability and inertness to chemicals (Mata et al., 2005) . Figure 18 illustrates the various steps for rapid prototyping using PDMS (McDonald and Whitesides, 2002). PDMS chips can be bonded to glass, silicon or PDMS itself using oxygen plasma bonding (Bhattacharya et al., 2005) or other partial curing techniques for PDMS-PDMS bonding which has been proven to be stronger than plasma bonding (Eddings et al., 2008). Masters for PDMS moulding could also be fabricated using 3D printing, micromachining, milling removing the requirement of expensive cleanroom facilities and extensive training but with a disadvantage of having bigger channel size.

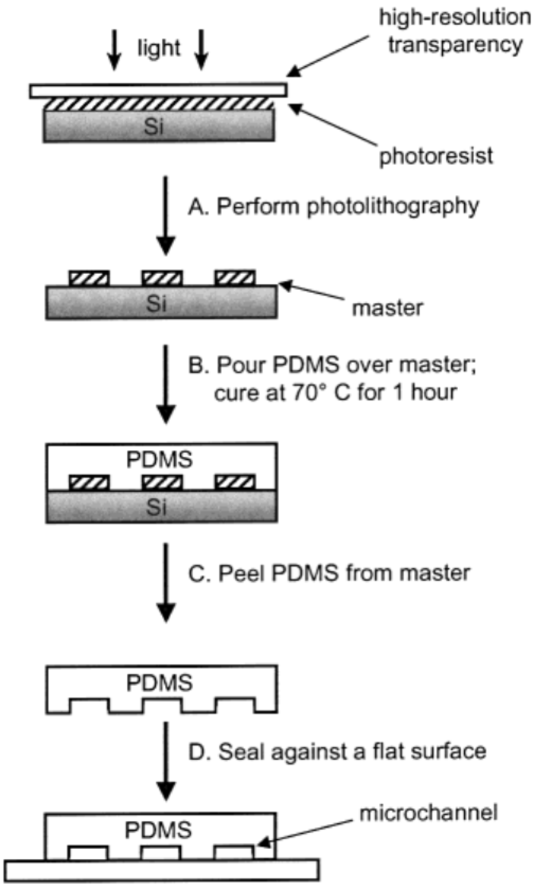

Figure 18. *Demonstration of the steps of rapid prototyping using PDMS (McDonald and Whitesides, 2002).*

In droplet microfluidics, hydrophobic surface are frequently required but chips made of non-fluorous materials such as PDMS, glass, cyclic olefin polymer, etc. are not ideal and require additional surface treatments to make the channels hydrophobic. This adds to the fabrication step and the surfaces are generally not durable. They may degrade over time due to use of high temperature or multiple day usage making them a liability for field deployable sensors. Fluoropolymers (PTFE, FEP, PFA) cater to this issue due to their inherent fluorous surface however, fabricating chips from them can be problematic due to high temperature requirements and difficulty in machining. Our group has implemented an easy method for fabricating "monolithic fluoropolymer chips" using Dyneon THV 500 GZ (Nightingale et al., 2020) as illustrated in Fig. 19.

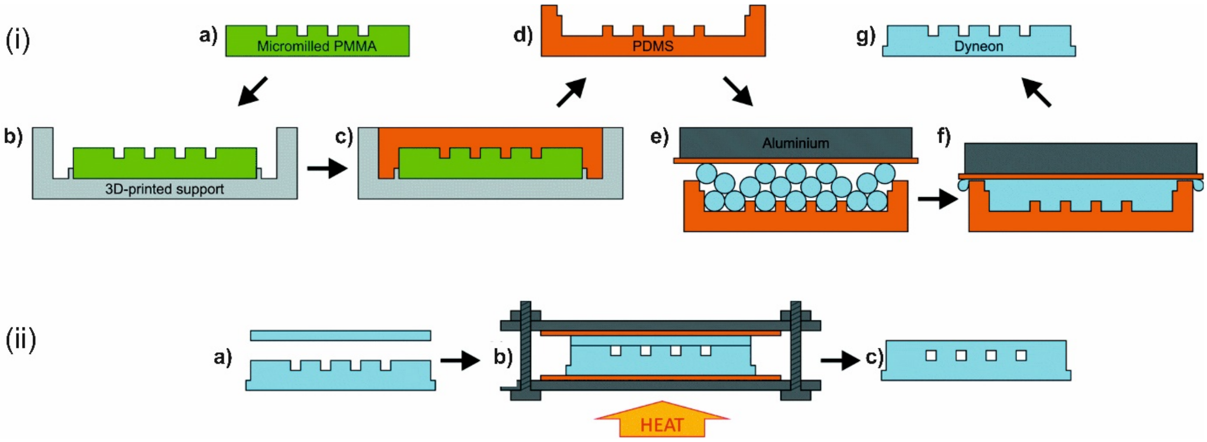

Figure 19. Illustration showing the fabrication of micro-patterned Dyneon THV chips (Nightingale et al., 2020). (i) A micro-milled PMMA unit (a) is held by a 3D printed support (b) and PDMS liquid is poured in it. After curing, the PDMS mould (d) is used for filling up with Dyneon THV pellets and covered with a silicone sheet and aluminium block on top. Curing in the oven and removing from the mould results in the patterned Dyneon THV structure (g). (ii) Illustration showing the bonding of a patterned and flat Dyneon layers to result in the final chip. The two layers are sandwiched using a metal plate clamp and silicone sheets and heated in the oven at 160 °C overnight to bond them.

Recent development in 3D printing has also brought about significant improvement in microfluidic chip fabrication such as reduction in cost, time and flexibility in achieving more complex structures with combination of materials. Polyjet, stereolithography (SLA), fused deposition modelling (FDM) have all been used extensively for printing fluidic features (Beauchamp et al., 2017) and printing of channels reliably down to 100 µm has been demonstrated. However, 3D printing still cannot compete with the resolutions allowed by lithography techniques and issues with biocompatibility, surface quality and optical transparency are being studied (Waheed et al., 2016).

The wetting condition of the channels are critical for the uniform formation and robust handling of droplets. In order for aqueous droplets to not come in contact with the channel walls, the continuous phase should preferentially wet the walls. Failure to coat the walls may lead to droplet adhesion and hence the prevent reproducibility of the chip. PDMS is mildly hydrophobic but plasma treatment for bonding in soft lithography can cause the channels to become hydrophilic. This effect is not permanent and exposure to air causes the channels to become hydrophobic again naturally. However, Aquapel glass treatment and other hydrophobic silanes can be used to make channels super hydrophobic (Tran et al., 2013, Glawdel et al., 2013).

2.6.6. Carrier fluids

The choice of carrier fluid is very important for droplet production as the carrier has to be inert to both the reagents/ samples within the droplet and to the material from which the chip is fabricated. Silicone oils have been used in glass devices but are suitable for PDMS ones as low viscosity silicone oils are easily absorbed by PDMS devices, causing them to swell and eventually altering the cross-section of the channels. High-viscosity silicone oil on the other hand does not cause much swelling but adds pressure requirements to drive the oil through the channels. Fluorocarbon oils are more favoured in biochemical analysis because they do not swell PDMS and work well at preserving droplets due to very high interfacial tension with water. Fluorocarbon oils also allow gaseous exchange which is vital for respiration of cells in droplets (Tran et al., 2013, Glawdel et al., 2013).

2.6.7. Surfactants

‘Surface Active Agents’ or ‘surfactants’ are an integral part of droplet-based microfluidics and are used to stabilize droplets and for storage applications. Surfactants are made of amphiphilic molecules, which makes them soluble in both oil and aqueous phases and as a result, they travel and stay on the surface of the droplets (Glawdel et al., 2013). Surfactants decrease the surface tension between phases, prevent the coalescence of close droplets and also keep the constituents of the droplets intact. The relation between the number of molecules adsorbed at the surface and the surface tension can be described by Gibbs adsorption isotherm

$$\Gamma = -\frac{c}{RT}\frac{d\gamma}{dc} \tag{10}$$

where Γ is the surface concentration, γ is the surface tension, c is the surfactant concentration and T and R are temperature and gas constant respectively. The surface tension decreases with the increase in adsorbed molecules at the surface (Baret, 2012). Baret has tabulated and reviewed a list of commercially available surfactants such as Triton X-100, ABIL EM90, Span80, Tween 20/80, etc. and their applications (Baret, 2012). A type of PFPE-PEG triblock co-polymer surfactant as shown in Fig. 20 has been widely used when fluorinated oil is chosen to be the carrier fluid. This fluorosurfactant contains a PEG hydrophilic head and two PFPE tails.

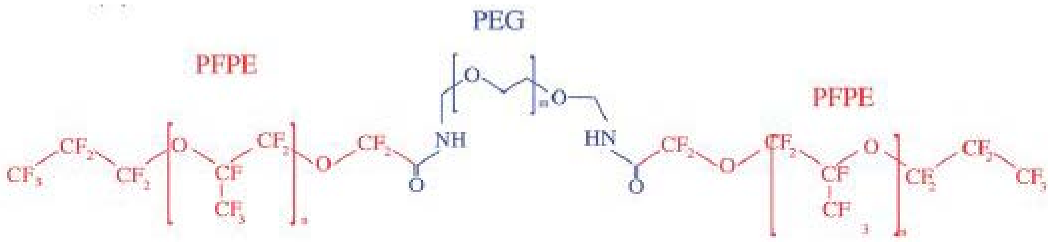

Figure 20. *PFPE-PEG triblock copolymer (Brosseau et al., 2014).*

At high temperatures, triblock co polymers like PFPE-PEG may show poor performance (such as droplet merging and transfer of small molecules between droplets) during bioanalytical procedures like thermal cycling during PCR. Recently di-block polymers with dendric head groups have been synthesized and demonstrated thermal stability of droplets (Chowdhury et al., 2019).

2.6.8. Droplet manipulation

After generation of droplets either by passive or active methods, droplets can be manipulated using various functions and utilised for biochemical sample processing and analysis (Simon and Lee, 2012). Droplets can be manipulated by droplet merging (Niu et al., 2008, Mazutis et al., 2013, Liu et al., 2007), fission (Adamson et al., 2006, Link et al., 2004, Song et al., 2003), mixing (Song et al., 2003, Hsieh et al., 2009, Wang et al., 2015a), sorting (Niu et al., 2007, Tan et al., 2004, Xi et al., 2017) and dilution (Niu et al., 2011, Postek et al., 2017).

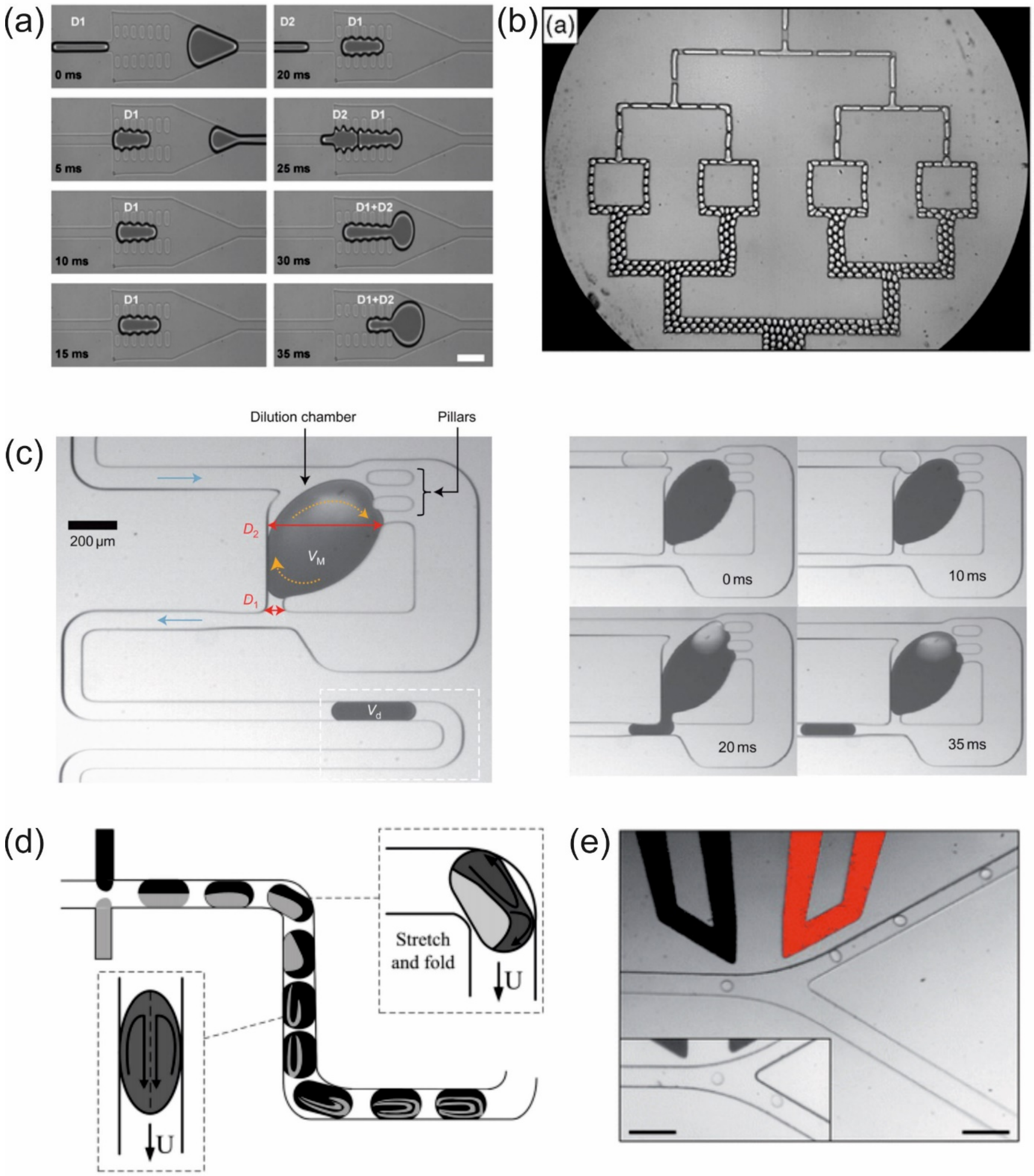

__Figure 21.__ Droplet manipulations. (a) Droplet merger using a tapered pillared structure (Niu et al., 2008). (b) Droplet splitting (Link et al., 2004). (c) Droplet dilutor (Niu et al., 2011). (d) Mixing in droplets (Wang et al., 2015a). (e) Fluorescence-activated cell sorting (FACS) (Baret et al., 2009).

Droplet merging is an important function since it allows combination of various reagents and analytes thus initiating biological and chemical reactions in microfluidic devices (Simon and Lee, 2012). In order to coalescence two or more droplets in microfluidic structures it requires the removal of the continuous phase separating them. Fluctuations in surface tension and destabilization of the aqueous and oil interface leads to fusion (Eggers et al., 1999). A tapering pillared, single input, single output microfluidic structure (Fig. 21 (a)) was developed by Niu *et al.* to passively merge droplets (Niu et al., 2008). The structure exploits the interaction of hydrodynamic and interfacial tension and could be introduced in any part of a microfluidic network without disrupting the mass and pressure distribution. When a droplet enters the pillared expansion chamber, it is trapped indefinitely until the next droplet merges with it. The structure allows the continuous phase to move to the main channel without being trapped by the droplet thus in a way acting like a filter. Active control methods have also been employed for merging droplets such as dielectrophoresis (Wang et al., 2009b), electrocoalescence (Priest et al., 2006) and optical tweezers (Lorenz et al., 2006). Using electricity can accelerate the fusion process and increase throughput but on the negative side, employing electrodes can lead to deposition and biofouling (Simon and Lee, 2012). Droplet merging has been applied in areas of research like single cell analysis (Mazutis et al., 2013) and for fusion of liposomes and cells (Tresset and Takeuchi, 2004).

Niu *et al.* have fabricated a droplet diluter (Niu et al., 2011) for high-throughput screening and applied it for a DNA binding assay (Fig. 21 (c)). A nanolitre sample droplet of a known concentration is trapped in a microfluidic chamber and smaller buffer droplets are fused with it to produce a droplet sequence resulting in a 'digital concentration gradient'.

Droplet fission is another critical droplet manipulation tool. Droplet fission is used to divide droplet plugs into multiple smaller droplets for increasing throughput, digitizing biological assays and giving systems ability to multiplex (Simon and Lee, 2012). Link *et al.* have demonstrated droplet splitting (Fig. 21 (b)) using bifurcation channel geometries (Link et al., 2004). Fission of plug like droplets occur at the bifurcation when droplet length is greater than the droplet edge circumference and the fluidic resistance of the daughter channels downstream are equal. Link *et al.* have also demonstrated an 'obstruction-mediated breakup' using a square obstruction in a microchannel to produce different sizes of daughter droplets based on the size and placement of the obstruction (Link et al., 2004). Active methods like EWOD (Sung Kwon et al., 2003), laser (Baroud et al., 2007) and microheaters (Yap et al., 2009) have also been implemented to split droplets.

Droplet sorting based on the contents (cells, biological particles, etc.) of the droplets is of utmost significance in droplet analysis (Xi et al., 2017). Simple sorting mechanisms do not require any active control and can be implemented using creative channel geometries exploiting droplet size. Tan *et al.*

have demonstrated droplet sorting (Tan et al., 2007) according to their sizes by simultaneously controlling the flow rate ratio of the daughter channels and modifying the bifurcating junction geometry. The same group have also developed a two layered microfluidic device with a circular reservoir to separate and filter out satellite droplets (which may interfere during analysis) produced while generating emulsions (Tan and Lee, 2005). Niu *et al.* implemented capacitive sensing using parallel electrodes to sort droplets based on the change in di-electric constant depending on the droplet content (Niu et al., 2007). Other methods such as fluorescence activated cell sorting (FADS) (Fig. 21 (e)) (Baret et al., 2009), magnet controlled sorting (involving ferrofluids or magnetic beads) (Chen et al., 2013) and optofluidic cell sorting (Kovac and Voldman, 2007) have also been demonstrated.

An advantage that droplet microfluidics has over continuous microfluidics is faster mixing due to reduced volumes, chaotic advection and faster heat transfer (Song et al., 2003). Mixing within plugs (droplet diameter larger than channel width) is improved due to ‘double recirculation flow’ caused by shear forces either from the continuous phase or channel wall contact. This phenomena of ‘double recirculating flow’ has been observed optically (Song et al., 2003) and quantified (Wang et al., 2007a). ‘Double recirculating flow’ limits the mixture of droplet contents across the centre-line and this limitation has been overcome by addition of channel windings. The windings result in uneven shear forces on the droplets causing them to ‘stretch and fold’ as can be seen in Fig. 21 (d). The uneven recirculating patterns cross the centre of the droplets and decrease diffusion time, thereby enhancing mixing (Song et al., 2003, Hsieh et al., 2009). Other groups have also introduced additional bumps to winding channels (Hsieh et al., 2009, Liau et al., 2005), and lasers (Cordero et al., 2009) to improve mixing. Therefore there are multiple operations that can be performed with droplets as elaborated above, making them extremely useful for different biochemical analysis needs.

2.7. Detection techniques for droplet microfluidics

Analytical detection of droplets and their contents is an integral part of droplet microfluidic platforms. A few main detection techniques have been described as follows:

2.7.1. Bright field microscopy

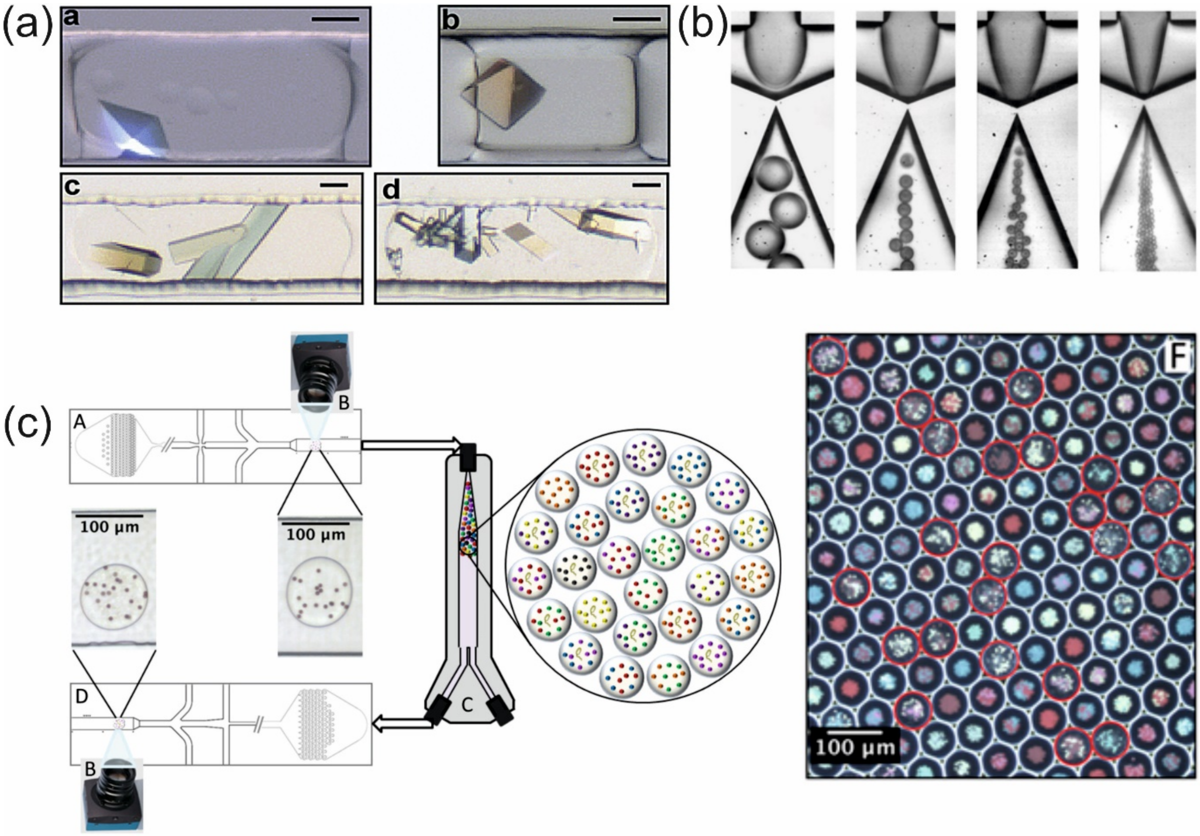

Figure 22. *Examples of bright field microscopy applications in droplets. (a) Studying protein crystallization (Zheng et al., 2003). (b) Studying droplet generation process in flow focus geometry (Yobas et al., 2006). (c) Studying droplets containing colour coded polystyrene beads with biological specimens for antibiotic susceptibility (Svensson et al., 2019).*

Parameters like the shape, size, and pathway of droplets can be identified using bright-field microscopy. In order to study the dynamics of droplet generation (Fig. 22 (b)) and manipulation, bright field microscopy together with high-speed cameras can be utilized to take images of the droplets and analyse their states. Fast mixing and reaction kinetics inside droplets can also be monitored by adding dyes or tracers. (Zhu and Fang, 2013). Zheng *et al.* have utilised a bright filed microscope with polarised light for screening protein crystallization conditions (Zheng et al., 2003) in droplets and some images obtained can be seen in Fig. 22 (a). Another application of bright field microscopy was to study droplets containing colour coded polystyrene beads with biological specimens (Fig. 22 (c)) for antibiotic susceptibility (Svensson et al., 2019). 8 different coloured beads were used per droplet to generate 20 different droplet populations having different environmental conditions which were then incubated and decoded via image analysis and machine learning.

2.7.2. Fluorescence detection

Another common and powerful technique used is fluorescence, for extracting analytical information from droplets containing fluorescence labelling or endogenous fluorescent molecules. Florescence imaging techniques can result in high sensitivity by utilising high resolution, high speed cameras and suitable filters and can be applied for high throughput screening (Brouzes et al., 2009b), single cell analysis, and time lapsed droplet monitoring for polymerase chain reaction (Casadevall i Solvas et al., 2011) or studying reaction kinetics (Song and Ismagilov, 2003). In an earlier study, Song *et al.* have measured the kinetics of ribonuclease A (RNase A) with millisecond resolution and in sub-microlitre droplets. Enzyme activity was measured at different time points using fluorescent images (Song and Ismagilov, 2003) as can be seen in Fig. 23 (a). Fluorescence measurements in droplets have been carried out by Marcoux *et al.* who employed a microfluidic platform to monitor enzyme activities of single cells (Marcoux et al., 2011). They encapsulated cells in picolitre droplets and a fluorogenic reporter MUG (4-Methylumbelliferyl β-D-glucuronide) was used to analyse the enzyme activity with the help of time-lapse images. Another interesting application of fluorescence detection was by Liu *et al.* in their microfluidic platform for automated DNA melting curve analysis (Liu et al., 2017) for the identification of single-nucleotide polymorphisms. Droplets containing DNA and a fluorescent dye were propagated through a channel subjected to a temperature gradient (Fig. 23 (b)) which caused the DNA to denature and release dye. Then spatially distanced fluorescence intensities were recorded and analysed. Apart from fluorescence imaging which relies on ‘field-of-view detection’, laser-induced fluorescence is also used for ultra-high throughput and sensitivity and is a popular choice for cell screening and sorting (Colin et al., 2015, Liu and Zhu, 2020).

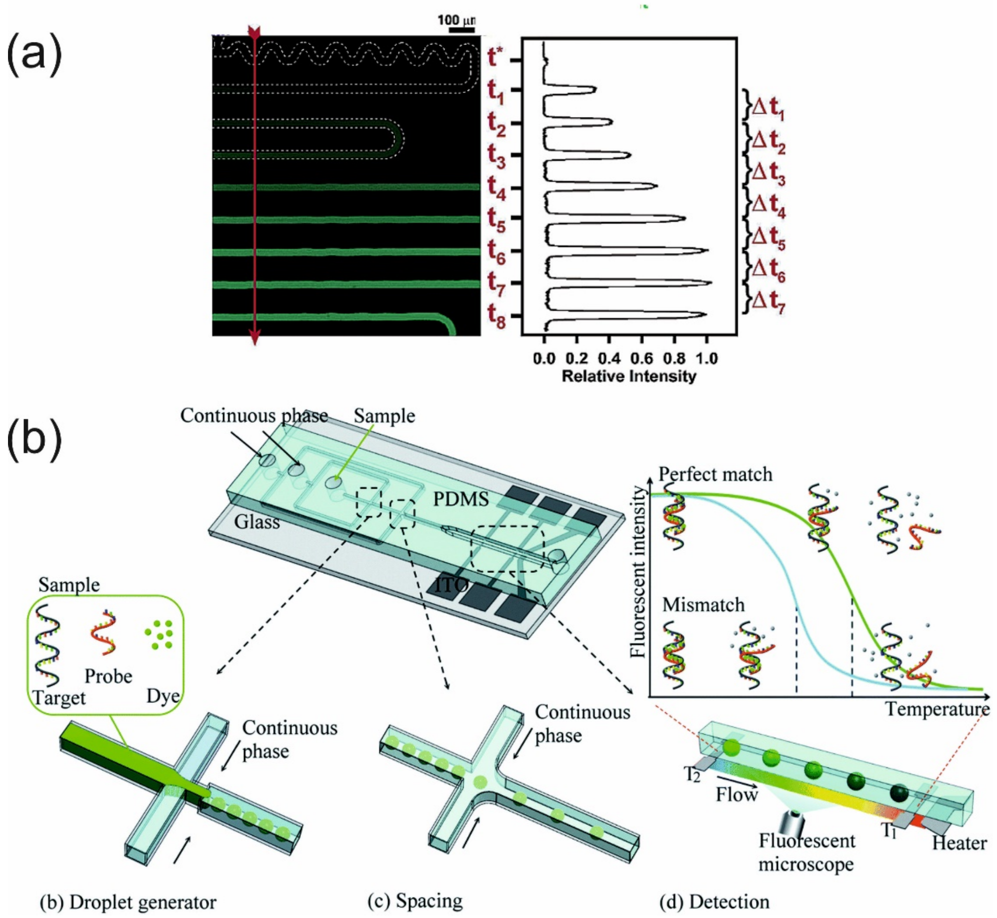

Figure 23. *Fluorescence detection in droplets. (a) Study of ribonuclease A (RNase A) enzyme kinetics (Song and Ismagilov, 2003) (b) Droplet based genotyping platform containing droplet generation, spacing and detection region. As the droplets pass through the temperature gradient in the detection region, the DNA strand disintegrates and fluorescent dye is released. Fluorescent intensities are measured spatially along a temperature gradient and DNA melting curves are obtained (Liu et al., 2017).*

2.7.3. Raman spectroscopy

Raman spectroscopy is a label-free, highly sensitive detection technique based on the Raman Effect. Raman spectroscopy provides structural information about molecules of interest by generating a characteristic vibrational spectrum or fingerprint of Raman shift and can be quantified based on the corresponding peak intensity. Probing droplet contents using Raman microspectroscopy was first demonstrated by Cristobal and co-workers (Cristobal et al., 2006) who used it to extract concentration profiles of chemicals. As the Raman effect is based on the inelastic scattering of photons, the signal received is very weak and suffers from poor signal-to-noise ratio thus limiting the detection for lower analyte concentrations. However, these limitations have been overcome by the recent developments in surface-enhanced Raman spectroscopy (SERS) (Jahn et al., 2017, Anna et al., 2017). SERS amplifies the Raman signal by bringing analytes in close proximity to metallic nanostructures. An interesting application of SERS in a droplet platform has been shown by Walter *et al.* where they created a database of 11200 spectra (1 spectra per second) and nine identified Escherichia coli bacterial strains with about 92.6% accuracy (Walter et al., 2011). Some other applications of droplet microfluidics based systems employing SERS include quantifying trace amounts of paraquat in water (Gao et al., 2010), measuring mercury (ll) ions (using gold nanoparticles and Rhodamine B tracer) (Wang et al., 2009a) and identifying prostrate specific antigen (PSA) cancer markers using a wash free magnetic immunoassay (Gao et al., 2016).

2.7.4. Mass Spectrometry

Mass-to-charge ratio of analytes can be found out using mass spectrometry (MS), where chemical species are bombarded with electrons causing them to break and the ions are separated by acceleration and deflection. Mass spectrometry can also provide information about the structure of analyte through the analysis of molecular fragments. It is a label-free detection technique providing high sensitivity together with the scope of parallel detection of several analytes. Electrospray ionization (ESI) and matrix-assisted laser desorption ionization (MALDI) mass spectrometry provide great sensitivity when incorporated with microfluidic devices (Zhu and Fang, 2013, Basova and Foret, 2015, Wang et al., 2015b). MALDI-MS was first demonstrated by Hatakeyama *et al*.. Nanoliter reagent droplets separated by fluorinated oil were fused with substrates and transported to a receiving tube. The tube was then sealed and the droplets were incubated and ultimately deposited on the MALDI plate, evaporated, MALDI matrix deposited and finally analysed by MS. A group of 44 chemicals were screened with minimal substrate consumption (20 µg) (Hatakeyama et al., 2006). Continuous phase oil can have adverse effects on the desorption/ionisation process and interfere with the analysis which was not addressed by Hatakeyama *et al*. Pereira and co-workers have addressed this issue and removed the oil phase in their system before spotting onto the MALDI target (Pereira et al., 2013). They developed a Liquid chromatography- MALDI-MS droplet interface and applied it for studying complex proteomic mixtures. However, MALDI-MS is an offline technique and procedures like droplet deposition on MALDI plates are labour intensive and time consuming thus limiting analytical throughput. Online analytical techniques like ESI-MS can overcome these issues. Kennedy group (Pei et al., 2009) have applied a simple method of analysing nanoliter plugs by ESI via coupling a droplet cartridge to a fused silica nano spray emitter tip. The cartridge consisted of droplets (as small as 13 nL) segmented by air or oil in a Teflon tube. Droplet samples were analysed with little carryover (<1%), high speeds (sample analysis rates of 0.8 Hz) and low detection limits (1 nM) were also achieved (Pei et al., 2009). They further matured the system for analysing samples down to 65 pL with throughput of 10 samples/s and applied the system for monitoring enzyme activity (Steyer and Kennedy, 2019).

2.7.5. Electrochemical detection

Dimension, frequency, velocity, conductivity and composition are some parameters that are hard to determine in droplet microfluidics but can be measured using electrical detection. In comparison to microscopes or high-speed cameras, electrical detection techniques are much easier to incorporate with microfluidics platforms due to their scalability and lower footprint (Basova and Foret, 2015, Zhu and Fang, 2013).

One of the first reported works of electrochemical detection (Luo et al., 2006) is of Lou *et al.* who applied low AC voltage to Au microelectrodes to determine the size and ionic concentration of droplets (pL to nL). Han *et al.* developed an amperometric method to monitor millisecond enzyme kinetics in droplets by inserting Pt and Ag/AgCl microelectrodes inside microchannels (Han et al., 2009). Thin film electrodes have been employed by Moiseeva *et al.* to measure electrical impedance when conductive droplets cross the electrodes (Moiseeva et al., 2011). Elbuken *et al.* demonstrated capacitive detection via the application of multiple coplanar electrodes to detect droplets and calculate the velocity and size. When a droplet passes the sensing region, there is a change in capacitance depending on the dielectric property of continuous and dispersed phase (Elbuken et al., 2011).

2.7.6. Colorimetry (Absorption) detection

Absorption detection is a popular method and various groups have integrated it in their microfluidic system for droplet detection (Liu and Zhu, 2020). As a target analyte reacts with a reagent, a coloured product is formed which can be quantified using absorption spectroscopy. An incident light passes though the coloured product and is partially absorbed. The analyte concentration is then quantified using the Beer Lambert Law (Swinehart, 1962),

$$A = \log_{10}\left(\frac{I_0}{I}\right) = \varepsilon c l \tag{11}$$

where, I_0 corresponds to the incident light and I corresponds to the light transmitted through the sample. Absorbance is the product of ε (molar absorption coefficient), c (concentration) and l (optical path length). It can be seen from the equation that absorption of light for a given analyte concentration is directly proportional to the path length and increasing the optical path length therefore increases the sensitivity allowing for lower concentrations to be measured.

Trivedi *et al.* have used fibre optic detection modules consisting of light emitting diodes (LEDs) and detectors for optical examination of droplets. LEDs are low cost, economical, compact, and robust and provide a variety of wavelengths (Trivedi et al., 2010). An optical flow cell with two adjacent LED-photodetector light paths has been developed by Hassan *et al.* to measure droplet size and velocity (Hassan et al., 2017). They have also demonstrated a multi-detector flow cell for monitoring reaction kinetics in continuous droplets (Hassan et al., 2016) as shown in Fig. 24 (a). The multiple detection points provided continuous measurement at different time scales which could be used to study Michaelis-Menten kinetics.

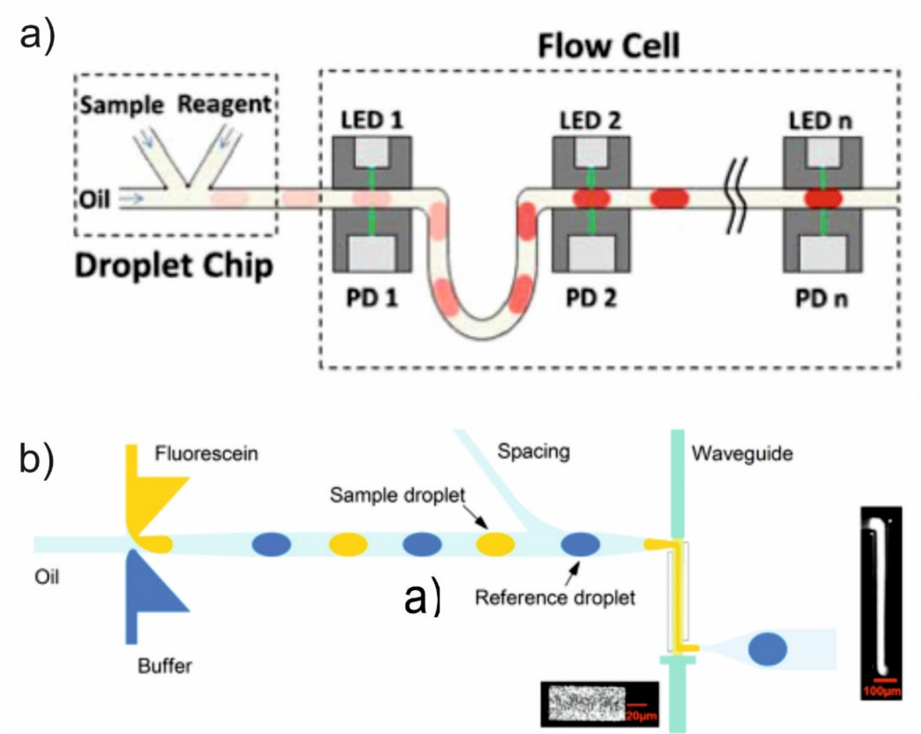

Figure 24. *(a) Schematic diagram of multi-detector flowcell designed by Hassan et al. to monitor reaction kinetics in droplets. (b) An optofluidic platform illustrating a Z-shaped flow path for increasing the detection sensitivity of droplets (Liu and Zhu, 2020, Hassan et al., 2016, Yang et al., 2017).*

Detecting pL-nL volumes in micro channels can be challenging due to smaller pathlength of micro channels. Yang *et al.* have developed an optofluidic platform with PDMS waveguides (Fig. 24 (b)) to cater to this issue (Yang et al., 2017). Having a Z shaped optical path significantly increased the patlength at the analysis point and allowed detection of fluorescein up to 400 nM. Nightingale *et al.* have also designed a fluropolymer chip (Dyneon THV) with “an array of concatenated Z-shaped flow cells” with the longest pathlength being 10 mm for highly sensitive measurement of droplets (Nightingale et al., 2020). Other than that, multi-pass techniques which exploit reflection of the excitation light multiple times through the sample has also been reported over the years (Rushworth et al., 2012) and very low limit of detections have been achieved.

2.7.7. Electrophoresis

Capillary and chip-based electrophoresis are widely used separation techniques in areas like gene sequencing (Durney et al., 2015), drug discovery (Ouimet et al., 2017), enzyme analysis, etc. for high-throughput and repeated analysis (Dolnik and Liu, 2005). When samples contain multiple electro-active or fluorescent components, a separation step is required before analysis by the detection methods mentioned in the previous sections. Capillary electrophoresis (CE) separation depends on the ‘differential migration’ of molecules/analytes in an electric field based on their size and charge (Ouimet et al., 2017). Edgar and co-workers have demonstrated capillary electrophoresis together with laser fluorescence microscopy and separated three fluorescein labelled amino acids (Edgar et al., 2006). Niu *et al.* demonstrated a novel technique for separating picolitre (pL) to nanolitre (nL) aqueous droplets into a separation chamber by removing the carrier oil phase (Niu et al., 2013) and further demonstrated parallel separations via a slip-chip platform (Hassan et al., 2015).

2.8. Biological and chemical analysis using droplet microfluidics

Droplet microfluidics provide a high throughput platform for various assays and has applications in chemistry, biotechnology, biomedicine and nanotechnology. As previously mentioned in this thesis, in comparison to conventional techniques, droplet microfluidics significantly reduces cost of reagents by utilising small volumes and generation of waste is also minimal (Mashaghi et al., 2016) due to the small scale. Therefore, a few applications of droplet microfluidics have been discussed in the following sections.

2.8.1. Cell manipulations

Though bioassays can be scaled down to picolitre volumes in microwells, they are subjected to liquid evaporation and capillary effects. Droplets remove the risk of liquid evaporation and dispersion of reagents providing a contained environment for single cell reactions (Basova and Foret, 2015, Köster et al., 2008) and allow high throughput cell screening (Brouzes et al., 2009a). Balance of proper nutrients and providing gaseous exchange via fluorinated oils can lead to cell culture in droplets (Mashaghi et al., 2016, Wang et al., 2014).

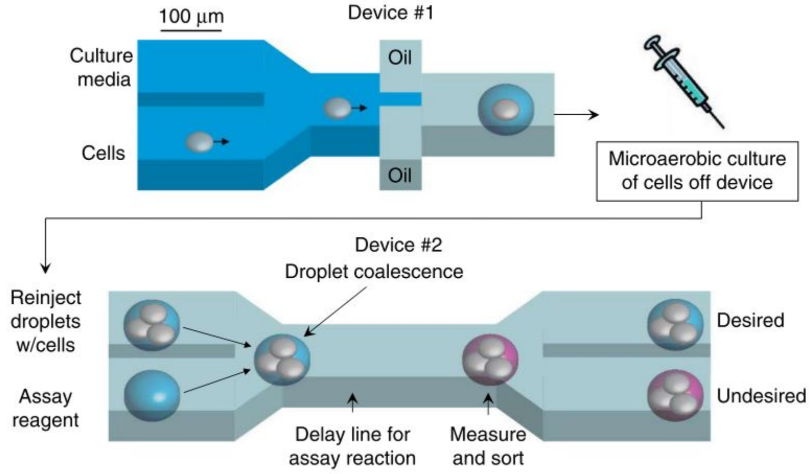

Figure 25. This diagram demonstrates cell culture and detection of extracellular metabolites using droplets (Wang et al., 2014).

Figure 25 demonstrates a microfluidics platform designed by Wang and co-workers for culturing cells and detecting extracellular metabolites (Wang et al., 2014). Device 1 was used to generate droplets containing cells and culture media. The droplets were collected and stored in a capped syringe, which acts as an incubator for cell culturing. The droplets were then reinjected into device 2 where they merged with reporter droplets containing fluorescent reagents. After a delay time, the fluorescence was measured and the desired metabolite was identified (Wang et al., 2014). When encapsulated cells secrete molecules which remain inside the droplets they can be rapidly detected. Also, intracellular biomolecules can be examined by lysis of the compartmentalized cells and this opens possibility for amplification of DNA or RNA.

2.8.2. Drug discovery and delivery

Understanding the dynamics between different drugs and target analytes is vital and droplet microfluidic techniques provide several advantages. Parallelization in case of microfluidics platforms offer significant benefits over conventional screening methods where the number of clones tested during one experiment is usually small. In context to drug delivery, encapsulation of the agent is carried out using microparticles or capsules and released in a controlled manner in the target area for high therapeutic efficacy. Droplets are highly reproducible with good encapsulation efficiency leading to reliable release of drug (Shang et al., 2017). Double or multiple emulsion droplets with tunable sizes and layers are of great scientific interest in the area of drug studies (Rajian et al., 2011).

Screening small compound libraries can lead to the discovery of new drugs but requires screening of about as much as a million variants, increasing time required and making the procedure very expensive. Droplet microfluidic assays address these needs by facilitating high-throughput screening (up to 10^8 samples per day), increasing sensitivity by compartmentalization and decreasing overall expense of procedures (Guo et al., 2012).

2.8.3. Analysis of biomolecules

The unique properties of droplet microfluidics and the efficiency, flexibility of the platform has led to the analysis of ions and small molecules together with bio macromolecules such as proteins and nucleic acid (Zhang and Jiang, 2016, Shang et al., 2017).

2.8.3.1. DNA analysis

In DNA analysis the Polymerase Chain Reaction (PCR) is a technique extensively used in areas ranging from evolution biology, criminology to clinical diagnostics, to amplify DNA and make millions of copies in a matter of hours. PCR is a three-step process consisting of denaturisation, annealing and extension to make copies of the target DNA. PCR in droplets provide many advantages over conventional techniques such as lower consumption of expensive reagents, less prone to contamination and decrease in time to reach optimum temperature for denaturisation and annealing steps due to large surface-to-volume ratios of the droplets. Moreover, droplets provide automation and parallelization and therefore, the opportunity to have multiplexed assays. Nucleic acids are crucial biomarkers for many diseases e.g. rare tumoral DNA and droplet-based PCR is highly sensitive and can accurately detect mutations (Zhang and Jiang, 2016, Shang et al., 2017). For example, Zeng and co-workers have demonstrated a multiplexed single cell PCR method using a microfluidic emulsion generator array (MEGA) device to distinguish and quantify wild type and pathogenic cells (using *Escherichia coli* bacterial cells as an example) utilizing functionalized microbeads (Zeng et al., 2010).

2.8.3.2. Assays

Droplet microfluidics provides the capability to measure multiple analytes in a small sample volume that could be significant in research of microfluidic cultures, organ-on-chips, and experiments involving small animals, etc. An automated microfluidic platform (Cedillo-Alcantar et al., 2019) was developed for “3-plex analysis” of glucose, lactate dehydrogenase (LDH) and bile acids from the culture media of hepatocyte spheroids which were exposed to a lipotoxic agent. Trains of droplets were generated using a series of valves to measure the cell metabolites from the cell medium using absorbance and fluorescence detection and the condition of the hepatocyte spheroids were monitored (Fig. 26). This application highlights the usefulness of droplet microfluidics coupled with optical detection techniques for measuring multiple analytes from small sample volumes.

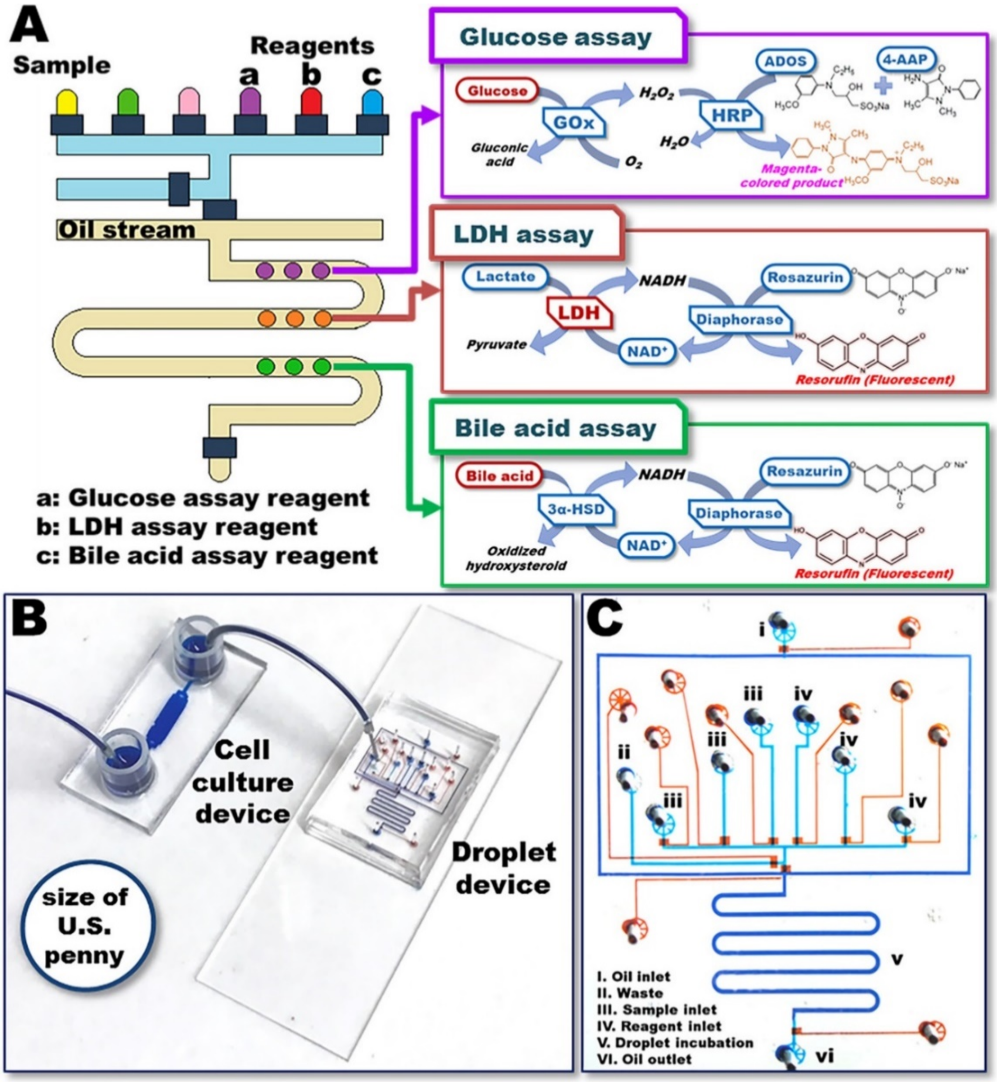

Figure 26. *(a) Schematic of droplet platform for multiplexed measurement of glucose, lactate dehydrogenase and bile acids for hepatocyte spheroids. (b) Actual photograph of cell culture and droplet generation microfluidic*

devices. (c) Photograph of droplet generation device with red and blue ink filling the flow and control layer respectively (Cedillo-Alcantar et al., 2019).

Though many assays have been implemented using droplet microfluidics (Nan et al., 2011, Kiss et al., 2008) it has been difficult to perform heterogeneous assays requiring several steps. Compartmentalizing reagents and taking single measurements are straightforward but removing constituents from one buffer to another requires more complex strategies. Multiple-step immunoassays are currently under development and has been demonstrated by a few groups which will be further discussed in the following section.

2.8.4. Immunoassays using droplet microfluidics

A widely used technique for measuring analytes in biological analysis is the immunoassay, which is based on the interactions between antigen and antibody. Depending on whether separation is necessary or not, the assay can be divided into heterogeneous or homogeneous. Analytes can be measured using either a competitive or a non-competitive mode depending on the chemistry. Competitive approach can be further divided into capture of antigen or capture of antibody based on what the solid phase is covered with. Labelled antigens and unlabelled antigens (sample) compete with each other to bind with the limited sites of the capture antibody in competitive antigen-capture approach. After the incubation, the immune complex is separated via chemical or physical procedures from the unbound reagents. The activity of the label can be in the form of fluorescence, radiation, etc. and quantification is done based on the activity. In case of competitive antigen-capture, the signal that is generated is inversely proportional to the concentration of sample antigen. Based on the signal received, a standard curve is generated using known concentrations of the analyte and is used to determine the concentration of the unknown samples (Darwish, 2006, Teste et al., 2013, Ng et al., 2012). Larger analytes which have multiple epitopes are used for the non-competitive approach. Two antibodies are needed to attach to "non-overlapping epitopes". There is one antibody out of the two which is bound to the solid phase and the other antibody has a label which is required for detection (Darwish, 2006).

Immunoassays have shown immense popularity since its invention in 1960's and considered the "gold standard" for immunodiagnostics (Lequin, 2005). There have been many automated analyser units for immunoassays since the 1980's, but they pose several disadvantages. The drawbacks include use of a large quantity of sample which is not ideal for disease diagnostics as samples are limited and reagents expensive, and analysis time can go up to several hours (Ng et al., 2012). These drawbacks can be mitigated by the application of microfluidics to miniaturise the immunoassays. Also, the liquid handling systems in the analysers are bulky, usually due to their expensive robotic instrument setup. Microfluidics can cater to this problem by making the fluid handling system more compact.

Multiple-step assays, as the name implies consist of several steps for removing or extracting reagents and washing, which are usually hard to achieve in droplets. One of the pioneering groups in miniaturizing assays and developing components to facilitate multiple steps is that of Jean-Louis Viovy's. Viovy *et al.* have developed several platforms combining droplet microfluidics, magnetic beads and magnetic tweezers. The use of magnetic beads ranging from nm to µm is quite common in microfluidic platforms as has been outlined (Pamme, 2006). The particles which are most widely used are superparamagnetic because they do not retain "magnetic memory" (Pamme, 2006) in comparison to ferromagnetic particles which are permanently magnetized and resuspension during washing steps of the assay is not possible (Ali-Cherif et al., 2012). Superparamagnetic particles can be found surface coated with a functional group such as amino or carboxyl groups which leads to easy attachment of biologically active substances such as antibodies or strands of DNA (Pamme, 2006).

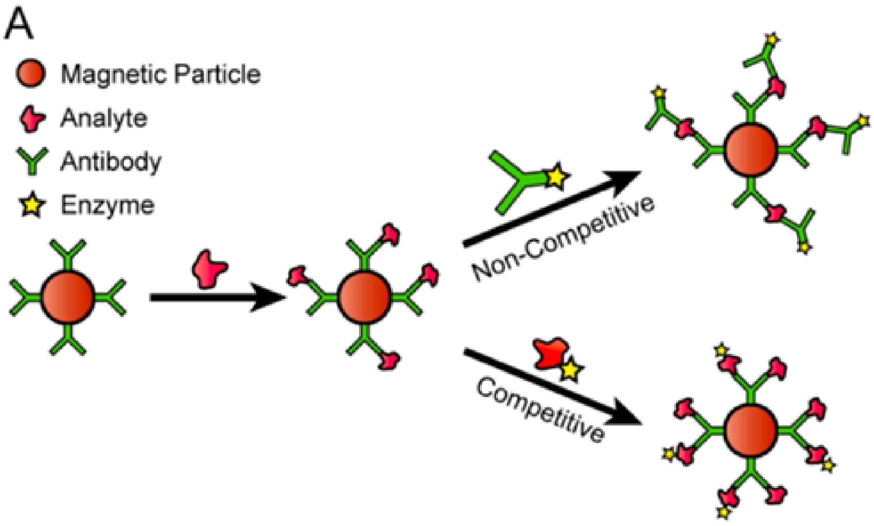

Figure 27. *Competitive and non-competitive immunoassay schematic utilizing magnetic beads (Ng et al., 2012).*

Superparamagnetic particles are gaining popularity as a solid-state support because they can easily bind with the analyte that needs quantification (Fig. 27), can be captured using a magnet from the fluid medium and then re-suspended into the washing buffer. However, conventional techniques pose difficulties such as poor mixing, washing and usage of larger volumes. Through the development of "programmable magnetic tweezers" Viovy *et al.* have tried solving the aforementioned problems. The tweezers execute multiple trapping and release sequences with less than 2% carryover of supernatant fluid between less than 80 nL volume droplets. Figure 28 demonstrates the bead trapping and release sequences, with the triangles representing the tweezers. As a droplet containing beads approach the tweezer tips, the tweezers are activated, and the beads tend to form a cluster. As the droplet passes through, the bead cluster (1 nL) pinches off from the droplet and is held stationary till the arrival of the next droplet. Two instances can occur after this; the beads can be held stationary so that the new washing droplet rinses the beads removing more supernatant fluid or else, the beads can be re-suspended to allow further circulation and incubation time (Ali-Cherif et al., 2012).

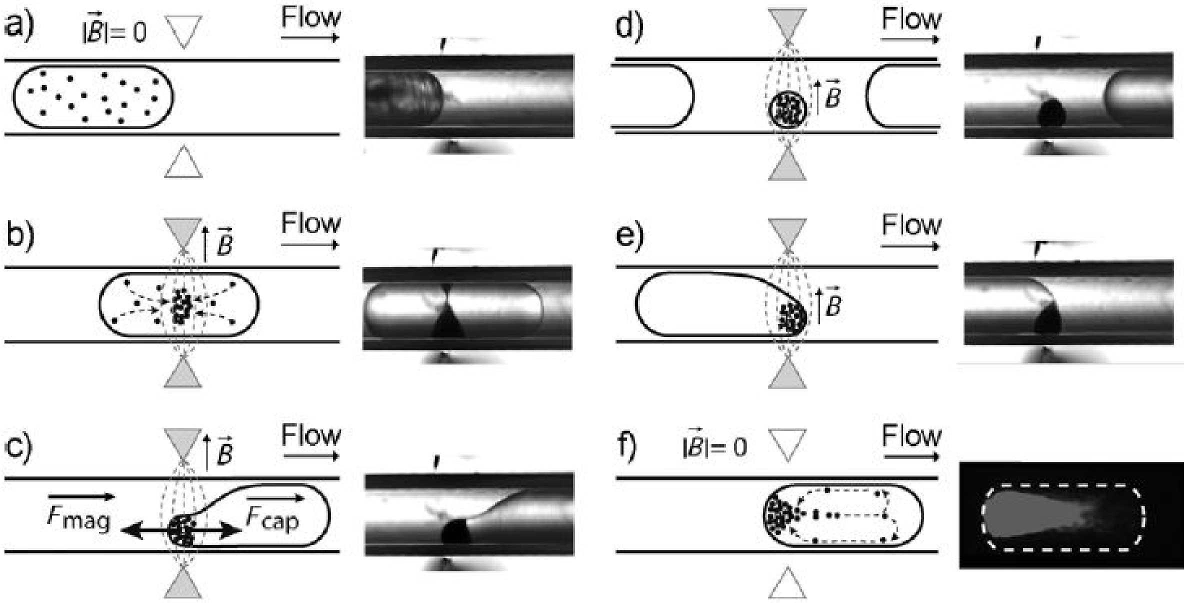

Figure 28. *Trapping and release sequence of magnetic beads using programmable tweezers inside a capillary. (a) Suspended magnetic particles in the droplet, (b) particle capture, (c) deformation of droplet, (d) retention of beads, (e) new droplet coalescing with the beads and (f) re-distribution of magnetic particles (Ali-Cherif et al., 2012)*

Ali-Cherif *et al*. have developed a liquid handling system consisting of a pipetting robot which generates droplets by repeated aspirations from a 96 well plate. In order to test their liquid handling and tweezer system, they implemented a 9 step sandwich immunoassay (Ali-Cherif et al., 2012) for the identification of neonatal congenital hyperthyroidism (CH); a condition which can cause child-development problems if not treated early. Mai *et al.* have developed an immunoassay for measuring amyloid-β peptide-based biomarkers (Aβ 1-42 and Aβ 1-40) for the diagnosis of Alzheimer's disease. Similar fluid handling and microfluidic system was incorporated as described earlier. Four magnetic tweezers were used in order to prevent the back-and-forth motion of the droplets to the tweezers, together with 4 CMOS cameras for observing droplets and a LED-detector pair were used for florescence detection (Fig. 29). Mixing plates were also inserted for better mixing of beads, in between each camera and tweezer unit. The ELISA assay was incorporated in the microfluidics system by using a sequence of five droplets as can be seen on the top-right hand side of Fig. 29.

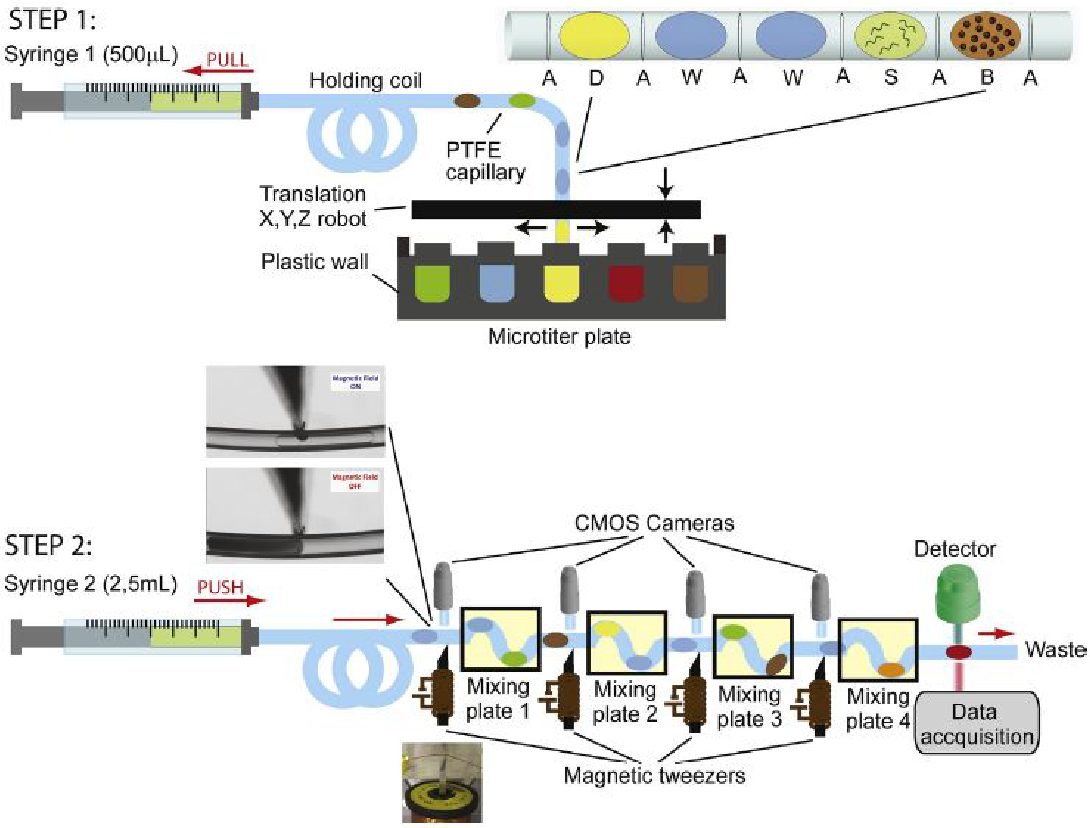

Figure 29. Immunoassay for measuring amyloid-β peptide-based biomarkers for the diagnosis of Alzheimer's disease. Step 1 shows the uptake of droplets using a robotic liquid handling system and Step 2 shows the delivery of the droplets through tweezers, CMOS cameras and mixing plates. On the top right corner, the droplet sequence is as follows, D indicates detection droplet, W is washing droplet, S is sample, B is droplet containing magnetic beads and A refers to air bubble (Mai et al., 2018).

The first droplet contained beads (B) coated with antibody, the second droplet had sample/standard (S) followed by two washing droplets (W) and finally the reporter (D) droplet (QuantaRed) (Mai et al., 2018). Similar pipetting systems and tweezers (Teste et al., 2013, Ferraro et al., 2016) have also been demonstrated but their droplet generation technique is complex, and the instrumentation is not compact thus restricting their usage only in laboratories. Hence, our approach is to utilise the advantages demonstrated by droplet microfluidics technology incorporated with magnetic beads and tweezers and make a portable, compact system which will prove to be a significant development in immunodiagnostics.

2.9. Environmental sensing using droplet microfluidics

Not only in the field of medical diagnostics, droplet microfluidics can also be utilized for *in situ* environmental monitoring with high temporal and spatial resolution. Transitioning from continuous flow microfluidic analyzers to droplet-based ones could provide a plethora of advantages. Removal of Taylor dispersion, reduction of sample and reagent size to nanoliter scale, reduction in reaction time, and prevention of cross-contamination between samples are a few that have been discussed throughout the thesis (Song et al., 2006).

Niu group have successfully deployed a droplet microfluidic sensor for monitoring nitrate and nitrite simultaneously and were able to generate data for a three week period in tidal river with a 6% error relative to spot samples (Nightingale et al., 2019a). During the trial phase of the sensor, crosstalk was discovered between the standard and sample which was due to nitrite being converted to an intermediate gaseous nitric oxide which was then migrating between droplets. It was found that the crosstalk between droplets could be predicted and was quantifiable post-hoc (Nightingale et al., 2018). Capabilities of this sensor technology (Nightingale et al., 2019a) has been expanded in this thesis (Chapter 4) and we have developed a first of its kind ammonium droplet sensor for monitoring river water and wastewater facilities.

2.10. Conclusion

Continuous monitoring with POC diagnostics and *in situ* environmental analysers provides us with invaluable real-time data which can assist us in understanding physiological and biogeochemical processes better. Several sensors used for continuous monitoring has been described and the advantages that droplet microfluidics provides in the avenues of high frequency measurement and monitoring has been highlighted.

This chapter reviewed how droplet microfluidics provides us advantages such as elimination of Taylor dispersion, efficient mixing and reduced reaction times compared to continuous flow microfluidics.

Active and passive droplet formation and manipulation (splitting, merging, mixing, dilution, sorting) techniques have been discussed. Reaction in droplets and several detection techniques such as fluorescence detection, mass spectrometry, and absorbance detection have been reviewed. Several assays such as mix-and-read, multiplexed and multiple step assays (such as ELISA) in droplets have been highlighted. Therefore, a wide range of functions combined with sophisticated detection techniques can be implemented using microfluidic platforms for automating biochemical assays.

However, there is still scope for improvement in making droplet microfluidics-based sensors more robust, programmable and versatile. A lot of the systems still use complex and bulky fluid handling systems making multiple-step and multiplexed assays tedious. Therefore, precise, compact and low power fluid handling systems are the need of the hour. Droplet detection methods need to be more compact, sensitive and low power as well to cater to long term monitoring needs and be applicable for low concentration analytes. This thesis addresses several avenues of microfluidic sensors in need of improvement and provides solution for further advancement of this very valuable analytical technology.

CHAPTER 3

DROPLET MICROFLUIDICS FOR HEALTHCARE APPLICATIONS - continuous ELISA

This chapter reports the design, fabrication and calibration of a droplet based continuous monitoring platform that can perform Enzyme-linked immunosorbent assay (ELISA) repeatedly and continuously. As an example application, we have measured cortisol concentrations via a competitive assay. Such a platform could have wide-ranging implications in our physiology and tracking its variation can guide diagnosis and treatment of several health conditions.

3.1. Continuous monitoring of cortisol

Prolonged stress can be detrimental to both mental and physical health, it is a predisposing factor for a number of chronic diseases. Low level stress is a component of normal human physiology and forms the basis of the fight or flight response, but chronic stress can have damaging effects. Stress causes the release of cortisol from the adrenal cortex, which is a steroid hormone and an important biomarker for indication of stress levels (Lee et al., 2015). Hypothalamus pituitary-adrenal (HPA) axis is an integral part of the adaptive system of the body and its primary function is to balance physiological process after subject to stimuli. Cortisol is an end product of the HPA axis as can be seen in Fig. 30 (a) and is synthesized from cholesterol. Most cholesterol binds to cytosolic receptors, this leaves trace amounts of extracellular cortisol that can be detected in body fluids (Fig. 30 (b)) (Lee et al., 2015). Around 90% cortisol circulating in human serum or plasma is attached to cortisol binding globulin (CBG) and serum albumin, and 3-5% of serum cortisol exist in biologically active and unbound form (Gracie et al., 2017, Gatti et al., 2009). Usually for determining cortisol in plasma or serum, assays measure total cortisol which is made up by bound and free cortisol. Then Cortisol Free Index (CFI) which is the free cortisol bioactive form is calculated using Coolen's method (Kaushik et al., 2014, Dorin et al., 2009). In humans, total serum cortisol ranges up to 600 ng/mL with normal levels of 140.60 ± 9.62 ng/mL in males and 101.03 ± 8.61 ng/mL for females (Gracie et al., 2017). Increased cortisol levels have been linked to the development of Cushing's syndrome, whereas decreased level leads to illnesses like Addison's disease (Kaushik et al., 2014).

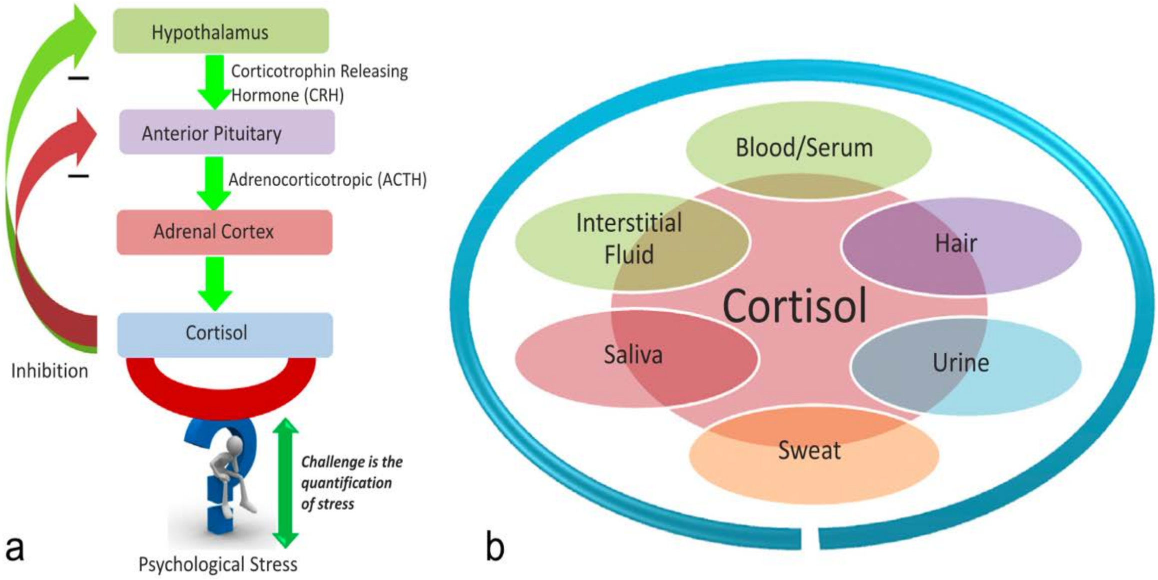

Figure 30. *(a) The HPA axis regulating the secretion of cortisol. (b) different biological fluids that can be used to measure cortisol (Kaushik et al., 2014).*

Secretion of cortisol follows a 24-hr circadian rhythm (Fig. 31) showing a peak about 30 minutes after a person wakes up and decreases gradually as night commences. In order to monitor the immediate fluctuations in cortisol above a baseline, analysis of cortisol containing body fluids must be rapid and accurate.

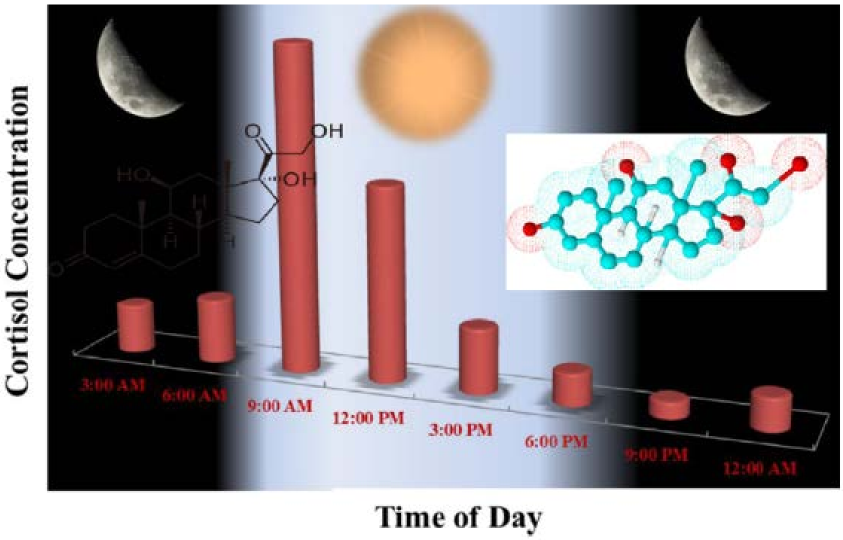

Figure 31. *Variation of cortisol levels with time of day. (Kaushik et al., 2014). There is a rise in cortisol levels soon after an individual wakes and then it slowly decreases throughout the day.*

Different assays and sensing technologies have been implemented for measuring cortisol (Kaushik et al., 2014, Gatti et al., 2009) but most of them are not designed to perform real-time analysis. The sample collection procedures are prone to manual error and the delay between collecting and analysing samples fail to provide an accurate picture of the instantaneous levels of cortisol. Many methods also require larger samples because of the trace amounts of cortisol available in the body (Gracie et al., 2017). Moreover, the conventional assay procedures like ELISA take hours to complete even by an experienced laboratory technician, and manual pipetting could lead to sample loss and contamination.

The aim of this study is to address the aforementioned issues by developing a system which can continuously monitor cortisol and provide faster and accurate result with high temporal resolution. A fully automated microfluidics platform for miniaturising ELISA for monitoring cortisol has been developed and calibrated. The lab-based assay has been developed by Dr. Susan Pang (LGC) and the microfluidic system has been developed in collaboration with Dr. Gareth Evans, Dr. Sharon Coleman, Brett Warren (SWS) and Dr. Sammer-Ul Hassan.

3.2. System overview

This fully automated system can be divided in to two parts; the fluidics and the electronics, which work coherently to miniaturize heterogeneous ELISA for monitoring cortisol. The fluidics section of the system consists of the liquid cartridge, peristaltic pump and a microfluidic chip for generating droplet trains. The electronics include automatic magnetic tweezers for magnetic bead manipulation and in-line spectrophotometer for detection of droplets, controlled by an Arduino prototyping Board.

3.2.1. System schematic and power flow diagram

Figure 32 below shows the fluidic diagram and system schematic of the miniaturising ELISA platform. The reagents and sample are pumped in through a peristaltic micropump to a 12-line PDMS microfluidic chip which produces a sequence of droplets (detailed later in section 3.4). The first droplet contains cortisol sample, cortisol-3-carboxymethyloxime horseradish peroxidase conjugate (cortisol-HRP) and antibody functionalized magnetic beads (MyOne Dynabeads). The next two droplets are phosphate buffered saline (PBS) wash droplets and finally 3,3',5,5'-tetramethylbenzidine (TMB) reporter droplet. The assay is then carried out with the aid of a pair of magnetic tweezers which extracts magnetic beads from the sample droplet and releases into the reporter droplet. The concentration of the analyte (cortisol) is then measured by colorimetric detection using an in house, in-line spectrophotometer.

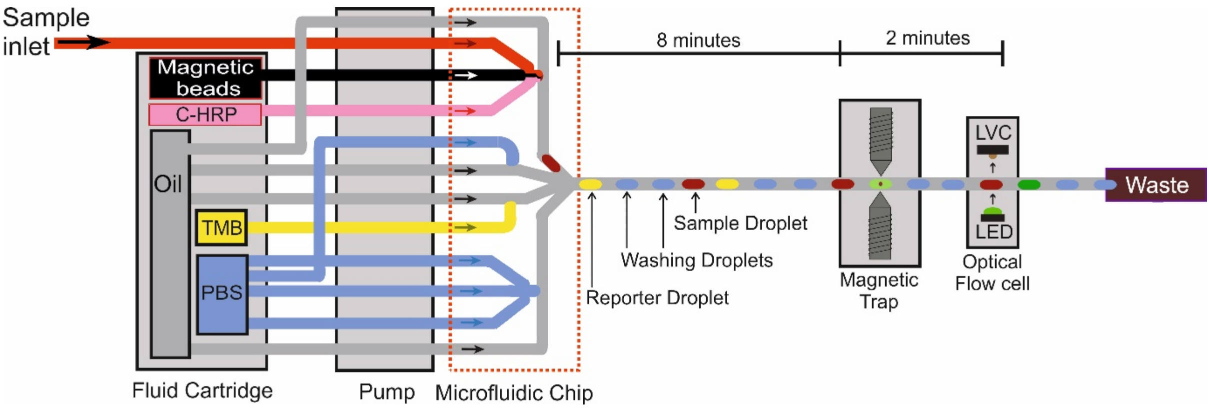

__Figure 32.__ Schematic diagram of microfluidics platform of miniaturized ELISA for continuous monitoring of cortisol (adapted from schematic by Dr. Gareth Evans).

Figure 33 illustrates the power flow to the different components of the system. An external power supply is used to power up the phased peristaltic pump. One USB connection is used to power the magnetic bead shifter (MBS) and the interfacing feather board. Another USB connection is utilized for powering an Arduino board and the detector flow cell.

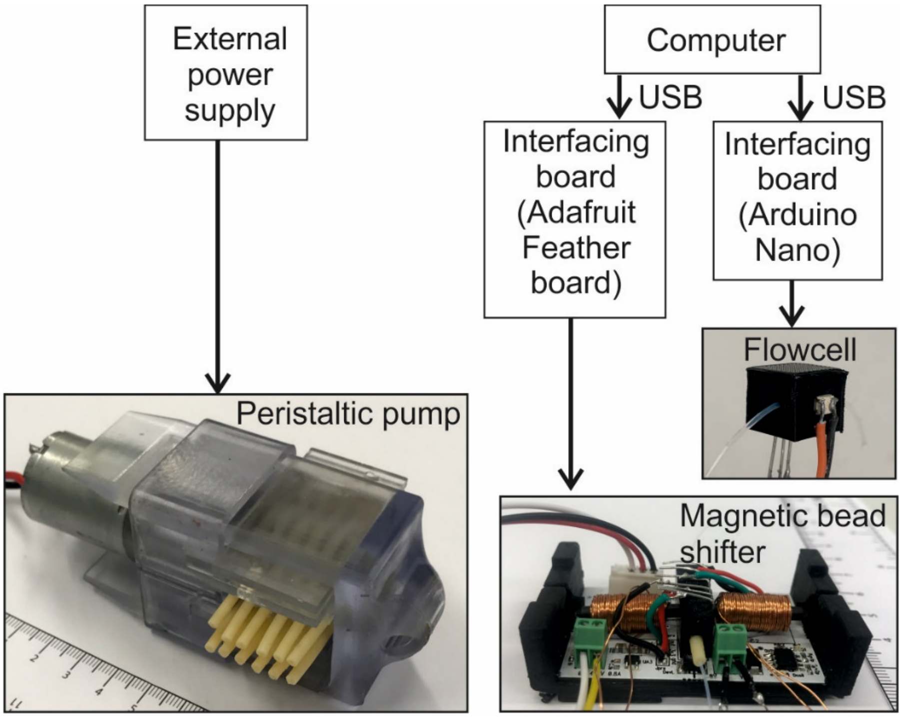

Figure 33. *Power flow diagram of the portable ELISA system.*

3.3. Fabrication, testing and optimization of electro-magnetic tweezers

One of the aims of this project is to miniaturize bead-based assays like ELISA using droplet based microfluidics. An integral part of platform technology is a small pair of electro-magnetic tweezers, which can extract the superparamagnetic beads in the assay and move them between droplets. The conceptualisation, fabrication and optimization of a magnetic tweezer unit for extraction of superparamagnetic beads has been highlighted in the following sections of this chapter. The designs show progression from a manually controlled unit to a completely autonomous one capable of completing magnetic beads manipulation and detection of the droplets. As shown in Fig. 32, the desired cortisol assay is implemented using a sequence of four aqueous droplets separated by fluorocarbon oil, with the first droplet containing sample and magnetic beads, then two wash buffer droplets and finally a reporter droplet (details can be found in the later sections of this chapter). The tweezers essentially extract magnetic beads from the first sample droplet, keep the beads positioned at the tip and let two washing buffer droplets pass through. Finally, the tweezers release the beads in the reporter droplet containing Tetramethylbenzidine (TMB) substrate for colorimetric detection.

Each electromagnetic tweezer is constructed by wrapping 200 windings of enamelled copper wire of 0.35 mm thickness around a ferrite rod. The ferrite rod has a diameter of 3 mm and a length of 25 mm and has been purchased from RS Components. The length of the coil is around 15-16 mm depending on the precision of manual winding. The tips of the ferrite core have been tapered in order to increase the magnetic field density and provide stronger force for the capture of magnetic beads. The extraction of magnetic particles require a delicate balance between interfacial, magnetic and hydrodynamic forces.

Pamme *et al.* have suggested that the force applied to a magnetic particle within a magnetic field is a function of the volume of particle (V), the variation between the magnetic susceptibilities (Δx) between the particle (x_p) and the medium (x_m) together with the gradient and strength of the magnetic field (B) and the permeability of free space (μ_0). Therefore, the formula of force on a magnetic particle in a magnetic field is as follows (Pamme, 2006):

$$F = \frac{V.\Delta x}{\mu_0}(B.\nabla)B \tag{12}$$

Dynabeads MyOne from Thermo Fisher (superparamagnetic beads) of 1μm diameter with carboxylic acid attached on their surface has been chosen for the experiments with tweezers. Later experiments have tosyl activated functional groups for binding anti-cortisol antibody. The beads have a hydrophilic surface, can be easily dispersed and used with various buffers. Their sedimentation rate is low, and the beads have high magnetic mobility making them appropriate for automated assays.

3.3.1. Variation of magnetic field density

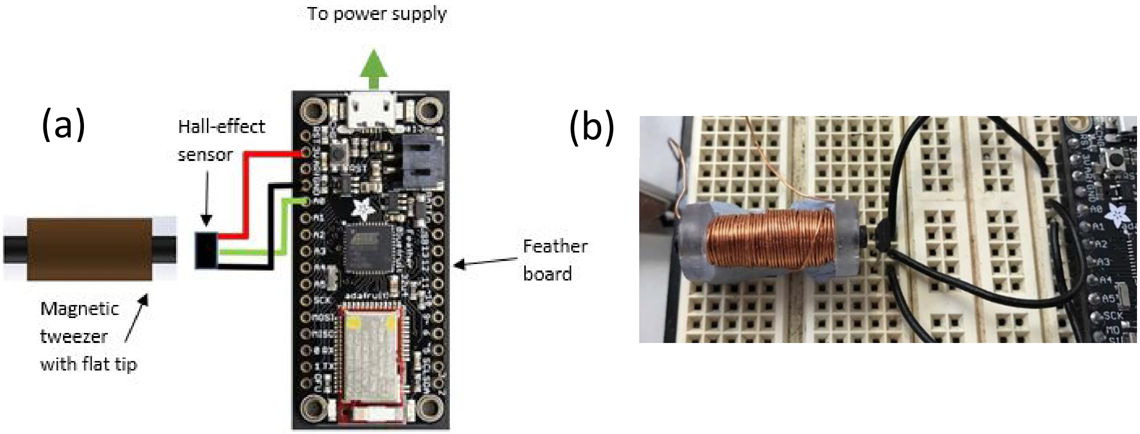

Figure 34. (a) Schematic of flat tip tweezer with a Hall Effect sensor connected to an Adafruit Feather 32u4 board to test magnetic field density. (b) Photograph of experimental setup.

Magnetic field density between the Hall Effect sensor and the flat electromagnetic tweezer tip was measured to quantify the reliability of the tweezers for bead extraction. Number of coil windings were varied from 50, 100 to 200 (coil wire thickness 0.35 mm) and the tweezers were excited with currents ranging from 0 to 1 A. The distance between the tweezer tip and sensor was also varied from 0.5 mm to about 5 mm. A low power 3.3 V Adafruit Feather 32u4 board and a bipolar Hall Effect sensor (DRV5053VAQLPG) with a sensitivity of -90mV/mT was used in order to measure the field density. The schematic of the experimental setup (a) and the photograph of the actual setup (b) can be seen in Fig. 34.

Figures 35 (a) - (c) illustrate the variation in magnetic field density with current for the tweezers with different windings. With increasing current, magnetic field density increased proportionally in similar projections for the three different coil windings. The closer the tweezer tip was, the higher the field density was indicating that there was less flux leakage. The tweezer with 50, 100 and 200 windings will be denoted by T_{50}, T_{100} and T_{200} respectively. T_{200} reached the saturation limit of the Hall Effect sensor which is 11.2 mT at lower current than the T_{100}. Similarly, T_{100} reached the saturation limit of the sensor at a lower current than T_{50}. In fact, for the range of current (0-1 A) that the tweezers were tested, T_{50} did not reach the limit at all. The highest field density obtained by T_{50} was about 10 mT for 1 A. Hence, T_{200} which showed faster increase in magnetic field density in comparison to others for a smaller range of current was chosen and 200 windings was decided as the most optimized number of windings for the given size restrictions and application.

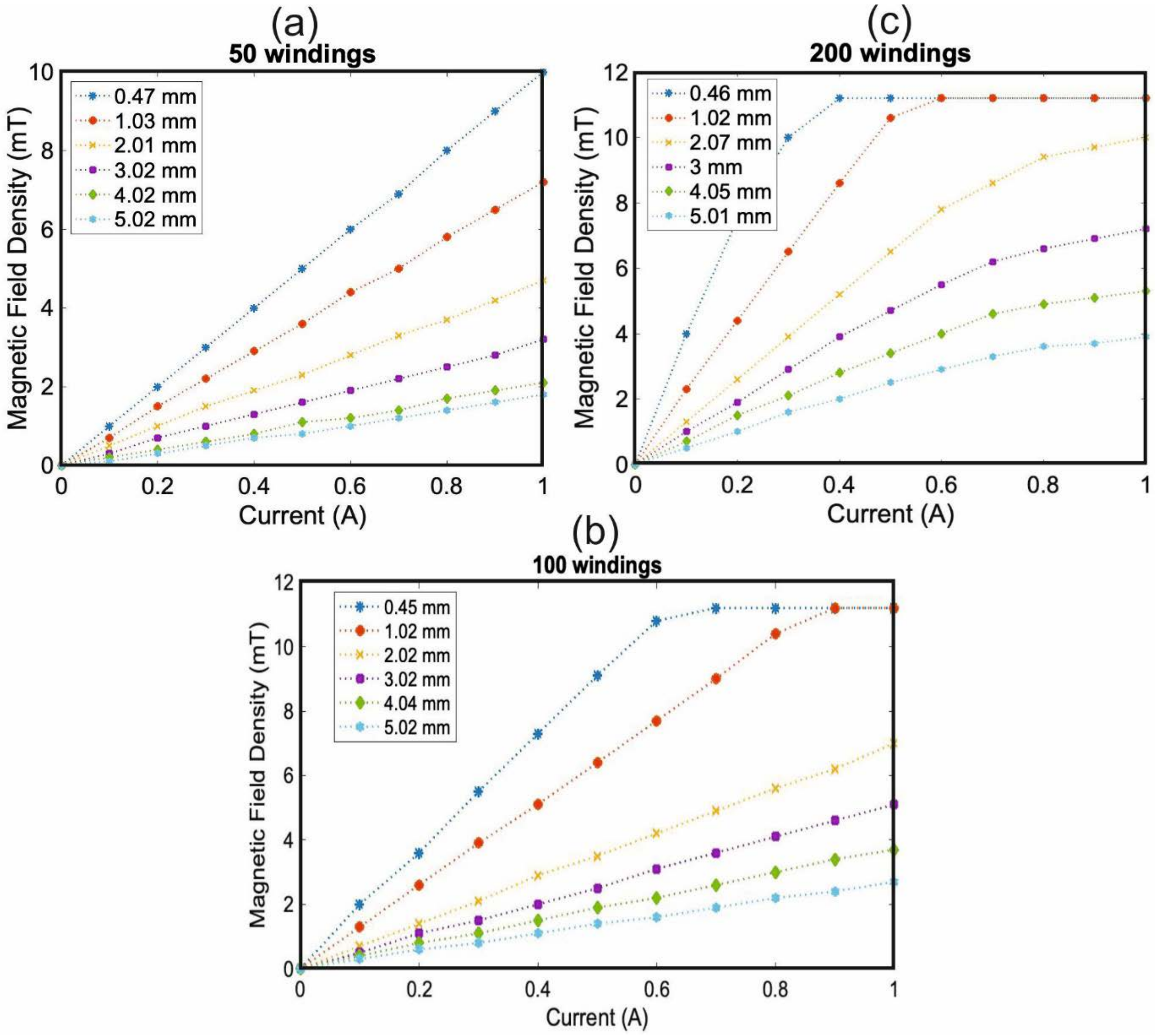

Figure 35. *Magnetic field density (mT) vs. current (A) for flat tip tweezer with (a) 50 windings, (b) 100 windings and (c) 200 windings.*

3.3.2. Magnetic bead extraction using tweezers with different tips

It is a challenge to produce a strong magnetic field from the tweezers and channel it appropriately in order to capture the beads effectively. Sharp, blunt and flat tips with the above-mentioned ferrite core (3 mm diameter and 25 mm length, RS Components) and 200 windings were tested in order to find out the most appropriate tip geometry. The sharp tips, blunt tips and flat tips had a tip diameter of 0.1 mm, 0.6 mm and 3 mm respectively. Figure 36 below shows the three pairs of tweezers with different shapes of tips positioned in 3D printed (white PLA, Ultimaker 2$^+$) holders. All of the tweezer pairs were aligned precisely and secured to tightly fit around the 0.3 mm inner diameter (ID) and 0.5 mm outer diameter (OD) polytetrafluoroethylene (PTFE) tubing (UT3) purchased from Adtech Ltd. Aligning the tweezer tip is important as slight misalignment usually leads to unfocused magnetic field and hence unsuccessful trapping of beads. Accordingly, the holders of the magnetic tweezers were designed in such a way that they keep the tweezers and PTFE tubing in place.

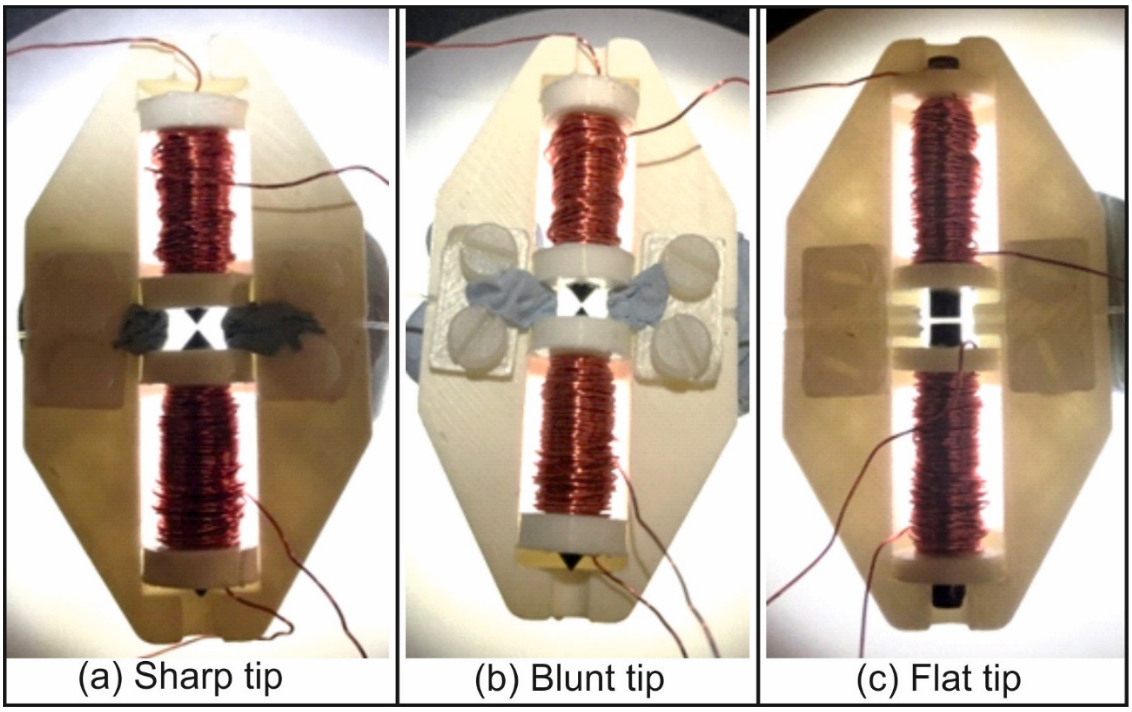

Figure 36. *Three pairs of magnetic tweezers held in 3D printed holder. Each pair of tweezers have a different tip, (a) sharp tip, (b) blunt tip and (c) flat tip. The sharp tips, blunt tips and flat tips have a tip diameter of 0.1 mm, 0.6 mm and 3 mm respectively.*

Figure 37 shows the schematic of experimental setup for testing the different tweezer pairs qualitatively, consisting of a syringe pump (Harvard Apparatus PHD 2000), an external power supply, microscope (AmScope) with camera (Thorlabs USB 2.0 Digital Camera), and computer display setup projecting from the digital camera mounted on the microscope for real-time monitoring of the droplets and manual capturing, releasing.

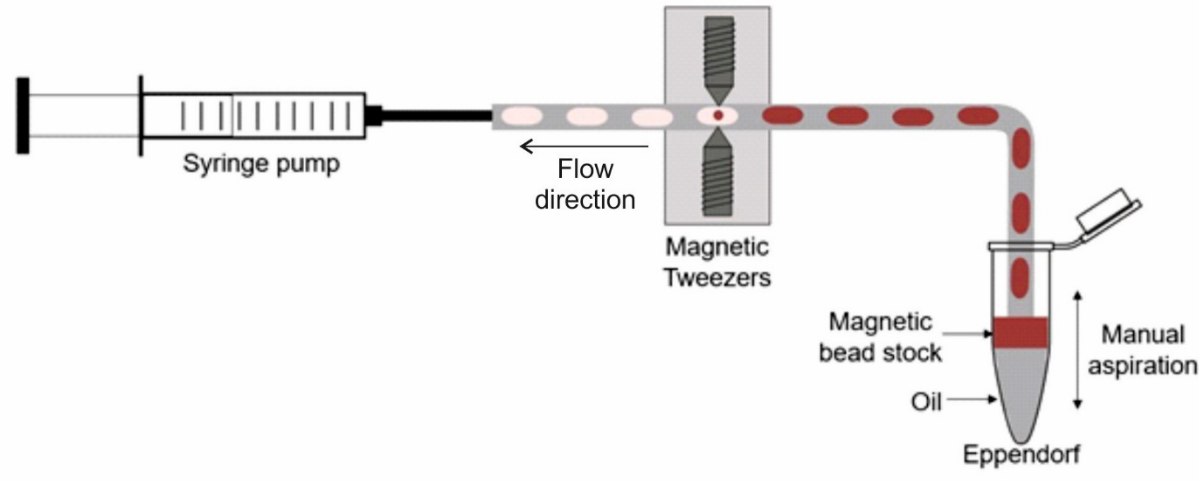

Figure 37. *Schematic showing manual aspiration of droplets containing magnetic beads from an Eppendorf tube using a syringe pump. The Eppendorf tube was filled with a layer of FC-40 oil and a top layer of magnetic bead stock.*

Syringe pumps are widely available and provide ease and controllability for generating droplets. It is possible to specify the flowrate using a syringe pump, which proves advantageous when needing to work with various flowrates during experiments. A sequence of single, aqueous magnetic bead droplets were generated by using the withdrawal mode of the syringe pump set at 10 µl/min. The PTFE tube connected to the syringe was dipped alternatively in bead stock and FC40 to aspirate droplets (Fig. 37). The bead stock used in the experiment was prepared using 50 µl of beads in 500 µl of phosphate buffered saline (PBS) with 1% bovine serum albumin (BSA) and 1% Tween20. FC40 carrier was used without any surfactant. Pipetting the magnetic beads proved to be a challenge as 100 percent of the beads could not be pipetted out while making the bead stock. So, the volume of the beads was approximately 50 µl. Figures 38, 39 and 40 display the (a) capture, (b) retention and (c) re-suspension of beads using sharp, blunt and flat tweezer tips respectively.

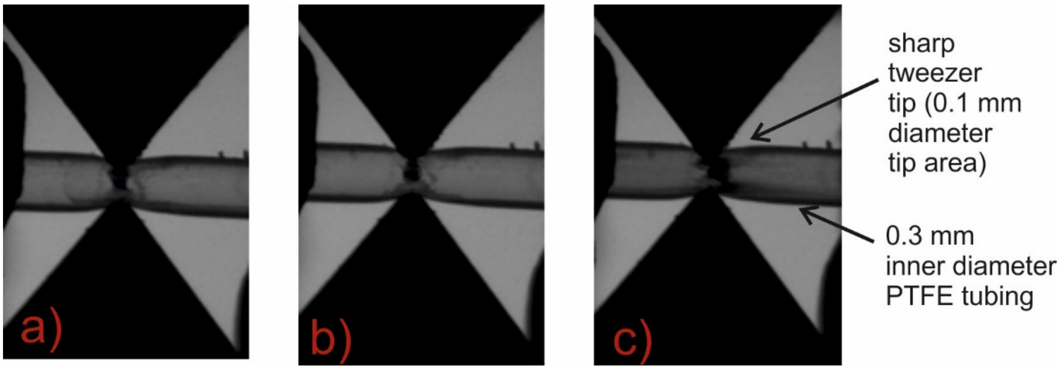

Figure 38. *(a) Capture, (b) retention and (c) re-dispersion of beads using sharp tips. The sharp tips have a diameter of 0.1 mm.*

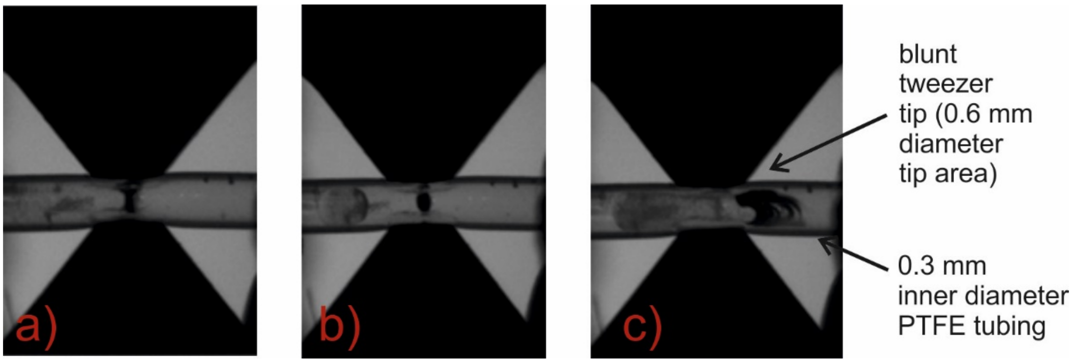

Figure 39. *(a) Capture, (b) retention and (c) re-dispersion of beads using blunt tips. The blunt tips have a tip diameter of 0.6 mm.*

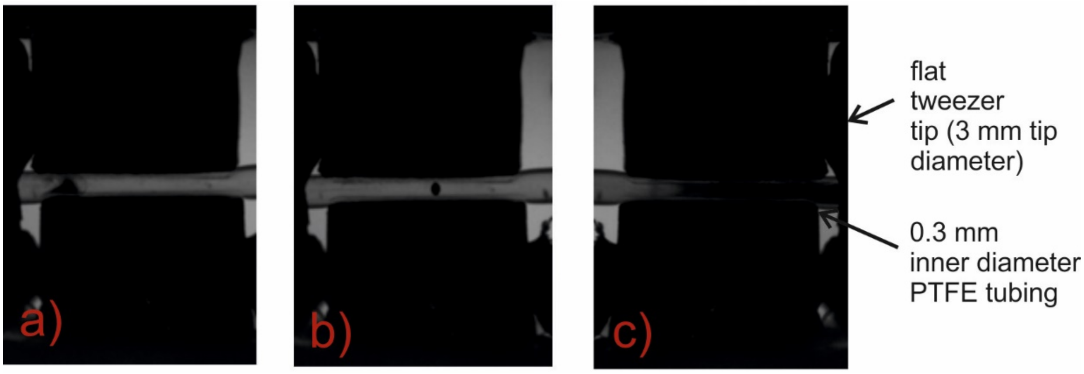

Figure 40. *(a) Capture, (b) retention and (c) re-dispersion of beads using flat tips. The flat tips have a diameter of 3 mm.*

Good capture is indicated by tweezer tips attracting the magnetic particles from the droplet and forming a bead pellet, which can overcome the interfacial tension of the droplet surface and remain in position without being carried away by the droplet. The sharp tips demonstrated good capture, but not as strong as blunt tips and the magnetic field seemed to be saturated. The blunt tips showed decent capture, retention and re-distribution of the magnetic beads. The capture, retention and redistribution also seemed good with the flat tips. After capture, the bead droplet had a tendency to move to the centre of the flat tips indicating that the magnetic field is strongest in the centre of the flat tips. Both capture and redistribution of beads took place over a larger area and the magnetic beads seemed to align with respect to different field lines. This behaviour indicated that the flat tips could be used for mixing purposes in the assay.

3.3.3. Bead extraction results using different tips

As the immediate requirement to perform the assay was to receive focused magnetic field for capturing beads efficiently, it was decided that the sharp and slightly blunt tips would be tested further for beads capturing. The following tests have been done in collaboration with Dr. Gareth Evans. The sharp and blunt tip tweezer pairs were subject to currents ranging from 0.1 A to 0.5 A for different flow rates (5 µl/min, 10 µl/min and 20 µl/min) of the droplet sequence. The bead stock was prepared using the procedure as mentioned in section 3.3.2 and the FC40 oil was used without any surfactant.

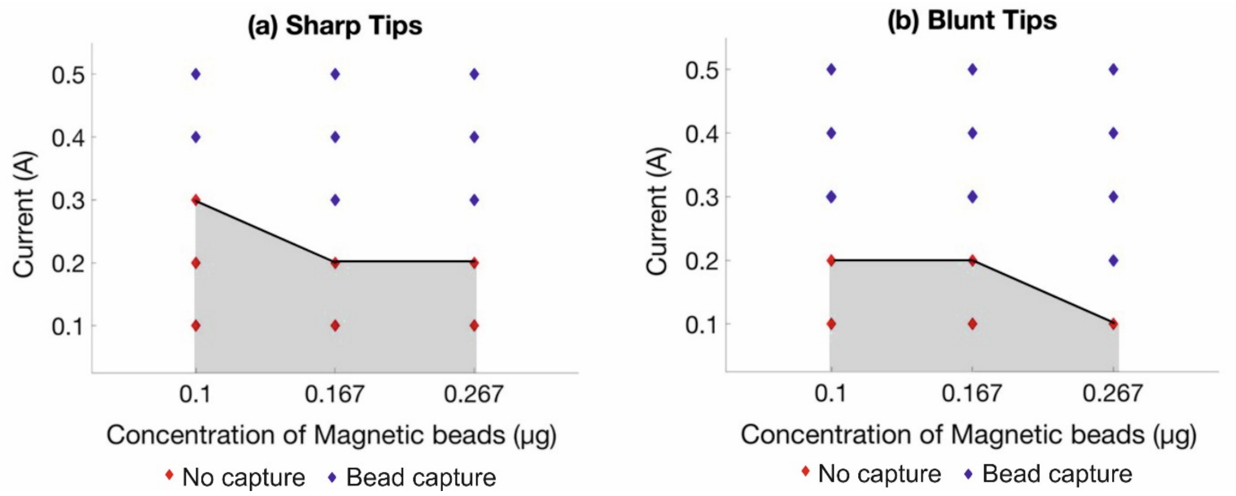

Figure 41. Bead capture for various currents (0.1-0.5 A) through the tweezers for flow rate of 5 µl/min using (a) sharp tip and (b) blunt tip. The red diamonds indicate no capture of beads (grey area) and the blue diamonds indicate capture.

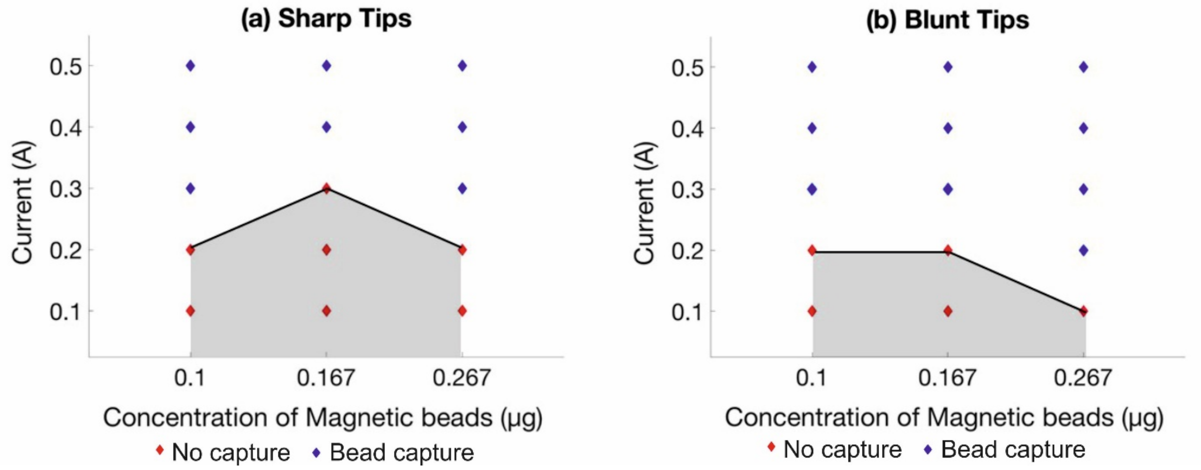

Figure 42. *Bead capture for various currents (0.1-0.5 A) through the tweezers for flow rate of 10 µl/min using (a) sharp tip and (b) blunt tip. The red diamonds indicate no capture of beads (grey area) and the blue diamonds indicate capture.*

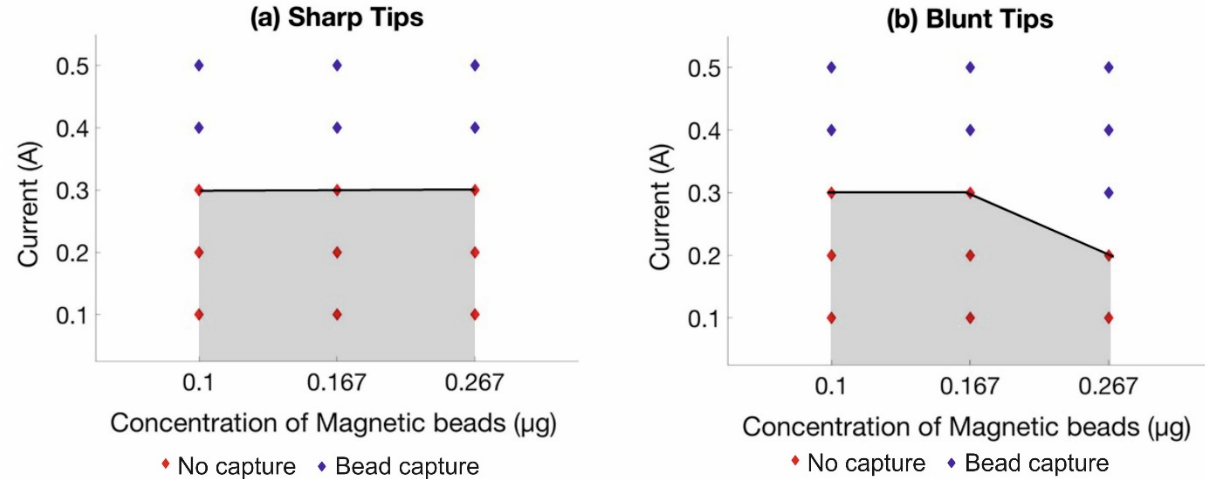

Figure 43. *Bead capture for various currents (0.1-0.5 A) through the tweezers for flow rate of 20 µl/min using (a) sharp tip and (b) blunt tip. The red diamonds indicate no capture of beads (grey area) and the blue diamonds indicate capture.*

Figures 41-43 show the scatter plot of current (A) versus concentration of magnetic beads (µg/ml) for the two different tweezer tips. The blue diamonds on the plots indicate bead extraction and the red diamonds indicate no extraction (grey area). Figure 41 shows the data for flowrate of 5µl/min, Fig. 42 shows for 10µl/min and Fig. 43 for 20µl/min. The droplets were aspirated manually with the syringe pump in withdrawal mode same way as has been described in the previous section (3.3.2). The overall experiments demonstrated that the blunt tips were better at capturing the beads than the sharp tips, at different flow rates and currents. The graphs demonstrate a few inconsistencies (not capturing beads where expected) which might have occurred due to the misalignment of the tweezer tips or maybe due to the inconsistencies in droplet generation due to manual aspiration. The sharp tip tweezers were harder to align (aligning means tweezer tips pointing directly at each other and slightly squeezing the PTFE tubing) and as a result, the magnetic field could not be focused at all times. The blunt tip tweezers fit more tightly around the PTFE tubing and the surface area of the tips aligned better (tip surfaces were parallel to each other). This gave field lines more area to cover and hence the field lines were effective in a larger volume suitable for interacting with all magnetic particles (volume matching field lines with the beads).

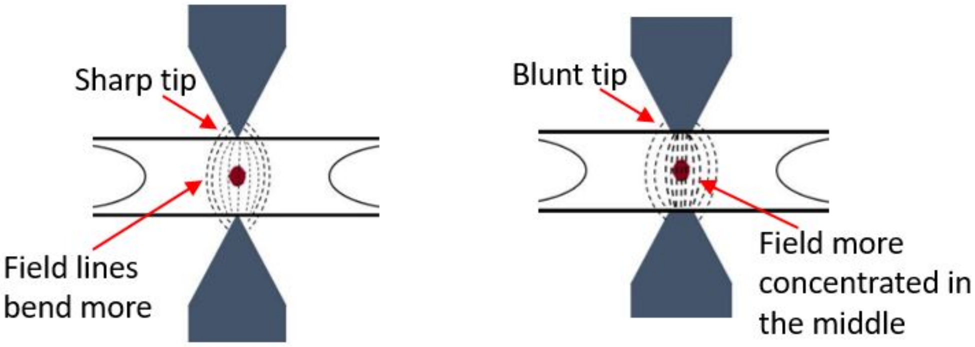

Figure 44. *Schematic diagram of sharp and blunt tips with magnetic field lines between the tips.*

Figure. 44 shows the schematic of blunt and sharp tips and the field lines between the tips of each tweezer pair. Due to the slightly larger suface area of the tips, the field density in between blunt tips is higher and there is less leakage of field which is vital for good extraction of beads. Therefore, the slightly blunt tips were chosen as the most suitable configuration for the assay based on the experimental results.

3.3.4. Washing Efficiency

In ELISA immunoassays, unbound proteins or analytes can create background noise and variability in test results. In order to obtain precise measurements with high sensitivity, efficient washing steps are required to remove the supernatant containing them. Keeping this in consideration, particular attention was given in designing tweezers to provide thorough washing of the magnetic beads. Hence, after selection of the most suitable tweezer tip (blunt), the washing efficiency was tested via a qualitative test. A train of four aqueous droplets separated by FC40 oil (0.1% surfactant) was generated (Fig. 45) using our group's novel peristaltic pump (Fig. 54). The droplet generation procedure has been described in detail later in section 3.4. The first of the four droplets consisted of magnetic beads with Rose Bengal dye in 50% PBS and 50% glycerol and the next three droplets were PBS buffer as can be seen in Fig. 45 (a). 50% glycerol was used to avoid sedimentation of beads in the PTFE tube (0.3 mm inner diameter) connecting the pump and chip, a problem which we had faced during experiments. The magnetic tweezers were activated upon the arrival of the first droplet and magnetic beads were captured. The tweezers were kept energised, and the bead cluster was held in place and the two washing droplets were allowed to pass through which can be seen from Fig. 45 (b). After washing, the beads were released into the third PBS buffer droplet (Fig. 45 (c)).

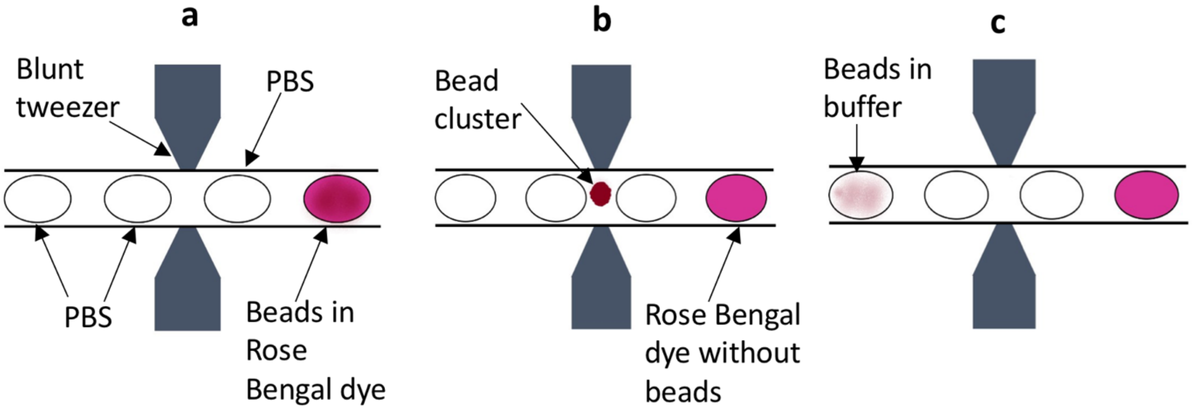

Figure 45. *Schematics showing (a) sequence of 4 droplets with blunt tweezers to test efficiency of bead extraction, (b) bead extraction after turning the tweezer on and (c) re-suspension of beads in third PBS buffer droplet by switching the tweezers off.*

The goal was to see if the last buffer droplet had Rose Bengal dye in it. The presence of dye would indicate the inefficiency of the tweezer pair. By naked eye, no Rose Bengal dye was seen in the last buffer droplet, where the beads were re-suspended. Also, after the extraction of the beads, the first droplet showed the exact colour of the dye indicating the absence of beads. A picture of the PTFE tube containing the droplet train after washing can be seen in Fig. 46.

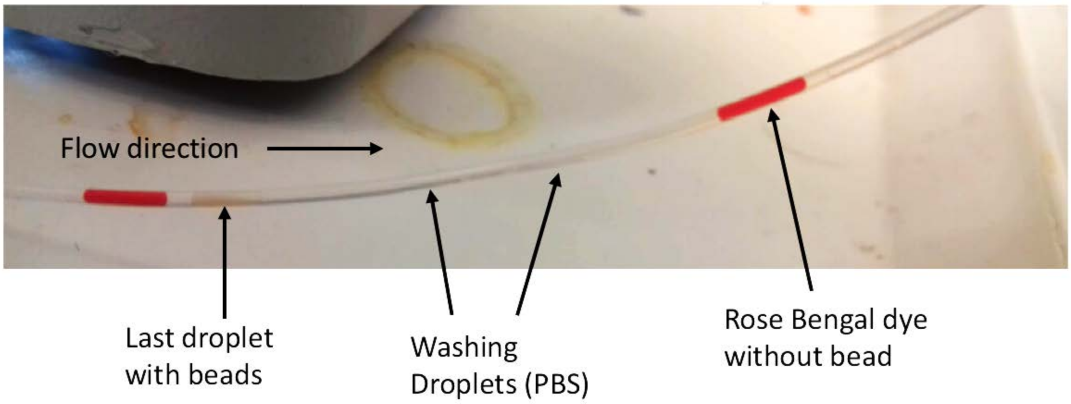

Figure 46. *Droplet sequence after extraction of beads from Rose Bengal dye, washing and redistribution.*

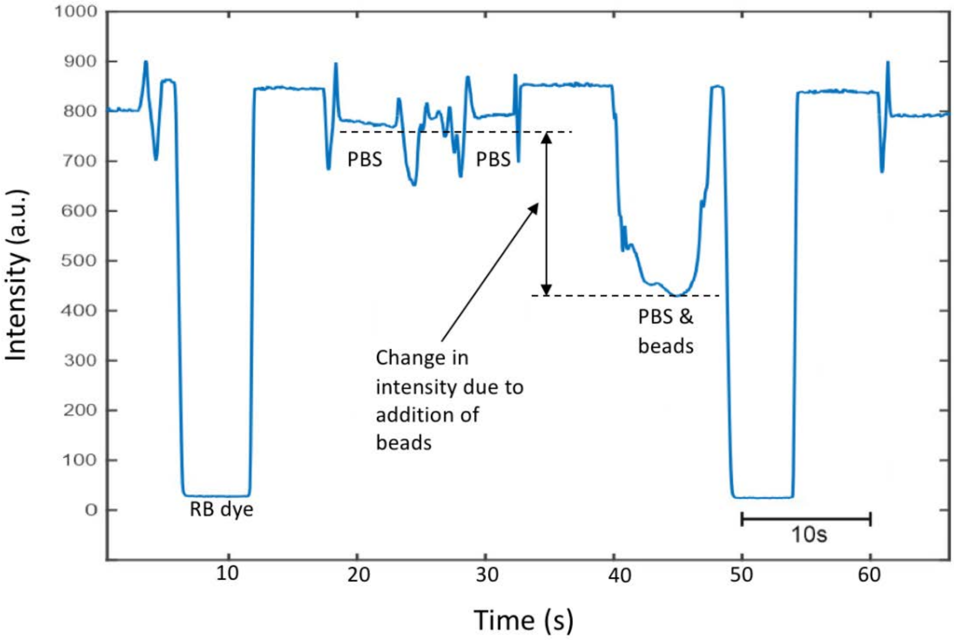

Figure 47. *Raw data of transmitted light intensity over time as the droplet sequence passes through the flow cell.*

The droplet trains in the experiment were passed through a flow cell, whose working principle has been explained later in section 3.6. The flow cell is made up of a detector and an LED and as the droplets pass through, the intensity of the transmitted light changes depending on the constituents of the droplets. Figure 47 shows the intensity of the transmitted light versus time as the droplet train travels through the flow cell. The first droplet to reach the flow cell was the one containing Rose Bengal dye from which the beads have been extracted. The next two were PBS buffers and the last one was the PBS droplet containing re-suspended beads. There was a change in intensity due to the release of beads in the 4th droplet. Therefore, the washing efficiency test of the tweezer seemed highly satisfactory by eye, however, further tests were carried out in collaboration with Dr. Gareth Evans to obtain quantitative results.

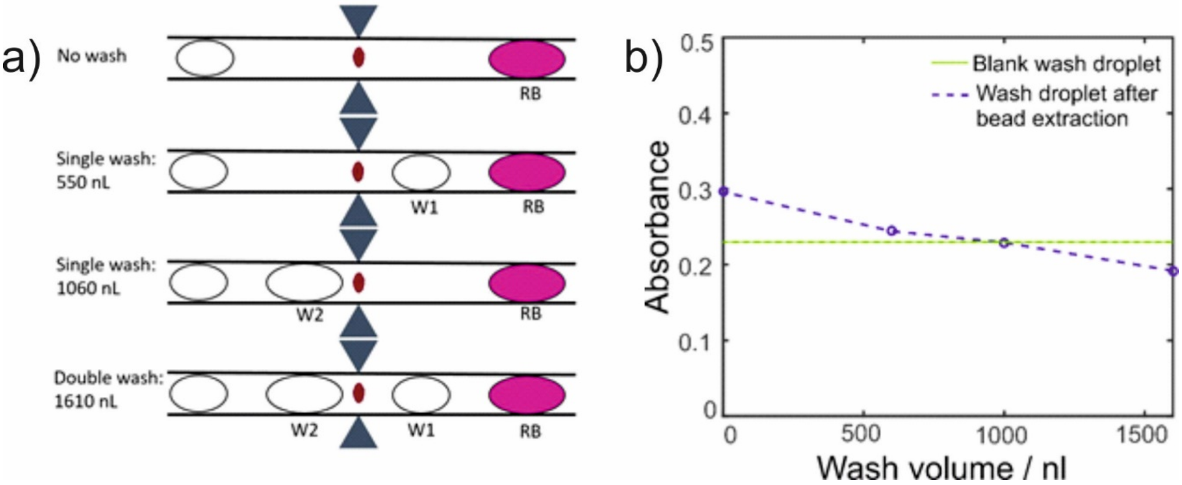

Figure 48. (a) Droplet sequences generated for testing washing efficiency of the magnetic tweezers. (b) Graph of absorbance vs wash volume for different washing protocols using different wash volumes.

Firstly, in order to obtain the absorbance of the Dyna beads, a droplet containing 1 mg/ml of bead stock was passed through the optical detector. Then using the same pump roller design (Section 3.4) as is to be used for the assay, four different sequences of droplets were produced. Every time the first droplet was composed of magnetic beads (1 mg/ml) with Rose Bengal dye in 50% PBS and 50% glycerol as used for the previous experiment. The other droplets were PBS wash buffers (with BSA for non-specific adsorption and Tween 20) of two different sizes (550 nL, 1060 nL) and all of them being carried by FC40 oil (0.1% surfactant). Every time a wash droplet passed through the bead cluster, it was seen to deform showing slight re-dispersion and then aggregating again when the oil passed through it.

The first sequence as illustrated in Fig. 48 (a) consisted of no washes and direct extraction of magnetic beads from Rose Bengal dye and re-dispersing into a PBS wash buffer. The second sequence involved extracting the beads and passing them through 550 nL PBS wash droplet and releasing them in the next PBS droplet. For the third sequence the beads were passed through 1060 nL PBS wash droplet and released them in the next PBS droplet. The fourth and final sequence involved washing through a 550 nL and a 1060 nL droplet giving a combined washing volume 1610 nL. For all sequences, the absorbance of the PBS wash buffer droplet in which the beads are finally re-dispersed was measured.

The absorbance values (Fig. 48 (b)) indicated that 1060 nL droplet was more effective in washing away the Rose Bengal Dye (mimicking supernatant) than the 550 nL droplet. However, both the wash droplets combined assured proper washing and it was chosen as the sequence to be used for the assay. The forth washing sequence caused the loss of some magnetic beads. The loss of beads have been quantified by measuring the difference in absorbance values of reporter droplet containing re-dispersed magnetic beads after washing compared to a blank containing the original bead concentration. Estimated loss of 50 ng per train after two washing steps, or 16% of the total weight of magnetic beads, on par with previously reported microfluidic platforms such as Wang *et al.* platform which had a total loss of 12% of the starting bead volume after all washes required in their assay (Wang et al., 2007b). Generally washing steps in other microfluidic platforms require mixing plates for recirculation or longer incubation time (Mai et al., 2018). The washing protocol in our platform, seemed fairly effective and quite straightforward to implement without the need of having longer lengths of tubing or mixing plates.

3.3.5. Automatic Magnetic Bead Shifter (MBS)

The magnetic tweezers are the core constituents of the assay, and optimization is required in order to make them robust and easy to handle. While testing the tweezers, two main concerns came up regarding their usability. Firstly, aligning the tweezers tips proved to be a difficult task giving discrepancies in results due to slight misalignments and also taking up a long time to set up for each experiment. Secondly, the capturing, retention and re-suspension of beads were being done by manually powering the tweezers on and off. This sometimes resulted in human error and delays in controlling the tweezer unit. As the goal is to miniaturise ELISA and develop a portable unit, making the magnetic tweezers work automatically was of priority. An automatic tweezer unit otherwise known as the Magnetic Bead Shifter (MBS), was conceptualised and fabricated. 3D schematic of MBS and actual picture of the unit can be seen in Fig. 49.

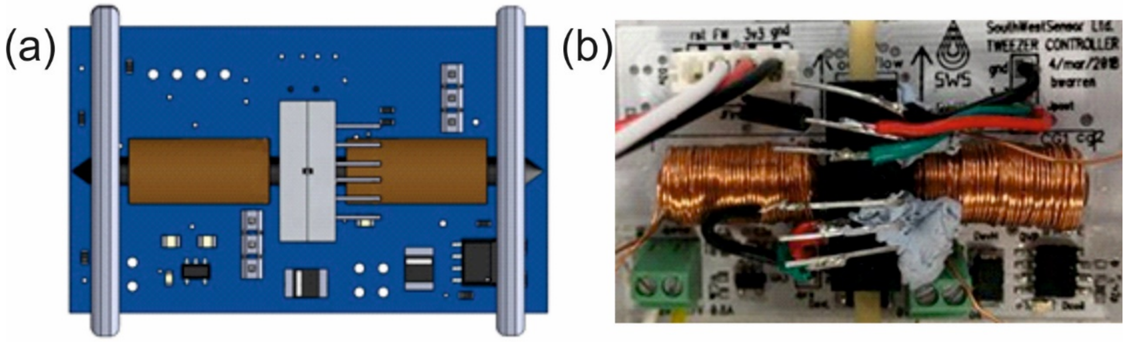

***Figure 49**. (a) Top view of 3D schematic of Magnetic Bead Shifter (MBS) on the left and (b) photograph of the actual unit on the right.*

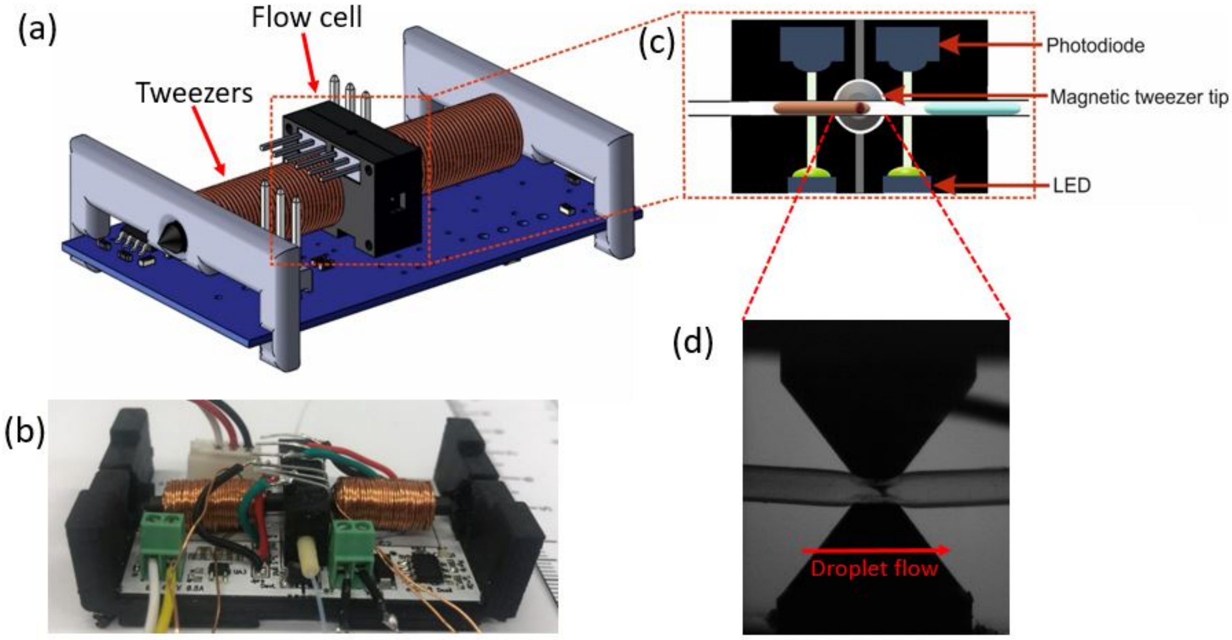

__Figure 50.__ (a) 3D SolidWorks CAD drawing of Magnetic Bead Shifter (MBS), (b) photograph of actual unit, (c) schematic of cross-sectional view of flow cell showing two light gates, magnetic tweezer tip and droplets in PTFE tubing and (d) zoomed in view of magnetic tweezer tips extracting magnetic beads.

The MBS is a fully autonomous unit programmed to extract magnetic beads and release the beads into the desired droplets. MBS consists of the following components (Fig. 50):

1. A pair of electromagnetic tweezers
2. A flow cell
3. MBS control PCB
4. Adafruit Featherboard 32u4

The heart of the MBS is a mini flow cell or spectrophotometer (fabricated by Dr. Sammer-ul Hassan) (Fig. 51) made up of two LEDs (Cree PLCC4 1-in-1 SMD LED CLM4B-BKW/GKW) and two detectors (TSL 257 photodiode with amplifier). There is a change in light intensity when different droplets pass between the LED and detector. These intensity values in the first detector suggests which droplet is going to next pass through the tweezers (magnetic beads, wash buffer or reporter droplet). Bead capture requires tweezers to be activated before the sample droplet arrives. The intensity value in the second detector suggests which droplet type is fully situated between the tweezer tips. Bead release should only be attempted once beads break the surface tension of the droplet. The software in the

MBS checks and reacts to the two detector levels to correctly grab and release beads in the passing droplets. The feather board allows the activity in an MBS to be sent to and presented on a nearby PC.

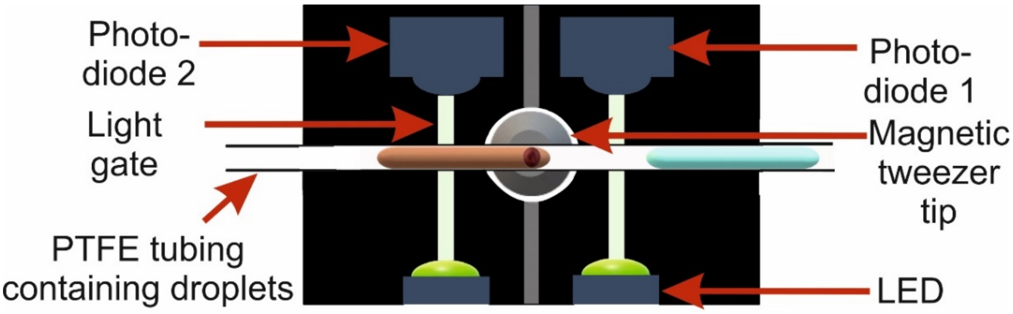

Figure 51. *Schematic of flow cell in MBS consisting of two LED and detector pairs.*

The tweezer circuit was designed using DipTrace and exported in Gerber format for printing the PCB. MBS software was developed using AVRStudio and it was also used to control an Atmel ISP chip programmer. Arduino IDE was used to develop and program the connection software running on the Adafruit Featherboard 32u4. The graphical user interface (GUI) was developed using Embarcadero C++ Builder. The GUI is used to view, define and upload different parameters for the tweezers such as the coil current and light intensity thresholds, required to reliably trigger the switching of the tweezers. The GUI lets the user either manually power the tweezers or set the MBS unit to a fully automatic mode. The PCB, software and the GUI for the MBS was developed by Brett Warren, SouthWestSensors Ltd based on our input. A screenshot of the GUI can be seen in Fig. 52.

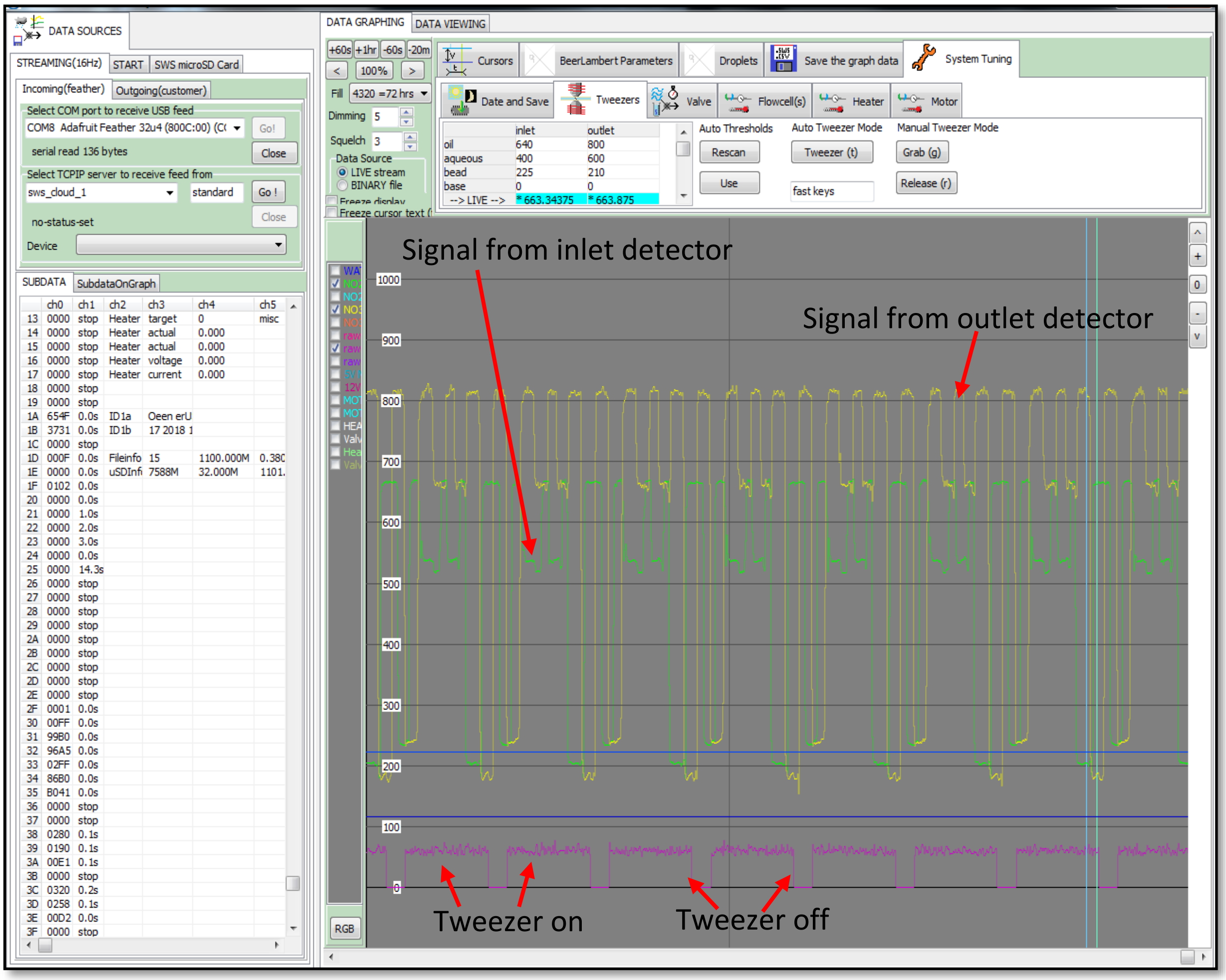

Select COM port to receive USB feed: COM8 Adafruit Feather 32u4 (800C:00) (C(
serial read 136 bytes
Select TCPIP server to receive feed from: sws_cloud_1 standard
no-status-set
Device:
Fill: 4320 =72 hrs
Dimming: 5
Squelch: 3
Data Source: ● LIVE stream ○ BINARY file

	ch0	ch1	ch2	ch3	ch4	ch5
13	0000	stop	Heater	target	0	misc
14	0000	stop	Heater	actual	0.000	
15	0000	stop	Heater	actual	0.000	
16	0000	stop	Heater	voltage	0.000	
17	0000	stop	Heater	current	0.000	
18	0000	stop				
19	0000	stop				
1A	654F	0.0s	ID1a	Oeen erU		
1B	3731	0.0s	ID1b	17 2018 1		
1C	0000	stop				
1D	000F	0.0s	Fileinfo	15	1100.000M	0.380
1E	0000	0.0s	uSDInf	7588M	32.000M	1101.
1F	0102	0.0s				
20	0000	0.0s				
21	0000	1.0s				
22	0000	2.0s				
23	0000	3.0s				
24	0000	0.0s				
25	0000	14.3s				
26	0000	stop				
27	0000	stop				
28	0000	stop				
29	0000	stop				
2A	0000	stop				
2B	0000	stop				
2C	0000	stop				
2D	0000	stop				
2E	0000	stop				
2F	0001	0.0s				
30	00FF	0.0s				
31	99B0	0.0s				
32	96A5	0.0s				
33	02FF	0.0s				
34	86B0	0.0s				
35	B041	0.0s				
36	0000	stop				
37	0000	stop				
38	0280	0.1s				
39	0190	0.1s				
3A	00E1	0.1s				
3B	0000	stop				
3C	0320	0.2s				
3D	0258	0.1s				
3E	00D2	0.0s				
3F	0000	stop				

	inlet	outlet
oil	640	800
aqueous	400	600
bead	225	210
base	0	0
--> LIVE -->	* 663.34375	* 663.875

Figure 52. *Screenshot of the GUI demonstrating MBS working in automatic mode.*

Figure 53 illustrates the detection sequence by the MBS controller PCB. The purple plot in Fig. 53 demonstrates the transmitted light reaching the inlet photodetector as the droplet train passes. The green plot is from the outlet photodetector and the red plot at the bottom of the graph represents the current flowing through the coil (arbitrary unit).

The highlighted delay in the figure (between the inlet plot changing and the tweezer being energised) is a careful balance of filtering out of droplet boundary events and allowing for the transition time from inlet to tweezer. When the droplets pass the path length, there is a peak generated at the beginning and the end (periphery) of the droplet due to the lensing of the light. This is considered as one of the boundary events. The delay assures beads are reliably recognised based on the set threshold.

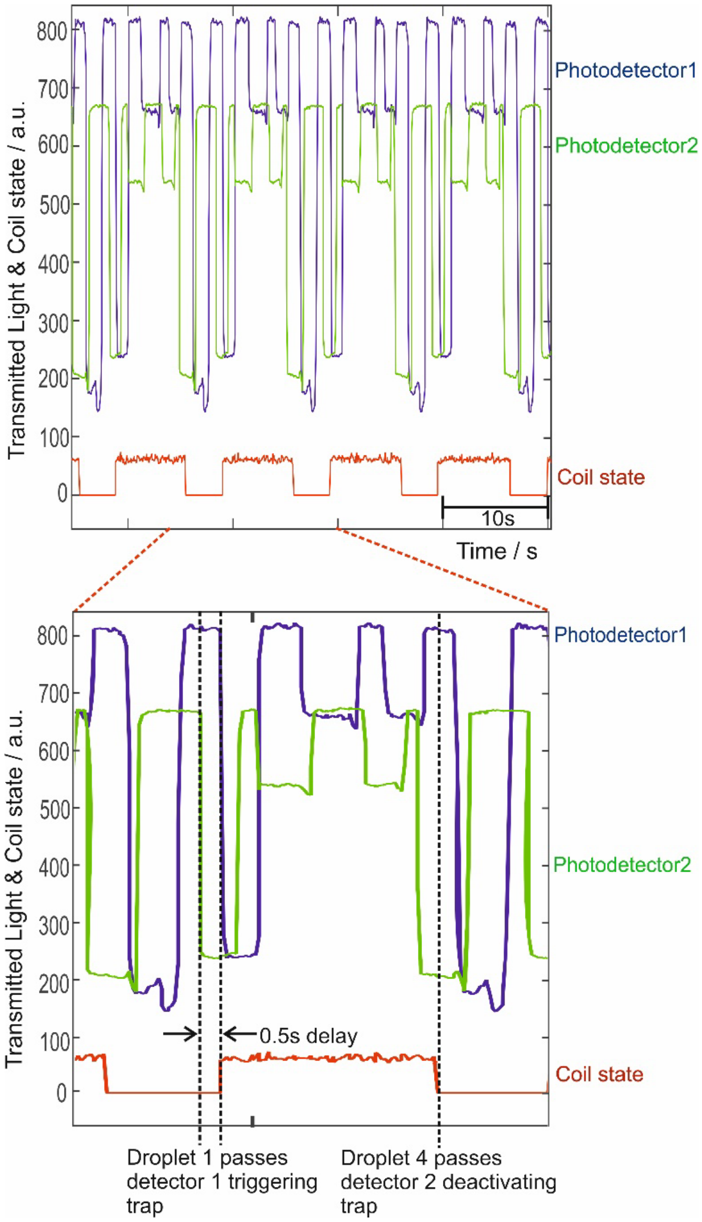

Figure 53. *Transmitted light received by the detectors (green and purple) and the current flowing through the coil (red) in the Magnetic bead shifter.*

Therefore, the MBS is capable of reliably recognising the bead droplet, extracting the beads and then releasing them in the reporter droplet as illustrated by the regular sequence in Fig. 53 (four extraction and release sequences can be seen in the top figure). Not only is this unit applicable for the cortisol ELISA but by changing the intensity thresholds for the different droplets and adjusting the current we can implement it for other bead-based assays with varying droplet size and magnetic bead concentration.

3.4. Pump

The droplet generation is facilitated by a peristaltic micropump and is based on the working principle previously shown by our group (Nightingale et al., 2017), which delivers oil and aqueous phases alternatively to the microfluidic junction, resulting in robust droplet generation. The pump consists of a motor (499:1 Metal Gearmotor 25Dx58L mm LP 6V), 3D printed chassis, rotor head with rollers, pump line bed and a cap to keep the pump line beds in position. The different 3D parts (Fig. 54) were designed in SolidWorks by Dr. Gareth Evans. The parts were printed using Objet500 Connex3 polyjet printer (Stanford Marsh Ltd) in the "VeroClear" material in 'glossy mode'.

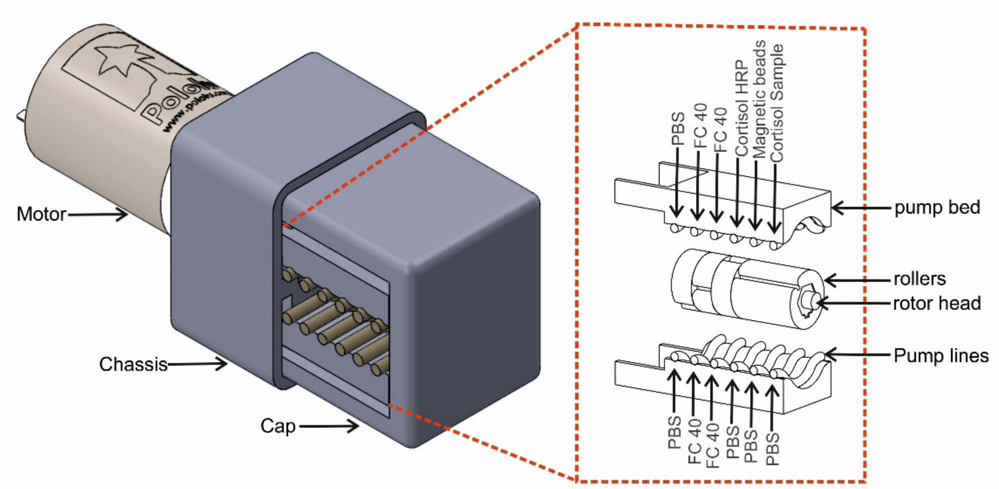

Figure 54. *12-line peristaltic pump. Exploded diagram showing different reagents and sample coming in to the pump lines.*

The rotor head consists of rollers with grooves cut into them and features which constricts the Santoprene tubing (purchased from Megaflex Ltd., UK) pump lines and facilitates the motion of the fluids by peristalsis. Droplet size is directly proportional to the size of the features and is independent of the motor speed (Nightingale et al., 2017).

There are 24, 0.5 mm ID PTFE tubing inserted into the 12 Santoprene tube pump lines from either side which are connected to the reagent/ sample containers (can be seen from the exploded diagram in Fig. 54) and 12 inlets of the PDMS microchip. The goal is to have the tubing connecting the pump lines and the chip short, so that effects of Taylor dispersion (Song and Ismagilov, 2003) is decreased and also so that sedimentation of magnetic beads are prevented.

3.5. Microfluidic chip

The characteristic properties of PDMS are highly suitable for fabricating microfluidic devices, as has been discussed by McDonald *et al*. (McDonald and Whitesides, 2002) and mentioned in section 2.6.5. The 12-inlet PDMS chip used in the system was fabricated using a 3D printed mould (Fig. 55 (a) designed in SolidWorks and printed using Objet500 Connex3 polyjet printer (Stanford Marsh Ltd) in the “VeroClear” material in glossy mode. The elastomer and the curing agent were mixed evenly in a 10:1 (McDonald and Whitesides, 2002) ratio and degassed to remove any bubble that had formed during mixing. The liquid PDMS was then poured into the mould containing the channel structure and baked in the oven at about 70 ℃ for an hour until it was completely cured. Later, the channel structure was sealed with a half-cured layer of PDMS that had been cured for about 17 minutes. 17 minutes is an optimum time for the other half to stick to the cured channel structure without fusing into the channels. Once the chip was fully cured, the channels were treated with hydrophobic coating (Aquapel), air dried and then once again the chip was placed in the oven overnight to make the channels hydrophobic (Nightingale et al., 2017). Finally, 0.5mm ID and 0.7 mm OD (UT5) PTFE tubes from Adtech Ltd were inserted into the inlets and outlet of the chip and were sealed with liquid PDMS, which was then dried on a hotplate. Sealing the tubes to the chip inlets and outlets prevents leakage of reagents and sample. Photograph of a fabricated PDMS chip can be seen in Fig. 55 (b).

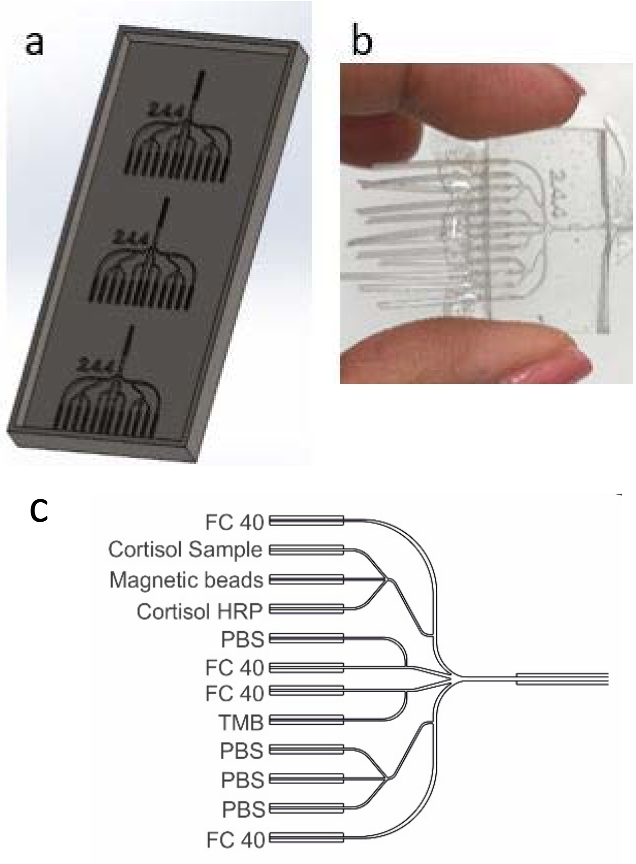

Figure 55. *(a) 3D Solidworks model of chip mould for cortisol ELISA. (b) Fabricated PDMS chip with 0.5 ID PTFE tubing inlets and outlets. (c) Schematic of chip showing the reagents and sample that enter through the 12 inlets.*

The microfluidic chip is composed of four parallel T-junctions which all contribute to the formation of a continuous sequence of four aqueous droplets separated by oil. Figure 55 (c) shows all the reagents and samples that enter the different channels of the PDMS chip, which are cortisol sample, cortisol-3-carboxymethyloxime horseradish peroxidase conjugate (cortisol-HRP), antibody functionalized magnetic beads (MyOne Dynabeads), FC40 oil, phosphate buffered saline (PBS) wash buffer and 3,3',5,5'-tetramethylbenzidine (TMB) reporter.

3.6. Detection flow cell

The detection flow cell (spectrophotometer) for quantifying the composition of droplets accurately is made up of two adjoining pieces of polymethylmethacrylate (PMMA) which have been micro milled to include an LED (150224BS73100 - LED, Blue, SMD, 20 mA, 3 V, 456 nm from Farnell) and a photodetector (TSL257) as can be seen in Fig. 56. The two sides also have a groove to fit in a 0.5 mm

ID PTFE tubing (UT5) purchased from Adtech Ltd. and another grove for light to pass. The LED and photodetector pair create a light gate and when a droplet passes through the light gate, the photodiode receives varying amounts of light based on the droplet constituents. The light received varies depending on the absorbance by the droplets and also due to the effects of refractive index (Hassan et al., 2017).

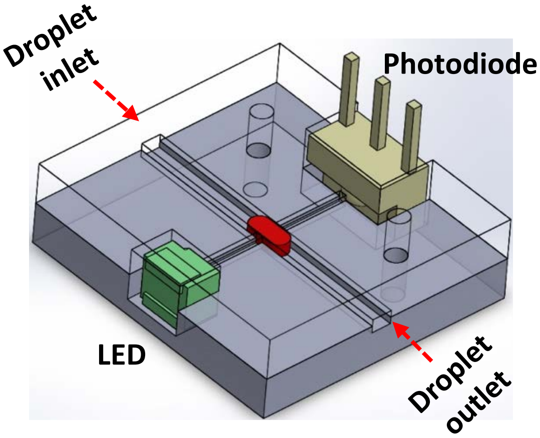

Figure 56. *3D schematic of flow cell (Hassan et al., 2017).*

The raw data from the photodiode was extracted using an Arduino Nano microcontroller and recorded using LabView software (designed by Dr. Adrian Nightingale) from National Instruments. A modified version of Beer Lambert law (Hassan et al., 2016) has been used to find out the absorption values of the droplets:

$$A = -\log_{10}\left(\frac{I_{sample\ droplet}}{I_{blank\ droplet}} \times \frac{I_{blank\ oil}}{I_{droplet\ oil}}\right) = \varepsilon c l \tag{13}$$

$I_{sample\ droplet}$ corresponds to the light transmitted through the sample droplets and $I_{blank\ droplet}$ for light through blank droplet which is usually introduced at the beginning of the experiment. For the assay, droplet containing TMB was used as the blank droplet. Transmitted light through adjacent carrier fluid droplets is denoted by $I_{blank\ oil}$ and $I_{droplet\ oil}$ for the blank and sample respectively. Absorbance is the product of ε(molar absorption coefficient), c (concentration) and l(optical path length).

3.7. Translation of assay into microfluidics platform

After the different components of the system were tested individually to check their reliability, the assay was implemented. Running the assay was a collaborative effort between Dr. Sharon Coleman, Dr. Sammer-Ul Hassan, Dr. Susan Pang (LGC), Dr. Gareth Evans and I. Dr. Sharon Coleman and Dr. Sammer-Ul Hassan helped functionalize the magnetic beads and prepare the reagents.

3.7.1. Grafting the antibodies onto the magnetic beads

Reagents were purchased from Sigma Aldrich unless mentioned otherwise. Dr. Susan Pang from London Government Chemist Group (LGC) optimised a protocol for coating magnetic micro beads. Anti-cortisol-3-BSA antibody (Calbioreagents) was used to coat the Tosylactivated Dynabeads (Invitrogen). The coating buffer was 0.1M sodium borate at pH 9.5 and 1 mL of coating buffer was used to rinse 250 µL of 100 mg /mL of beads two times. The beads were then re-suspended in 100 µL coating buffer and a vortex mixer was used for thorough mixing. Neodymium magnets were used for extraction, washing and re-suspension of the beads. 735 µL of coating buffer (722.9 µL) and reconstituted antibody (12.1 µL) in 0.5mL Phosphate Buffered Saline, PBS was added to the beads together with 415 µL of 3 M ammonium sulphate for a 500 µg of coating antibody. The antibody coated beads were incubated at room temperature for 24 hours with slow tilt rotation. The antibody coated Dynabeads were then removed from the coating buffer and re-suspended in 1250 µl of blocking buffer (PBS with 2% w/v Bovine Serum Albumin and 0.05% Tween 20). The beads were incubated for another 24 hours with a slow tilt rotation. Finally on the third day, the beads were extracted from the blocking buffer, washed twice and then finally suspended in storage buffer. The storage buffer was made of PBS, 0.1% Bovine Serum Albumin and 0.05% Tween 20. The final concentration of the beads in storage buffer was 1 mg/mL (assuming 100% recovery), and stored in the fridge (4°C) to preserve for later application.

3.7.2. Assay in bulk laboratory protocol

The assay was performed in 96 well micro titre plates (StarLab Ltd). Serial dilutions of cortisol (CalBioreagents) were made from 100 ng/mL to 1.56 ng/mL using PBS wash buffer. Cortisol-3-carboxymethyloxime horseradish peroxidase conjugate (cortisol HRP) (CalBioreagents) tracer solution was prepared by 1:2500 dilution in wash buffer (2 µL cortisol-HRP in 5 mL buffer). The supernatant storage buffer was removed from the beads by manual pipetting. Cortisol-HRP and cortisol standards were added together in equal volumes and from there 100 µL was added to the beads. Incubation took place at room temperature with fast rotation. The well plate was then placed on a plate shaker at 37°C and incubated for 15 minutes. The beads were then washed three times using fast rotation for two minutes and re-suspended in PBS wash buffer. 100 µL of 1-step Ultra TMB ELISA (Thermo Scientific) was added to the bead solution and incubated for 10 minutes for colour formation. The resulting chromophore was measured at 450 nm (BMG Labtech OMEGA fluorostar plate reader).

3.7.3. Running the magnetic beads-based assay in the microfluidics platform

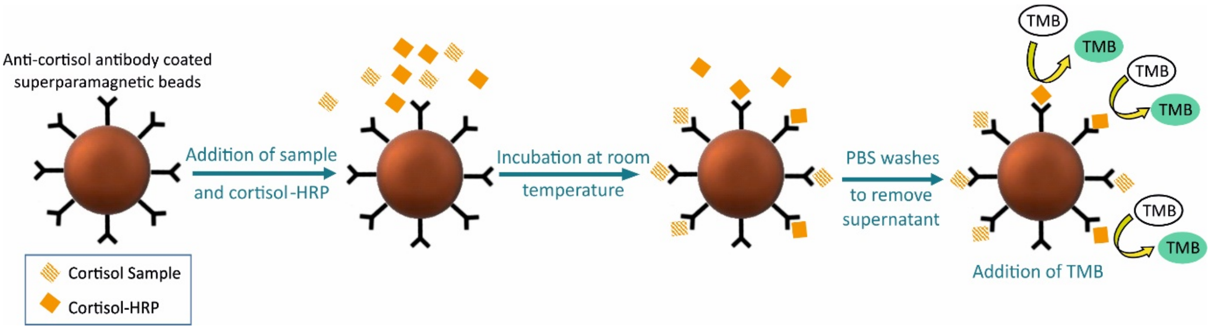

Figure 57. *Schematic of magnetic bead-based competitive heterogeneous ELISA assay showing competitive binding of Cortisol and Cortisol-HRP to Anti-cortisol antibody coated superparamagnetic beads at room temperature. After washing the supernatant with PBS washing buffer, chromogenic Tetramethylbenzidine (TMB) was added and catalysed by HRP from its native diamine form into blue-green, one electron oxidation state product.*

Figure 57 shows the schematic of the magnetic bead-based competitive heterogeneous ELISA for cortisol. Before running the assay using the droplet platform, the droplet generation unit consisting of the pump and the PDMS chip were tested using food dye for checking connections and surface chemistry. As soon as stable droplets were achieved, the food dye was replaced with the reagents and sample for the assay. The reagents/standards were all stored in Eppendorf tubes. The fluids coming into the pump consisted of cortisol sample, cortisol-3-carboxymethyloxime horseradish peroxidase conjugate (cortisol-HRP), antibody functionalized magnetic beads (MyOne Dynabeads) in PBS and 50% glycerol, FC-40 oil with 0.1% of PFPE-PEG surfactant and phosphate buffered saline (PBS) washing buffer with 0.1% bovine serum albumin (BSA) (BSA prevents non-specific binding) and 0.1% Tween20. 0.1% surfactant seemed optimum for proper extraction and re-suspension of beads. The surfactant lowers the surface tension of the droplet boundary thus ensuring the bead pellet to be extracted with ease after the tweezers are turned on. Adding glycerol to the bead stock acts as a thickening agent to increase viscous drag and hence increases the sedimentation time of the beads in the tubing leading up to the pump before droplet generation. There was also, 1- Step Ultra TMB (3,3',5,5'-tetramethylbenzidine) coming into the pump which would ultimately be the detection droplet.

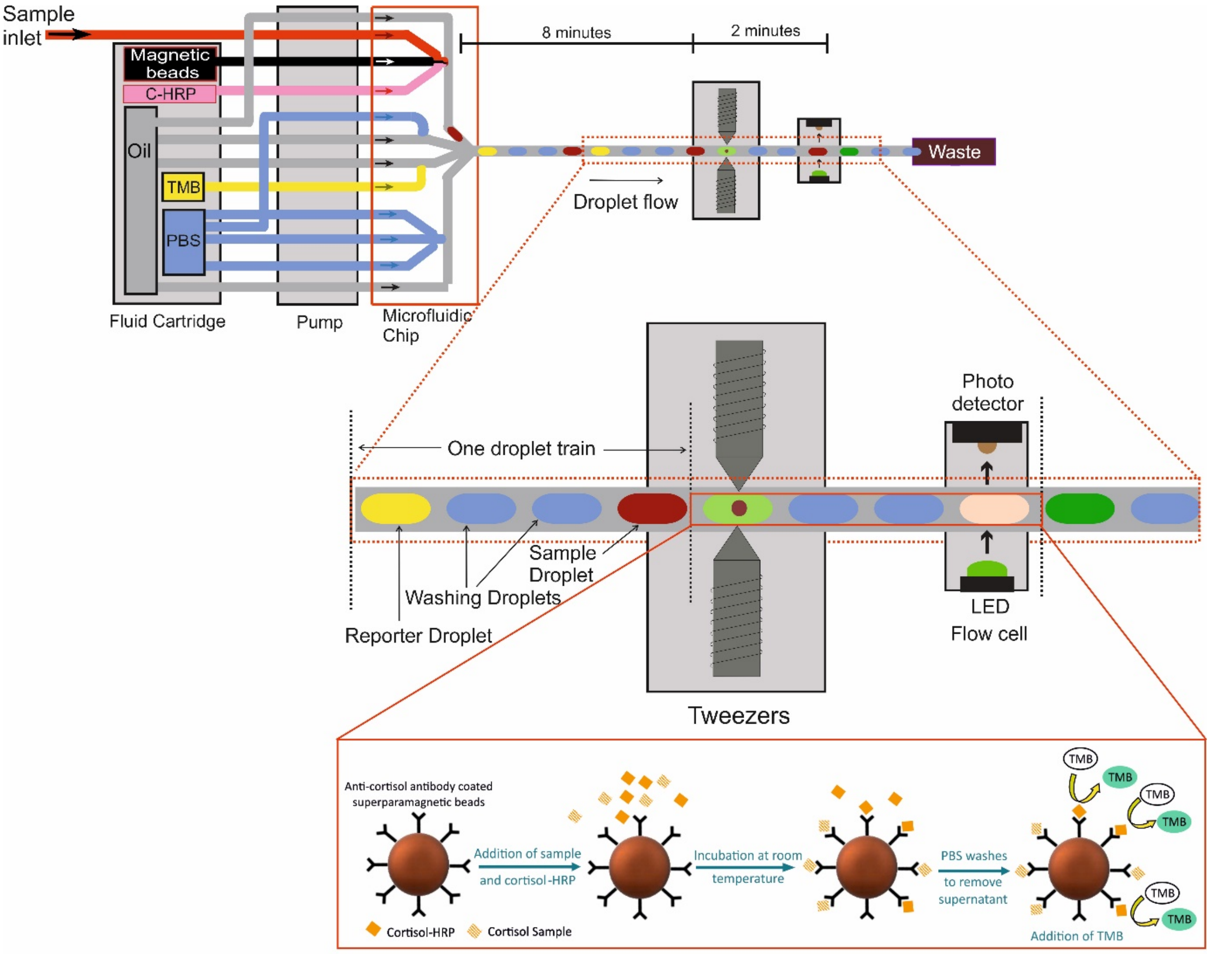

Figure 58. *Schematic diagram of microfluidics platform and fluidic pathway for miniaturizing ELISA for continuous monitoring of cortisol. The assay steps have been translated to droplets using a sequence of four droplets as can be seen in the dashed box. The first droplet in the droplet train contains, cortisol sample, cortisol-HRP and magnetic bead followed by two PBS wash droplets and finally a TMB reporter droplet. The first droplet of the train contains sample, magnetic beads and cortisol-HRP. The second and third droplets are washing droplets containing only PBS. The fourth droplet contains the TMB indicator. As the droplet train passes the magnetic trap (from left to right), the beads are captured, washed and finally re-dispersed in TMB indicator droplet where HRP catalyses colour changes.*

The reagents and sample were pumped through to the different channels of the microfluidic chip resulting in a continuous sequence of four aqueous droplets as can be seen in Fig. 58. Fig 58 shows the system schematic with exploded diagram of the droplet sequence and the bead-based assay. The droplet sequence is generated by eight separate phases. The term ‘phase’ is used to denote separate phases of fluidic flows (aqueous and oil) driven by the rotorhead of the pump per rotation. The 1st phase is co-flow of sample, beads suspension and cortisol-HRP, 2nd FC-40 oil, 3rd PBS, 4th FC-40 oil, 5th PBS, 6th FC-40 oil, 7th TMB, and 8th FC-40 oil. After the 2nd phase, the three aqueous inputs of sample, magnetic beads and cortisol-HRP are segmented into a droplet by the oil at a T-junction and finally moved into the main output channel of the chip. Then at the 4th and 6th phases, two PBS washing droplets are produced and enter the main outlet channel. Phase 8 produces the TMB indicator droplet which is the fourth and last droplet in the sequence, hence completing the droplet train.

An incubation time of about 8 minutes was allowed for competitive binding to occur between cortisol sample and cortisol-HRP with the functionalized beads. In order to provide the incubation time, the generation was stopped for about 8 minutes and then the droplets were allowed to pass through the tweezers. The tweezers were switched when an approaching bead droplet was detected from the feedback by the flow cell on the tweezer board. Switching on the tweezers caused the bead pellet to form due to the applied magnetic field. The bead pellet was then held in place and the two wash droplets were allowed to pass. Finally, the beads were re-suspended in the reporter droplet containing TMB and colour change was detected using the flow cell in section 3.6.

3.7.3.1. *Calibration curve*

Cortisol samples (3.175, 12.5, 25, 50 and 100 ng/mL) were used in the droplet platform to generate a calibration curve. The droplet assay in droplets was performed in collaboration with Dr. Gareth Evans. The amount of cortisol-HRP was kept constant at 100 ng/mL. Figure 59 shows the transmitted light to the detection flow cell for 3.175ng/mL and 100 ng/mL cortisol sample for a train of droplets. The signal varies as oil and aqueous droplets alternately pass through the light path giving a real-time data of absorption. The intensity values were taken for each concentration and the absorbance was found out by the modified Beer Lambert law mentioned in section 3.6. The measured absorbance is inversely proportional to the concentration of cortisol present as expected for a competitive heterogeneous assay. In healthy individuals the basal serum free cortisol level is typically 4.7125 ng/mL ± 0.725 ng/mL as estimated by Coolens’ method (Dorin et al., 2009).

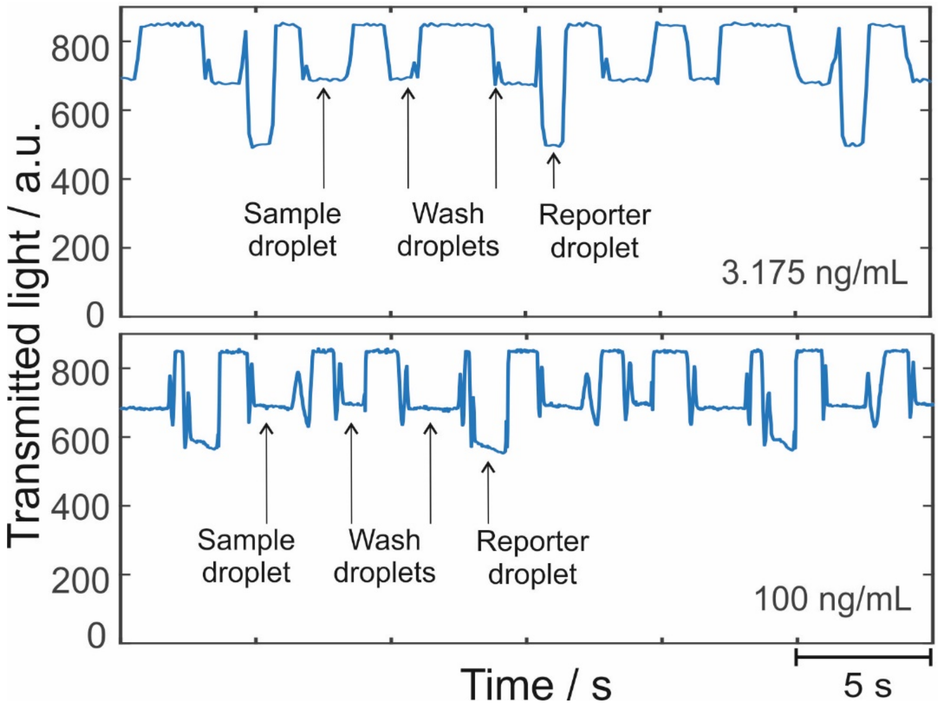

__Figure 59.__ Raw data of transmitted light from flow cell for 3.175 ng/mL and 100 ng/mL.

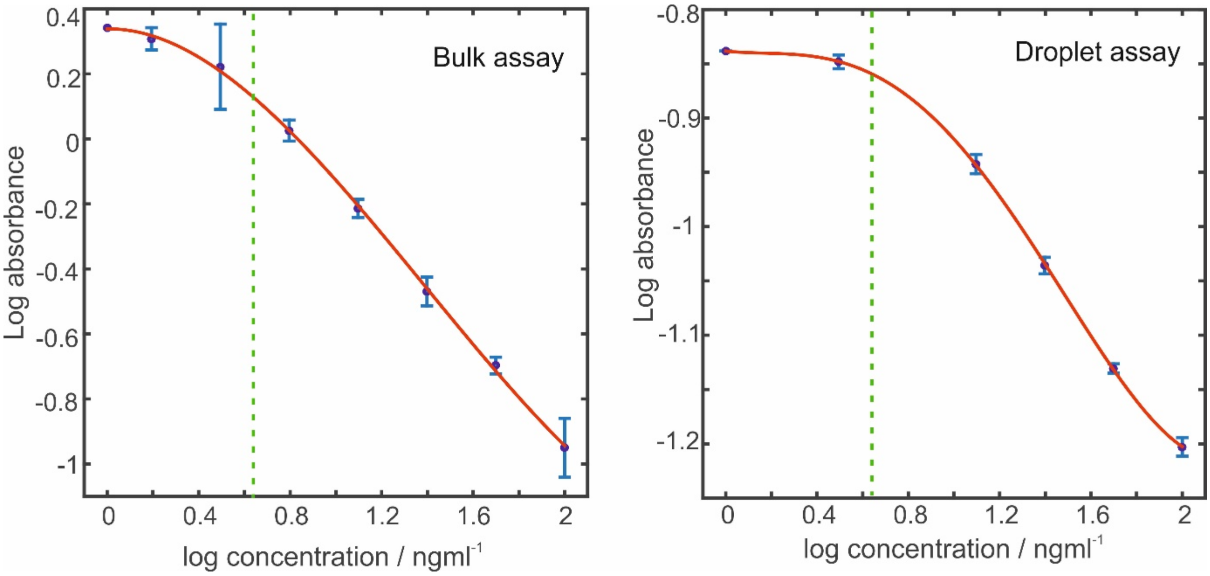

__Figure 60.__ Calibration curves for the competitive heterogeneous Cortisol assay obtained from the bulk technique (n=3) and the droplet platform (n=10). The dashed line indicates serum free cortisol in healthy individuals typically 4.7125 ng/mL ± 0.725 ng/mL as estimated by the Coolen's method (Dorin et al., 2009).

The calibration curves (Fig. 60) obtained from the bulk assay technique and the droplet platform have similar qualitative trends for the range of samples measured. However, the absorbance for the droplet assay is lower than the well plate reading because of the differing path lengths of the two detectors, which is 0.5 mm for the optical detector in the droplet platform compared to 5 mm for the well plate reader.

The well plate-based assay calibration curve shows large RSD which might have been due to manual handling errors. In comparison, each point in the droplet assay is taken from 10 repeats and show much less variation, indicating the advantage of using an automatic system. For the droplet assay, the RSD is much lower (less than 1%) which can be attributed to the automated process, precise volumetric control of the fluids and enhanced mixing in droplets. Two additional samples of 12.5 ng/ml and 100 ng/ml were tested in the system and concentration values were recovered from the standard curve as 14.96 ng/ml with a standard deviation of 1.33% and 102.8 ng/ml with a standard deviation of 1.05%. The error for the 12.5 ng/ml is about 19.7% and for the 100 ng/ml is about 2.8%. This is not abnormal considering the cortisol assay used is a competitive assay and 12.5 ng/ml lies near the plateau as shown in Fig. 60, therefore a small error of absorbance reading could cause a bigger percentage deviation in concentration. The time for each assay in the droplet platform is about 10 minutes, which is significantly lower than about 3 hours required for the laboratory bulk method. Also, compared to the 150 μl of sample and reagent that the bulk method uses per assay, the liquid consumption using the droplet platform is merely 3 μl and consequently much cheaper.

Therefore, this chapter described the fabrication and working principle of each individual component of the microfluidics platform for the continuous measurement of cortisol. The individual components have been successfully integrated and the system was able to perform the desired ELISA and provide preliminary data. The calibration curve (Fig. 60) that has been obtained from the droplet platform is very promising and indicates that the miniaturised implementation of the assay is feasible.

3.8. Chapter conclusion

This chapter illustrates the development of a droplet microfluidic platform capable of miniaturising heterogeneous assays like ELISA. In this chapter I have:

(i) Described the importance of high frequency measurement and monitoring of biomarkers like cortisol.

(ii) Illustrated the development and fabrication of an automatic magnetic bead shifter (MBS) capable of manipulating superparamagnetic beads and is an integral part for implementing ELISA in droplets.
(iii) Described the fabrication and integration of various components to build an automated microfluidic platform for miniaturising ELISA for cortisol.
(iv) Described the translation of lab-based ELISA for cortisol to a droplet-based approach.
(v) Obtained preliminary data to validate the feasibility of the droplet-based approach for miniaturising ELISA.

The future direction for this study would be to validate the system performance over time and then take the microfluidic platform to a clinical setting and validate with real patients. This work opens doors for miniaturising other heterogeneous assays for measuring and monitoring a range of different biomarkers.

Chapter 4

ENVIRONMENTAL MONITORING APPLICATIONS

In this chapter, a droplet microfluidic platform was developed for monitoring of chemical fluctuations, in particular ammonium. Although the aquatic ecosystems are normally dynamic and are influenced by numerous parameters, our focus here has been on monitoring ammonium in natural waters and wastewater treatment facilities. The results show that the sensor can track the ammonium levels accurately and with high frequency of measurement (10 seconds per sample). This application provides a further convincing example of suitability of droplet microfluidic platform in environmental monitoring.

4.1. Monitoring Ammonia

Ammonia is one of the key components of the nitrogen cycle and a fundamental nutrient for microbes within the aquatic ecosystem (Lin et al., 2019). Protonated (NH_4^+) and deprotonated ammonia (NH_3) together make up total ammonia (N) and the concentrations of $NH_4^+$and NH_3 are dependent on temperature and pH. Below the pH value of 8.75 the predominant form is the comparatively non-toxic NH_4^+ and above pH 9.75 is the toxic form NH_3. Therefore, total ammonia concentration (ammonia nitrogen-N) consisting of both the concentration of NH_4^+ and NH_3 is measured from water samples for indicating water quality. Ammonia though naturally makes up a much smaller percentage but can make its way into water as agricultural run-off or municipal/industrial wastewater discharge. High levels of ammonia can be toxic for aquatic life impairing fish growth and polluting water quality (Camargo and Alonso, 2006, Šraj et al., 2014).

Increased levels of ammonia have various implications in the aquatic ecosystem and is an ecological stressor causing biotic impoverishment. Higher levels of ammonia can encourage primary production in phytoplankton and therefore cause algal bloom and eutrophication which may in turn lead to hypoxia. Marine fish and invertebrates become more susceptible to ammonia toxicity in hypoxic water and both these stressors work hand in hand to destabilise the aquatic life balance. Ammonia can also cause irreversible damage especially to marine fish whose gills have more ‘ionic permeability’ than their fresh water equivalents. Ammonia exposure therefore damages gills, reduces oxygen carrying capacity, deteriorates liver and kidney function ultimately weakening the immune system making them vulnerable to parasitic and bacterial diseases. Long term exposure and build-up of toxin can lead to extinction of important aquatic populations and cause irreversible damage to the ecosystem (Šraj et al., 2014, Camargo and Alonso, 2006). Therefore, monitoring ammonia in natural waters and in wastewater pathways could provide us valuable information for early warning and effective remediation.

4.1.1. Conventional methods for measuring ammonia

Several techniques have been used for measuring ammonia which include spectrophotometric, fluorometric and electrochemical methods (Lin et al., 2019, Šraj et al., 2014). The Nessler’s reagent method is a classic method for measuring ammonia nitrogen (Lin et al., 2019). Consisting of mercury (II) iodide and potassium iodide as reagents in an alkaline solution, the reaction with ammonia results in the formation of a yellow solution. Nessler's method provides advantages such as the usage of one reagent and that the reaction does not require heating however, it is toxic and prone to ion interferences (calcium, magnesium). Another popular spectroscopic method is the indophenol blue (IPB) method, which is based upon the Berthelot's reaction (Cho et al., 2018, Searle, 1984). IPB method is made up of a two-step reaction but is less toxic compared with Nessler's reagent method therefore was chosen as the method for miniaturisation here. The detailed reaction is discussed further in section 4.3. Chemical molecules in matrix such as calcium, magnesium, etc. (Lin et al., 2019) could interfere with the aforementioned assays, therefore gas diffusion techniques have also been implemented (van Son et al., 1983, Plant et al., 2009) to minimize the interference by generating ammonia from ammonium in alkaline conditions. The ammonia then transports through a membrane into an indicator solution leading to a colour change to be measured by a spectrophotometer. In the o-phthaldialdehyde (OPA) method (Genfa and Dasgupta, 1989) (fluorometric method), where OPA in an alkaline solution with 2-mercaptoethanol reacts with amino acids and ammonia to produce a strong fluorescent product. Replacing 2- mercaptoethanol with sulfite results in a more selective and sensitive method for ammonia. Electrochemical methods (Lin et al., 2019) involve ion chromatography, capillary electrophoresis and gas diffusion with conductometric, potentiometric and amperometric sensing (section 2.2.1.1).

Each method for determining ammonia has its own merit (Lin et al., 2019, Šraj et al., 2014), however, most assay-based methods are conducted in a laboratory environment requiring discrete sampling, complex equipment, substantial reagent consumption and long turn-around times. Electrochemical sensors are widely used for *in situ* measurement, but electrodes are usually susceptible to ion interferences and hence not suitable for sea water monitoring.

In situ analyzers resolve the issues regarding manual sampling, transport and manual analysis and hence have gathered growing research interest as described in section 2.3. Ma *et al*., have developed a syringe-pump-based environmental-water-analyzer (iSEA) for real time determination of ammonium by spectroscopic method (Ma et al., 2018). Simultaneous detection of ammonia (OPA method) and phosphate has been achieved by a sequential injection analysis system (Frank et al., 2006) using a combination of computer controlled syringe pump, valve and detectors. However, both these systems mentioned require large volumes per sample, have complex fluid handling systems and also they need to be flushed in between samples.

Droplet microfluidic systems have shown promise in miniaturizing wet chemistry protocols and providing *in situ* monitoring capability with laboratory accuracy, high measurement frequency and reduced sample/reagent consumptions, as demonstrated in NO_2/NO_3 monitoring for both fresh and sea water (Nightingale et al., 2019a). Here we report the development of a microfluidic platform for quantifying aqueous ammonium in droplets using the indophenol blue method. The system has been used to measure ammonium in river water and later has been modified for continuously monitoring ammonium levels in a sequential batch bioreactor.

4.2. Preparation of reagent and standards

All the chemicals used in the experiments were analytical grade and purchased from Sigma Aldrich if not otherwise specified. 18.2 MΩ.cm pure water (Triple Red water technology) was used for all the sample and reagent preparation and dilutions. For preparing Ammonium Chloride stock solution (1g/L N), 0.382 g anhydrous ammonium chloride (dried at 105 °C for at least 2 h) was dissolved in Milli-Q water and diluted to 100 ml using volumetric flask (Stored in a glass bottle in a fridge; this solution is stable for at least 1 month).

100 ml of Salicylate reagent was prepared by dissolving 13 g of sodium salicylate, 13 g of tri-sodium citrate dehydrate and 0.0097 g of sodium nitroprusside in Milli-Q water. For 100 ml sodium dichloroisocyanurate reagent (DIC), 3.2 g of sodium hydroxide and 0.2 g of sodium dichloroisocyanurate dehydrate were dissolved in in Milli-Q water.

The standard ratio for spectrophotometric detection was 10.5:1:1 for standard/sample: salicylate reagent: sodium dichloroisocyanurate reagent. Once prepared, the reagents and standards were stored in the refrigerator (4 °C) and used for up-to 1 month.

4.3. Bulk assay protocol

The highly sensitive protocol for ammonium detection is based on the indophenol blue method or the modified Berthelot's reaction for the formation of indophenol blue derivative from ammonia, salicylate and dichloroisocyanurate in alkaline solution. It is addressed as modified because the phenol in the original reaction protocol has been replaced by the less toxic salicylate (Cho et al., 2018). Figure 61 illustrates the protocol for the production of indophenol dye. Sodium dichloroisocyanurate in alkaline solution produces hypochlorite ions which react with ammonia to form monochloroamine. Monochloroamine further reacts with salicylate to form 5-aminosalicylate. The structure resonates from an amino to imino to allow for a bonding pair of electrons to be accessible. Finally the amino attacks the salicylate to form the indophenol blue derivative and no further reaction occurs due to the steric hindrance of the salicylate rings (Cho et al., 2018). The end compound is believed to provide the blue colour to be utilised for the spectrophotometric detection at around 660 nm wavelength. A typical calibration range for this method is 0.05 mg/L to 2 mg/L ammonium (Standardization, 2013). The absorbance of light is directly proportional to the concentration of ammonium.

The assay detects the level of free ammonia (NH_3), so basic conditions release all ammonia leading to an accurate result. Therefore, the reaction takes place in basic conditions to shift the equilibrium of ammonia-ammonium towards ammonia formation, as follows:

In acidic conditions, the following reaction is favoured: $NH_{3(aq)} \rightarrow NH^{+}_{4(aq)}$

In basic conditions, the inverse is favoured: $NH^{+}_{4(aq)} \rightarrow NH_{3(aq)}$

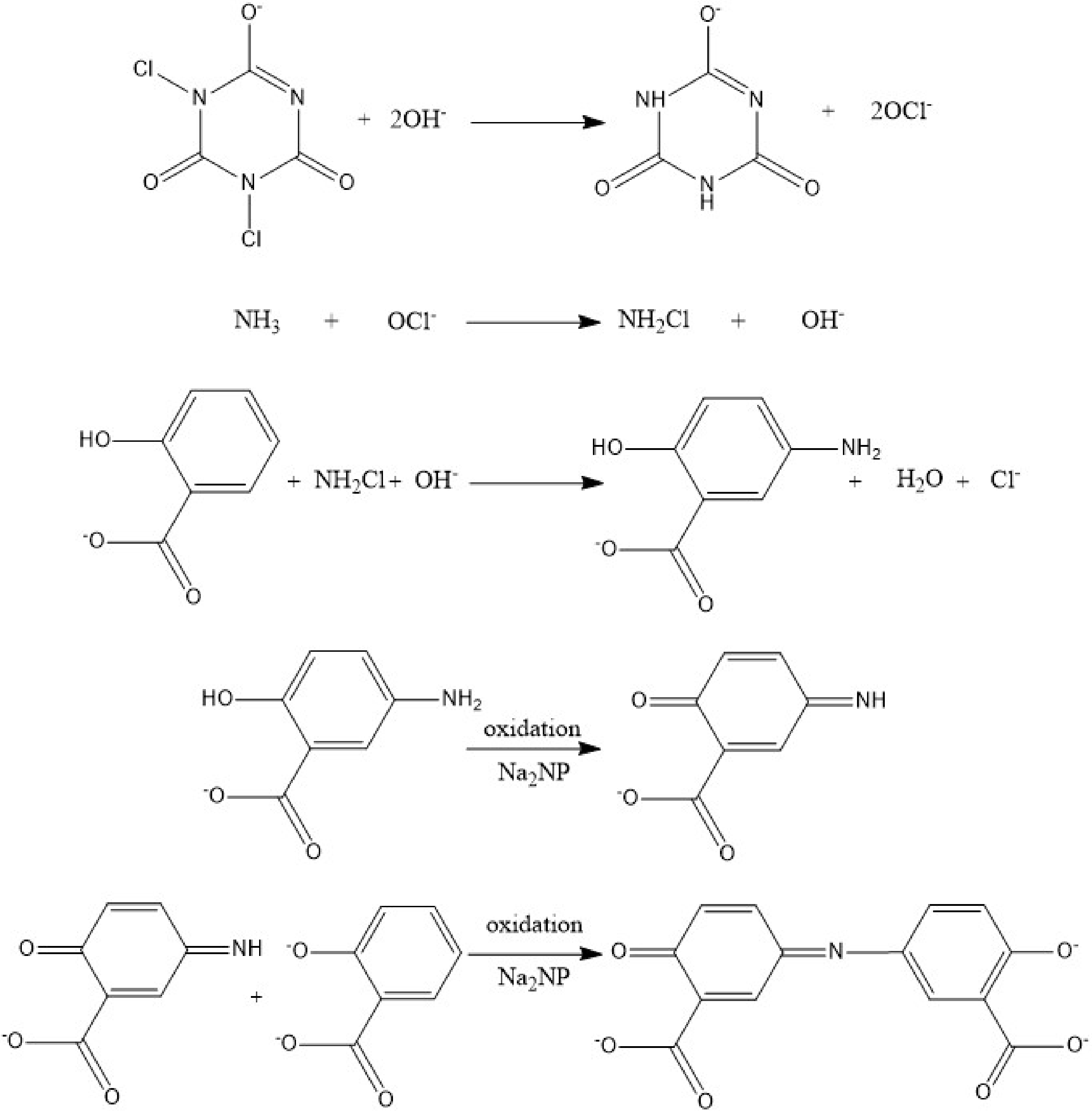

Figure 61. *Mechanism for the production of indophenol blue dye from ammonia, salicylate and dichloroisocyanurate using the modified Berthelot's reaction. It is called modified Berthelot's reaction because the toxic phenol has been replaced by salicylate for this mechanism. The oxidation is catalysed by sodium nitroprusside (NA$_2$NP). This reaction mechanism has been reproduced from (Cho et al., 2018).*

4.4. Well plate-based assay development

The assay was carried out in a 96 well plate using the original mixing ratio of 10.5:1:1 (Fig. 62) for 0.2 to 1 mg/L range of ammonium. Colour development took approximately 20 minutes at room temperature compared to about 30 minutes as stated in literature before (Qiu et al., 1987).

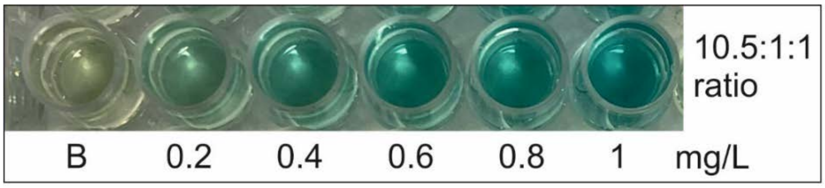

***Figure 62**. Well plate row showing 10.5:1:1 ratio of standard: DIC reagent: Salicylate for indophenol blue assay for a range of ammonium standards as indicated.*

The BMG Labtech OMEGA fluorostar plate reader was set to 25 °C for obtaining absorbance values at different concentrations for a range of wavelengths. Maximum absorbance value was found to be at 660 nm wavelength as shown in Fig. 63.

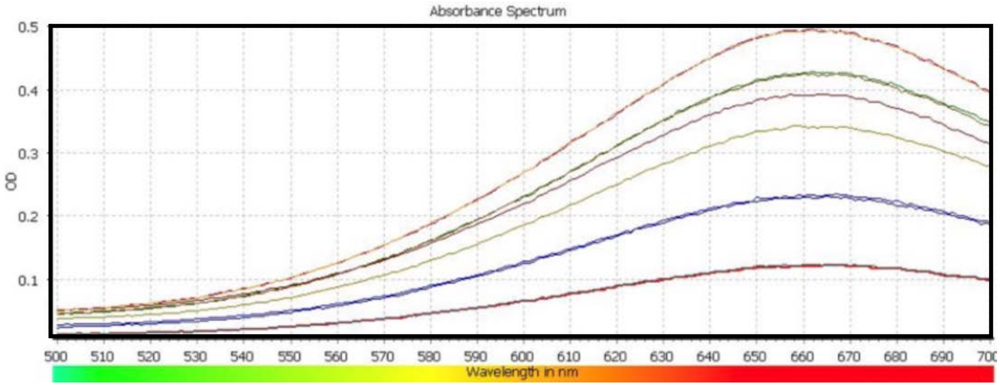

***Figure 63**. Absorbance spectra for the assay showing maximum absorbance at 660 nm.*

4.5. Adjusting the mixing ratio to scale down for droplets assay

The standard ratio for sample/standard: DIC reagent: Salicylate reagent is 10.5:1:1 which has been implemented for the assay in the previous section and is feasible to carry out in well plate or cuvette formats. However, when translating the assay to droplets, it is hard to have a roller feature which would provide about 10 times the volume of sample per turn without making the roller feature for reagents extremely small and unreliable. Therefore, the mixing ratio was firstly adjusted by diluting the reagents accordingly for 1:1:1 and 3:1:1 ratio of sample/standard: DIC: Salicylate whilst keeping the final concentration of reagents in the mixture to remain the same as for the standard ratio. The colour in the well plate for 1:1:1 and 3:1:1 mixing ratios after completion of reaction can be seen in Fig. 64. The colour increases linearly with increase in ammonia concentration; with the 3:1:1 mixing ratio showing stronger colour due to less dilution of sample than the 1:1:1 ratio. This is also supported by the gradient obtained from each mixing ratios which is 0.506 for 3:1:1 and 0.3345 for 1:1:1 (Fig. 65). The standard calibration curves for both the mixing ratios follow the Beer-Lambert's law trend.

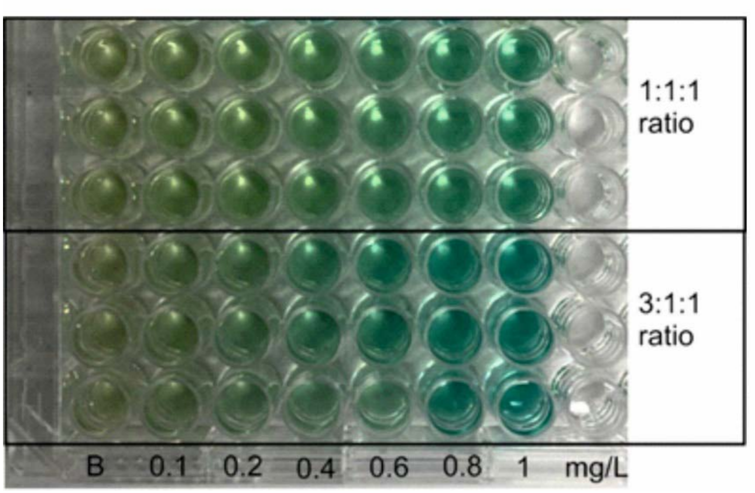

Figure 64. *96 Well plate showing three repeats of 1:1:1 and 3:1:1 ratio for 0.1 to 1 mg/L ammonium standards. Gradual colour development can be seen from left to right and the 3:1:1 ratio shows darker colour due to less dilution of the sample.*

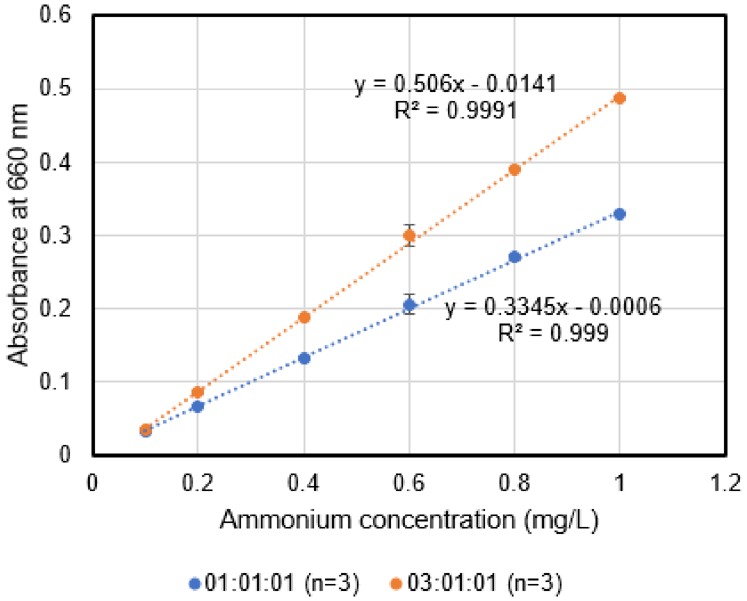

Figure 65. *Calibration curve for two different ratio of sample to reagent for indophenol blue assay. A linear relationship can be seen between the increase in ammonium concentration and absorbance.*

4.6. Sensitivity in well plate

In order to find out the sensitivity of the well plate assay, concentrations ranging from 0.15 mg/L all the way down to 0.01 mg/L were tested. Figure 66 shows the colour development in well plate for 3:1:1 and 1:1:1 ratios for 0.01 mg/L to 0.15 mg/L. Absorbance values were obtained for up to 0.03 mg/L. The calibration curves show a linear trend as can be seen in Fig. 67.

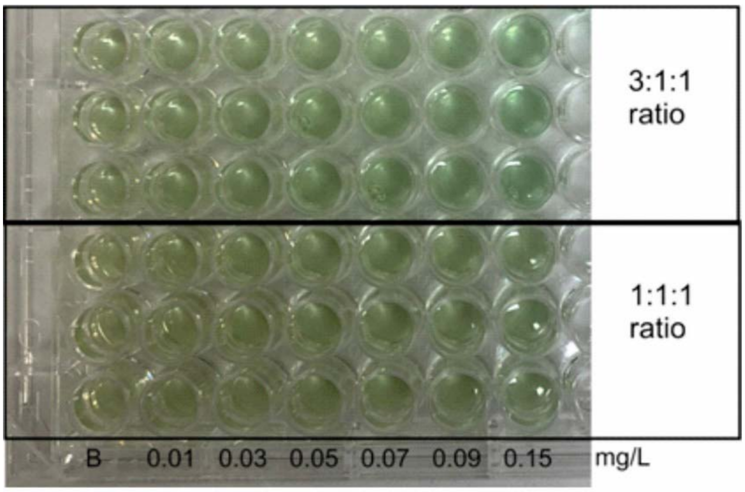

Figure 66. *96 well plate showing three repeats of the assay for two ratios. The 3:1:1 ratio displays more colour than 1:1:1 ratio.*

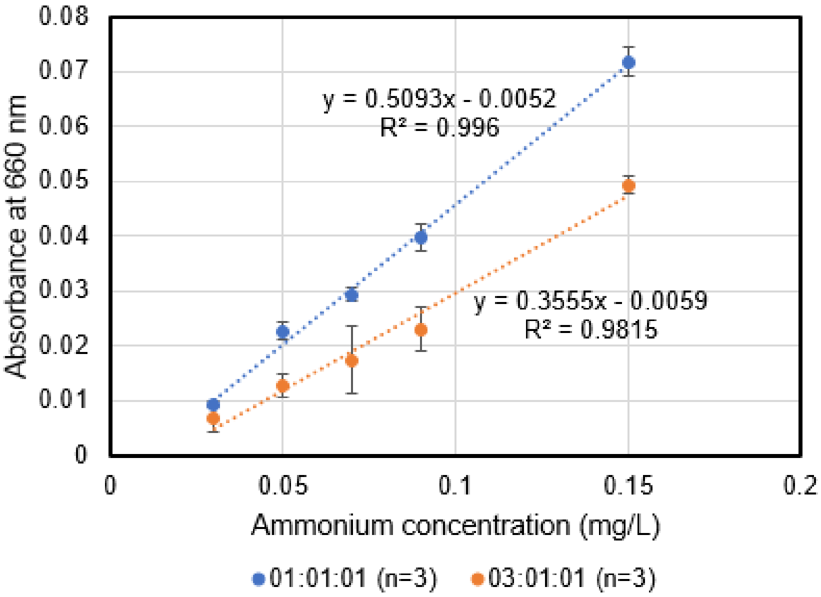

Figure 67. *Calibration curve to check sensitivity of the indophenol blue assay in well plate. A linear relationship can be seen between the increase in ammonia concentration and absorbance down to 0.03 mg/L.*

4.7. Reaction kinetics

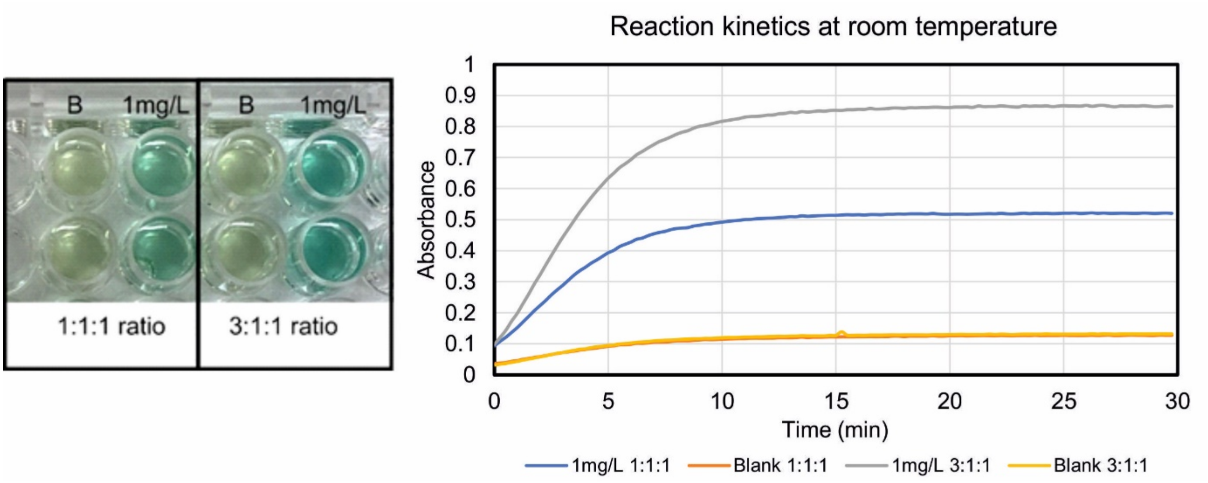

Figure 68. *Reaction kinetics of indophenol blue assay at 25°C for 30 mins. Two repeats of two different ratios of sample to reagent using 1 mg/L ammonium standard in order to check the reaction kinetics. Picture of the well plate shown on the left was taken after the kinetics measurement at 25°C using the plate reader, after completion of reaction.*

The reaction seemed to reach completion by 15 minutes at room temperature for the 1:1:1 ratio and by 20 minutes for the 3:1:1 ratio as can be seen from the kinetics plot in Fig. 68. The plot for 45 degrees could not be retrieved from the database but as seen while running the kinetics measurement, increase in temperature did not significantly increase the reaction time.

4.8. Translation of indophenol blue assay to droplets

4.8.1. Microfluidic sensor fabrication

Miniaturising the indophenol assay to droplets requires thorough design and integration of different components which have been discussed in the following sections.

4.8.1.1. Phased peristaltic pump

The multi-pump system described in section 5.4 has been implemented to perform the initial droplet assay and to optimize the reaction time, droplet size and mixing ratio of sample and reagents.

For majority of the other experiments described throughout this chapter a stepper motor (Dual Shaft, 57.2 mm, Bipolar, Unipolar, 0.53 N-m, 600 mA) peristaltic pump (fabricated by SWS) has been used. Figure 69 shows photographs of the (a) pump after assembly, (b) the pump with pump bed unclipped, revealing the roller design and (c) the 3D printed pump head and a pump bed with 4 Santoprene tubing pumplines glued on. The stepper motor has a USB power supply which can either be powered from the mains using an adaptor or via a laptop. This version of the pump has been fabricated by SouthWestSensor Ltd.

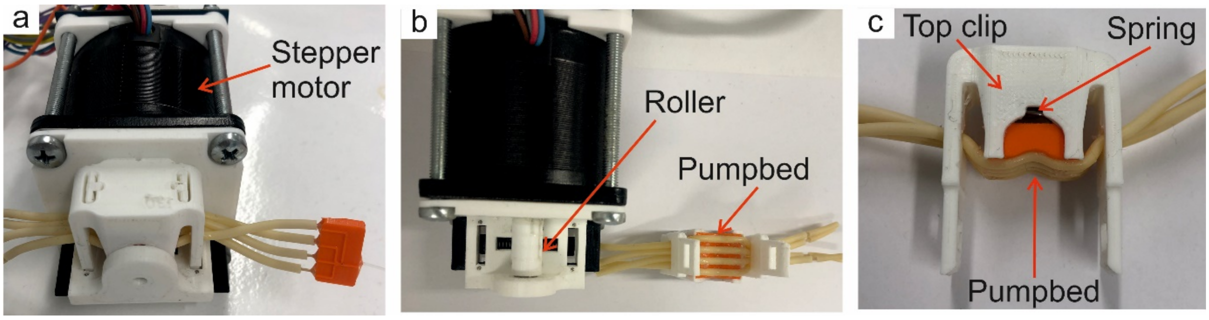

Figure 69. *Photographs of the stepper motor peristaltic pump. (a) Pump after assembly, (b) the pump with the pump bed unclipped, revealing the roller design and (c) the 3D printed pump head and a pump bed with 4 Santoprene tubing pumplines.*

4.8.1.2. Microfluidic chip

Two types of microfluidic chips were used for the various experiments discussed in this chapter. One type is PDMS chip and the other 3D printed chips. A PDMS microfluidic chip (100 µm × 600 µm channels) with three- inlets leading to a Y-junction and an oil line at 90 degree (Fig. 70 (c) (ii)) was used for the first set of experiments. A 3D printed mould (Fig. 70 (a)) designed in SolidWorks and printed using Objet500 Connex3 polyjet printer (Stanford Marsh Ltd) in the "VeroClear" material in glossy mode was used to fabricate the PDMS chip (McDonald and Whitesides, 2002). 0.5mm ID and 0.7 mm OD (UT5) PTFE tubes from Adtech Ltd were inserted into the inlets and outlet of the chip and sealed with liquid PDMS to prevent any leakage. Fabrication steps have been explained in detail in section 3.5 (cortisol chip section). A more durable 3D printed (PLA material) microfluidic chip (650 µm diameter channels) designed and fabricated by collaborator SWS was used for further experiments and for the field deployment prototype as can be seen in Fig. 70 c (i). PEEK tubing (0.51 mm ID) was used for inlet and outlets and were glued in position using epoxy glue. The 3D printed microfluidic chip does not require surface treatment for hydrophobicity like the PDMS chip and hence is more robust for long term usage. Sealing the tubes to the chip inlets and outlets prevents leakage of reagents and sample. Care has to be taken while inserting the PTFE and PEEK tubing for PDMS and PLA chip outlets respectively so that no gap remains between the chip channel and the tubing. A seamless transition from the chip channel to the outlet tubing prevents accumulation of product which may lead to cross contamination and droplet breakup.

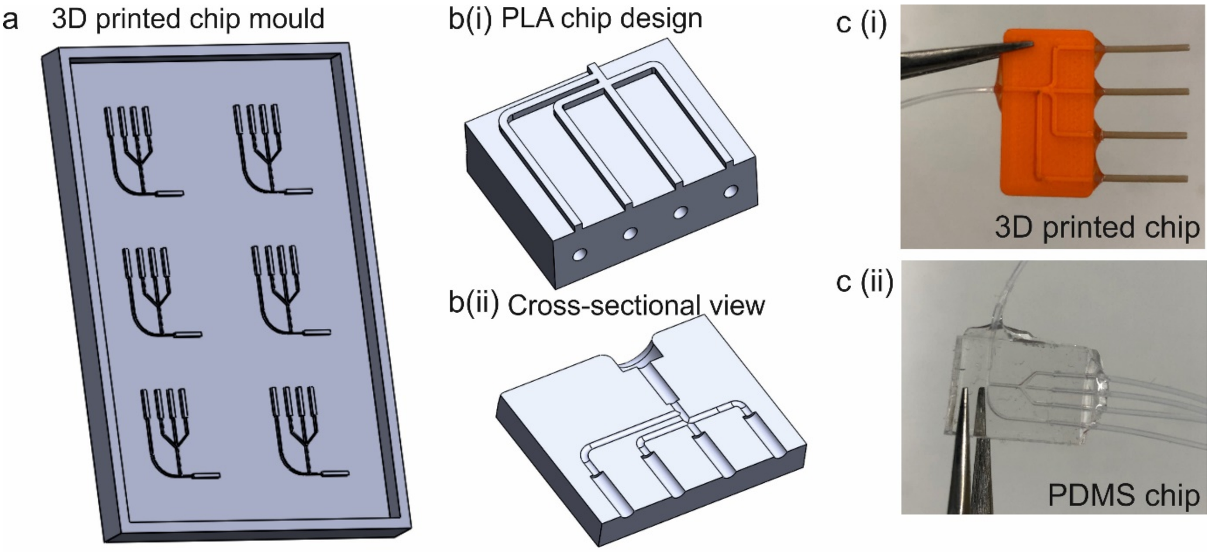

Figure 70. *Microfluidic chips used for experiments presented in this chapter. (a) Solidworks CAD file of mould (to be printed using VeroClear material) for fabricating the PDMS chip in (c. ii). (b. i,ii) Solidworks CAD file of microfluidic chip to be printed using PLA material. (c. i) Photograph of 3D printed microfluidic chip (650 µm channels) with PEEK tubing inlets and a PTFE tubing outlet. (c. ii) Photograph of a PDMS microfluidic chip with PTFE tubing inlets and outlet.*

4.8.1.3. In-line absorbance flowcell

The miniaturised flowcell for quantifying the droplet composition consists of a single 3D printed (Black PLA material) unit with grooves for an LED (2.5 V Red LED PLCC 2 SMD, Kingbright KA-3528SRT, RS components), photodetector (TSL257-LF, RS components) and 0.7 mm ID PTFE tubing (UT7, Adtech Ltd). Two more variations of this flowcell design were fabricated with 0.5 mm ID tubing (UT5) and 0.6 mm ID tubing (UT6). A multipath flow cell designed by Dr. Bingyuan Lu was also tested for an experiment to increase the limit of detection of the assay whenever is necessary. The design of the multipath flow cell consists of a 3D printed (black PLA material) unit with groves for an LED (2.5 V Red LED PLCC 2 SMD, Kingbright KA-3528SRT, RS components) and photodetector (TSL257-LF, RS components) as used for the design mentioned above with the addition of two plastic mirrors (laser cut to 4 x 10 mm, 4 x 6 mm and 4 x 4 mm) on either side to reflect the light through the tubing and increase the pathlength by internal reflection. The LED and photodetector are positioned at an angle (73.3°) to allow the light to reflect several times before reaching the detector and provide an optical path length of 24 mm. A PTFE (TR20 from Adtech Ltd) tubing was used which was shrunk using a heat gun into 2mm width and height square channel by inserting a metal rod. Solidworks CAD files of the flowcell designs can be seen in Fig. 71.

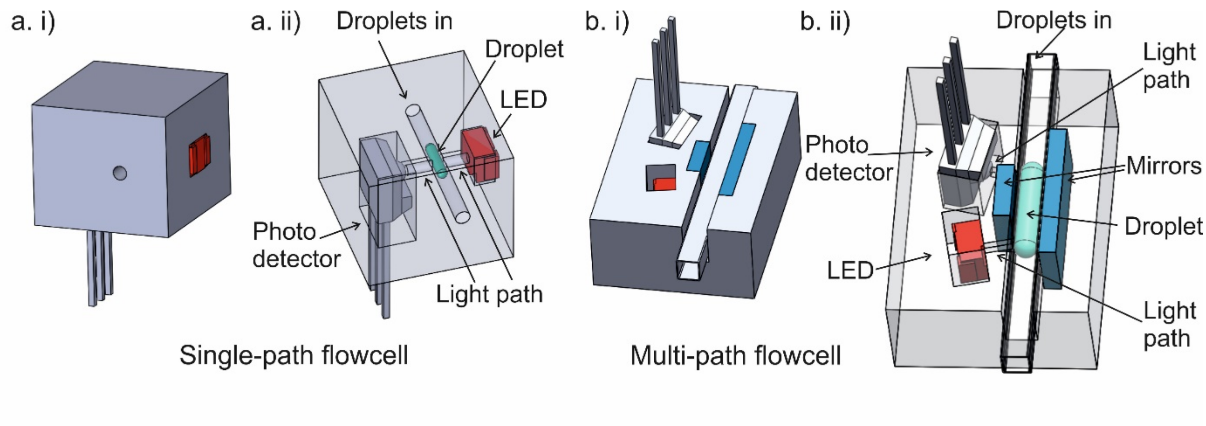

Figure 71. *(a. i-ii) Solidworks 3D CAD model of a single path flow cell with 0.7 mm pathlength, consisting of a LED-detector pair and a 0.7 mm ID PTFE tubing (b. i-ii) Solidworks 3D CAD model of a multipath flowcell consisting of an LED-detector pair, plastic mirrors and a square 2mm PTFE tubing.*

4.8.2. Initial qualitative test for observing colour development in droplets

A qualitative experiment was designed to observe colour development in droplets and to optimize the sample and reagents mixing ratio and droplet composition. In order to do so, a multiple pump platform (details in Chapter 5, Section 5.4) was incorporated and three pumps were utilised. One pump was used for pumping the ammonium sample, another pump introduced both Salicylate and DIC reagents and the third pump pumped in the required amount of oil. The setup also consisted of a heating plate for increasing the reaction time and a single path 660 nm wavelength flowcell (section 4.8.1.3). Approximately 15 cm of 0.5 mm inner diameter PTFE tubing was attached on the heating plate in a serpentine layout to observe change in colour and the temperature of the heating plate was set to 55°C. Figure 72 shows a picture of the multiple pump set up, the system schematic and the development of colour in droplet in approximately 10 minutes.

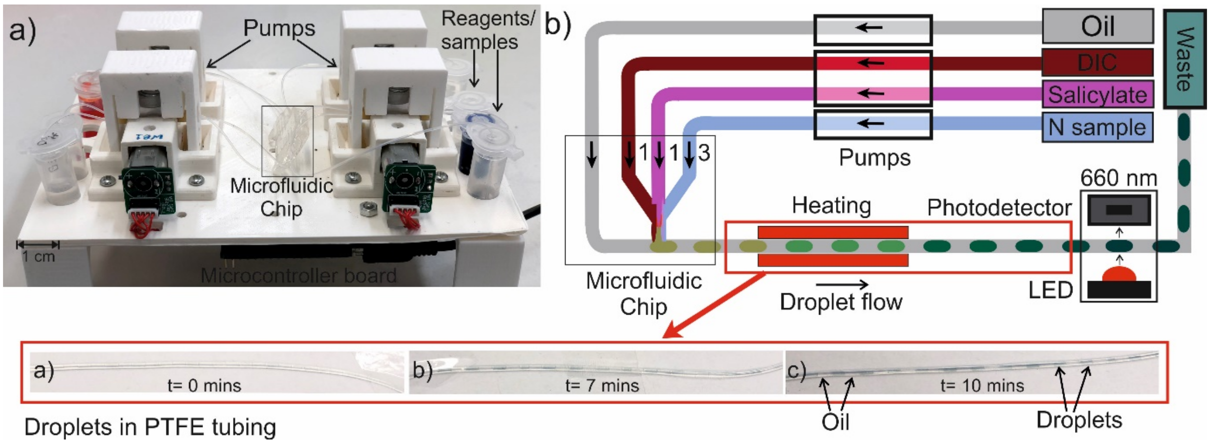

Figure 72. *Indophenol blue assay colour development in droplets by optimizing the sample: DIC: Salicylate mixing ratio and droplet composition. a) Multiple pump setup used to generate droplets of desired volume and ratio and observe colour development. b) Droplet platform schematic with inset of photographs of droplets in PTFE tubing showing gradual colour development.*

The first sequence of droplets were generated by introducing the sample and reagents in 1:1:1 ratio. Very light colour development was observed even for higher concentrations such as the 2 mg/l standard. Another sequence was then implemented by pumping the sample and reagents in 3:1:1 ratio. The colour development was more visible. This was predicted as the 3:1:1 ratio of sample to reagent means less dilution of the sample than the 1:1:1 ratio. Based on this primary observation, the sample: DIC: salicylate ratio was selected to be 3:1:1. An increase in droplet length by 1.67 times also meant slightly longer droplet plateau at the detector end and less influence of lensing effect of light around droplet edges on the plateau detection.

Once a mix-and-read assay has been optimised using multiple pump system, the multiple pumps can be replaced with a single, high-power pump as has been the case in this application. For field deployment, the multiple pump platform has been replaced by a stepper motor pump which has better long-term performance as has been shown in our nitrate/ nitrite sensor (Nightingale et al., 2019a). Therefore, multiple pumps can be replaced by a single pump in case they become redundant after assay optimisation. However, multiple step assays or assays which require droplet volume or ratio adjustment on-demand, will always benefit from having multiple pumps as can be seen in Chapter 5.

4.8.3. Indophenol blue assay in droplets

After finalizing the mixing ratio of reagents and standards/ sample and observing colour development, the assay was carried out using a single peristaltic pump set up. The experimental setup consisted of a stepper motor peristaltic pump (section 4.8.1.1) connected to a 3D printed microfluidic chip (section 4.8.1.2) and a 3D printed single path 660 nm wavelength flowcell (section 4.8.1.3). The four line pump introduced ammonium standard, DIC reagent and Salicylate reagent to the 3D printed PLA microfluidic chip forming 4 mm length droplets of approximately 752 nL in 0.5 mm ID tubing. The roller features were designed for generating 3:1:1 ratio droplets separated by a pulse of oil per rotation. Figure 73 shows the schematic diagram of the experimental setup of the prototype sensor system. After generation, the droplets travelled through the PTFE tubing on a heating plate set at 55°C which was used to accelerate the reaction. The droplets then travelled to the in-line spectrophotometer for colorimetric detection at 660 nm.

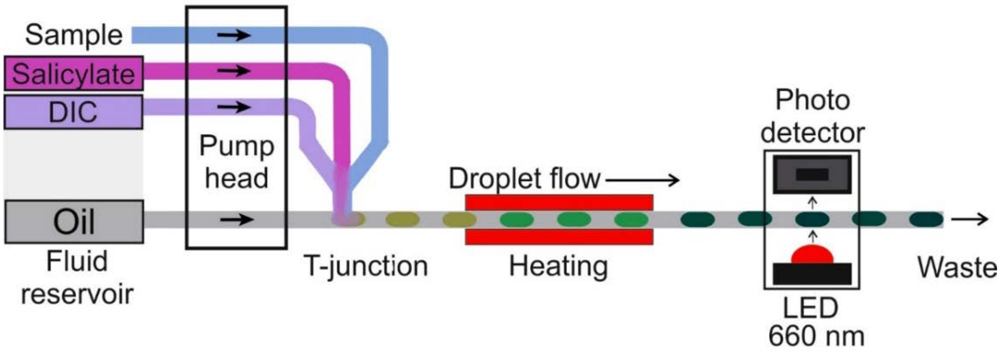

Figure 73. *Schematic of microfluidic platform and fluidic pathway for continuously measuring ammonium. A stepper motor peristaltic pump in conjunction with a 3D printed microfluidic chip generates droplets for ammonium measurement and after heating at 55°C the colour change is detected by an in-line spectrophotometer.*

4.8.4. Raw intensity data from inline spectrophotometer

The inline flowcell/ spectrophotometer was used to characterise the colour change from yellow (colour pre-reaction due to salicylate reagent) to blue due to the formation of the indophenol product. The colour development is directly proportional to the concentration of ammonium. A 0.7 mm pathlength flowcell (3D printed, Black PLA material) was used to quantify the droplet constituents (Fabrication details in section 4.8.1.3). Figure 74 is a screenshot of the GUI (full screenshot of GUI in appendix, Fig. 125) showing the gradual increase in raw light intensity from the flowcell detector as the concentration of the ammonium standard decreases. The top part of the raw data indicates oil level (which acts as a baseline) and the plateaus below 700 intensity are either blank droplets or standard droplets. The sudden drop in the intensity value in between the different standards indicate introduction of air bubbles in the system when changing the standards for producing the calibration curve. The inset in Fig. 74 shows the characteristic square wave signal generated from the flow cell due to passage of coloured droplets and oil alternatively. The signal quality deteriorates for lower concentrations as the lensing effect becomes more pronounced indicated by the large spikes on either side of each plateau. However, the 0.7 mm pathlength still allows us to measure up to 0.1 mg/l regardless of the drop in signal quality. There is a slight shift in oil level as the experiment proceeds but the effect of it is post corrected while calculating the concentration.

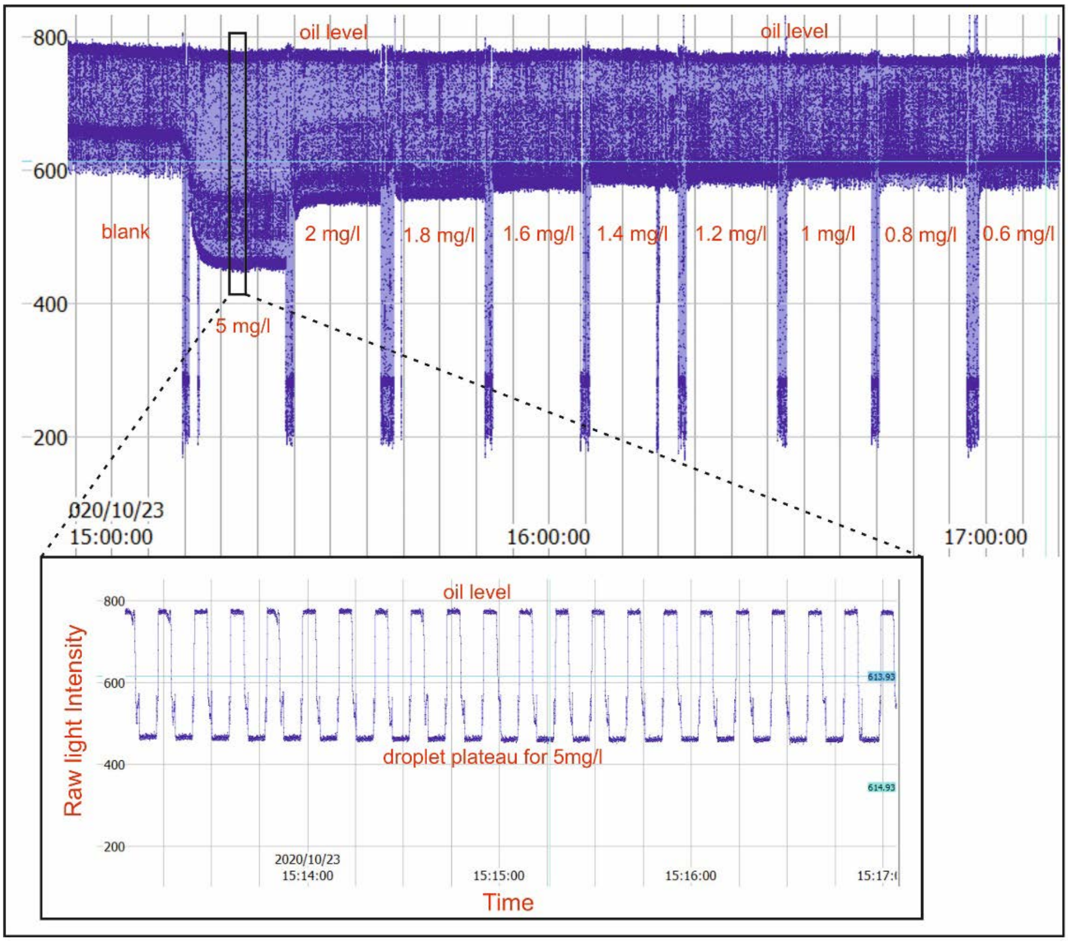

__Figure 74.__ Screenshot from the SWS GUI displaying raw intensity data obtained from the 0.7 mm single path flowcell. The raw light intensity signal shows the oil level and droplet plateaus for different ammonium standards starting from 5 mg/L all the way down to 0.1 mg/L. The top part of the raw data indicates oil level (which acts as a baseline) and the plateaus below 700 intensity are either blank droplets or standard droplets. The sudden drop in the intensity value in between the different standards indicate introduction of air bubbles in the system when changing the standards. The inset shows a zoomed in picture of the droplet plateaus obtained for 5 mg/L ammonium standard for a duration of about 4 minutes.

4.8.5. Standard calibration curve from raw intensity data

Once the raw intensity data were obtained, the Beer Lambert law was used to calculate absorbance values and a calibration curve was generated for 0.1 mg/L to 5 mg/L ammonium standards. The calibration curve showed a linear trend validating the assay for the measured range as can be seen in Fig. 75. 10 droplets were measured for each standard data point. The limit of detection was determined to be 0.05 mg/L for the optical pathlength of 0.7 mm following the 3-sigma method. The limit of detection has been calculated by the formula $OD = {}^{3S_D}/_{m}$, where S_D is the standard deviation of the blank and *m* is the slope of the calibration curve.

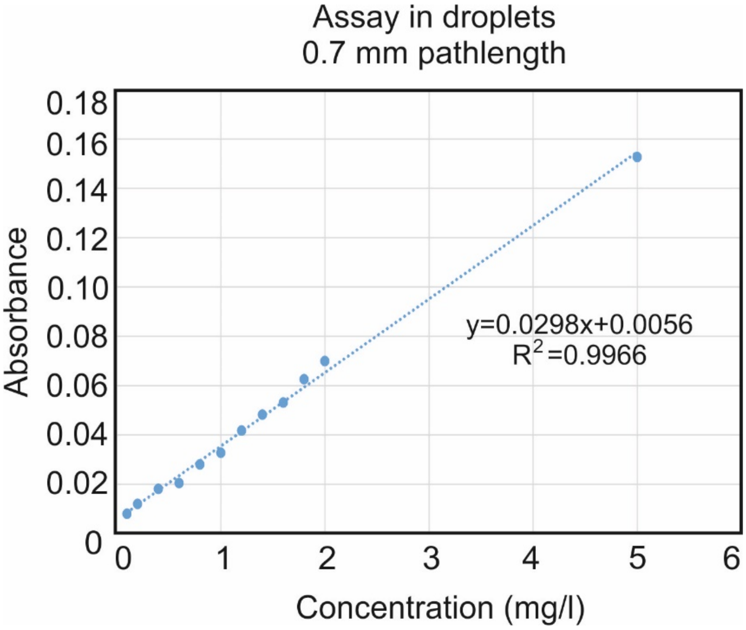

Figure 75. *Standard calibration curve obtained for the indophenol blue assay for ammonium generated from the absorbance data obtained from 0.7 mm single pathlength flowcell. The calibration curve shows a linear trend for the 0.1-5 mg/L range. The limit of detection was determined to be 0.05 mg/L using the 3-sigma method.*

4.8.6. Droplet data vs spectrophotometer data

The assay was also carried out in cuvettes for spectrophotometric detection with the same reagents and standards that were used in the droplet assay described in the previous section. A few higher concentrations were also passed through the spectrophotometer and a linear calibration graph was obtained for the 0-5 mg/L range. Fig. 76 (a) shows a picture of cuvettes containing different ammonium standards (increasing concentration from left to right) after completion of reaction. Fig. 76 (b) presents the calibration curve generated from the absorbance data obtained from the spectrophotometer. Saturation can be seen beyond 5 mg/L indicating either that all of the reagents have been used up or that the spectrophotometer has reached its maximum possible detection.

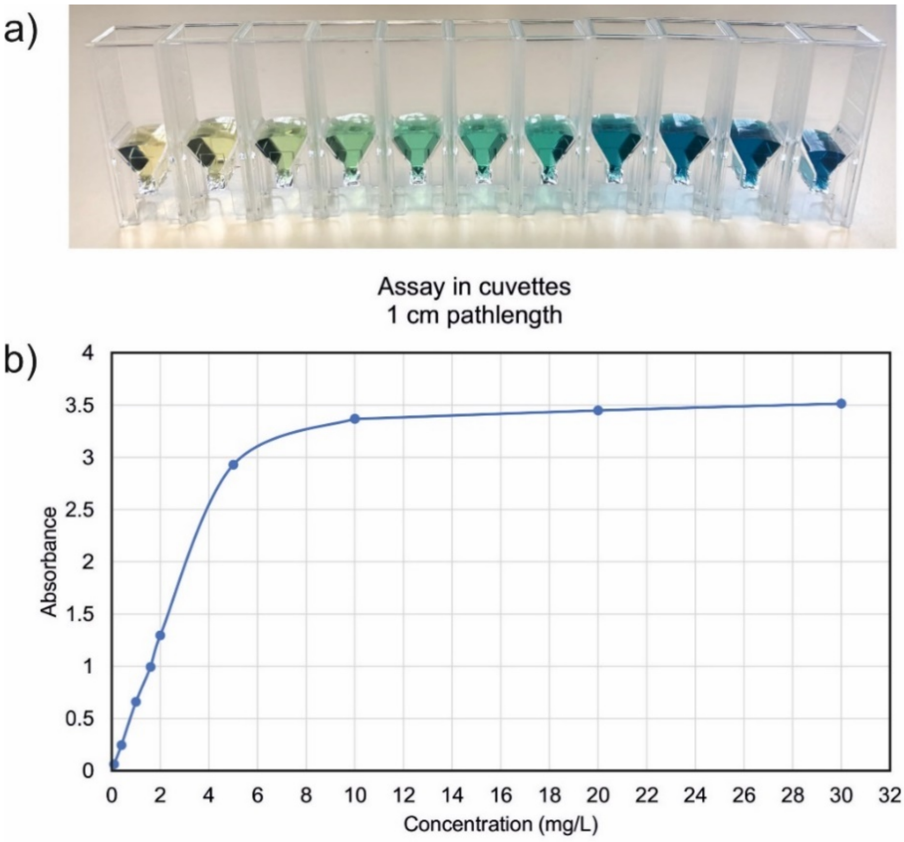

Figure 76. *Indophenol blue assay in cuvettes. (a) Photograph of cuvettes containing different ammonium standards (increasing concentration from left to right) after completion of reaction. (b) Calibration curve generated from the absorbance data obtained from the spectrophotometer for an optical pathlength of 1 cm.*

When compared for the range 0 - 5 mg/L, the calibration curve for both the spectrophotometer and droplet assay shown in Fig. 77 demonstrated similar linear trend. The absorbance values are roughly 14 times smaller for the droplets, as expected for smaller pathlength of the flow cell which is 0.7 mm as compared to that of the spectrophotometer which is 10 mm.

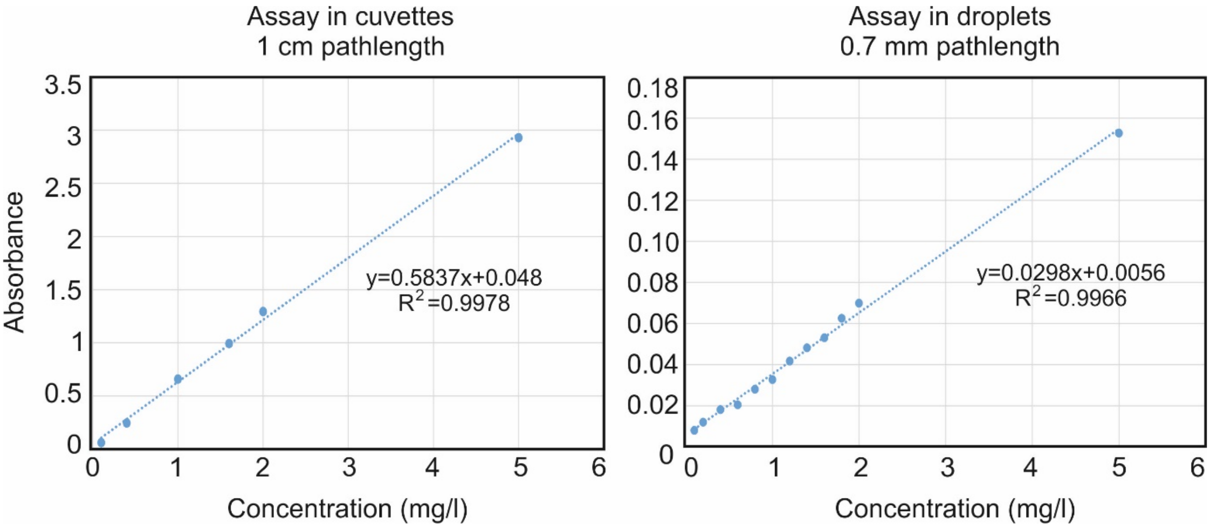

Figure 77. *Comparison of assay carried out in cuvettes with the droplet assay. Both the calibration curve show a linear trend. The assay in droplets show much lower absorbance due to the smaller pathlength of the flow cell (0.7 mm) compared to that of the cuvettes (10 mm).*

4.9. Flow cell calibration comparison and finding the lower limit of the droplet assay

Increasing the optical path length can result in achieving lower detection limits and this can be implemented in different ways. Two methods that we have tested for this application are increasing the tubing diameter so that the droplet diameter increases and hence the optical path length. Another method has been implementing mirrors inside the flowcell on either side of the droplet and positioning the LED and detector at an angle so that the light from the LED reflects through the droplet several times before reaching the detector. The detector designs and fabrication steps have been described in section 4.8.1.3.

A series of flowcells with different pathlengths such as 0.5 mm, 0.6 mm and 0.7 mm and 24 mm (multi-path flowcell) were tested with 5 different ammonium standards (0.156 mg/L, 0.3125 mg/L, 0.625 mg/L, 1.25 mg/L and 2.5 mg/L). Raw light intensity data obtained from each flow cell was used to generate calibration curves which demonstrated good linearity and sensitivity. The 0.5 mm, 0.6 mm and 0.7 mm pathlength flowcells behaved in a similar way and the absorbance values obtained from them were very close (Fig. 78). The 0.5 mm flowcell demonstrated the lowest absorbance values as expected but interestingly, the 0.6 mm flowcell gave higher absorbance than the 0.7 mm pathlength flowcell for all the ammonium standards. The reason for this variation could have been due to fabrication error during 3D printing. The limit of detection has been calculated by the 3-sigma method where, $OD = {}^{3S_D}/_{m}$, S_D is the standard deviation of the blank and m is the slope of the calibration curve. The LOD for 0.5 mm, 0.6 mm and 0.7 mm pathlength were 0.078 mg/L, 0.023 mg/L and 0.05 mg/L respectively. Micro milling the flowcell channel and light path on PMMA material could result in finer groves and better alignment but that requires much longer time for fabrication and assembly.

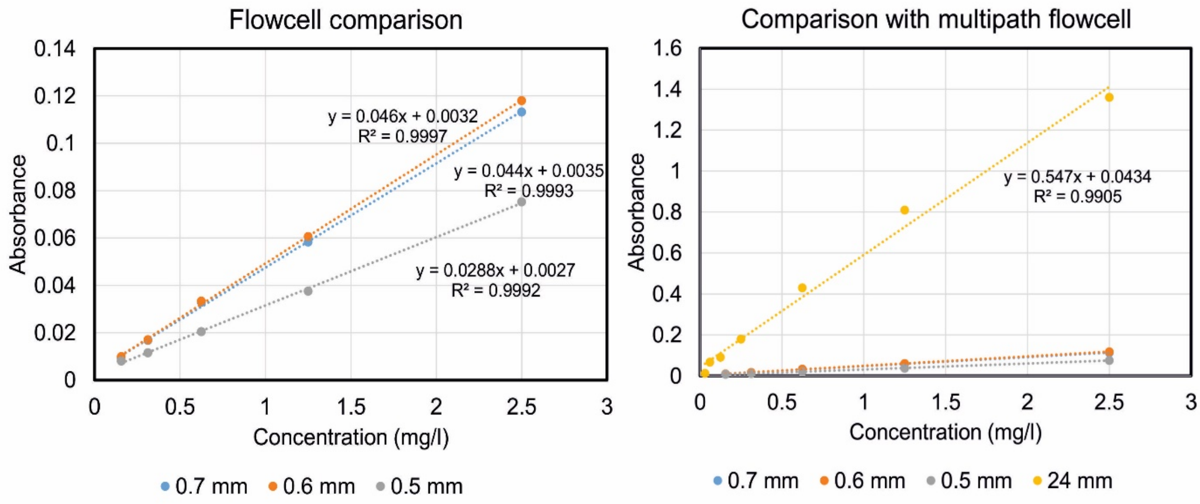

Figure 78. *Calibration curves generated from raw light intensities obtained for 0.5 mm, 0.6 mm and 0.7 mm flow cell for different ammonium standards. A 24 mm multipath flowcell was used to increase the lower detection range. All the flowcells demonstrated good linearity and sensitivity. The LOD for 0.5 mm, 0.6 mm, 0.7 mm and 24 mm pathlength were 0.078 mg/L, 0.023 mg/L, 0.05 mg/L and 4.6 µg/L respectively.*

A 24 mm pathlengh flowcell (Fabrication procedure explained in section 4.8.1.3) was utilized in order to reach a lower detection limit. The absorbance measurements from the 24 mm pathlength flow cell generated a linear calibration (Fig. 79) curve giving us values until 0.06 mg/L which is considerably better than the lower limit (0.3 mg/L) reached by the UT7 flow cell and the LOD using the 3-sigma method was 4.6 µg/L. The LOD of the assay can be further improved by changing the angle of the mirror in the multipath flowcell, hence increasing the pathlength and making the droplet assay more applicable for different scenarios.

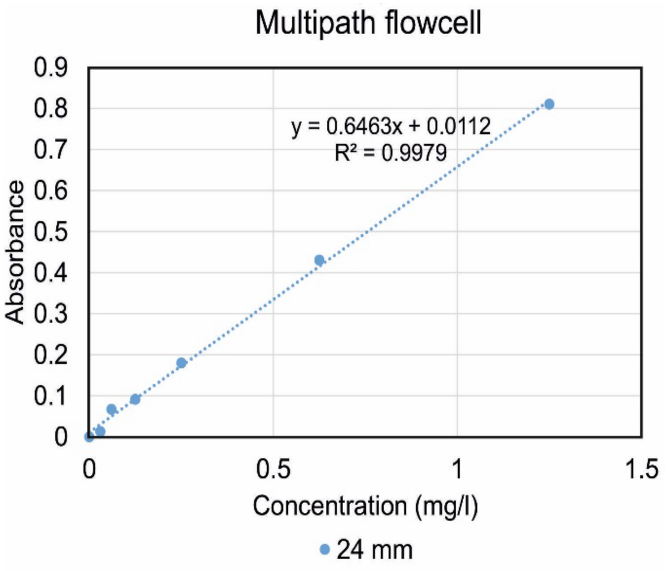

***Figure 79.** Calibration curve generated from raw light intensities obtained for 24 mm flow cell for different ammonium standards. Graph shows good linearity and sensitivity. The LOD using the 3-sigma method was calculated to be 4.6 µg/L.*

Other than increasing the pathlength, the limit of detection and range could also be increased by adjusting the concentration of reagents. A quick test performed by Carla Ruggiero (SouthWestSensor Ltd) showed that higher absorbance values could be achieved by using undiluted reagents for the 3:1:1 ratio, as illustrated in Fig. 80. Indeed, undiluted reagents did give higher absorbance values compared to the diluted reagents indicating that the sample was not fully being used up when the reagents were diluted.

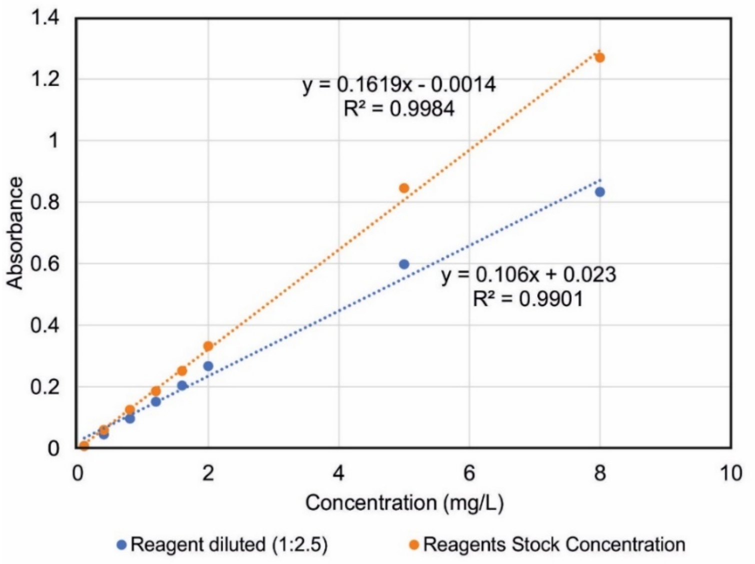

***Figure 80.** Standard calibration curves generated for assays using undiluted and 2.5 times diluted samples.*

4.10. Measuring ammonium in river water samples

After characterising its functions using lab samples, the droplet system was validated by measuring ammonium in river water samples at high tide. Grab samples were obtained from 5 different sites in River Itchen which is a chalk stream river lying in the south coast of England, leading up to the English Channel. The river water samples were collected by Dr. Adrian Nightingale. The samples were collected using a syringe, filtered and stored in centrifuge tubes. The syringe (25 mL, BD Plastipak) was rinsed three times. 20 mL sample was then passed through the syringe filter (Biofil PES 0.45 µm). The centrifuge tubes (15 mL) were also rinsed thrice before finally filling up. The map in Fig. 83 (a) displays the sample collection points. The sample collection locations lay both upstream and downstream from the Woodmill tidal barrier (Fig. 83 (b)) as indicated on the map. Figure 81 shows the colour development of the standards and samples in well plate from the five different river water sites after completion of the assay. The mixing ratio used was 3:1:1 for Sample/standards: DIC: Salicylate reagent.

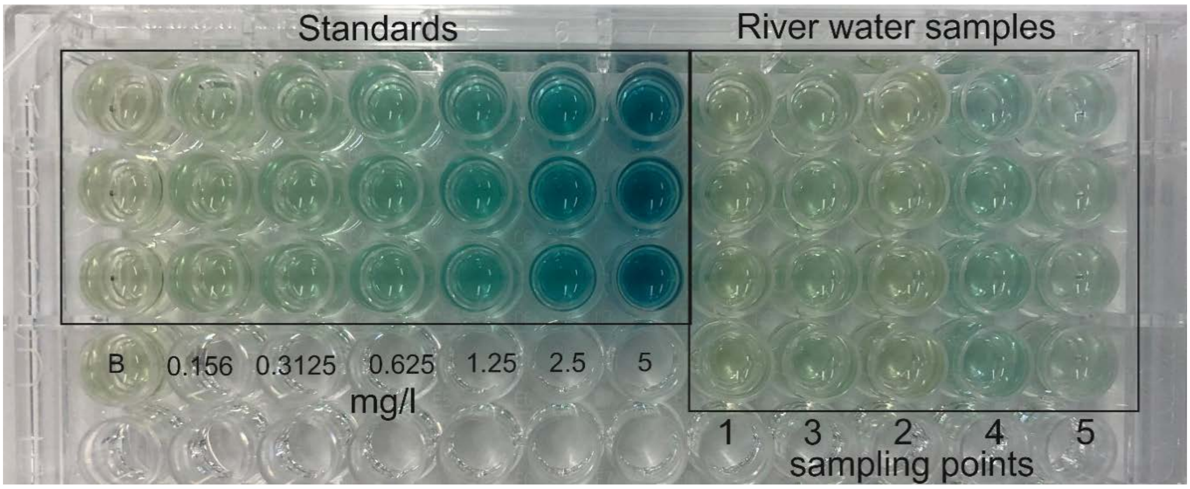

Figure 81. Well plate assay for ammonium standards and river water samples for measuring ammonium. Standards show a gradual increase in colour from left to right indicating increase in concentration of ammonium. River water samples show light colour development with sample from point 4 showing most colour.

The assay was carried out in both the well plate and droplets on the same day and calibration curves were generated for the range 0-5mg/l and 0-2.5 mg/l respectively. The calibration curves obtained from the absorbance values of the spectrophotometer for the well plate assay and for droplet assay can be seen in Fig. 82. Both the assays show linear trend and as expected, the absorbance values obtained from the flowcell are lower due to the smaller pathlength. The ammonium concentrations of the river water samples were recovered from the calibration curves for both the droplet and well plate assay.

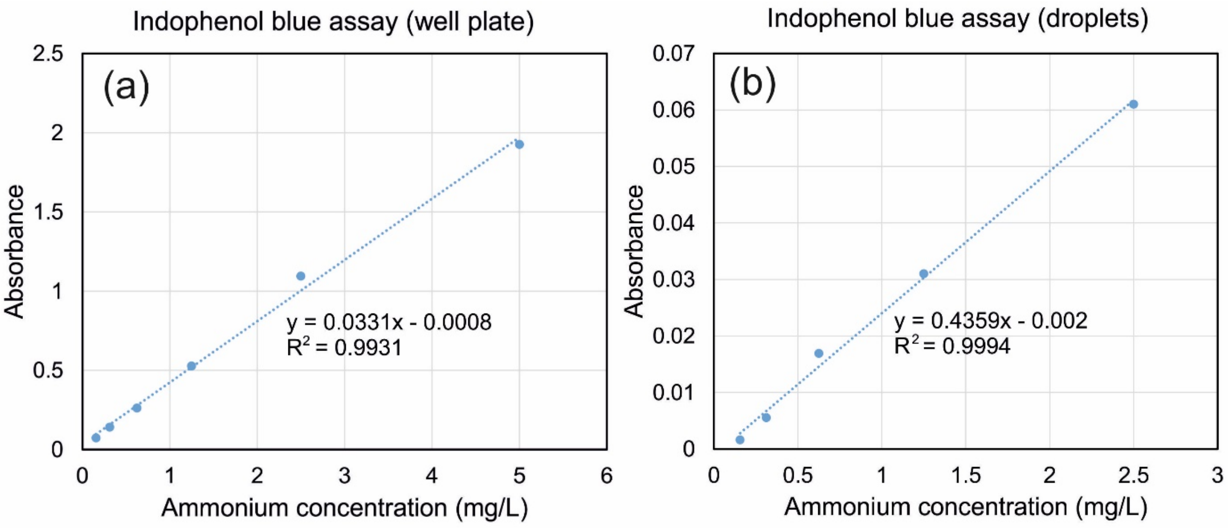

Figure 82. *Standard calibration curves obtained from well plate and droplet assays for river sample analysis. (a) Standard calibration curve plotted from well plate assay for river water sample analysis. (b) Standard calibration curve plotted from droplet assay for river water sample analysis.*

Comparing between the concentration values obtained from the droplet and well plate-based assays, the values are fairly close to each other for sampling sites 1, 2 and 3, however, larger deviation is seen for sample points 4 and 5 which are further away from the tidal barrier and slightly closer to the sea. There is a sharp increase in ammonium concentration at sampling point 4 which can be attributed to there being an effluent outlet. The measurement from sample point 5 is marked in red in Fig. 83 (c) as during the well plate-based assay, precipitate formation was observed deeming this particular result inconclusive.

The error bars for the well plate assay represent the standard deviation in absorbance values of three repeats. The error bars from the droplet assay droplet assay represent standard deviation of 10 droplet data points per analysis. The droplet system does demonstrate good performance in measuring the ammonium levels when compared to the spectroscopic method (Fig. 84).

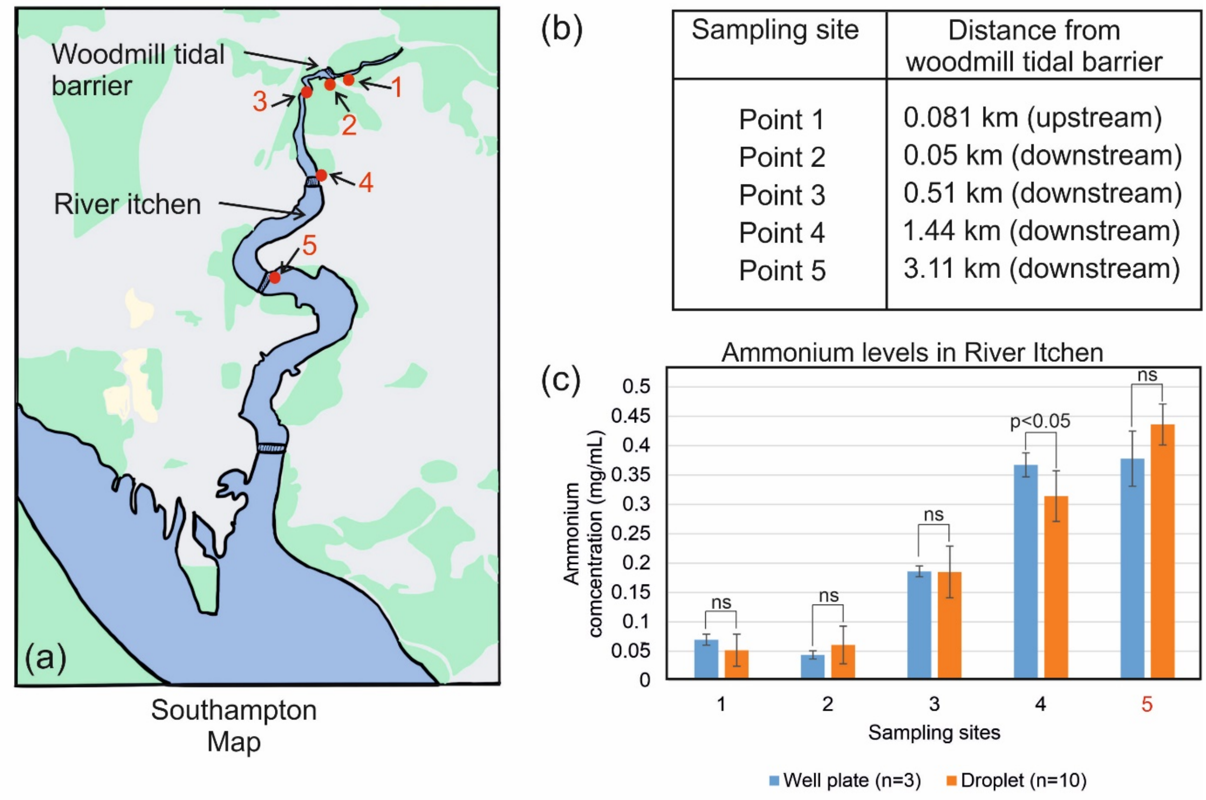

Figure 83. *Measuring ammonium levels in River Itchen. (a) Map showing River Itchen leading to the English channel. River water samples were collected from the labelled positions (1-5). (b) Distances of sampling points have been tabulated as upstream or downstream from Woodmill tidal barrier on River Itchen, Southampton. (c) Bar chart comparing concentration of ammonium in river water samples obtained from the well plate and droplet assay. Statistical analysis was performed using two-tailed Student's t test (Two sample assuming unequal variances). Sample point 5 is marked in red as during the well plate based assay, precipitate formation was observed deeming this result inconclusive.*

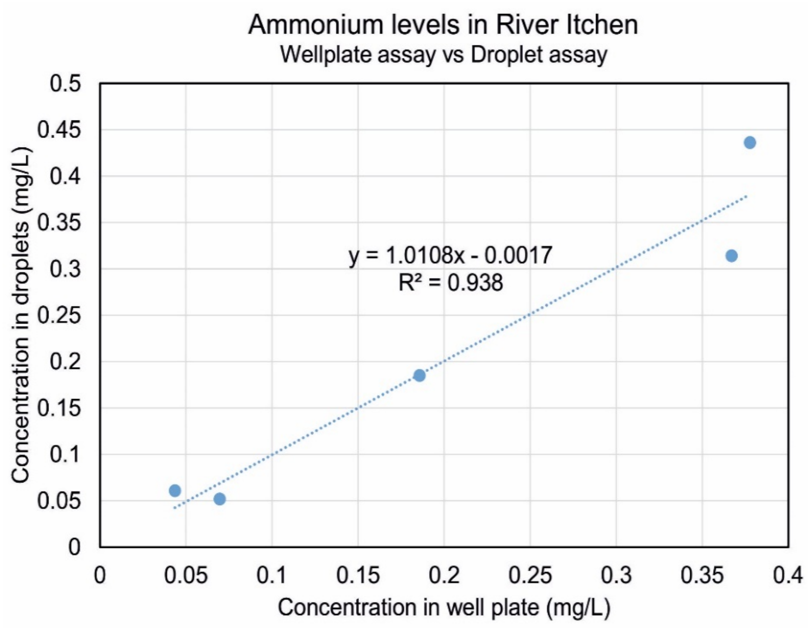

Figure 84. *Comparison between ammonium concentrations of the river water samples obtained from the well plate assay and the droplet assay.*

While carrying out the indophenol blue assay for the river waters samples, the solution in the well for sample point five went cloudy indicating precipitation. Reaction kinetics of the standards and river water samples showed characteristic trend with higher absorbance values for higher concentrations and a completion time of approximately 5 minutes. However, the reaction kinetics of river water from sampling point 5 showed inconsistencies in absorbance as time passed (Fig. 85). The absorbance spectra revealed a characteristic curve of precipitate formation and it followed a completely different trend from rest of the samples and standards (Fig. 86). All the sample points demonstrated peak absorbance at around 660 nm unlike the river water sample from sampling point 5. The formation of a cloudy precipitate was deemed to be due to the higher salinity as sampling point 5 is closest to the sea in comparison to all the other sampling points.

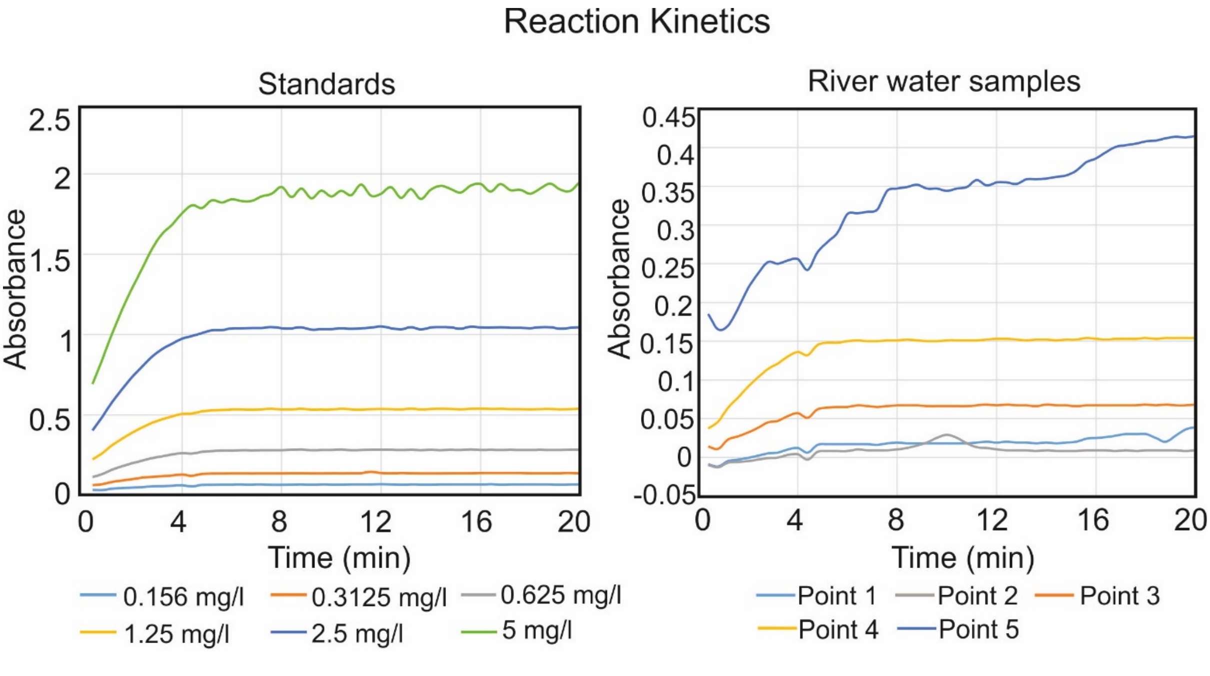

Figure 85. *Reaction kinetics of ammonium standards and river water samples for measuring ammonium. All samples and standards show full colour development by approximately 6 minutes except river water sample from sampling point 5.These values are all blank corrected.*

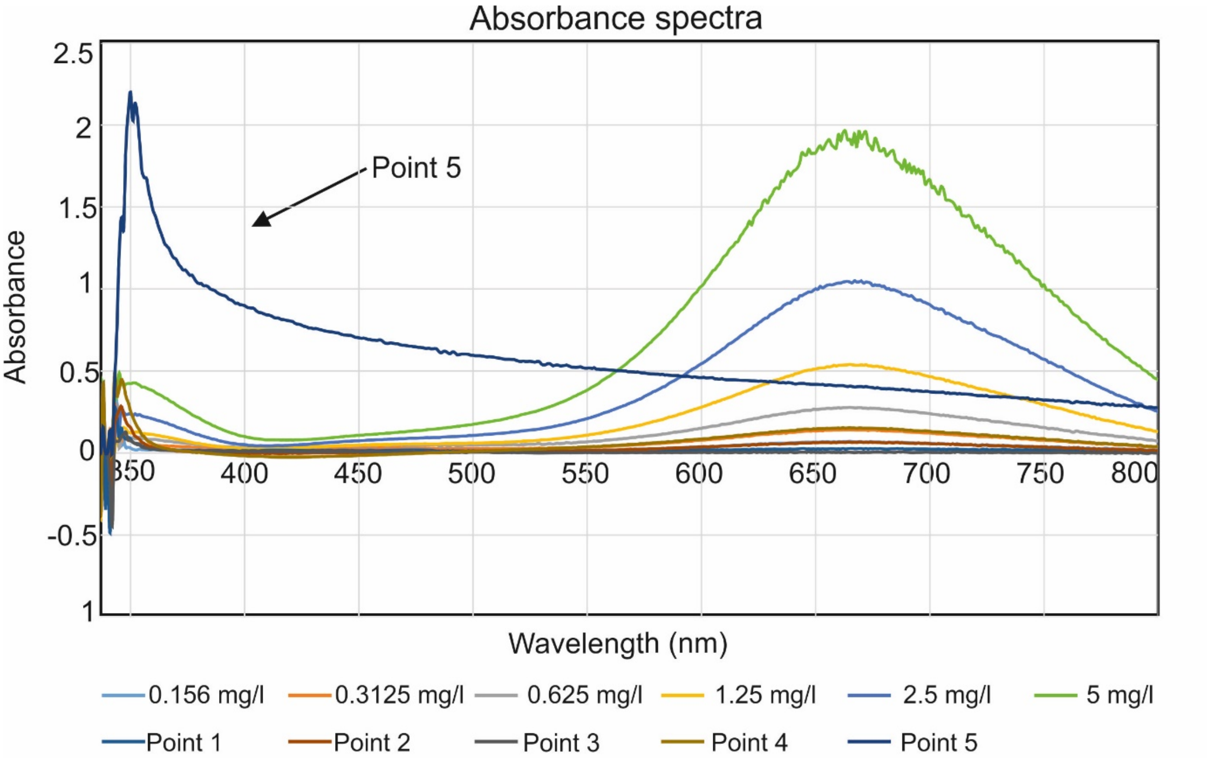

Figure 86. *Absorbance spectra from 350 nm to 800 nm wavelengths for river water samples and ammonium standards. All samples and standards excepting river water sample 5 demonstrate characteristic absorbance spectra with peak absorbance at 660 nm wavelength. Sample 5 shows absorbance spectra for precipitate formation.*

4.11. Crosstalk experiment

Although the current method we have been incorporating to measure ammonium in well plate, limits us from measuring at higher salinity, droplets offer us other advantages. So far we have utilised droplets as individual reaction chambers however, recent studies have shown that analytes/solutes can leave the droplets and migrate to neighbouring droplets via surfactant driven mechanisms or as has been observed by our group via gas mediated crosstalk (Nightingale et al., 2018). Gas mediated cross talk has been demonstrated successfully in droplets for measuring nitrate by our group (Nightingale et al., 2018). An experiment was designed and carried out with Dr. Adrian Nightingale to check if gaseous transport of ammonia is possible and detectable with the current assay protocol. This would help us circumvent events of precipitation and get reliable absorbance measurement in droplets.

The reaction protocol for the indophenol blue assay involves the conversion of the ammonium present to ammonia which in turn reacts with the salicylate. For the crosstalk demonstrating experiment, 150 µl of 1 M NaOH was used with 150 µl of sample/ standard to raise the pH of the droplet and hence formation of ammonia for migration. The reactions were carried out in petri dishes each containing two 300 µl droplets in close proximity to each other as can be seen in Fig. 87. One droplet had 150 µl standard/sample and 150 µl NaOH and the other droplet contained 150 µl of DIC and 150 µl of salicylate reagents.

Two standard and two sample droplets were used for the experiment. The blank droplet consisted of 150 µl deionised water and 150 µl NaOH. The other droplets included 5 mg/L ammonium standard, river water sample 4 and river water sample 5 instead of the de-ionised water. All these droplets had an adjacent reagent droplet. Once both the droplets were added, the petri dishes were covered, and time was allowed for the deprotonation of the ammonium and hence migration of NH_3 to the reagent droplet. The petri dishes were closely observed for a duration of 30 minutes for any colour change.

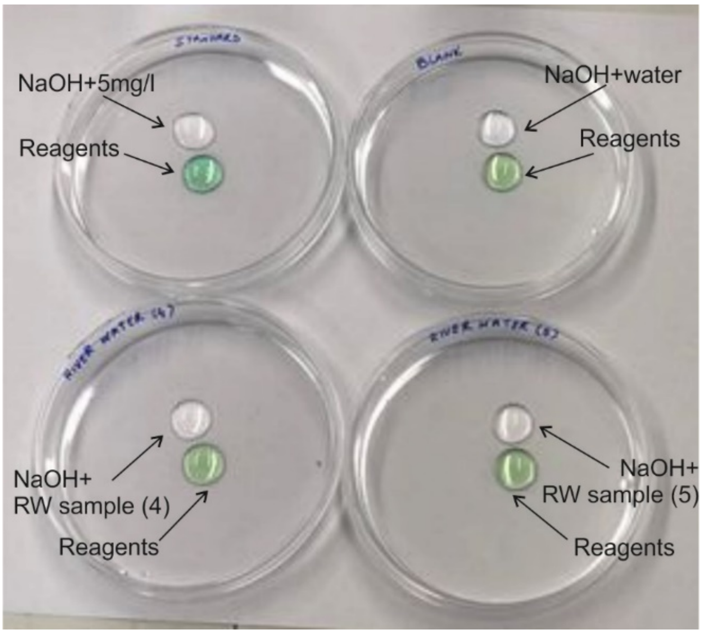

Figure 87. *Photograph of ammonium sample droplets with adjacent reagent droplets in a covered petri dish in the absence of oil. The sample compositions were NaOH+5mg/l ammonium, NaOH+river water sample 4 and NaOH+river water sample 5 of 150 µl each. The blank consisted of NaOH+water and the reagents droplets consisted of DIC and Salicylate (150 µl each). The picture was taken after approximately 20 minutes from when the droplets were deposited.*

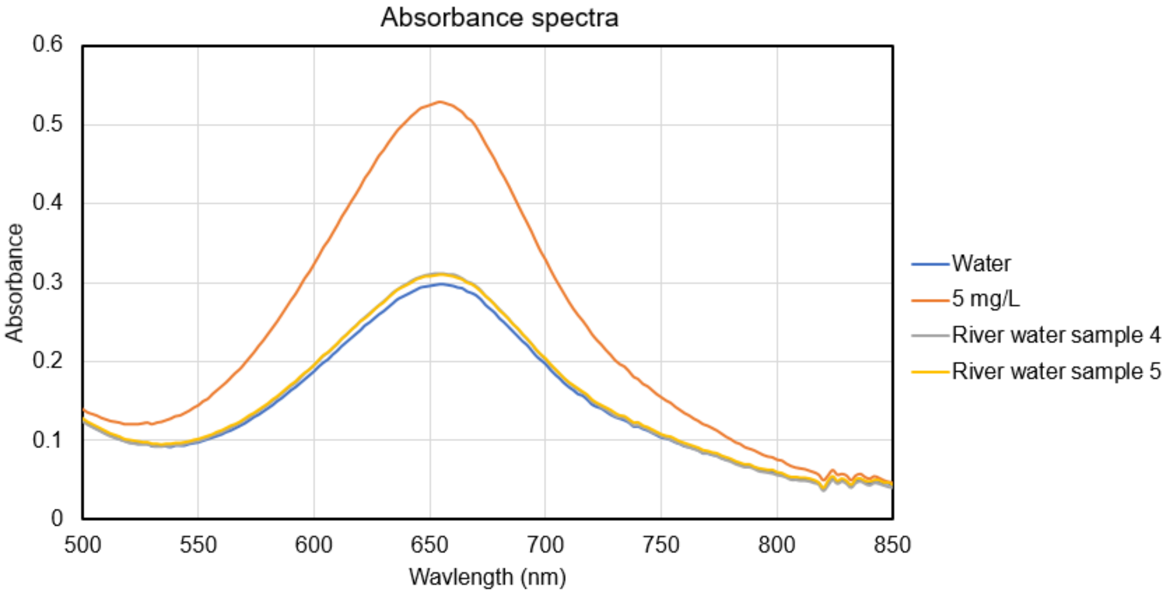

Figure 88. *Absorbance spectra of water, 5 mg/L ammonium standard and river water sample 4 and 5.*

All the reagent droplets developed a greenish blue colour indicating the transport of NH_3 and the formation of the indophenol derivative. After 30 minutes the reagent droplets were transferred to a well plate and absorbance measurements were taken. The graph in Fig. 88 shows the blank corrected absorbance measurements for the 5 mg/L ammonium standard and both the river water samples. All three samples show absorbance peaks at 660 nm with the 5 mg/L standard showing highest value. This experiment shows the potential that an alternative approach can be used with droplets for the measurement of ammonia for samples with higher salinity content. Further experiments need to be performed to validate this approach.

4.12. Monitoring ammonium in a sequential batch bioreactor

The ammonium sensor was further developed and deployed to a sequential batch bioreactor enriched with polyhydroxyalkanoates (PHAs) accumulating bacteria for continuous monitoring. Polyhydroxyalkanoates (PHA) are microbially produced polyesters which are biodegradable, biocompatible, and have tuneable mechanical and thermal properties and their microbial production has garnered vast research interest (Chen et al., 2011).

4.12.1. Components of ammonium sensor drybox

The ammonium sensor drybox (details of fluidic diagram and system schematic in section 4.12.2) was designed for deployment in a sequential bioreactor enriched with PHA accumulating bacteria. The system consists of the stepper motor peristaltic pump as detailed in section 4.8.1.1, a 3D printed microfluidic chip, flowcells (section 4.8.1.3) for colorimetric detection and heating module. A diaphragm pump (RS PRO, 4.5 V 11 psi, -8 psi Direct Coupling Water Pump, -360 ml/min, 580 ml/min) was used initially to transport the sample from the bioreactor to the peristaltic pump and was later changed to another commercial peristaltic pump due to performance failure. An in-house 3D printed filter was used to filter the sample before providing the sample to the peristaltic pump. The ammonium drybox sensor system components have been designed and fabricated by Simon Willis and Akash Srivastava of SouthWestSensor Ltd.

The PCB design and software development have been done by Brett Warren (SWS). The PCBs for the system have been designed using DipTrace CAD software and have been manufactured by third party based on Gerber export. The electronics for the system have been designed based on a 3-step approach. The first step is a set of dual-task digital sensor modules, and each is controlled by a Microchip AVR module from the AVR-1 series (ATTiny412 through ATTiny1614) and each controller runs the same code. The first task is to turn a resistor-based heater element on and off using a

MOSFET. There is a single target temperature. Measurement is taken using a Vishay surface mount NTC thermistor. The second task is to report colorimetry signal intensity of each passing droplet. An LED is used as a light source and a linear light level sensor measures the intensity of light that passes through the droplet. The LED is controlled with microprocessor PWM. The module reads raw intensity and detects transition of oil and aqueous phases. The LED PWM is adjusted automatically to keep Oil raw intensity at a fixed level. The calculation of absorbance and then of concentration is done on the mainboard. The flowcell module uses a 3D printed light path piece to ensure only the LED (2.5 V Red LED PLCC 2 SMD, Kingbright KA-3528SRT, RS components) light passing through the droplet is sensed using a detector (TSL257-LF, RS components).

The heater task is used to maintain the LED and light path piece at a stable temperature, which aids consistency of readings. The Heater modules uses the heater task to self-heat the entire PCB to a stable (35-65*C) temperature. The PTFE tubing containing the droplets can then be placed in direct contact with the surface using a coil or serpentine formation. Further plastic or metal pieces maximise the heat transfer before being placed in an insulation layer. The simplified module architecture means the module can be formed on single sided aluminium substrate PCB, which increases transfer efficiency.

The second step of the electronics is an interface conversion PCB. A single Microchip AVR DA series microprocessor (AT128DA28) captures data from the three sensor modules. Since tasks are identical between modules, the cable position is used to determine each module's purpose, and hence meaning of readings the sensor is reported. The interface conversion PCB then reports to the main board (3rd step of the system) controlling the entire system using a protocol specific to the main board.

4.12.2. System schematic of ammonium sensor drybox

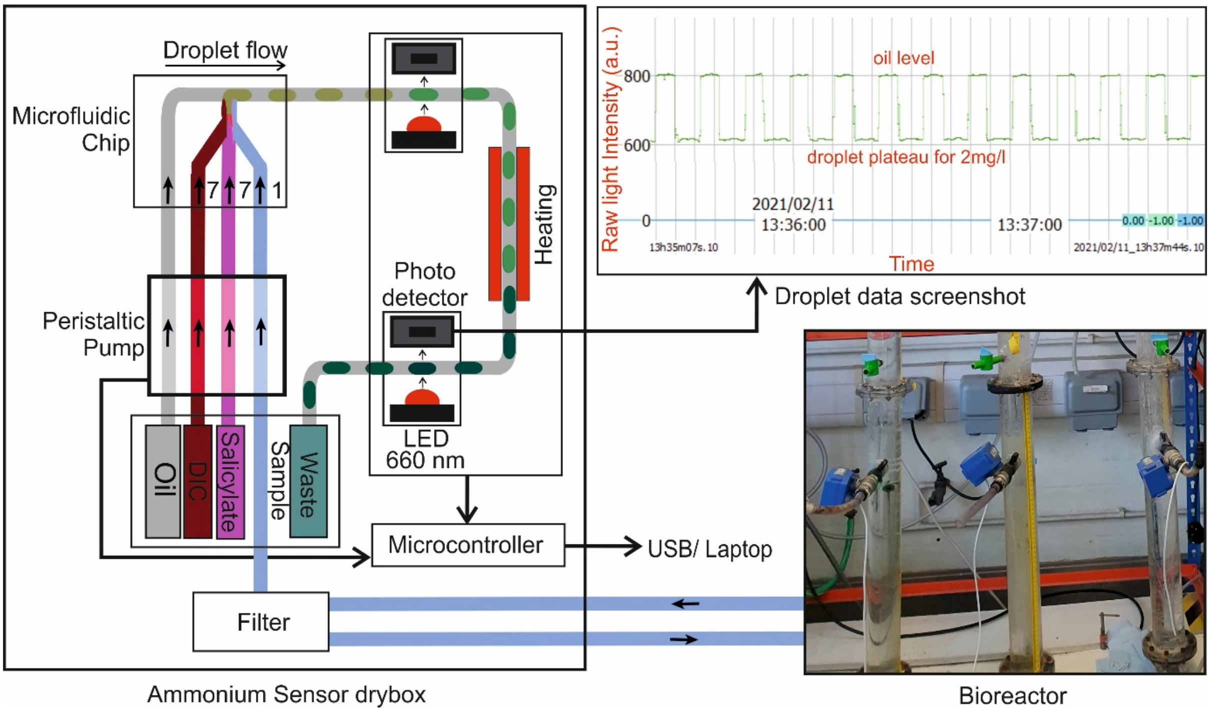

Figure 89. *Schematic of droplet microfluidic sensor system for monitoring ammonium levels in bioreactor enriched with PHA accumulating bacteria. Left panel displays the components of the drybox containing the liquid cartridge for reagents, a filter, peristaltic pump for fluid propagation, microfluidic chip, heater unit and flowcells.*

As shown in Fig. 89, a commercialized peristaltic pump was used to continuously circulate liquid sample from the bioreactor column at a flow rate of 60 mL/min. The microfluidic system utilized the stepper motor peristaltic micropump (section 4.8.1.1) and the sample liquid (via a filter), sodium dichloroisocyanurate (DIC) and salicylate solutions were pumped to a 3D printed chip (ABS material) where the aqueous co-flow was segmented into droplet by FC-40 oil. The droplet generation frequency is about 5 per minute and each droplet has a volume of approximately 1800 nL. A flowcell was placed just before the heater to ensure the quality of the droplets being produced. A homemade heater unit (section 4.12.1) kept the temperature of the droplets at 55 °C for 5 minutes while they were traveling downstream to a 0.7 mm direct path flow cell (section 4.8.1.3) for colorimetric detection at a wavelength of 660 nm. The raw light intensity data and waveform are shown in Fig. 89 top right panel and the concentration of ammonium can be calculated using Beer-Lambert law. Onboard calibration standards could also be added for quality control purposes over longer deployment periods (Nightingale et al., 2019a).

Figure 90 shows the raw intensity data generated during calibration of the sensor system before deployment. Ammonium standards from 0.1 mg/L to 20 mg/L were used to calibrate the sensor. The inset shows a zoomed in picture of the droplet plateaus and the characteristic square wave obtained for 2 mg/L ammonium standard.

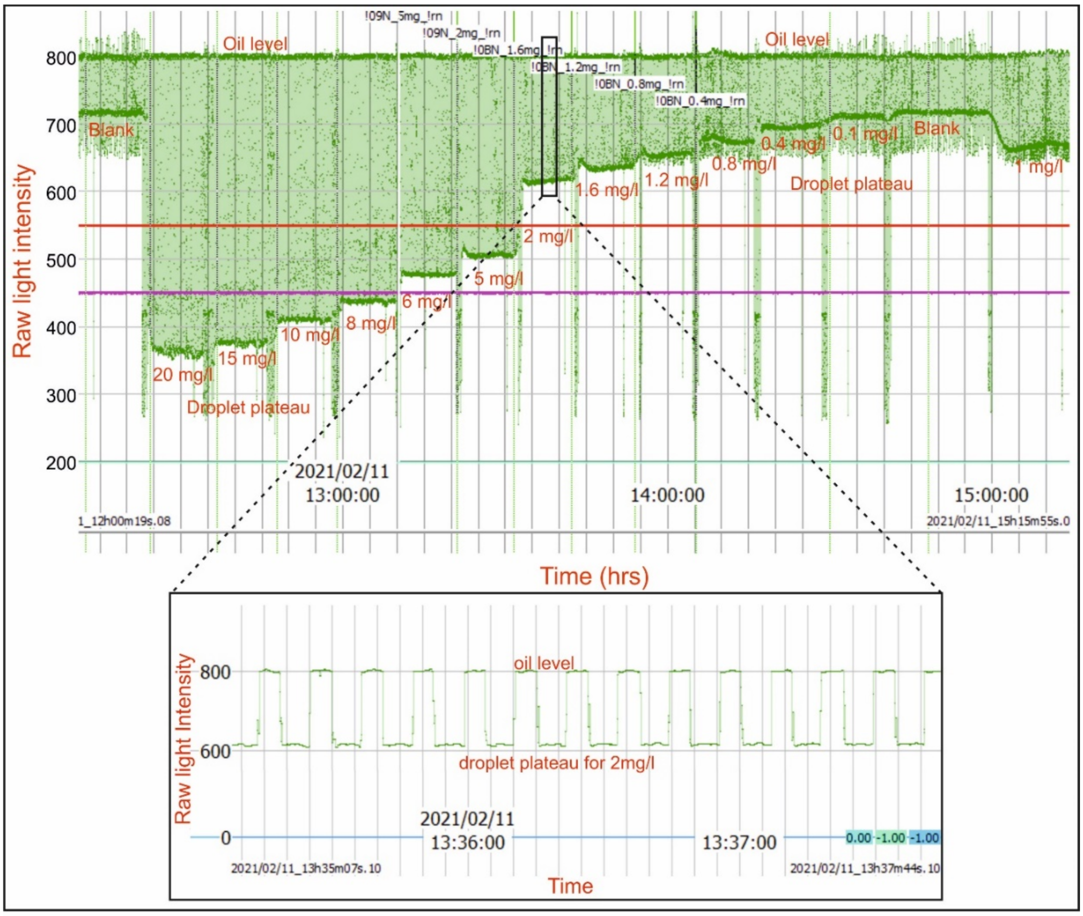

Figure 90. *Screenshot from the SWS GUI displaying raw intensity data obtained from the 0.7 mm single path flowcell while calibrating the sensor before deployment. The raw light intensity signal shows the oil level and droplet plateaus for different ammonium standards starting from 20 mg/l all the way down to 0.1 mg/l. The inset shows a zoomed in picture of the droplet plateaus obtained for 2 mg/l ammonium standard for a duration of about 4 minutes.*

Figure 91 shows the calibration curves obtained a few days apart from each other. Both the calibration curves are highly comparable indicating the robustness of the sensor measurements. Reagent stability studies were also performed in order to make sure that the reagents do not degrade during deployment period.

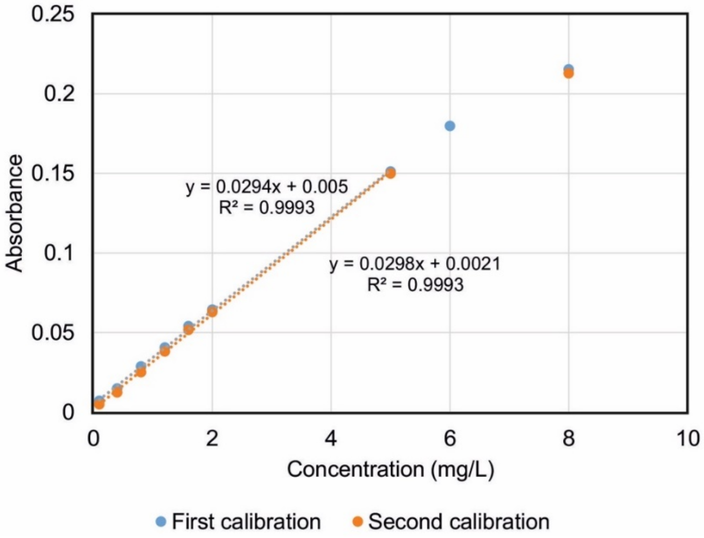

Figure 91. *Standard calibration curves generated a few days apart for ammonium sensor before first deployment.*

4.12.3. Sensor deployment

Continuous monitoring data was obtained from the bioreactor over four days, as shown in Fig. 92, with data from a few grab samples as comparison. The continuous data showed much lower ammonium concentrations over the four day deployment period than expected (could reach as high as 21 mg/L). However, the data still represented increased peaks of ammonium (indicated by the arrows) coinciding with stock feeding events (automatic addition of ammonium and phosphate solution into the column as nutrients to the bacteria).

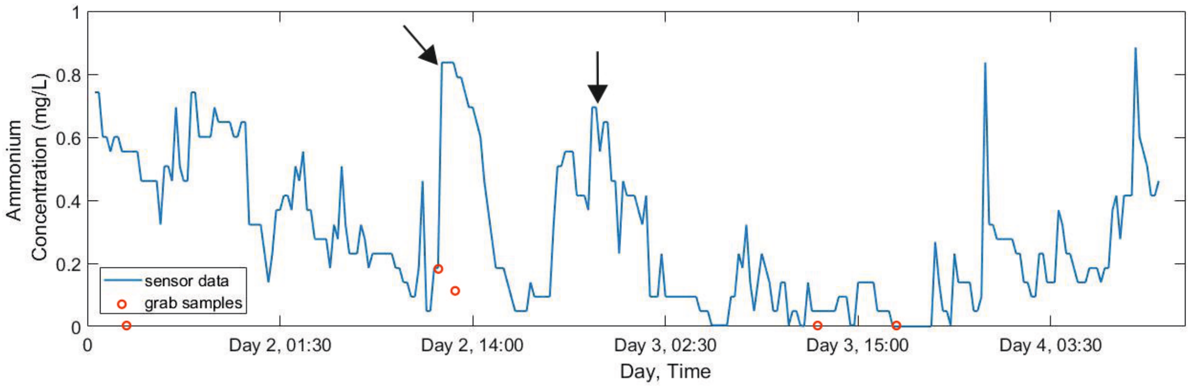

Figure 92. *Continuous data from the first deployment of the in situ sensor to the sequential batch bioreactor. Four days of continuous data shows fluctuations in ammonium levels and also peaks corresponding to introduction of feeding stock.*

The grab samples were analysed in spectrophotometer by using the 3:1:1 ratio and concentration values obtained indicated large variations from the sensor data prompting further investigation. The grab samples were also analysed in a different laboratory by Seongbong Heo using the original mixing ratio of 10.5:1:1 (section 4.2). Before the assay, the samples were diluted four times (required when measuring higher ammonium concentration according to protocol). The absorbance values obtained were higher and at par with what we were expecting (Table 2). This indicated that there was possible matrix interference in the bioreactor samples (likely to be thiourea, to be further verified in future experiments) which we did not face while calibrating the sensor (ammonium standards made using DI water) or when doing the river water analysis. Further investigation and analysis of more grab samples by Carla Ruggiero (SouthWestSensor Ltd) revealed that dilution of sample from the bioreactor is necessary before analysis.

Table 2. *Comparing ammonium concentration of grab samples from the bioreactor using 3:1:1 and 10.5:1:1 ratio of sample: DIC reagent: Salicylate reagent for analysis.*

Day	Time	Concentration (mg/L) (3:1:1)	Concentration (mg/L) (10.5:1:1)
Day1	15:11	0	0.37
Day 2	12:05	0.247	6.11
Day 2	13:21	0.104	4.32
Day 3	12:59	0	0.30
Day 3	17:14	0	0.28

In order to incorporate dilution of the sample into the sensor system, the volumetric ratios for sample to DIC reagent and salicylate reagent was set to 1:7:7 in order to remove matrix interference and provide a large analytical range. The sensor system was also modified by changing the roller design of the pump head and the heating volume. Figure 93 compares the standard calibration curve (up to 30 mg/L ammonium standards) for the assay carried out in the lab (spectroscopic detection) and the one for the sensor (assay in droplets with LOD of 0.11 mg/L). The difference in absorbance is due to the difference in pathlengths: 1cm for spectrophotometer versus 0.7 mm for sensor flow cell. After calibration the system was redeployed in the bioreactor.

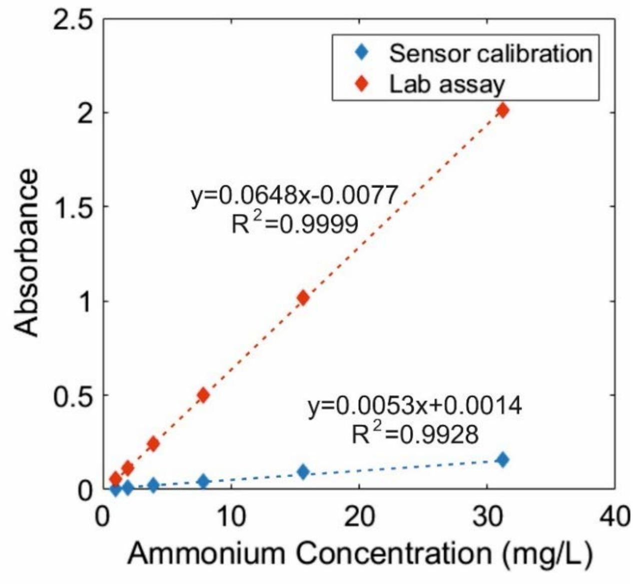

Figure 93. *Standard calibration curves for droplet based assay and assay in cuvettes for spectroscopic detection.*

Continuous monitoring data was obtained from the second deployment of the bioreactor for over four days, as shown in Fig. 94, with data from a few grab samples as comparison. Grab samples taken throughout the sensor deployment (limited numbers due to restricted lab access), coincided with the reading from the sensor therefore validating the assay in droplets. The slight discrepancy between the grab samples and the sensor data at low ammonium levels is thought to be due to the samples degrading between sampling and analysis and ongoing testing is looking to explore this. Four peaks of high ammonium concentrations are clearly visible, which correspond well with the stock feeding events. After each pulse feeding, there was a sharp decrease in ammonium concentration within 1.5 hour due to the intake of the ammonium by bacteria.

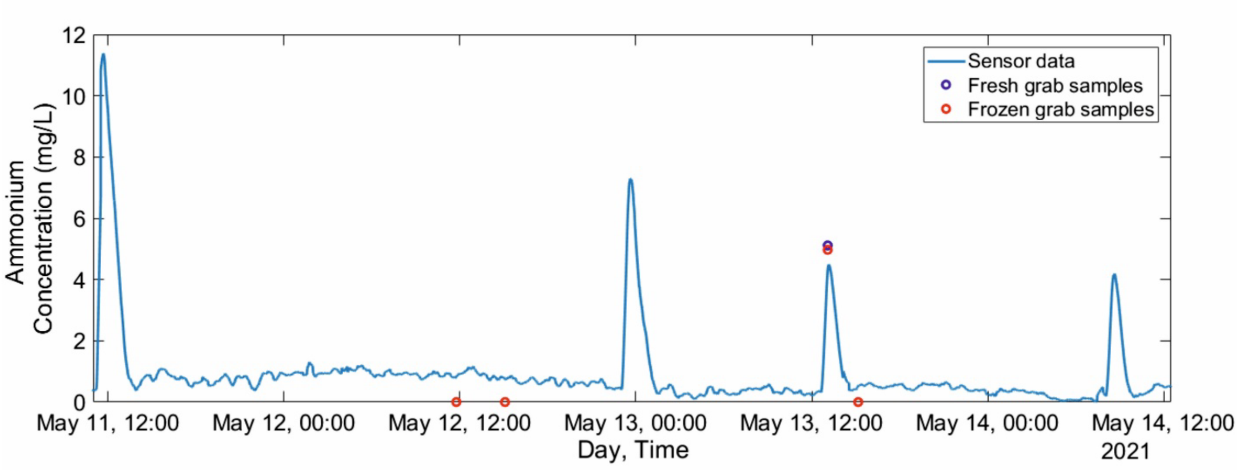

Figure 94. *Continuous monitoring data from in situ sensor deployed for 4 days in sequential batch bioreactor showing fluctuations in ammonium levels. Red and bule data points showing grab sample values.*

When compared with the data from the first deployment (Fig. 92) the second deployment (Fig. 94) generated a data set with expected ammonium levels. The sensor system is capable of performing high frequency and accurate measurement and provide long period of monitoring with minimal reagent consumption (1700 nL per analysis). This preliminary data obtained over a four day period shows high resolution monitoring and reveals the fast feeding behaviour of the bacteria, which could lead to the design of more efficient bioreactors and feedback controlled bioprocessing. These type of sensors could form the next generation of *in situ* sensors, to address wide applications in monitoring for wastewater treatment, environmental monitoring, aquaculture and others, especially when transient and episodic events are involved.

4.13. Chapter Conclusion

In this chapter I have:

(i) Shown the optimisation of the indophenol blue assay for implementing it in droplets for measuring ammonium levels in water.
(ii) Demonstrated the early calibration data for measuring ammonium in fresh water.
(iii) Shown the measurement of river water samples through the microfluidic system.
(iv) Shown the optimisation of the flow cell for achieving higher sensitivity and lower detection limit.
(v) Demonstrated the cross talk method as another possible approach to carry out the indophenol blue assay in droplets.
(vi) Shown the deployment of the ammonium sensor drybox in a sequential batch bioreactor enriched with PHA accumulating bacteria for continuously monitoring ammonium levels.
(vii) Obtained preliminary continuous monitoring data from bioreactor indicating robust performance of sensor system.

In order to further validate the ammonium sensor system, redeployment to the sequential batch bioreactor and obtaining multiple grab samples is necessary. Grab sample degradation due to transportation or storage needs to be further investigated as well.

After thorough testing, the way forward for this sensor system would be integrating with existing sensors in our group and develop into a system capable of multiplexing various assays for ammonium, nitrate/nitrite and phosphate. Physical sensors for measuring pH, dissolved oxygen, etc. could also be incorporated in order to produce a low cost and multi-parameter water sensor.

Chapter 5

MULTIPLE MICRO PERISTALTIC PUMPS FOR DROPLET GENERATION WITH ARBITRARY COMPOSITION AND SEQUENCING

This chapter details the design and fabrication of a novel, robust and programmable droplet on-demand platform based on peristaltic micro pumps capable of generating arbitrary sequences of droplets with variable size, spacing and composition. The system does not require redesigning of hardware, offers the flexibility to implement various multiplexed, 'mix-and-read' and multiple-step biochemical assays.

5.1. Multiple pump approach

Being able to generate reliable droplet sequences is extremely important for implementing heterogeneous, multiple-step and multiplexed assays using droplets. This will allow the platform to generate droplet sequences based on the requirement of assays, to fully exploit the true potential of droplet microfluidics.

As has been reported (Ferraro et al., 2016, Ali-Cherif et al., 2012), droplet assays require complex liquid handling systems involving robotic pipetting system or syringe pumps for generating droplet sequences, which can be time consuming for system to stabilise and the microfluidic chip surfaces are prone to surface contamination. In order to prevent contamination, the channels can be washed between different liquids, however this will result in higher complexity of the system as switch valves are commonly required, and lower the system throughput. Our group's novel 12-line peristaltic pump in Chapter 3 (Section 3.4, Fig. 54) provides a solution to address the aforementioned problems. It is self-priming and as each inlet is connected to a single liquid, it does not require any switching between samples and hence washing of channels. The liquid flow is based on peristalsis and the rotor head features facilitate pumping a defined volume every time. This pump has 6 pumplines on each side of the pump beds and rotor features were designed such that a sequence of four droplets are produced per revolution of the rotor. However, due to the limited peripheral length, this pumping system is limited by the volume of droplets or oil gap that can be produced as the rotorhead features have to be small enough to ensure that the channels are fully occluded.

Another engineering consideration is the system robustness. The 12-line pump took long time to assemble (about 10-15 mins) and de-assemble. Moreover, if one of the pump lines did not work, the entire pump bed had to be discarded and replaced. This led to loss of material and also time in replacing and reassembling. As the sequence is hardcoded and a pre-defined droplet sequence is produced every turn of the rotor, if an additional wash droplet is required for example, a new rotor design needs to be printed. Adding more features into a multi roller rotor head is difficult as it has limited space on the surface as well.

To overcome these problems aforementioned, a multi-pump approach was considered in this chapter. Various smaller and easier to assemble units were conceptualised, designed, fabricated and tested. These smaller pumps can be separately controlled and operated in synchronisation to produce desired droplet sequences. The very first version of the pump involved a pump design consisting of dual disc springs and later based on the needs of the application and reliability, design approach was shifted to a spring version which is capable of generating droplets with coefficient of variation of less than 0.7%. The evolution of the micropump has been illustrated in the subsequent sections.

5.2. Design and fabrication of dual disc spring peristaltic micropump

In order to shift from the single pump to multiple-pumps, the fundamental requirement was the ability to control the position of the roller features and to be able to trigger different pumps at different times. As shown in Fig. 95, this was achieved by using two magnets and a Hall Effect sensor. A magnet holder was designed to contain two magnets (part-F332-50, 3mm diameter 2mm thickness neodymium magnets, Magnet Expert) to rotate with the motor shaft and a fixed Hall Effect sensor (AH372, DiodesZetex) was positioned on the chassis. The two magnets were placed 180 degrees to each other on the holder with one positioned to indicate the north pole and another the south to allow a position feedback signal produced by the Hall Effect sensor per half turn.

Having multiple pumps reduce the need for several pump lines per pump bed and hence a smaller, lower power motor can overcome the torque required for pumping. A G12-N20 Geared Mini DC motor with a 20 mm shaft was used. Another major change in the design was to use metal springs instead of shims to fix the pumpbeds. As the pump lines on the pump bed squeezed over time and became more elastic, the shim sizes need to be increased. On the other hand, a spring can provide pressure with less variation to the pump beds and keep the engagement with the pump.

To fulfil these design criteria, a dual disc spring pump (Fig. 95 (a)) was firstly designed that consisted of a chassis (26.4mm X 16 mm; height 25.9 mm for two-line pump bed; height 21.9 mm for single line pump bed) enclosing a pair of disc springs (6890: CSW-NM 12,7X8X4,7 from Lesjöfors), two pump beds and a roller. A bearing was used to keep the motor shaft in place and reduce friction. All the components of the pump are illustrated in the exploded diagram in Fig. 95 (b) and (c).

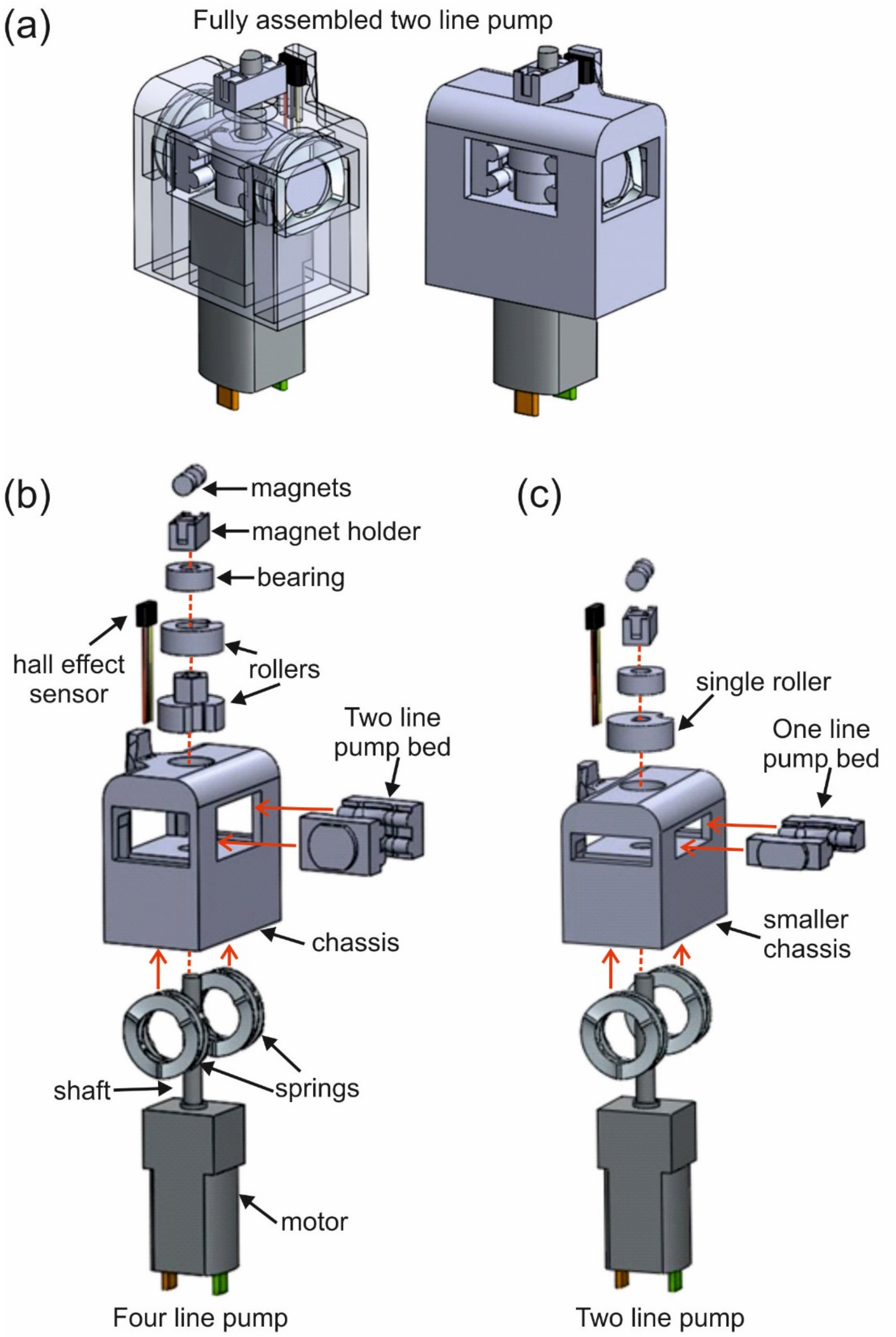

Figure 95. *Solidworks CAD model of the fully assembled dual disc spring peristaltic pump. (a) Inside view and outside view. Exploded Solidworks model of (b) four line and (c) two-line, dual disc spring pumps.*

The constituents of the pump were designed using SolidWorks and printed in VeroClear material using the Objet500 Connex3 Polyjet printer (Stanford Marsh Ltd). Two versions with the same design principle were fabricated but one containing pump beds with two pump lines (Fig. 95 (b)) and the other version with single pump lines (Fig. 95 (c)). The four-line pump (two pump lines on each pump bed) was designed so that it is able to generate the droplet containing three aqueous phases (e.g. one sample and two reagents) in one single shaft rotation. The two-line (single line in each pump bed) pump on the other hand was for generating droplets contains wash buffer or others.

The 3D printed prototypes were assembled and tested to check their stability and capability of reliable pumping. The initial testing immediately showed several challenges. The assembly was unexpectedly difficult and time consuming, as the pump bed and the spring had to be inserted and aligned carefully. Once assembled and run, the springs wobbled, did not seem to apply uniform pressure on the pump bed and resulted in instability of the pump beds. This led to the introduction of varying amounts of aqueous sample every time producing highly polydisperse droplets. Generation of air bubbles occasionally were also seen disrupting the droplet flow (images provided in the Appendix in Fig. 126). As qualitative testing demonstrated the unreliability of the pump, further quantitative tests were not performed.

The following sections elaborate upon the design and fabrication of single coil spring micro pumps which are significantly reliable, durable, and much easier to assemble.

5.3. Design and fabrication of single coil spring peristaltic micropump

5.3.1. Transition to coil spring and single pump bed

Learned from previous design and testing, it is clear that to obtain a robust system, the component needs to be durable and aligned in position. As the two side springs brought in huge variations, it seemed feasible and necessary to shift to a pump unit with a single pump bed and coil spring. Coil spring also provides uniform vertical pressure. This would offer some immediate advantages, like decreasing the amount of friction that the rotor must overcome per rotation, easier assembly, and removal of one entire pump bed. This design would also eliminate an extra spring and in turn, decrease the overall size. Having a single spring and pump bed would also introduce the possibility of having a ‘clip-on’ top cap for the pump.

The new version of the single spring one sided pump was designed with a chassis (34.8mm X 37.2 mm X 17.36 mm), a ‘clip-on’ top (17.85 mm X 29.5mm X 38.2 mm), a motor (G12-N20 Geared Mini DC motor with a 20 mm shaft), a spring (LC 047E 01 M from Lee Springs), pump bed with Santoprene tubing pump lines, hardcoded rollers, two bearings and a Hall affect sensor (AH372), to provide feedback on the position of the roller features. The pump has been designed using SolidWorks and the different parts have been printed using two different printers. The chassis and the 'clip-on' top have been printed using Ultimaker2+ in Polylactic acid (PLA) material. The rollers and pump bed have been printed using Objet500 Connex3 polyjet printer in VeroClear material in 'glossy mode' because they require good surface finish. PLA provides more flexibility than the VeroClear material, which is stronger but more brittle. The magnet cam holding the two small magnets (part-F332-50, 3mm diameter 2mm thickness neodymium magnets, Magnet Expert) attached to the motor shaft was also printed in VeroClear material. The different components of the single spring pump have been illustrated using an exploded diagram in Fig. 96.

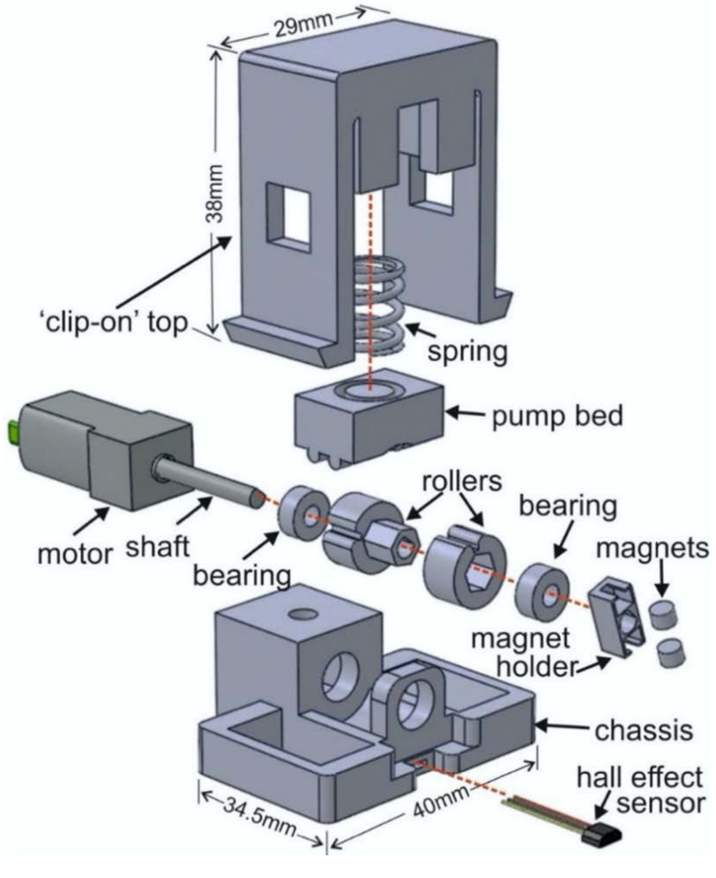

Figure 96. Exploded diagram of two-line, single spring pump showing the different components: chassis, 'clip-on' top, spring, pump bed, motor, motor shaft, bearings, rollers, magnet holder with magnets and a Hall Effect sensor.

Designing the 'clip-on' top and the pump bed were the most challenging aspects of single spring pump. Having a 'clip-on' top which would be flexible in plugging in and out and also strong enough to pump liquids through two or three pump lines required a delicate balance between the strength, size and user friendliness. Initially the top cap was printed using Objet500 Connex3 polyjet printer in VeroClear material (Fig. 97 (i)) however, as soon as it was plugged in and taken out a few times, it developed fractures and cracked around the top corners and around the stoppers on the bottom. The next iteration involved increasing the thickness of the sides of the top cap and printing in Polylactic acid (PLA) using Ultimaker 2+, for the same chassis. It was less brittle than the VeroClear top cap, but still felt rigid while inserting. Another design involved making the top cap wider with the side edges designed to hook on to the chassis (Fig. 97 (ii)), which would keep the cap locked in position and prevent it from springing out. The chassis as a result was also increased in size to match the top. However, the cap had to be pushed down and then squeezed inwards to be unclipped. This proved to be difficult and also caused unnecessary compression of the spring.

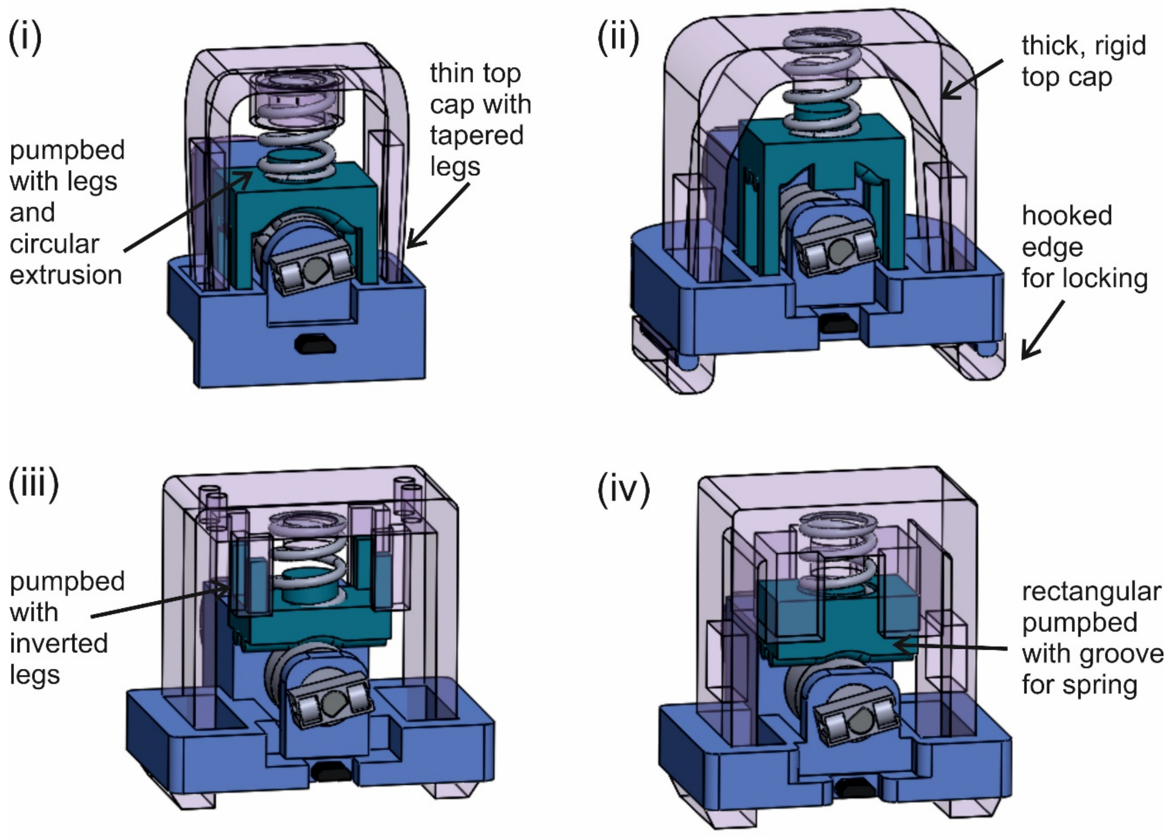

Figure 97. *3D CAD assemblies of the single spring pump showing the evolution to the current working version.*

While doing iterations of the design, the chassis was also printed using PLA, as printing in VeroClear did not add any structural benefits compared to PLA. The next iterations (Fig. 97 (iii-iv)) had a similar chassis and top cap. The chassis evolved from having a straight slot for the top clip to enter to a tapered slot, thus allowing less stress while plugging the cap in (Fig. 97 (iv)). Photographs of the different versions can be seen in Fig. 127 in the Appendix. The detailed evolution of the single coil spring pump design has been illustrated in Fig. 128 in the Appendix.

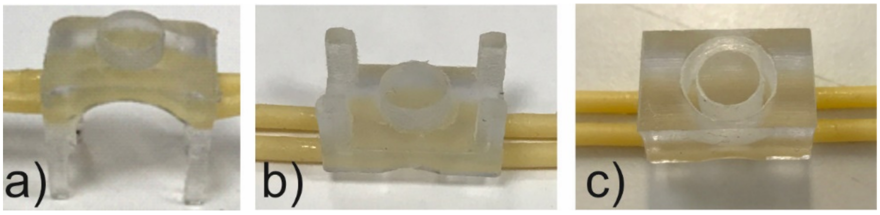

Figure 98. *Improvement in design of pump bed for single spring pump. (a) Two-line pump bed containing four legs to restrict lateral motion of pump bed. (b) Pump bed with four legs on the top surface. (c) Rectangular pump bed with circular groove to insert spring.*

From the initial designs, the spring was held in position using circular extrusions underneath the cap top and on the top of the pump bed. The extrusions ensured that the spring just had vertical compression and expansion and any lateral movement was restricted. The pump bed design also evolved from having four legs (Fig. 98 (a), 98 (b)) on each corner to a more solid, modular structure (Fig. 98 (c)). Four vertical extrusions were designed on the inside of the 'clip-on' top to confine the modular pump bed and prevent sideways motion during pumping. Final iteration of the pump bed involved having a circular groove cut on the top of the pump bed to insert the spring (Fig. 98 (c)). All the pumpbeds shown in this section and all the iterations of the pumps had Santoprene tubing (purchased from Megaflex Ltd., UK) pumplines due to the robustness that the tubing provides over its silicone counterparts. Santoprene tubing has been tested for long term usage in different pumps in our group (Nightingale et al., 2019a, Nightingale et al., 2020).

The purpose of the several iterations was to identify the possible limitations of the micropump assembly and come up with a compact, robust and user-friendly module.

5.3.2. Droplet generation using single spring two-line micropump

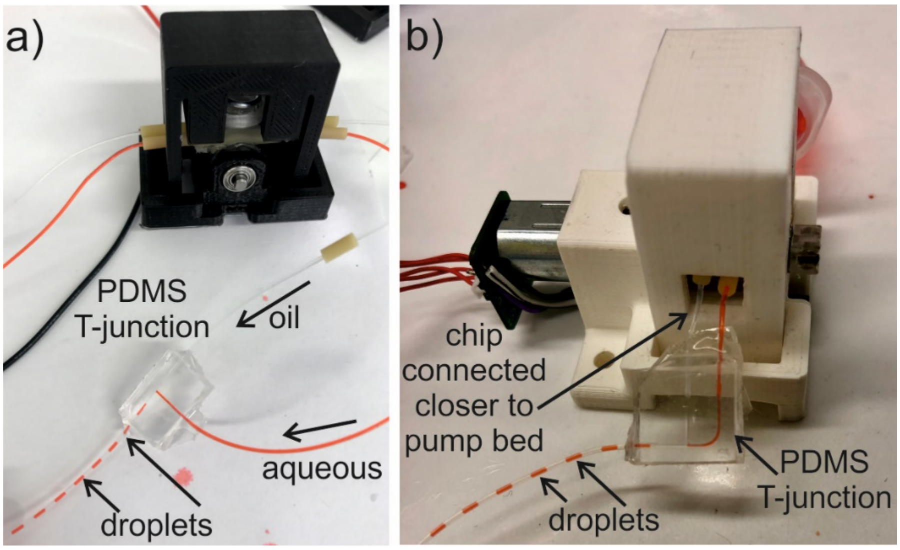

Figure 99. *(a) Monodisperse droplet generation by two-line pump when connected with a T-junction PDMS chip. (b) Modified version of the two-line pump (discussed in later sections of this chapter) with microfluidic chip very close to the pump and pump bed. This reduces Taylor dispersion leading up to the chip junction.*

In order to investigate the stability and repeatability of the pump design and assembly, droplets were produced using a basic PDMS chip and a T-junction with channel dimension 600 µm X 100 µm (Fig. 99 (a)). To thoroughly quantify the performance of this design, three complete units were fabricated, assembled, and tested. To compare the droplet generation of the three pump units, the experimental set up was kept constant.

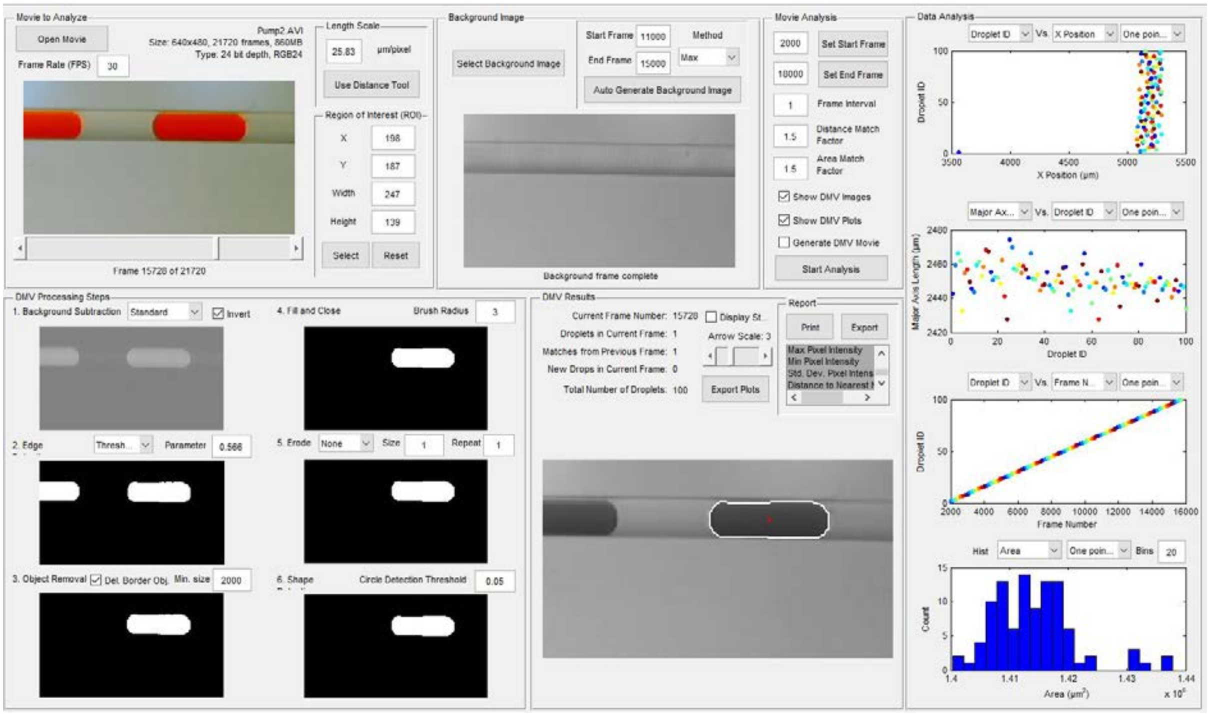

Movie to Analyze
Pump2 AVI
Size: 640x480, 21720 frames, 860MB
Type: 24 bit depth, RGB24
Frame Rate (FPS): 30
Frame 15728 of 21720

Length Scale: 25.83 µm/pixel

Region of Interest (ROI)
X: 198
Y: 187
Width: 247
Height: 139

Background Image
Start Frame: 11000
End Frame: 15000
Method: Max
Background frame complete

Movie Analysis
2000 Set Start Frame
18000 Set End Frame
Frame Interval: 1
Distance Match Factor: 1.5
Area Match Factor: 1.5
☑ Show DMV Images
☑ Show DMV Plots
☐ Generate DMV Movie

DMV Processing Steps
1. Background Subtraction: Standard ☑ Invert
2. Edge: Thresh... Parameter: 0.566
3. Object Removal ☑ Del. Border Obj. Min. size: 2000
4. Fill and Close: Brush Radius: 3
5. Erode: None Size: 1 Repeat: 1
6. Shape: Circle Detection Threshold: 0.05

DMV Results
Current Frame Number: 15728
Droplets in Current Frame: 1
Matches from Previous Frame: 1
New Drops in Current Frame: 0
Total Number of Droplets: 100
☐ Display St
Arrow Scale: 3

Report
Max Pixel Intensity
Min Pixel Intensity
Std. Dev. Pixel Intens
Distance to Nearest I

Data Analysis
Droplet ID Vs. X Position One poin...
Major Ax... Vs. Droplet ID One poin...
Droplet ID Vs. Frame N... One poin...
Hist Area One poin... Bins: 20

Figure 100. *Screenshot of DMV software interface while analysing a droplet video.*

Around 100 droplets were produced using each pump unit for a duration of about 12 minutes. The droplets were recorded using a dnt Digimicro Mobile Mikroskop camera and analysed using Droplet Morphometry and Velocimetry (DMV) video processing software (Basu, 2013). DMV uses bright field digital videos and takes advantage of the darker boundary of the droplets due to the refractive difference between the two different phases. DMV image processing steps include a background image generation which is generally an empty channel without any droplets. Then the background is subtracted, image is inverted, and edge detection is used to recognise the boundary of the droplet. Users can then set a threshold to keep the droplets but remove other smaller objects which create noise. DMV can track individual droplets over several frames, giving each of them a unique identity and tracking their trajectory, calculating velocity, shape, and a range of other variables. The data generated from DMV is then exported to a .txt file and imported to Matlab. Figure 100 shows a screen shot of the DMV software interface while analysing a droplet video. A total of 100 droplets produced by each pump were analysed with the data obtained shown in Fig. 101 (a) - 101 (d).

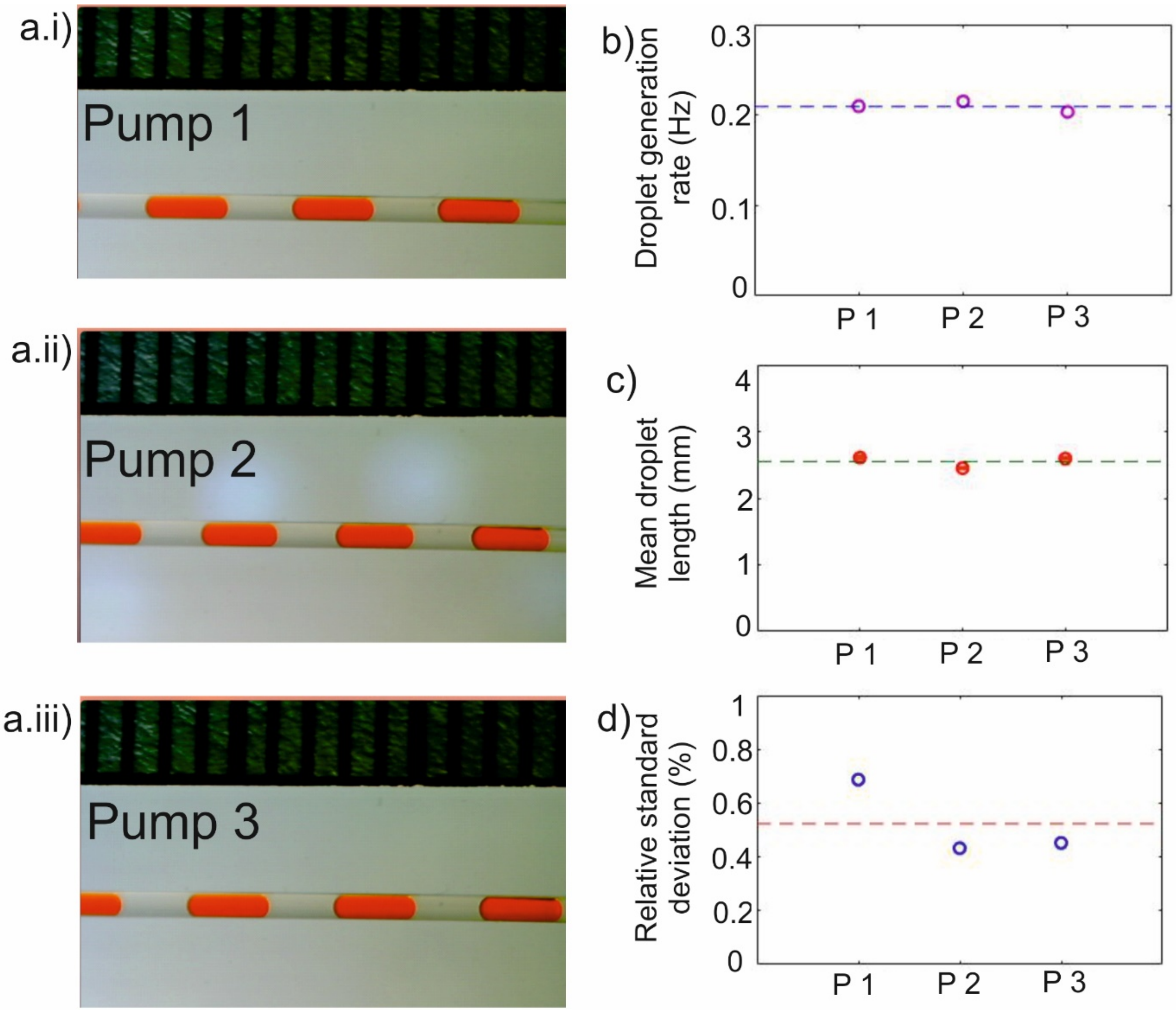

***Figure 101**. (a) Monodisperse droplet generation by single spring two-line pump (i) unit one, (i) two and (i) three. The droplets are in a PTFE tubing of 0.5 mm inner diameter. (b) Comparison of droplet generation rate of the three pump units. (c) Mean droplet length produced by the three pump units. The error bars represent the standard deviation of droplet length for each pump unit for the same roller design. (d) Relative standard deviation (%) of droplet length over 100 droplets for each pump unit.*

Figure 101 a (i)- a (iii) show photographs taken using the dnt Digimicro Mobile Mikroskop camera, of the droplets generated by pump unit 1, 2 and 3. Droplet generation rate (Hz), mean droplet length (mm) and relative standard deviation (%) of droplet length per 100 droplets for all three pump units have been plotted in Fig. 101 (b)-(d) respectively. Pump-to-pump mean droplet generation rate was 0.209 Hz with a standard deviation of 0.581%. Mean droplet length produced by each pump unit were 2.61 mm, 2.45 mm and 2.59 mm with a mean of 2.55 mm and a pump-to-pump standard deviation of 8.76%. However, the relative standard deviation of droplet length for each individual pump unit was always less than 0.687%, which compares favourably with the other droplet generation methods reported (Jung et al., 2010, Garstecki et al., 2005).

5.3.3. Comparing the flow in each pump line

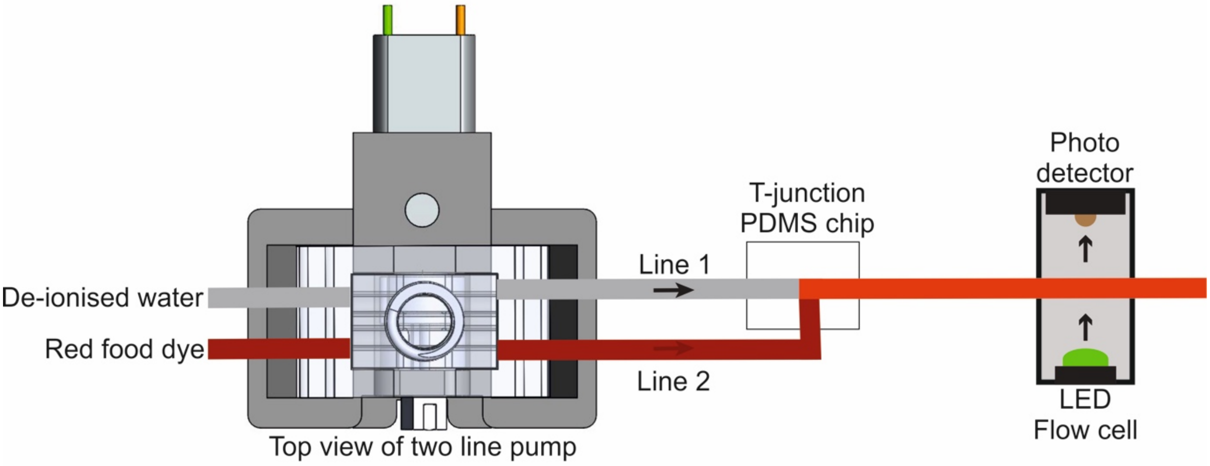

Figure 102. *Schematic of experimental setup for comparing the flow in each pump line in a two-line pump unit. The set up consists of a two-line pump, a T-junction PDMS chip and an optical detector.*

A series of simple tests were performed to quantify if both the pump lines in the two-line pump are pumping at the same rate. The experimental setup consisted of a two-line pump coupled with a basic PDMS T-junction (600 µm X 100 µm channel dimension) and an optical detector, as can be seen in Fig. 102. A roller with same feature size for both the pumplines was used. Red food dye and de-ionised water were switched alternatively between the two lines of the pump and the raw intensity values were obtained from the optical detector connected to the outlet of the T-junction chip. The pump line which would be pumping in more dye would generate lower intensity values (due to darker colour) at the detector and hence higher absorbance.

Three, two-line pump units were tested on two different days (about a week apart) to compare and to check their reliability over time. The absorbance values obtained from the raw intensity data using the Beer Lambert law can be seen in Fig. 103. The raw intensity data can be seen in Fig. 130 in the Appendix. Absorbance is directly proportional to concentration for a fixed path length.

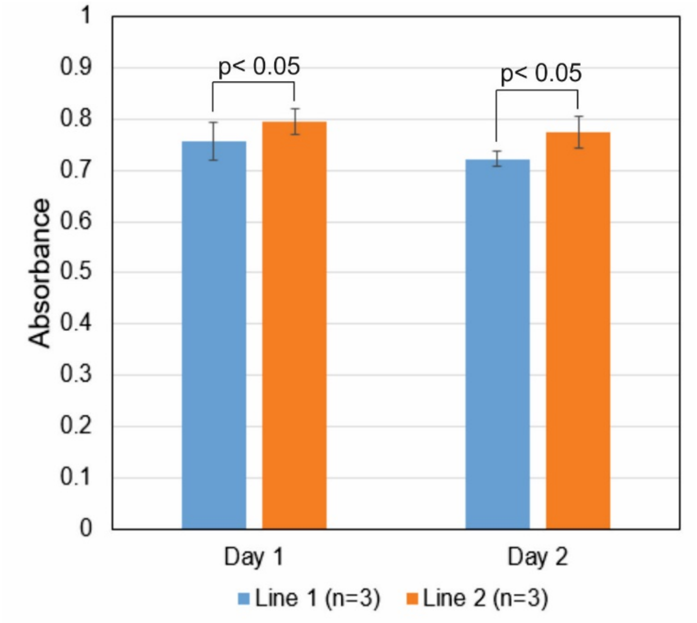

Figure 103. *Absorbance values of diluted red dye passing through flow cell to compare 3 different two line pump units. Statistical analysis was performed using the two-tailed Student's t test. The p value for day 1 and day 2 are 0.0244 and 0.0314 respectively.*

All the pumps seemed to pump more during the first set of tests (Day 1) than the second set (Day 2) with a mean absorbance value of 0.776 compared to 0.748 for all the pump lines. The tests also highlight a fact that the two pump lines pump slightly different amounts with the smallest difference being 3.32% and the highest being 8.55%. An interesting trend that comes forward is that pump line 2 (both data sets in Fig. 103) always has more red dye passing through than pump line 1, all throughout the tests and for all the pump units. This brings forth possible design error which has been further explored in the following section.

5.3.4. Observation regarding two different rollers types

As there was a trend noticed for one pump line always pumping more liquid than another, a quick test was done by using a roller with just one feature instead of two rollers with out of phase features as used for the previous tests (section 5.3.2, 5.3.3). Single roller with one feature caused both the pump lines to pump in at the same rate as can be seen from the absorbance values in Fig. 104 (raw intensity data can be seen in Fig. 131 in the Appendix). The discrepancy in both the results can be due to the fabrication of the rollers. When two rollers are used, one roller is designed to be inserted on to another roller. Even though the feature spacings are the same in the SolidWorks design, the insertion of one roller into another might cause the top roller spacing to slightly increase. On the other hand, when one roller is used, it has one uniform feature which is used for both the pump lines. A conclusive reason has still not been identified for the disparity and other tests need to be performed to further investigate the reason for this trend. However, as only one feature is used for pumping in aqueous followed by another feature for the oil, the slight difference can be ignored as long as monodisperse and repeatable droplets are produced.

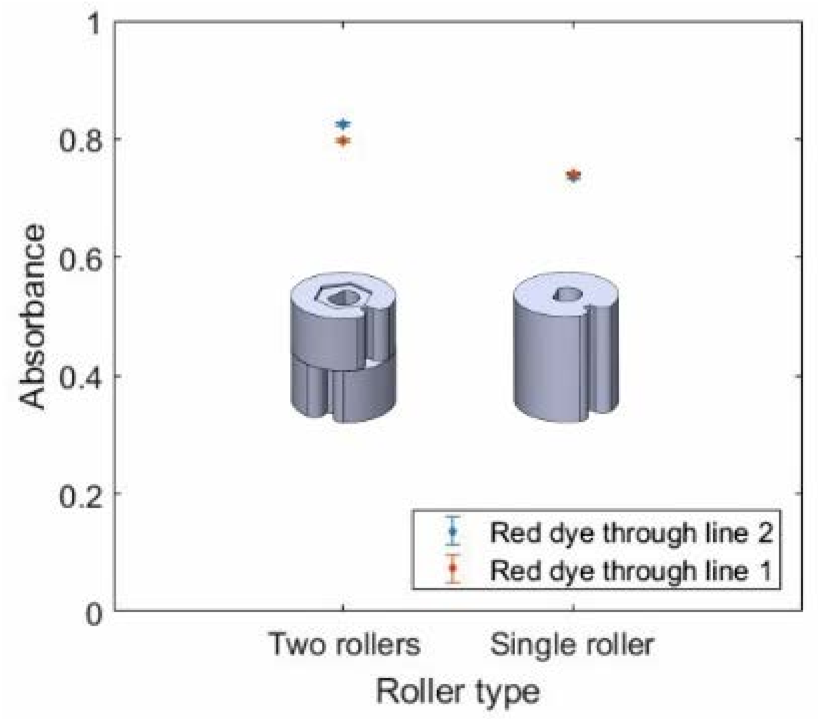

Figure 104. *Absorbance values of diluted red dye passing through flow cell when using two different roller types.*

5.3.5. Droplet generation with the two-line pump

The novel pumping technology developed by our group (Nightingale et al., 2017), as mentioned previously in this thesis generates fixed volume of droplets per rotation. The aqueous pulses are restricted by the feature spacing in the roller and tuning the spacing leads to producing desired volumes of droplets.

This concept was verified further using the two-line pump. The invariance of droplet volume for different motor speed was tested using rollers with different feature spacings (Fig. 105). Three different roller spacings 0.73 mm, 1.021 mm and 1.702 mm with the same radius (5 mm) roller were implemented and droplets were produced using a basic T-junction PDMS chip (600 µm X 100 µm channel dimension). For different motor speed varying between 0 to 0.5 Hz and roller spacing, a set of 100 droplets were produced, recorded and finally analysed using DMV.

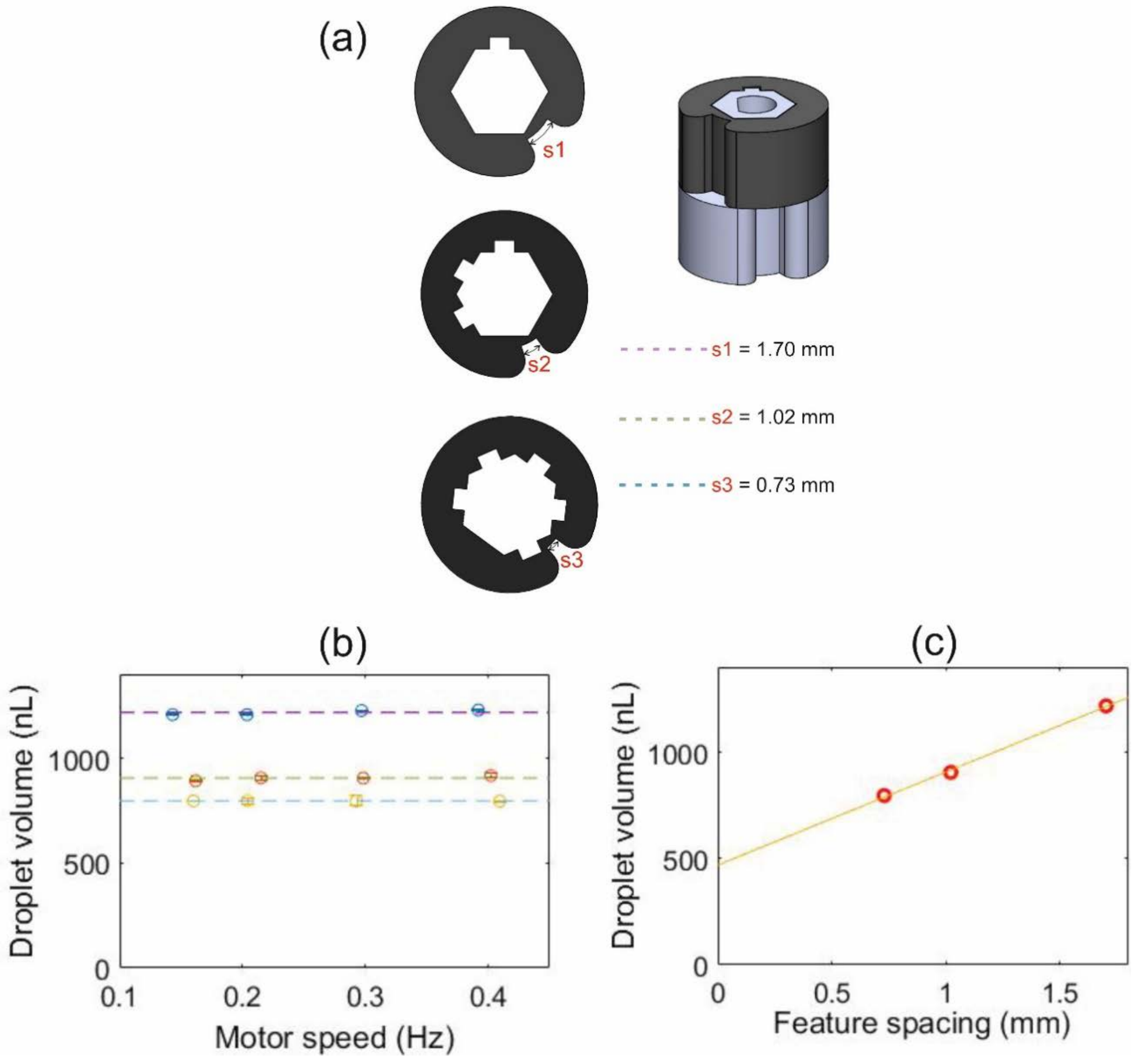

Figure 105. *Design and fluidic testing of two-line roller. (a) Shows 0.73 mm, 1.021 mm and 1.702 mm feature spacing of the roller for aqueous phase. (b) Graph of droplet volume (nL) vs motor speed (Hz) for three different feature sizes 0.73 mm, 1.021 mm and 1.702 mm. (c) Droplet volume (nL) vs feature spacing (mm). For each motor speed a set of 100 droplets were produced, recorded and analysed.*

For all the tests, the coefficient of variation of droplet volume remained less than 1%, which indicates the reliable performance of the pump with different rollers and different motor speeds (Fig. 105 (b)). The droplet sizes increased as the roller spacing increased (105 (c)), with mean volumes of 796 nL, 905 nL and 1217 nL being produced from feature spacing 0.73 mm, 1.021 mm and 1.702 mm respectively. The positive y-intercept in Fig. 105 (c) for the droplet volume (nL) vs feature spacing (mm) indicates that even if the feature spacing is zero, some volume of liquid will still be pinched off by the circular edges of the feature on the roller.

5.3.6. Droplet generation with three-line pump

The three-line pump is a basic unit capable of carrying out fundamental reactions with one line each for sample, reagent, and oil. The three-line pump design was based on the two-line one, with a slight modification to the pump bed and the height of the top cap. For the same dimension of the pump bed, three lines were added in place of two lines as can be seen in Fig.106 (a) (ii). The height of the top cap was decreased by 2mm for the three-line pump, as a higher pressure is required to pump through three lines. A set of two rollers were designed; one roller (with one feature) for pumping in oil and another larger roller (with one feature) for pumping through two aqueous lines. The three-line pump was connected to a 3 inlet, 3D printed junction chip (Fig. 106 (b)) printed using Vero Clear material (Objet500 Connex3 polyjet printer) and droplets were produced using red food dye and pure FC 40 oil (Fig. 106 (c)).

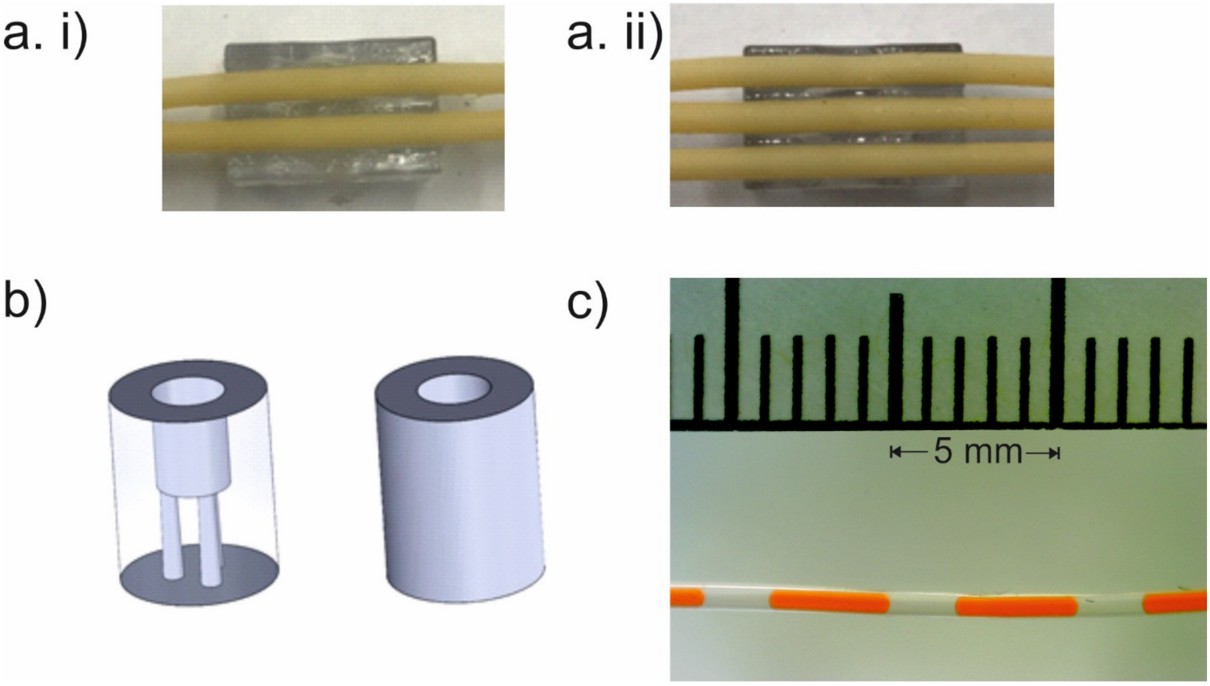

Figure 106. *Components of the three-line pump. Comparison between (a. i) two-line and (a. ii) three-line pump bed for single spring micro pump. Generation of monodisperse droplets by three-line pump when connected to a 3D printed junction chip. (b) SolidWorks model of three inlet junction chip. (c) Picture of monodisperse droplets produced with three-line pump flowing through a PTFE tube of inner diameter 0.5mm.*

The invariance of droplet volume for different motor speed was tested using different sized roller features for the three-line pump as well as can be seen in Fig. 107. Three different roller spacing 0.73 mm, 0.851 mm and 1.021 mm with the same radius (5 mm) roller was implemented and droplets were produced using the 3D printed three-inlet junction chip. For each motor speed and roller spacing, a set of 100 droplets were produced, recorded, and finally analysed using DMV.

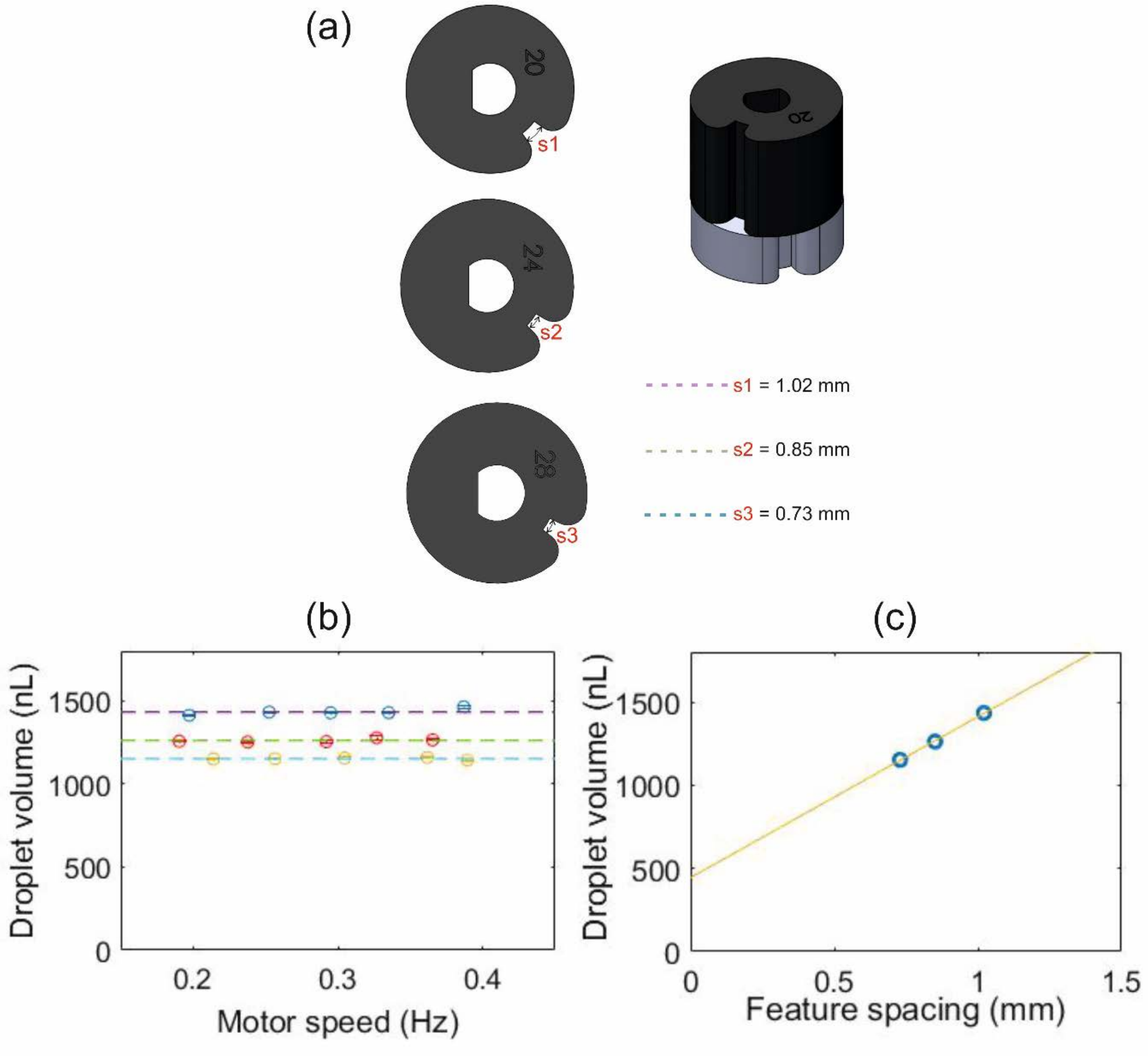

Figure 107. *Design and fluidic testing of the 3 line roller and pump. (a) Shows 0.73 mm, 0.851 mm and 1.021 mm feature spacing of the roller for aqueous phase. (b) Graph of droplet volume (nL) vs motor speed (Hz) for three different feature sizes 0.73 mm, 0.851 mm and 1.021 mm. (c) Droplet volume (nL) vs feature spacing. For each motor speed a set of 100 droplets were produced, recorded and analysed.*

For all the tests, the coefficient of variation of droplets remained less than 1% indicating robust performance of the pump with different rollers and different motor speeds (Fig. 107 (b)). The droplet size increased as the roller spacing increased (Fig. 107 (c)), with mean volumes 1152 nL, 1262 nL and 1434 nL being produced from feature spacing 0.73 mm, 0.851 mm and 1.021 mm respectively. The droplet volumes remained consistent for different motor speeds for each feature spacing.

5.4. Multiple pump synchronisation and platform development

Once the two-line and three-line single spring pumps showed repeatability in generating droplets and were stable in performance, they could be used separately to produce a single type of droplet or as a group to produce different droplets in a train. A control circuit was implemented to operate the multiple micro-pumps for the generation of the droplet sequences. The individual pump units are triggered to rotate at different instances using the digital pins of an Arduino and MOSFETs (IRF7103). A Hall Effect sensor (AH372) with each pump unit feeding back the position of the rotor head of that pump. As has been shown in the preceding sections each pump has two magnets (N and S) mounted on the opposite sides of its shaft. When the shaft rotated, these magnets were sensed by the Hall Effect sensor for each half rotations. The information is fed through the analogue input port of an Arduino board. Once a pump executed the desired half rotations *'n'* times set by the user, the next pump in the sequence was triggered. Therefore, the different pumps work in sequence to generate the desired droplet sequence which the user codes into the Arduino. A schematic of the control circuit for the multi-pump system can be seen in Fig. 108 (a).

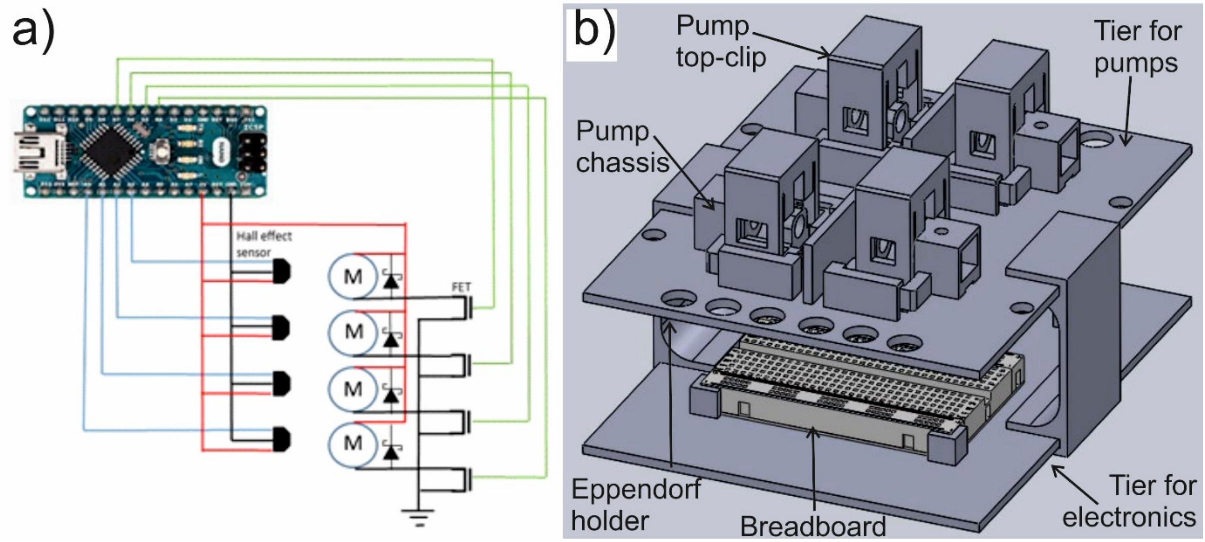

Figure 108. *Multiple pump synchronisation and platform. (a) Control circuit for operating multiple pumps for arbitrary droplet sequencing. (b) Two tier stand for mounting the four-pump system for laboratory testing and droplet generation.*

A two tier platform with corner stands was designed using Solidworks and printed in black PLA material , to mount the four pumps and control board for laboratory testing. The Solidworks model can be seen in Fig. 108 (b). The top tier includes holders for the four pumps so that two units are on either side facing the other pair. There is a gap in between for the chip and connecting PTFE tubing coming from either side. The pumps were oriented in such a way that shortest length of tubing would be required from each pump to reach the inlets of the microfluidic junction chip. The top platform also has slots for eppendorf tubes, to hold the liquid close to the pump inlets. The lower tier holds the breadboard containing the arduino control circuit.

The multipump system is run using a laptop and an Arduino board. Currently one motor is turned on at one time. Each motor consumes around 40 mA current and is run at nominal 5 V (Arduino port is not able to provide full 5 V). Therefore the power consumed by each pump is around 0.2 W. Arduino board iself consumes about 0.095W. If we have the Arduino and pump system connected to a 75Ah, 12V car batter, we would be able to run it for approximately 127 days. If all the four pumps are turned on simultaneoesly, the system would be able to run for about 41 days.

5.4.1. PCB design for multiple pump platform

After the design, assembly and successful operation of the first multiple pump platform (appendix Fig. 132), a PCB was fabricated to streamline the involved electronics and secure all the electronic connections. The circuit as can be seen in Fig. 109 for the PCB was designed using Dip Trace software. The circuit illustrates the connections between the Arduino microcontroller board and the different components of the platform such as the pumps, flow cell and heater. The circuit provides the capability to connect 5 pump units (additional pump one in case an assay requires it) from the digital pins of the Arduino to MOSFETs to control the switching on and off of the pumps according to demand. Diodes have been used in between the positive and negative connections of the motor to prevent reverse current. The position of the rotor head is fed back by the Hall- effect sensors through the analog input ports of the Arduino as explained in the previous section. The flowcell and heater units have also been connected to have feedback control.

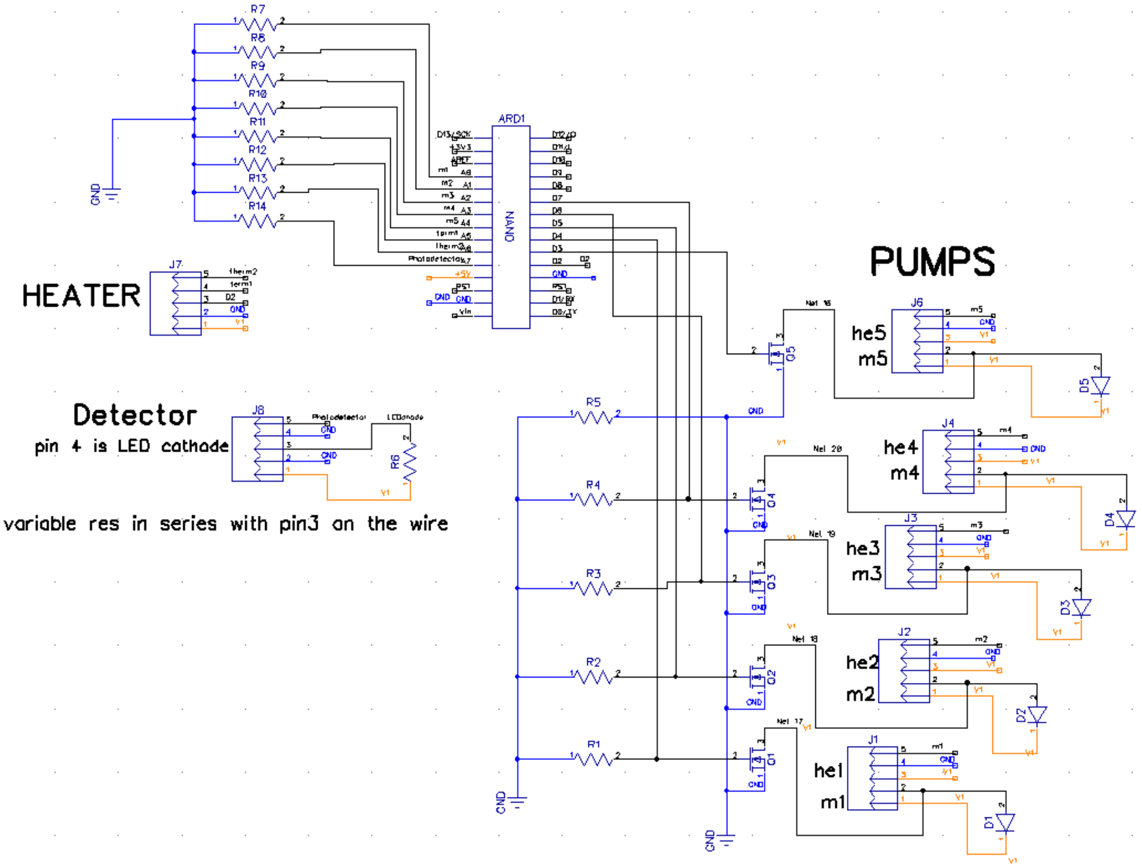

Figure 109. Circuit schematic for PCB for controlling the multiple pump system.

The PCB routing schematic and the STEP file can be seen in figure 110 (a) and 110 (b) respectively.

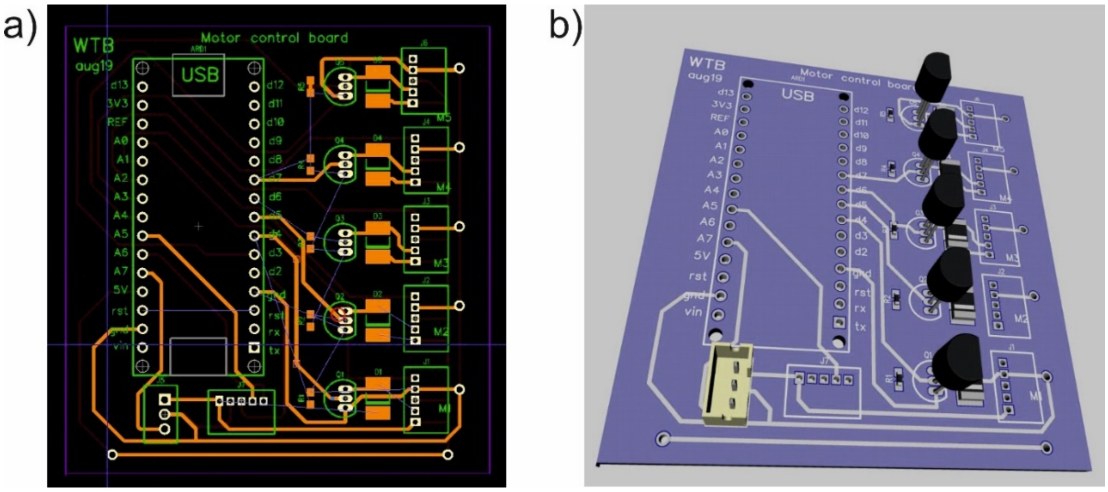

Figure 110. PCB for multiple pump platform. (a) PCB routing schematic and (b) STEP file showing PCB with mounted electronics.

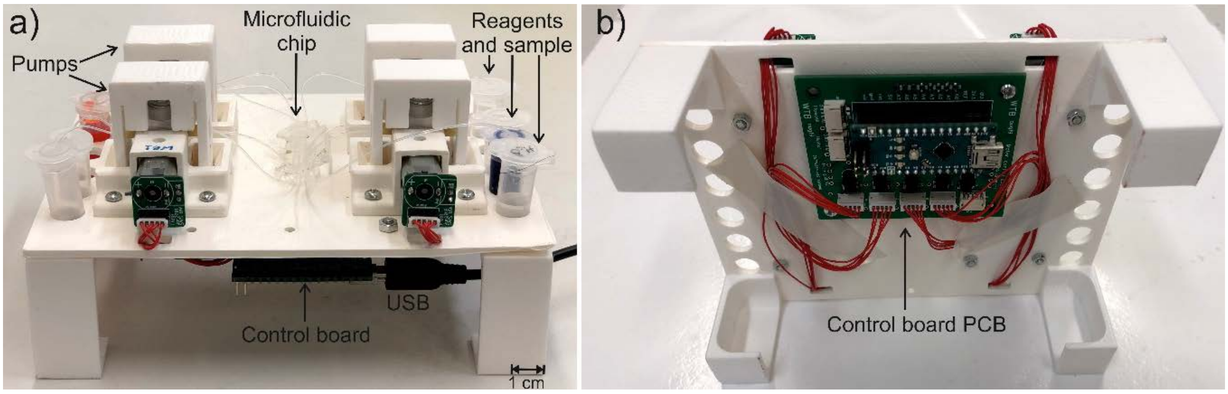

Figure 111. *(a) Second prototype of the multiple pump platform which has been modified from the first prototype (Fig. 132 in Appendix) to secure the pump units and the PCB in position with M3 screws. (b) The bottom side of the platform showing the electronics PCB secured in position using M3 screws.*

Figure 111 (a) and (b) show photographs of the second prototype of the multiple pump unit. A few modifications were made for the second prototype compared to the first prototype. The pump chassis was redesigned to accommodate M3 screws to secure them down to the platform. The PCB was also mounted on the bottom of the platform via M3 screws. Ribbon wires were then connected from the back of the motors to the main PCB.

Another compact two-pump system was also designed to be implemented in field deployable sensor units. The design consists of the two pumps keeping in mind that one would be used for sample and reagents and another one would be utilised just for pumping in oil (the benefits of having an independent oil pump has been discussed in the following sections). The design (Fig. 112) consists of a combined chassis and pump bed holder for the two pumps. The two layers have been spaced by metal separators and secured in position using screws. Two metal reinforcement plates have been used on either side to prevent the 3D structure from losing integrity. This pumping system is stable in operation and capable of producing highly monodisperse droplets as well.

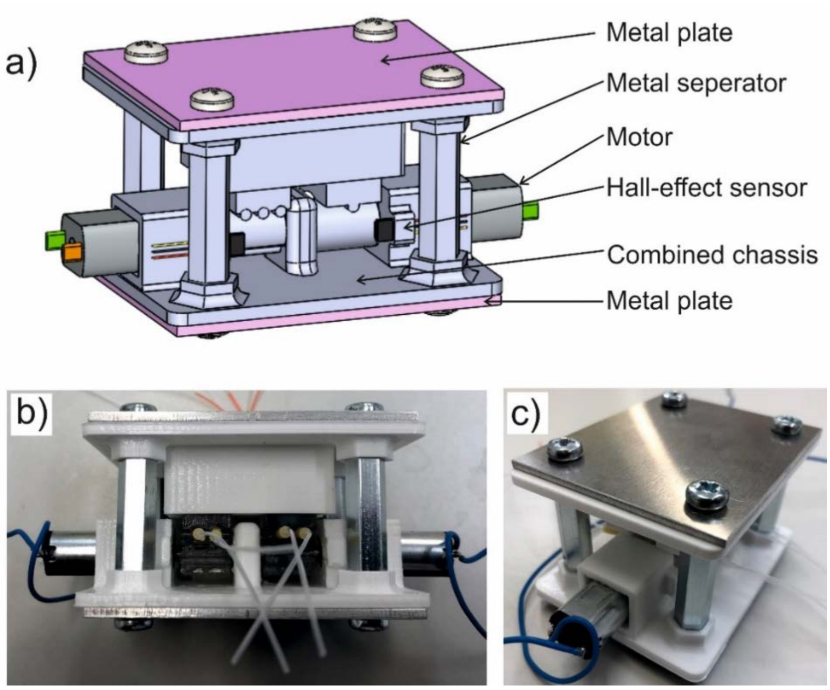

Figure 112. *Two-pump system assembly for field deployable sensors. (a) Solidworks CAD file displaying the various components of the pumping system. (b) and (c) photographs of the actual assembled unit.*

5.5. Applications: Droplet train generation using multiple motors

The combined pumps can vastly save time and expense required for fabricating hardcoded pumps individually for different assays. The platform has been used for various applications which have been demonstrated in the following sections.

5.5.1. Droplet sequences using two T-junctions

This section demonstrates how the multi-pump platform can be utilised to produce droplets on-demand and with different sequences. Three peristaltic micro pumps were implemented in conjunction with a PDMS chip (600 µm x 100 µm channels), which has two T-junctions with an extra oil line. Two, out of the three, two-line pump introduced an aqueous and an oil pulsation per rotation and the third one introduced additional oil when required (schematic in Fig. 113). Figure 113 (b)(ii)-(vi) shows the a few different sequences that can be produced using this set up of three pumps and Fig. 113 (b)(i) shows the chip used to do so. Green and yellow food dye were used for the aqueous phases and pure FC 40 used as carrier. Figure 113 (b)(ii) demonstrates single droplet generation per rotation using pump 3. Figure 113 (b)(iii) demonstrates all three pumps in action, producing alternating droplets separated by one oil pulse. All the consecutive figures show droplet trains generated using three pumps as well. Figure 113 (b)(iv) shows one rotation of pump 3 producing one yellow droplet and two rotations of pump 1 producing two consecutive green droplets with an additional oil pulsation in between each droplet by pump 2. Figure 113 (b)(v) shows two rotations of pump 3 producing two yellow droplets, two rotations of pump 1 producing two consecutive green droplets and the oil pump pumping after every rotation of the other two. Figure 113 (b)(vi) shows three rotations of pump 3 producing three yellow droplets, one rotation of pump 1 producing one green droplet and the oil pump pumping after every rotation of the other two. This sequencing shows that any two biomarkers or environmental analytes can be measured alternatively and in repeats using this combination of pumps and microfluidic chip. This can also be implemented for monitoring standard and sample for a single analyte.

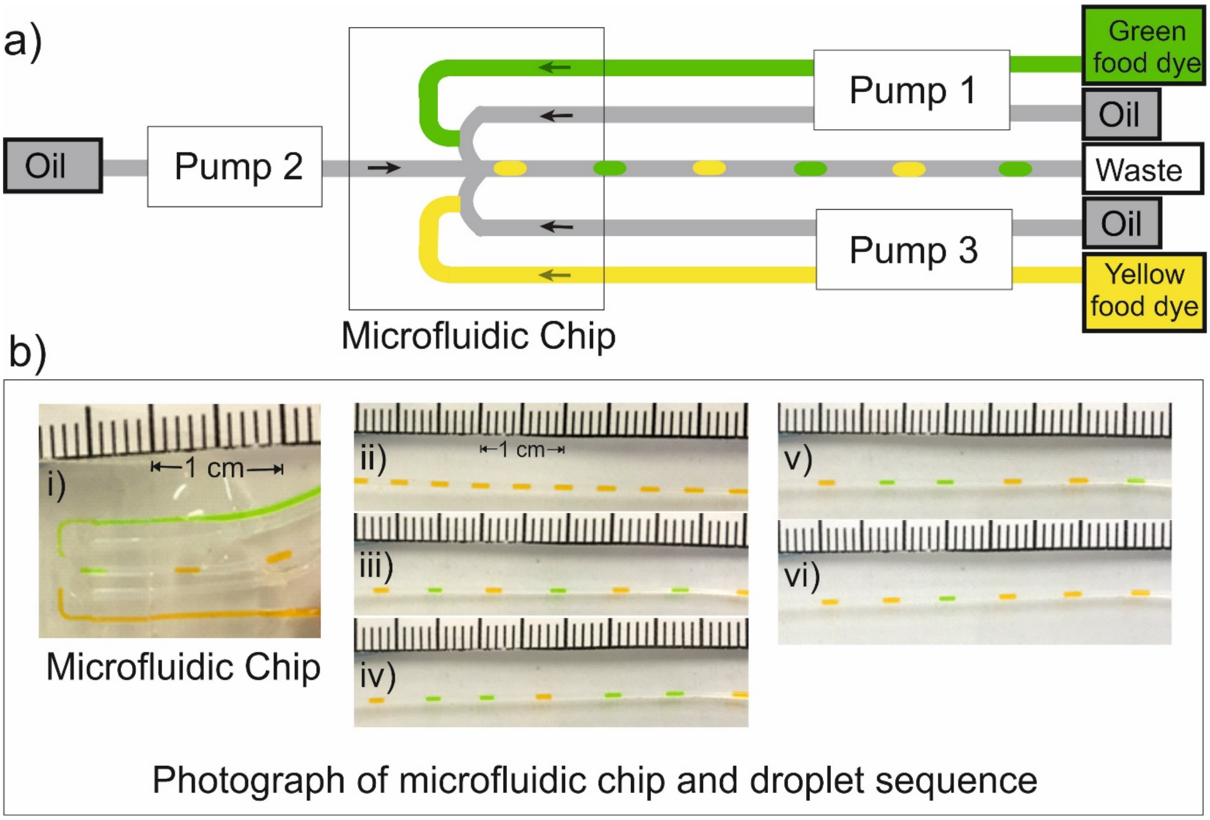

Figure 113. *(a) Schematic showing the three-pump system with parallel T-junction microfluidic chip, generating droplets. (b) (i) PDMS microfluidic chip with two parallel T-junction and an additional oil line. (b) (ii-vi) Different droplet sequences produced by the combination of three pumps and the PDMS chip in (b) (i).*

5.5.2. Four droplet train suitable for cortisol assay

Another example application of the multi-pump platform was the generation of a four-droplet train (400-500nL) for miniaturising continuous immunoassays such as ELISA in droplets (Evans et al., 2021), as demonstrated in Chapter 3. Here a droplet-based heterogeneous assay was explored for cortisol monitoring. The assay requires sampling cortisol-containing fluids into the first droplet with cortisol-HRP (cortisol-3-carboxymethyloxime horseradish peroxidase conjugate) and anti-cortisol functionalized magnetic beads (MyOne Dynabeads), forming a competitive assay. After the competitive binding process is complete, the magnetic beads are collected by a magnetic field and moved to the subsequent droplets in the train including PBS washing buffer and finally into 3,3',5,5'-Tetramethylbenzidine (TMB) reporter droplet.

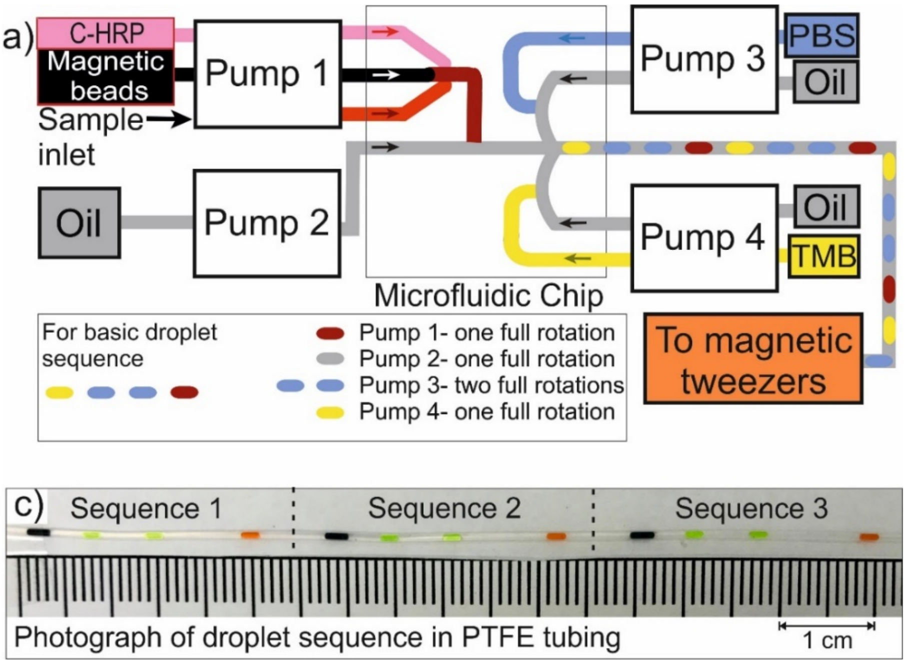

__Figure 114.__ (a) Schematic of four pump system generating four droplet sequence for carrying out ELISA assay for cortisol in droplets. Each sequence is produced by one rotation of pump 1, then pump 2, two full rotations of pump 3 and finally one rotation of pump 4. (b) Actual picture of droplets produced using red (420 nL), green (410 nL) and black dyes (580 nL) food dyes.

This pump system (Fig. 111) reliably produces these droplet trains on-demand. As can be seen from Fig. 114 Pump 1 in the system introduces the aqueous pulse containing, cortisol, cortisol-HRP and magnetic beads per rotation followed by one rotation of pump 2 introducing oil to break off the first droplet at the T-junction. Then pump 3 introduces the two PBS wash droplets followed by oil by completing two full rotations (the importance of having two wash droplets has been discussed in detail in Chapter 3, section 3.3.4). Final TMB reporter droplet is produced by one rotation of pump 4. The oil gaps between droplets are adjustable and the droplet trains can flow or stop at any time meaning the reaction time, bead capturing and transferring between droplets can be easily optimised. Figure 114 (c) shows actual photograph of droplets produced using red (420 nL), green (410 nL) and black dyes (580 nL).

5.5.2.1. Evolution of the junction chip

Each assay requires a tailored microfluidic chip, whose design is based on the number of inlets and the dimensions are based on the volume of droplets to be generated. Figure 115 demonstrates the evolution of the PDMS junction chip for the cortisol assay, which is crucial for smooth operation of the four-pump system. The first version of the chip (Fig. 115 (a)) comprised three parallel T-junctions which was derived from the chip used to perform the assay with a single 12-line pump (section 3.5, Fig. 55). However, the droplets produced were not clearing the outlet junction, resulting in droplet merging. The second chip Fig. 115 (b)) was designed taking into consideration the respective positions of the motors as shown in the schematic (Fig. 114 (a)) above. This chip had two oil lines for pumping in more oil with less rotations required from the oil pump (pump 2). However, this chip caused droplet instability due to having the extra oil line. The extra oil line was removed in the next chip shown in Fig. 115 (c)) however, the length of the channel connecting the 3-line T-junction to the main junction was not long enough for droplet formation before reaching the junction and caused droplet break up. Figure 116 (a) shows a picture of the droplet train generation (using chip in Fig. 115 (c)) but with droplet break up and merging, resulting in contamination and different volumes. Hence, in the final version (Fig. 115 (d)) of the chip, the channel length was increased and as a result, stable, monodisperse and repeatable droplet sequence was obtained as can be seen in Fig. 116 (b) (the dimensioned chip can be seen in Fig. 133 in the appendix).

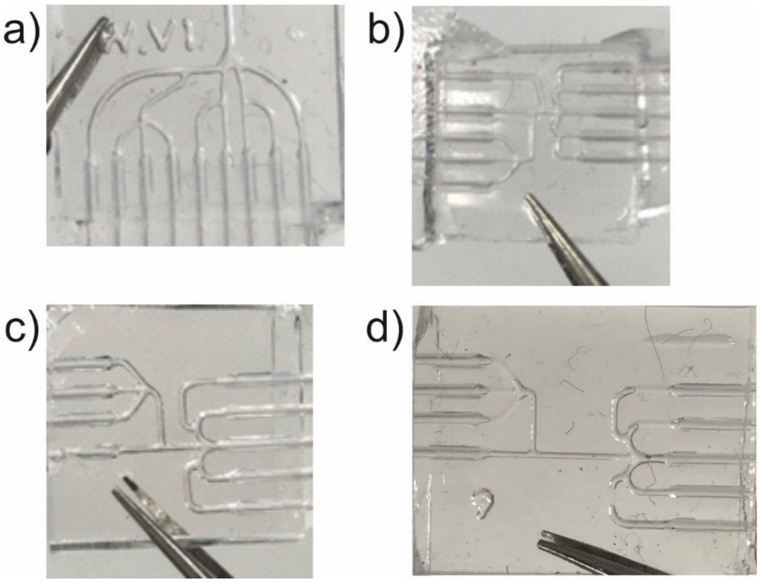

Figure 115. *Evolution of the PDMS junction chip for cortisol assay using the four-pump system. (a) Junction chip derived from design made for 12 line peristaltic pump (details in chapter 3). (b) Junction chip tailored for four-pump system. (c) Removal of additional oil line and re-arrangement of T-junctions from chip shown in (b). (d) Extension of channel connecting T-junction on the left side to the main junction resulting in the final chip.*

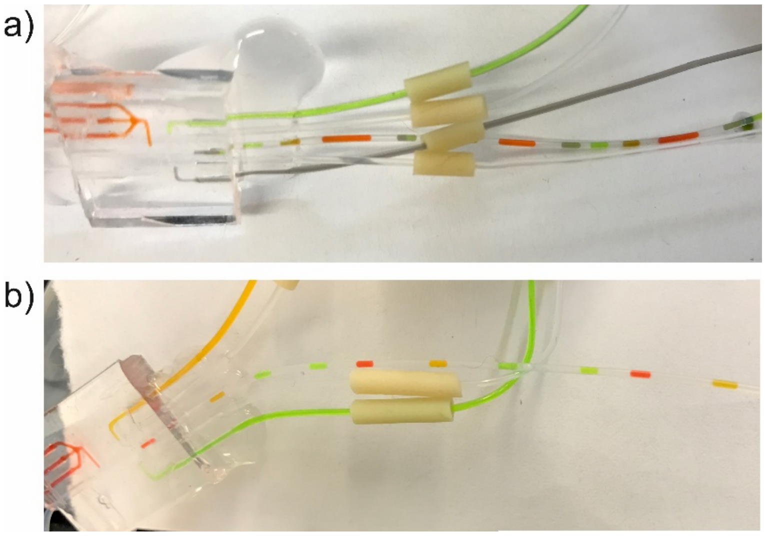

Figure 116. *Four droplet train generation using (a) an older version of PDMS junction chip (Fig. 115 (c)) and (b) latest version of PDMS junction chip (Fig. 115 (d)). The latest version shows stable and uniform droplet generation with no cross contamination.*

5.5.2.2. Dyneon chips

Although currently chips are fabricated using PDMS, from our experience, it is worthwhile to investigate other materials. PDMS chips require surface treatment, and the surface quality degrades over time resulting in pinning of the droplets to the channels and cross-contamination. A more robust and durable alternative to using PDMS would be fabricating chips using fluorinated thermoplastic polymer (Dyneon THV) supplied in pellet form (Begolo et al., 2011) which does not require any surface treatment like PDMS. The fabrication procedure is also straightforward compared to multi step procedures requiring laser cutting for making other Teflon chips (de Haas et al., 2012).

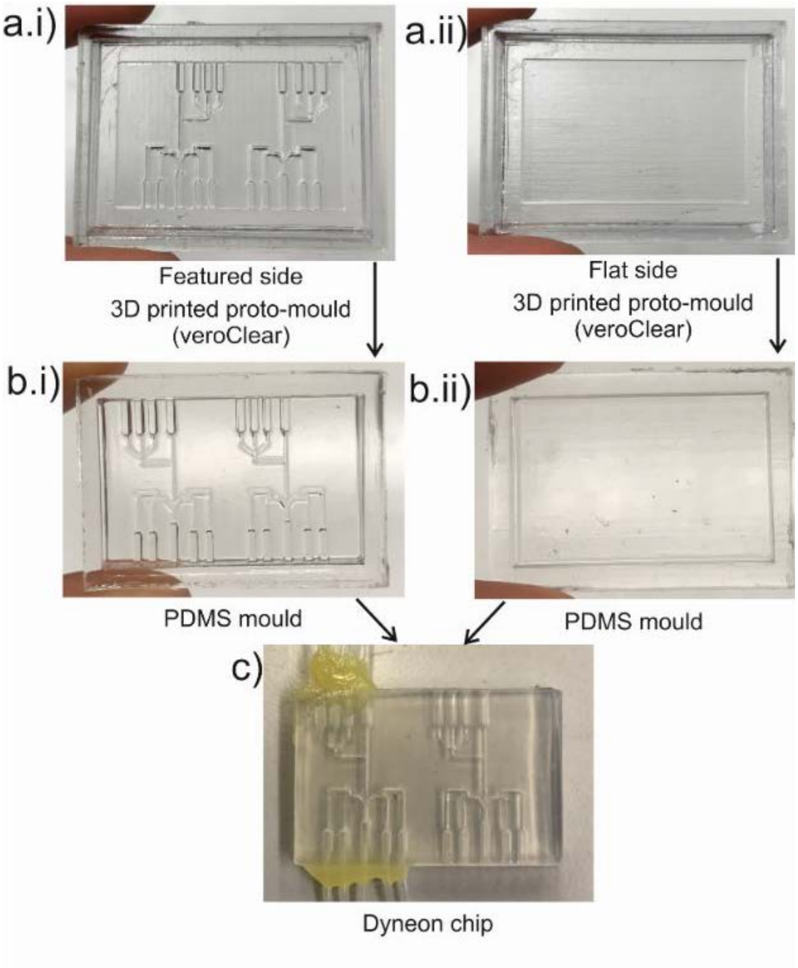

Figure 117. *Fabrication steps of Dyneon microfluidic chip. (a) 3D printed proto-mould for curing PDMS showing (i) featured side and (ii) plain side. (b) PDMS mould. (c) Finished Dyneon chip with PTFE tube (0.5 mm inner diameter) inlets and outlet.*

The fabrication steps (Nightingale et al., 2020) involve making a 3D printed proto-mould for a PDMS mould to pour the Dyneon pellets into. The proto-moulds for the cortisol junction chip which has been

3D printed using VeroClear material in glossy finish can be seen in Fig. 117 (a) (i) showing the featured side and Fig. 117 (a) (ii) showing the plain side. Compared to PDMS chip moulds which have extrusions for channels, these proto-moulds have grooves cut for the channels. The 3D printed proto-mould has channel dimensions of 400 µm X 450 µm (detailed dimensions in Fig. 134 in Appendix) which is supposed to produce a Dyneon chip of the nominal width and height of a 100 µm X 600 µm PDMS chip (dimensions used for the PDMS junction chips). PDMS mould are made using the 3D proto-moulds (curing in the oven at 70°C for about an hour) and after curing the PDMS moulds are then carefully peeled off (Fig. 117 (b) (i)-(b) (ii)). Dyneon pellets are then tightly packed in a mono layer in the PDMS mould and then placed in the oven to stay overnight at 190°C. Both sides of the chip are then taken out (one side containing channel structures and the other one plain) from the oven and left to cool down for about 10 minutes. The PDMS moulds are then peeled off to obtain the two sides of the Dyneon chip. The two different sides are aligned and carefully sandwiched, pressed using two steel plates and screwed until finger tightness is achieved using a torque screwdriver (0.2-1.5 Nm) at its lowest setting. The sandwiched Dyneon chip is then placed in the oven at 160°C and left overnight for bonding.

Finally, the Dyneon chips are finished off with inserting primed PTFE tubing (0.5 mm inner diameter) which are then glued on to the chip using epoxy. The finished Dyneon junction chip can be seen in Fig. 117 (c). The Dyneon chips are still to be tested and if they prove to be successful, the monitoring platform would become much more durable.

5.5.3. Generation of different sized droplets by altering pumping ratio

The multi-pump system gives us the ability to change the droplet size instantly providing advantages such as using less reagents/ samples per analysis and for optimizing the sensitivity of an assay by adjusting the amount of reagents or sample required instantly. Figure 118 (a) shows photographs of different volumes of droplets produced by defining the pumping ratio of the pump introducing red food dye (representing the aqueous phase). From Fig. 118 (a) (i) to (a) (vi) each droplet was produced using a basic T-junction (600 µm x 100 µm channels) by introducing red food dye pulse/ pulses and an oil pulse to break off the droplet in 0.5 ID PTFE tubing. Increasing size of droplets were produced (i to vi) by increasing the number of turns the pump introducing red food dye from one for Fig. 118 (a) (i) to six for Fig. 118 (a) (vi). The graph in Fig. 118 (b) presents a linear relationship between number of red dye pulses and volume of droplets generated indicating robust droplet generation.

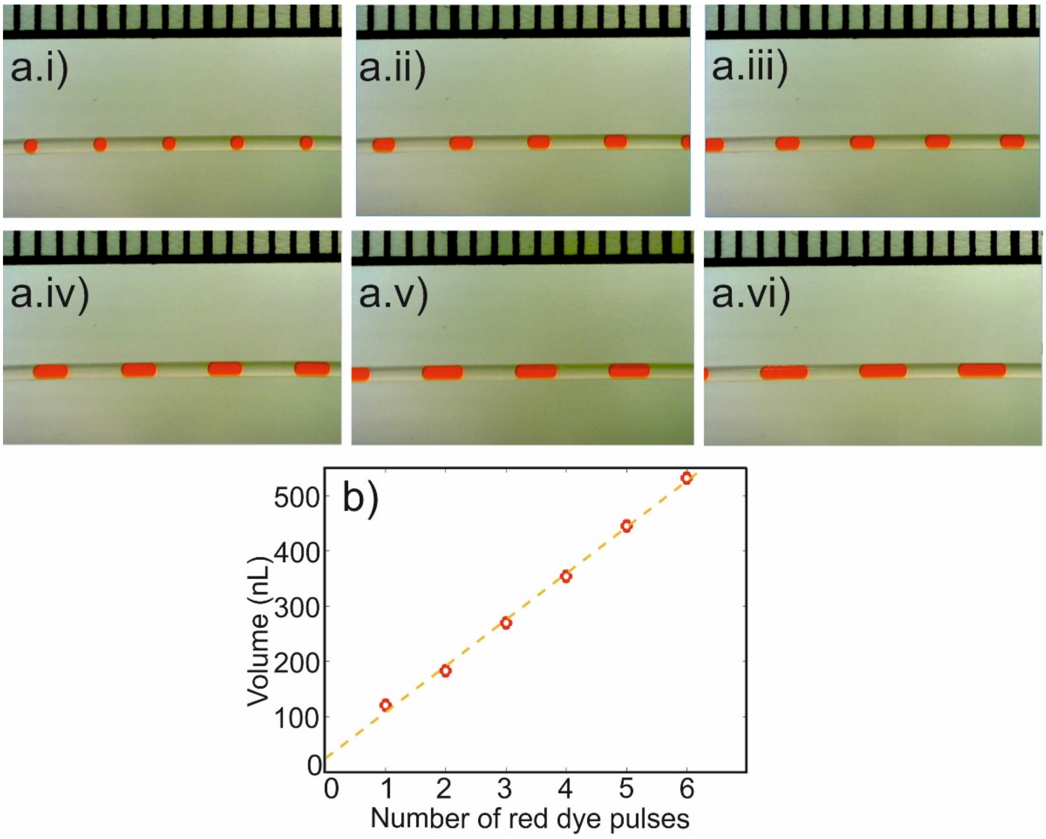

Figure 118. *Different sizes of droplets generated by multi-pump system on-demand. (a) (i-vi) Robust droplet generation of different sized red food dye droplets by increasing the number of rotations of the aqueous line. (b) Volume (nL) of droplets directly proportional to the number of red dye pulses.*

5.5.4. Increasing sensitivity of Dyneon flow cells

The multi-pump platform was implemented to test the sensitivity of Dyneon flow cells fabricated by Dr. Adrian Nightingale (Nightingale et al., 2020). An experiment was designed to verify the increase in sensitivity by increasing the path length of Dyneon flow cells and was performed in collaboration with Dr. Adrian Nightingale.

The flow cell had different pathlengths starting from 1.7 mm to 10 mm and the multi-pump system was used to produce droplets which would completely fill up the 10 mm flow cell (Fig. 119 (c)). For this particular application, the multi-pump system overcomes some limitations posed by the single pump approach. Comparatively larger droplets are required to fill up the 10 mm flow cell which would mean designing a very large roller feature for the single pump system or increasing the diameter of the roller and hence the overall pump head to accommodate the larger droplet volume requirement.

Instead by using the multi-pump system, larger droplets were generated by increasing the number of aqueous pulses before introducing oil to cut off, as demonstrated in the previous section as well (section 5.5.3). Figure 119 (a) shows the schematic of the pumps and the fluidic map. Two pumps were implemented for this application: one to introduce the reagent and standard and another one to introduce oil to the 3-inlet microfluidic chip (600 µm x 100 µm channels). An 8 mm droplet was produced by introducing 8 aqueous pulses (8 complete rotations of pump 2) followed by the introduction of oil. Figure 119 (b), shows the droplets generated to flow through the Dyneon flow cell.

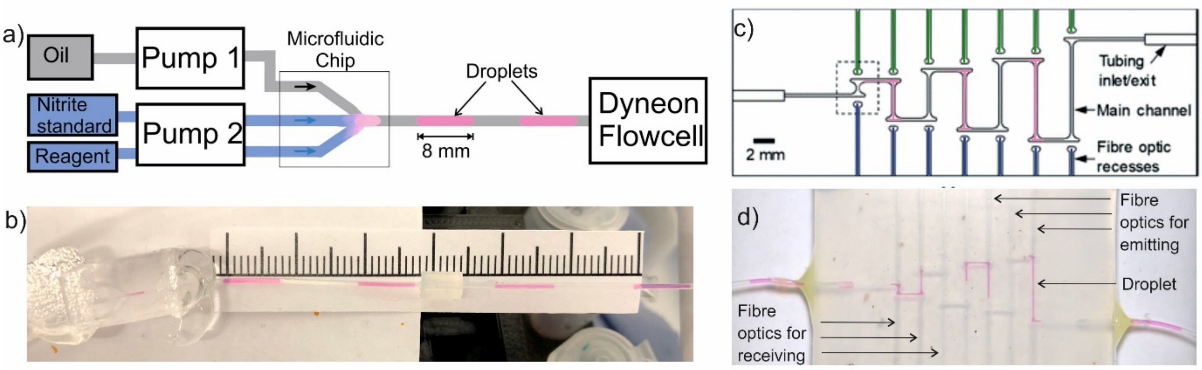

__Figure 119.__ Multiple-pump system used to generate droplets to check sensitivity of multipath Dyneon flow cells. (a) Schematic showing the utilization of two pumps to producing large droplets (modified Greiss assay in droplets) to pass through Dyneon flow cell. (b) Actual photograph of PDMS microfluidic chip and droplets (approximately 8 mm in length inside 0.5 ID PTFE tubing). (c) Layout drawing of the Dyneon flow cell designed by Dr. Adrian Nightingale. The green and blue lines represent fibre optics for emitter and receiver ends respectively and the pink lines represent droplets. (d) Actual photograph of Dyneon flow cell and droplets passing through it filling up the different optical paths (Nightingale et al., 2020).

In order to check the sensitivity of the flowcell, a modified Greiss assay for nitrite was implemented. Nitrite standards and Greiss reagent were added in 1:1 ratio to form a diazonium product which is purple in colour with an absorbance peak at about 525 nm. For the absorbance detection light was transmitted from an LED source through fibre optics to a photodetector. The recesses for the fibre optics and the layout of the Dyneon flow cell can be seen in Fig. 119 (c). A photograph of the Dyneon flow cell with coloured droplets filling up the different pathlengths can be seen in Fig. 119 (d). Increasing the pathlength indeed increased the sensitivity and lowered limit of detection (Nightingale et al., 2020).

5.5.5. Varying concentration and composition by changing pump ratio

In Fig. 120, three micro-pumps produce a continuous train of droplets (here four droplets in each group). The varying compositions of droplets are achieved by changing the number of rotations of pump 2 (introducing green dye) and pump 3 (introducing red dye), totalling five rotations (1700nL) per droplet. In Fig. 120 (b), the left most droplet in each sequence is produced by four rotations of pump 2 and one rotation of pump 3 and vice versa for the rightmost droplet. The number of different droplets with varying compositions can be increased by having smaller feature size of rollers allowing finer tuning of the composition together with permitting more variations for the same size of droplets. This example clearly demonstrates that the pumping system can reliably vary the concentration of analyte/reagent in the droplets, which is critical for droplet-based screening and analysis.

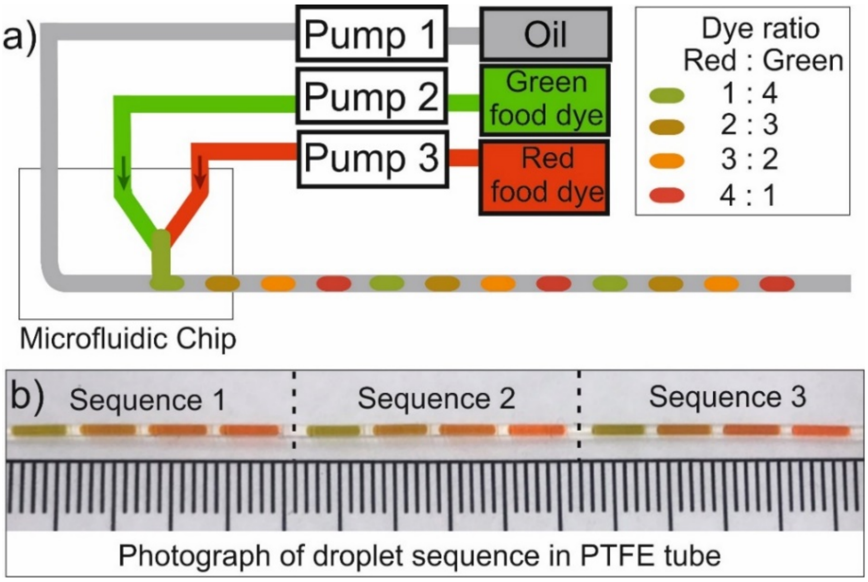

Figure 120. *(a) Schematic of 3 peristaltic pump system generating repeated four droplet trains having different compositions. (b) Picture of droplets with varying compositions indicated by the change in colour gradient from a green hue to red hue.*

A combination of three pumps can also produce different dilutions. In Fig. 121, three micro-pumps produce a continuous train of droplets with varying dilutions/ compositions. The varying dilutions of droplets are achieved by changing the number of rotations of motors in for two pumps introducing red food dye and de-ionised water totalling six rotations/ pulses (2040 nL) per droplet. Mixing ratio varies resulting in higher concentration of red food dye to lower concentration per six droplets and the cycle is repeated. The droplet generation and their composition show good reproducibility as seen by figures 121 (a), 121 (b) and by the cyclic change in absorbance in Fig. 121 (c). The leftmost droplet of each sequence comprises of 6 red food dye pulses and the rightmost droplet contains one red food dye pulse and 5 pulses of de-ionised water forming a much diluted droplet.

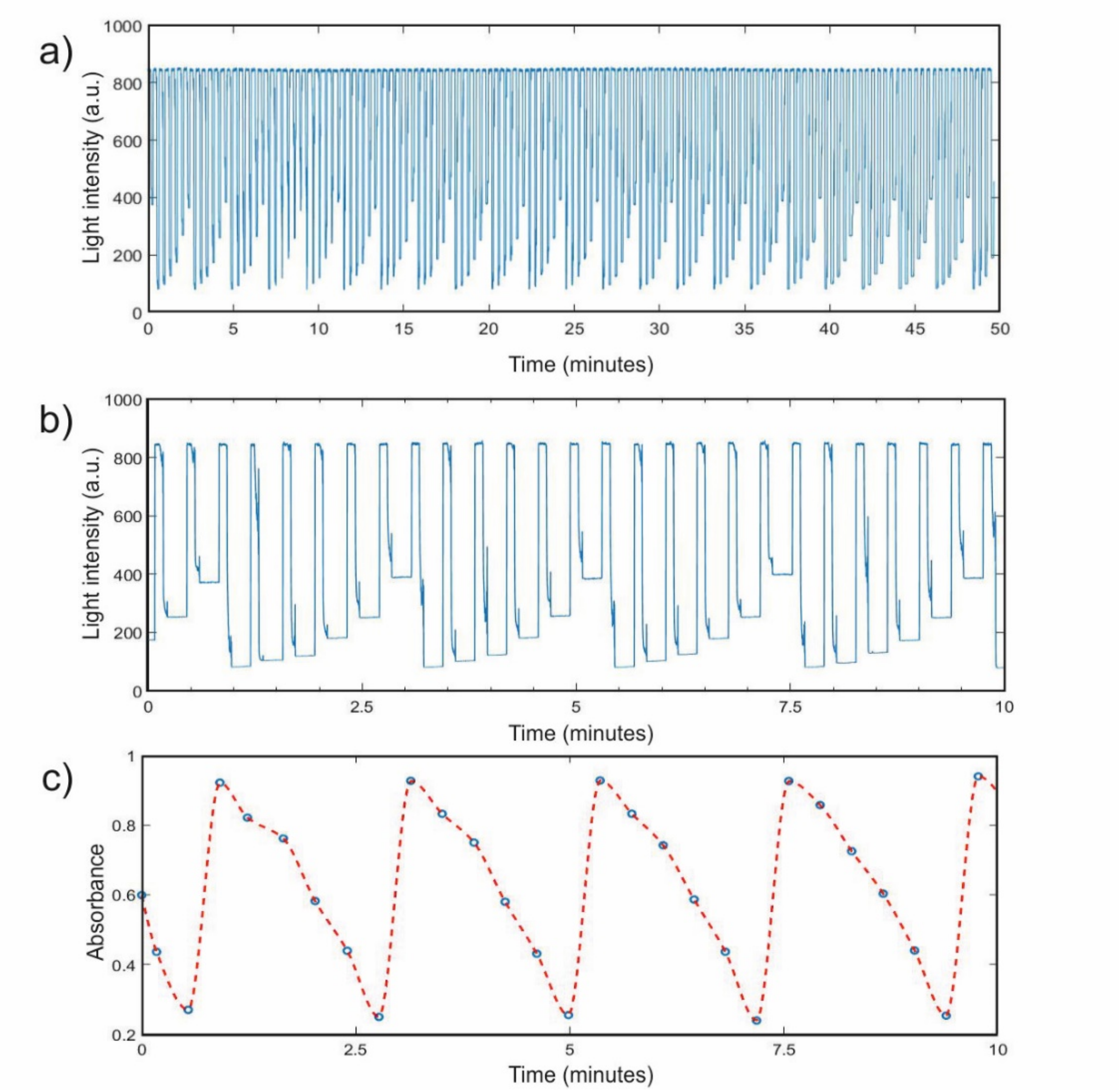

Figure 121. *Different dilutions generated in droplets using multiple-pump system. (a) Raw light intensity data showing different dilutions of droplets being generated repeatedly. Each square pulse refers to one droplet. (b) Graph zoomed in from (a). (c) Corresponding absorbance values of (b).*

Figure 122 shows the relationship between the number of red dye pules and the absorbance calculated using Beer Lambert's law from the raw intensity values in Fig. 121. The absorbance value increases as the concentration of red food dye increases. The absorbance value increases as the number concentration of red dye increases.

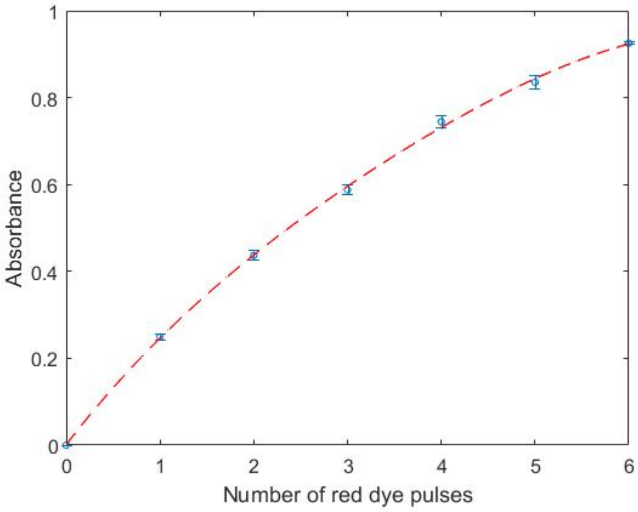

Figure 122. *Absorbance versus number of red dye pulses. As the number of red dye pulses increase per droplet (concentration of dye increases), the absorbance value also increases.*

Another variation of the test was done by using different pumping ratios but not keeping the droplet the same size, as having different droplet sizes does not affect the path length in this case. Photographs of the different compositions of the droplets can be seen in Fig. 123 (a). Relative concentrations of the droplets for different mixing ratios (1:1, 1:3, 1:5 and 1:7) were plotted against absorbance. Linear relationship between absorbance and relative concentration with absorbance values less than RSD 1.08% for more than 50 droplets of each composition shown in Fig. 123 (b).

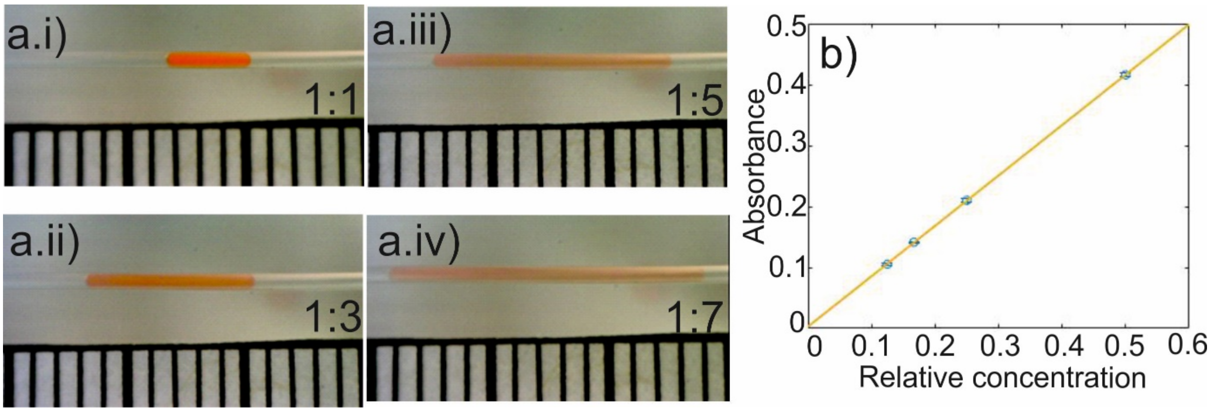

Figure 123. *(a).(i-iv) Changing the mixing ratio of red food dye and de-ionised water results in different concentration of droplets as shown. b) Linear relationship between absorbance and relative concentration with absorbance values < RSD 1.08% for >50 droplets of different ratios shown in (a).*

5.6. Chapter Conclusion

This chapter elucidates the development of a multi-pump platform capable of generating on-demand, arbitrary droplet trains of different volume and composition. In this chapter I have:

(i) Explained the rationale behind moving from a single pump system to a multiple pump platform.
(ii) Described the design evolution and fabrication of a single spring micropump.
(iii) Described the design and fabrication of a control circuit and PCB for automating the multiple pump platform.
(iv) Demonstrated different applications that can be achieved using multiple pumps like serial dilutions and generation of droplet trains e.g. for heterogeneous ELISA for cortisol.

This novel, versatile platform lays the foundation for exploring various multiple-step and multiplexed assays and could also facilitate different biochemical protocols which have been discussed further in the future works section.

CHAPTER 6

CONCLUSION AND FUTURE WORK

This chapter summarises the conclusion, key contributions, and avenues of future work.

6.1. Conclusion

This thesis has developed various microfluidic platforms and demonstrated that droplet microfluidics is indeed a powerful tool for biochemical analytics and for continuous monitoring. Both cortisol and ammonium have been analysed from healthcare and water monitoring applications. The sensors demonstrate high degree of automation, provide data with high temporal resolution, reduce sample-to-signal time and significantly reduce reagent consumption. We envisage that this platform technology would revolutionize immunodiagnostics by providing automated and cost effective multiplexed and multiple-step assays, for a multitude of applications. This platform technology also has the potential to be the next generation of *in-situ* environmental sensors and be implemented for high frequency nutrient profiling in natural waters and soil, wastewater monitoring, and aquaculture.

Novelty of different aspects of the thesis and study:

1. This is the first demonstration of miniaturising the magnetic based ELISA into a train of droplets for monitoring Cortisol. Fabrication of an autonomous platform consisting of a 12-line peristaltic pump for droplet train generation, electromagnetic tweezers for magnetic bead manipulation and inline spectrophotometer for colorimetric detection has been demonstrated.

2. This thesis is the first to report an *in-situ* droplet microfluidic based ammonium sensor. The well-established indophenol blue method using the modified Berthelot's reaction has been miniaturised into droplets in order to quantify ammonium. The sensor has been used to measure river water samples and has also been deployed in a sequential batch bioreactor for continuous monitoring.

3. Development of a robust and programmable droplet-on-demand platform utilising peristaltic micropumps. The platform is capable of generating arbitrary sequences of droplets with variable size, spacing and composition as desired without the need to redesign hardware. This offers the flexibility to implement various multiplexed 'mix-and-read' and multiple steps biochemical assays.

6.2. Future work

6.2.1. Further development of droplet platform

Currently in the multiple pump platform, low power geared DC motors (driven by an USB powered Arduino board) are used to drive the pumps. As the pumps are not turned on simultaneously, the power provided by the USB port is sufficient to support the system. However, if all the pumps in the platform are turned on simultaneously for filling inlet channels with reagents/sample, external power would be required. The motor lifetime has not been tested quantitatively but during experiments it was noticed that the motors did not last longer than a few days during continuous usage and also generated noise during rotation. Therefore, brushless DC motors with high torque could be tested and implemented in the future prototype system.

PDMS chips have been implemented in the droplet platforms throughout this thesis due to the ease of rapid prototyping and for achieving channel dimensions (down to 100 µm) with smooth surface finish, however there are still areas of improvement. PDMS chips require surface coating treatment which wears off after 2-3 days, therefore the chips have limited lifetime. Other alternative approaches have been explored in this thesis such as the use of Dyneon THV fluoropolymer (Begolo et al., 2011) for microfluidic junction (section 5.5.2.2). Although Dyneon chips did not require surface treatment and have demonstrated a longer lifetime for a period of around 16 weeks (Nightingale et al., 2020) with simple sample such as DI water and food dye solutions, smearing of the surface and cross contamination were observed when other acid or base regents were used. More hydrophobic materials and related fabrication techniques should be explored in the future. 3D printed (using Ultimaker 3) chips using PLA material have also been implemented in the ammonium sensor (section 4.8.1.2) which demonstrated good droplet generation over 4 days during the sensor deployment to the bioreactor. The channel diameter of the chips however could not go below 650 µm due to the printing resolution. Further long-term testing is required to validate the robustness of the chip.

6.2.2. Integrating with other detection technologies

One of the biggest advantages of this platform technology is its adaptability to perform various assays by a slight change in system hardware. The assays that have been implemented in this thesis like the ELISA for cortisol or the Indophenol blue assay for ammonium are both colorimetric assays and implement absorbance spectrometry. We are able to fabricate relatively cheap, simple, and robust 3D printed flowcells to carry out the detection. Absorbance measurements provide us with certain advantages over electrochemical sensing which is subject to ionic interferences, signal drift and biofouling (Heikenfeld et al., 2018) as mentioned earlier in this thesis. However, absorbance detection does come with some disadvantages and one such is not being able to achieve very low detection limits. The applications in this thesis have not required very low detection limits, however, it is an area that can be explored more using this platform technology. The detection limits have been improved in this thesis by changing the optical pathlength of the detectors and two ways on how that has been achieved has been explained in section 4.9. We have implemented flowcells with various tubing diameters to increase the droplet diameter and hence the path length. A multipass flowcell designed by Dr. Bingyuan Lu has also been implemented which applied to mirrors to reflect light through a droplet several times, thus increasing pathlength.

However, in order to get higher sensitivity, fluorescence-based detection can be implemented as well as has been detailed in section 2.7. Research efforts are being made to make fluorescence detection in droplets compact and versatile. Laser coupled optical fibres have been implemented for multicolour fluorescent detection by exciting different sections of a microfluidic channel thus shifting from using bulky epifluorescence microscopes (Cole et al., 2016). Yang and co-workers have demonstrated the fluorescence detection in picolitre droplets up to 400 nM of fluorescein using an optofluidic platform implementing liquid waveguides (Yang et al., 2017). Translation of fluorescence-based assays into droplets using this platform and developing miniaturised fluorescence detectors would lead to major improvement in detection sensitivity.

Therefore, different testing scenarios bring in different challenges but our droplet platform can be adapted for different scenarios rapidly. The technology is therefore very powerful and the options for continuous monitoring are abundant.

6.2.3. Applications

6.2.3.1. Utilization of multiple pump system for measuring Seawater Total Alkalinity

There could be endless applications with the droplet platforms developed in the thesis. Chapter 5 has demonstrated a method of flexible droplet train generation which could be used for measuring seawater total alkalinity. Increased atmospheric carbon over the last few decades has led to the absorption of carbon by the oceans causing a decrease in the ocean pH levels. This ocean acidification has cascading effects through the marine ecosystem. As the ocean acidity increases, it becomes harder for calcifying organisms to form shells and skeletons, and the existing ones become susceptible to dissolution (Millero, 2007). Seawater total alkalinity (A_T) is the measure of the buffering capacity of seawater and has been described by Dickson (1981) as the moles of protons (H^+) that needs to be added to quench every molecule of proton acceptors (bases) (Dickson, 1981, Seelmann et al., 2019). Measuring A_T together with three other parameters: pH, partial pressure of CO_2 (pCO_2) and total dissolved inorganic carbon (C_T) is required to accurately describe ocean carbonate chemistry (Millero, 2007).

Traditionally seawater total alkalinity is measured in laboratories using multipoint titration (Millero et al., 1993) involving pH electrode (disadvantages - frequent recalibration and impossible to implement in field deployable sensors) which is time consuming (10-20 minutes), requires precise handling of the related sample (transportation) and reagent. *In situ* analysers based on single point titration and spectrophotometric detection have been developed (Spaulding et al., 2014, Li et al., 2013) which work by adding in a large quantity of acid in one go, extracting any CO_2 that is given off (by removal of bicarbonate) and then measuring the final pH with a dye. These analysers cater to increasing the temporal resolution and decreasing the analysis time, however there are still some avenues which can be improved. Most of these analysers require flushing between samples which takes significant amount of time or else the measurements get compromised due to the sticking of titrant and sample mixture in the optical pathway (Seelmann et al., 2019). Removal of CO_2 (due to the dissolved inorganic carbon from the sample) is necessary and analysers usually employ additional components which increases system complexity. For their spectrophotometric analyser, Li *et al.* implemented an in line CO_2 remover consisting of a Teflon tube immersed in a box of 1M NaOH (Li et al., 2013). Another major issue is that the final pH needs to be in the 3-3.5 range and in order to do so, the amount of acid to be added needs to be known roughly (Seelmann et al., 2019). Therefore, a system which would be able to adjust the amount of acid on-demand would be well suited for this application.

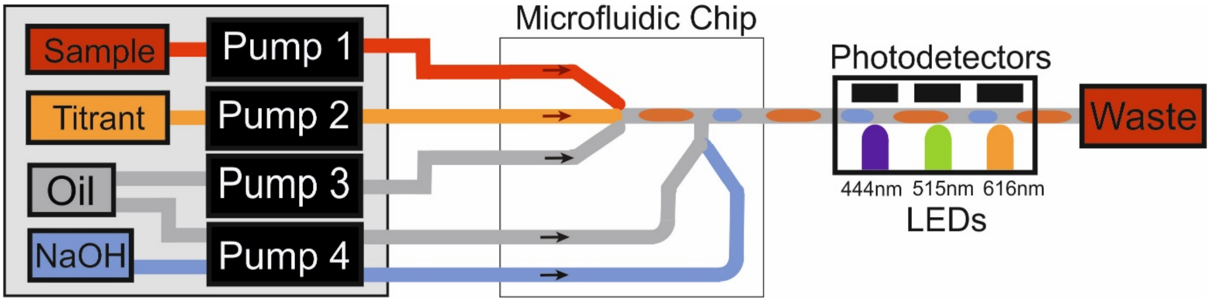

__Figure 124.__ System architecture of droplet microfluidic platform for monitoring Seawater Total Alkalinity. A combination of four pumps is used to generate alternating droplets containing sample+titrant and NaOH in fluorocarbon oil. The droplets then travel downstream to a 3 LED- detector flow cell for absorbance measurements.

Droplet microfluidics gives us an advantage of having the mixtures in droplets transported by an oil carrier. This removes the need for the system to be flushed in between samples and also provides us an easy way to remove CO_2 by having alternating NaOH droplets. The multi-pump system described in Chapter 5 allows different pumping ratios and would eliminate the need to always use a predetermined volume of acid for the analysis like other systems. We therefore, would be able to change the volume and mixing ratios of sample and titrant and as a result adjust measurements based on the total alkalinity values. Therefore, we propose an *in situ* seawater total alkalinity platform (Fig. 124) comprising of the multi-pump system, a PDMS microfluidic chip, a three LED and photodetector pair flowcell and cartridges for storage of sample, titrant and waste. Seawater, titrant (consisting of acid and indicator), oil and sodium hydroxide (NaoH) would be introduced to the microfluidic chip via the pumps. Therefore, a droplet train of alternate seawater+titrant and NaOH would be generated. The mixing ratio of seawater and titrant would be adjustable. The NaOH droplets on either side of each seawater+titrant droplet would absorb the CO_2 that would be generated and could interfere with the absorbance measurement. The three LED (615nm, 440 nm, 515 nm) pairs would provide the absorbance values required for calculating pH and hence the total alkalinity. The 444 nm wavelength LED and 616 nm one has absorbance maxima for acid and base indicator. An additional 515 nm wavelength LED would also be incorporated for the isosbestic point which is not supposed to change regardless of the shift in absorbance of the other two peaks thus acting as a reference point. Preliminary investigation using the multi-pump system has been performed in collaboration with Dr. Adrian Nightingale and a multi-LED flow cell has been fabricated (Fig. 135 in Appendix). However, further conclusive work could not be performed due to Covid-19 closure of the laboratories and future works are required.

6.2.3.2. Development of a total water monitoring sensor

An *in situ* sensor has already been developed by our group (Nightingale et al., 2019a) for monitoring nitrate/nitrite in river water. A sensor for monitoring phosphate concentrations is also in development in our group. This thesis has demonstrated the development of an ammonium sensor. Therefore, the development of a universal sensor for multiplexed measurement of all four nutrients like nitrate, nitrite, ammonium and phosphate would be of high value for environmental monitoring. It would provide us rich nutrient profiles, especially when other traditional sensors like temperature sensor, dissolved oxygen sensor and pH sensor are also integrated.

References

Abate, A. R., Romanowsky, M. B., Agresti, J. J. and Weitz, D. A. (2009) 'Valve-based flow focusing for drop formation', *Applied Physics Letters,* 94(2), pp. 023503.

Abate, A. R. and Weitz, D. A. (2009) 'High-Order Multiple Emulsions Formed in Poly(dimethylsiloxane) Microfluidics', *Small,* 5(18), pp. 2030-2032.

Abraham, G. E., Buster, J. E. and Teller, R. C. (1972) 'Radioimmunoassay of Plasma Cortisol', *Analytical Letters,* 5(11), pp. 757-765.

Adamson, D. N., Mustafi, D., Zhang, J. X. J., Zheng, B. and Ismagilov, R. F. (2006) 'Production of arrays of chemically distinct nanolitre plugs via repeated splitting in microfluidic devices', *Lab on a Chip,* 6(9), pp. 1178-1186.

Ahmed El-Laboudi, N. S. O., Anthony Cass, and Desmond Johnston (2013) 'Use of Microneedle Array Devices for Continuous Glucose Monitoring: A Review', *Diabetes Technology & Therapeutics,* 15(1), pp. 101-115.

Ali‐Cherif, A., Begolo, S., Descroix, S., Viovy, J. L. and Malaquin, L. (2012) 'Programmable Magnetic Tweezers and Droplet Microfluidic Device for High‐Throughput Nanoliter Multi‐Step Assays', *Angewandte Chemie International Edition,* 51(43), pp. 10765-10769.

Anna, S. L. (2016) 'Droplets and Bubbles in Microfluidic Devices', *Annual Review of Fluid Mechanics,* 48(1), pp. 285-309.

Anna, S. L., Bontoux, N. and Stone, H. A. (2003) 'Formation of dispersions using “flow focusing” in microchannels', *Applied Physics Letters,* 82(3), pp. 364-366.

Anna, T., Jan, P. and Frantisek, F. (2017) 'Recent strategies toward microfluidic‐based surface‐enhanced Raman spectroscopy', *ELECTROPHORESIS,* 38(16), pp. 1977-1987.

Appel, D., Schmid, R. D., Dragan, C. A., Bureik, M. and Urlacher, V. B. (2005) 'A fluorimetric assay for cortisol', *Anal Bioanal Chem,* 383(2), pp. 182-6.

Bandodkar, A. J. and Wang, J. (2014) 'Non-invasive wearable electrochemical sensors: a review', *Trends in Biotechnology,* 32(7), pp. 363-371.

Baret, J.-C. (2012) 'Surfactants in droplet-based microfluidics', *Lab on a Chip,* 12(3), pp. 422-433.

Baret, J.-C., Miller, O. J., Taly, V., Ryckelynck, M., El-Harrak, A., Frenz, L., Rick, C., Samuels, M. L., Hutchison, J. B., Agresti, J. J., Link, D. R., Weitz, D. A. and Griffiths, A. D. (2009) 'Fluorescence-activated droplet sorting (FADS): efficient microfluidic cell sorting based on enzymatic activity', *Lab on a Chip,* 9(13), pp. 1850-1858.

Baroud, C. N., Delville, J.-P., Gallaire, F. and Wunenburger, R. (2007) 'Thermocapillary valve for droplet production and sorting', *Physical Review E,* 75(4), pp. 046302.

Baroud, C. N., Gallaire, F. and Dangla, R. (2010) 'Dynamics of microfluidic droplets', *Lab on a Chip,* 10(16), pp. 2032-2045.

Basova, E. Y. and Foret, F. (2015) 'Droplet microfluidics in (bio)chemical analysis', *Analyst,* 140(1), pp. 22-38.

Bastos, L., Bio, A. and Iglesias, I. (2016) 'The Importance of Marine Observatories and of RAIA in Particular', *Frontiers in Marine Science,* 3(140).

Basu, A. S. (2013) 'Droplet morphometry and velocimetry (DMV): a video processing software for time-resolved, label-free tracking of droplet parameters', *Lab on a Chip,* 13(10), pp. 1892-1901.

Beaton, A. D., Sieben, V. J., Floquet, C. F. A., Waugh, E. M., Abi Kaed Bey, S., Ogilvie, I. R. G., Mowlem, M. C. and Morgan, H. (2011) 'An automated microfluidic colourimetric sensor applied in situ to determine nitrite concentration', *Sensors and Actuators B: Chemical,* 156(2), pp. 1009-1014.

Beauchamp, M. J., Nordin, G. P. and Woolley, A. T. (2017) 'Moving from millifluidic to truly microfluidic sub-100-µm cross-section 3D printed devices', *Anal Bioanal Chem,* 409(18), pp. 4311-4319.

Begolo, S., Colas, G., Viovy, J.-L. and Malaquin, L. (2011) 'New family of fluorinated polymer chips for droplet and organic solvent microfluidics', *Lab on a Chip,* 11(3), pp. 508-512.

Belder, D. (2005) 'Microfluidics with Droplets', *Angewandte Chemie International Edition,* 44(23), pp. 3521-3522.

Bhattacharya, S., Datta, A., Berg, J. M. and Gangopadhyay, S. (2005) 'Studies on surface wettability of poly(dimethyl) siloxane (PDMS) and glass under oxygen-plasma treatment and correlation with bond strength', *Journal of Microelectromechanical Systems,* 14(3), pp. 590-597.

Blaen, P. J., Khamis, K., Lloyd, C. E. M., Bradley, C., Hannah, D. and Krause, S. (2016) 'Real-time monitoring of nutrients and dissolved organic matter in rivers: Capturing event dynamics, technological opportunities and future directions', *Science of The Total Environment,* 569-570, pp. 647-660.

Bogojevic, D., Chamberlain, M. D., Barbulovic-Nad, I. and Wheeler, A. R. (2012) 'A digital microfluidic method for multiplexed cell-based apoptosis assays', *Lab on a Chip,* 12(3), pp. 627-634.

Booth, M. A., Gowers, S. A. N., Leong, C. L., Rogers, M. L., Samper, I. C., Wickham, A. P. and Boutelle, M. G. (2018) 'Chemical Monitoring in Clinical Settings: Recent Developments toward Real-Time Chemical Monitoring of Patients', *Analytical Chemistry,* 90(1), pp. 2-18.

Brasier, N. and Eckstein, J. (2019) 'Sweat as a Source of Next-Generation Digital Biomarkers', *Digital Biomarkers,* 3(3), pp. 155-165.

Brossaud, J., Ducint, D., Gatta, B., Molimard, M., Tabarin, A. and Corcuff, J. (2012) 'Urinary cortisol metabolites in corticotroph and adrenal tumours', *Endocr. Abstr.,* 29.

Brosseau, Q., Vrignon, J. and Baret, J.-C. (2014) 'Microfluidic Dynamic Interfacial Tensiometry (µDIT)', *Soft Matter,* 10(17), pp. 3066-3076.

Brouzes, E., Medkova, M., Savenelli, N., Marran, D., Twardowski, M., Hutchison, J. B., Rothberg, J. M., Link, D. R., Perrimon, N. and Samuels, M. L. (2009a) 'Droplet microfluidic technology for single-cell high-throughput screening', *Proceedings of the National Academy of Sciences,* 106(34), pp. 14195-14200.

Brouzes, E., Medkova, M., Savenelli, N., Marran, D., Twardowski, M., Hutchison, J. B., Rothberg, J. M., Link, D. R., Perrimon, N. and Samuels, M. L. (2009b) 'Droplet microfluidic technology for single-cell high-throughput screening', *Proceedings of the National Academy of Sciences of the United States of America,* 106(34), pp. 14195-14200.

Brower, K. K., Khariton, M., Suzuki, P. H., Still, C., Kim, G., Calhoun, S. G. K., Qi, L. S., Wang, B. and Fordyce, P. M. (2020) 'Double Emulsion Picoreactors for High-Throughput Single-Cell Encapsulation and Phenotyping via FACS', *Analytical Chemistry,* 92(19), pp. 13262-13270.

Camargo, J. A. and Alonso, Á. (2006) 'Ecological and toxicological effects of inorganic nitrogen pollution in aquatic ecosystems: A global assessment', *Environment International,* 32(6), pp. 831-849.

Casadevall i Solvas, X., Niu, X., Leeper, K., Cho, S., Chang, S.-I., Edel, J. B. and deMello, A. J. (2011) 'Fluorescence detection methods for microfluidic droplet platforms', *Journal of visualized experiments : JoVE,* (58), pp. 3437.

Cedillo-Alcantar, D. F., Han, Y. D., Choi, J., Garcia-Cordero, J. L. and Revzin, A. (2019) 'Automated Droplet-Based Microfluidic Platform for Multiplexed Analysis of Biochemical Markers in Small Volumes', *Analytical Chemistry,* 91(8), pp. 5133-5141.

Chan, C. P. Y., Mak, W. C., Cheung, K. Y., Sin, K. K., Yu, C. M., Rainer, T. H. and Renneberg, R. (2013) 'Evidence-Based Point-of-Care Diagnostics: Current Status and Emerging Technologies', *Annual Review of Analytical Chemistry,* 6(1), pp. 191-211.

Chang, Y.-H., Lee, G.-B., Huang, F.-C., Chen, Y.-Y. and Lin, J.-L. (2006) 'Integrated polymerase chain reaction chips utilizing digital microfluidics', *Biomedical Microdevices,* 8(3), pp. 215-225.

Chapin, T. P., Caffrey, J. M., Jannasch, H. W., Coletti, L. J., Haskins, J. C. and Johnson, K. S. (2004) 'Nitrate sources and sinks in Elkhorn Slough, California: Results from long-term continuous in situ nitrate analyzers', *Estuaries,* 27(5), pp. 882-894.

Chapin, T. P., Jannasch, H. W. and Johnson, K. S. (2002) 'In situ osmotic analyzer for the year-long continuous determination of Fe in hydrothermal systems', *Analytica Chimica Acta,* 463(2), pp. 265-274.

Chen, A., Byvank, T., Chang, W.-J., Bharde, A., Vieira, G., Miller, B. L., Chalmers, J. J., Bashir, R. and Sooryakumar, R. (2013) 'On-chip magnetic separation and encapsulation of cells in droplets', *Lab on a Chip,* 13(6), pp. 1172-1181.

Chen, G. Q., Wu, Q., Jung, Y. K. and Lee, S. Y. (2011) '3.21 - PHA/PHB', in Moo-Young, M. (ed.) *Comprehensive Biotechnology (Second Edition)*. Burlington: Academic Press, pp. 217-227.

Chin, C. D., Linder, V. and Sia, S. K. (2012) 'Commercialization of microfluidic point-of-care diagnostic devices', *Lab on a Chip,* 12(12), pp. 2118-2134.

Chin, C. S., Johnson, K. S. and Coale, K. H. (1992) 'Spectrophotometric determination of dissolved manganese in natural waters with 1-(2-pyridylazo)-2-naphthol: application to analysis in situ in hydrothermal plumes', *Marine Chemistry,* 37(1), pp. 65-82.

Cho, Y. B., Jeong, S. H., Chun, H. and Kim, Y. S. (2018) 'Selective colorimetric detection of dissolved ammonia in water via modified Berthelot’s reaction on porous paper', *Sensors and Actuators B: Chemical,* 256, pp. 167-175.

Choi, K., Ng, A. H. C., Fobel, R. and Wheeler, A. R. (2012) 'Digital Microfluidics', *Annual Review of Analytical Chemistry,* 5(1), pp. 413-440.

Chong, D., Liu, X., Ma, H., Huang, G., Han, Y. L., Cui, X., Yan, J. and Xu, F. (2015) 'Advances in fabricating double-emulsion droplets and their biomedical applications', *Microfluidics and Nanofluidics,* 19(5), pp. 1071-1090.

Chong, Z. Z., Tan, S. H., Ganan-Calvo, A. M., Tor, S. B., Loh, N. H. and Nguyen, N.-T. (2016) 'Active droplet generation in microfluidics', *Lab on a Chip,* 16(1), pp. 35-58.

Chowdhury, M. S., Zheng, W., Kumari, S., Heyman, J., Zhang, X., Dey, P., Weitz, D. A. and Haag, R. (2019) 'Dendronized fluorosurfactant for highly stable water-in-fluorinated oil emulsions with minimal inter-droplet transfer of small molecules', *Nature Communications,* 10(1), pp. 4546.

Churski, K., Kaminski, T. S., Jakiela, S., Kamysz, W., Baranska-Rybak, W., Weibel, D. B. and Garstecki, P. (2012) 'Rapid screening of antibiotic toxicity in an automated microdroplet system', *Lab on a Chip,* 12(9), pp. 1629-1637.

Claustre, H., Johnson, K. S. and Takeshita, Y. (2020) 'Observing the Global Ocean with Biogeochemical-Argo', *Annual Review of Marine Science,* 12(1), pp. 23-48.

Cole, R. H., Gartner, Z. J. and Abate, A. R. (2016) 'Multicolor Fluorescence Detection for Droplet Microfluidics Using Optical Fibers', *Journal of visualized experiments : JoVE,* (111), pp. 54010.

Colin, P.-Y., Kintses, B., Gielen, F., Miton, C. M., Fischer, G., Mohamed, M. F., Hyvönen, M., Morgavi, D. P., Janssen, D. B. and Hollfelder, F. (2015) 'Ultrahigh-throughput discovery of promiscuous enzymes by picodroplet functional metagenomics', *Nature Communications,* 6(1), pp. 10008.

Cordero, M. L., Rolfsnes, H. O., Burnham, D. R., Campbell, P. A., McGloin, D. and Baroud, C. N. (2009) 'Mixing via thermocapillary generation of flow patterns inside a microfluidic drop', *New Journal of Physics,* 11(7), pp. 075033.

Cramer, C., Fischer, P. and Windhab, E. J. (2004) 'Drop formation in a co-flowing ambient fluid', *Chemical Engineering Science,* 59(15), pp. 3045-3058.

Cristobal, G., Arbouet, L., Sarrazin, F., Talaga, D., Bruneel, J.-L., Joanicot, M. and Servant, L. (2006) 'On-line laser Raman spectroscopic probing of droplets engineered in microfluidic devices', *Lab on a Chip,* 6(9), pp. 1140-1146.

Daniel, A., Laës-Huon, A., Barus, C., Beaton, A. D., Blandfort, D., Guigues, N., Knockaert, M., Munaron, D., Salter, I., Woodward, E. M. S., Greenwood, N. and Achterberg, E. P. (2020)

'Toward a Harmonization for Using in situ Nutrient Sensors in the Marine Environment', *Frontiers in Marine Science,* 6(773).

Darwish, I. A. (2006) 'Immunoassay Methods and their Applications in Pharmaceutical Analysis: Basic Methodology and Recent Advances', *International Journal of Biomedical Science : IJBS,* 2(3), pp. 217-235.

de Haas, T. W., Fadaei, H. and Sinton, D. (2012) 'Laminated thin-film Teflon chips for petrochemical applications', *Lab on a Chip,* 12(21), pp. 4236-4239.

De Menech, M., Garstecki, P., Jousse, F. and Stone, H. A. (2008) 'Transition from squeezing to dripping in a microfluidic T-shaped junction', *Journal of Fluid Mechanics,* 595, pp. 141-161.

Denuault, G. (2009) 'Electrochemical techniques and sensors for ocean research', *Ocean Sci.,* 5(4), pp. 697-710.

Dickson, A. G. (1981) 'An exact definition of total alkalinity and a procedure for the estimation of alkalinity and total inorganic carbon from titration data', *Deep Sea Research Part A. Oceanographic Research Papers,* 28(6), pp. 609-623.

Dinnes, J., Deeks, J. J., Berhane, S., Taylor, M., Adriano, A., Davenport, C., Dittrich, S., Emperador, D., Takwoingi, Y., Cunningham, J. and et al. (2021) 'Rapid, point-of-care antigen and molecular-based tests for diagnosis of SARS-CoV-2 infection', *Cochrane Database of Systematic Reviews,* (3).

Dolnik, V. and Liu, S. (2005) 'Applications of capillary electrophoresis on microchip', *J Sep Sci,* 28(15), pp. 1994-2009.

Dorin, R. I., Pai, H. K., Ho, J. T., Lewis, J. G., Torpy, D. J., Urban, F. K. and Qualls, C. R. (2009) 'Validation of a simple method of estimating plasma free cortisol: Role of cortisol binding to albumin', *Clinical Biochemistry,* 42(1), pp. 64-71.

Dreyfus, R., Tabeling, P. and Willaime, H. (2003) 'Ordered and Disordered Patterns in Two-Phase Flows in Microchannels', *Physical Review Letters,* 90(14), pp. 144505.

Du, W., Li, L., Nichols, K. P. and Ismagilov, R. F. (2009) 'SlipChip', *Lab on a Chip,* 9(16), pp. 2286-2292.

Durney, B. C., Crihfield, C. L. and Holland, L. A. (2015) 'Capillary electrophoresis applied to DNA: determining and harnessing sequence and structure to advance bioanalyses (2009-2014)', *Analytical and bioanalytical chemistry,* 407(23), pp. 6923-6938.

Eddings, M. A., Johnson, M. A. and Gale, B. K. (2008) 'Determining the optimal PDMS–PDMS bonding technique for microfluidic devices', *Journal of Micromechanics and Microengineering,* 18(6), pp. 067001.

Edgar, J. S., Pabbati, C. P., Lorenz, R. M., He, M., Fiorini, G. S. and Chiu, D. T. (2006) 'Capillary Electrophoresis Separation in the Presence of an Immiscible Boundary for Droplet Analysis', *Analytical Chemistry,* 78(19), pp. 6948-6954.

Eggers, J., Lister, J. R. and Stone, H. A. (1999) 'Coalescence of liquid drops', *Journal of Fluid Mechanics,* 401, pp. 293-310.

Elbuken, C., Glawdel, T., Chan, D. and Ren, C. L. (2011) 'Detection of microdroplet size and speed using capacitive sensors', *Sensors and Actuators A: Physical,* 171(2), pp. 55-62.

Evans, G. W. H., Bhuiyan, W. T., Pang, S., Warren, B., Makris, K., Coleman, S., Hassan, S.-u. and Niu, X. (2021) 'A portable droplet microfluidic device for cortisol measurements using a competitive heterogeneous assay', *Analyst,* 146(14), pp. 4535-4544.

Fang, C., Lee, D., Stober, B., Fuller, G. G. and Shen, A. Q. (2015) 'Integrated microfluidic platform for instantaneous flow and localized temperature control', *RSC Advances,* 5(104), pp. 85620-85629.

Ferraro, D., Champ, J., Teste, B., Serra, M., Malaquin, L., Viovy, J.-L., de Cremoux, P. and Descroix, S. (2016) 'Microfluidic platform combining droplets and magnetic tweezers: application to HER2 expression in cancer diagnosis', *Scientific Reports,* 6, pp. 25540.

Frank, C., Schroeder, F., Ebinghaus, R. and Ruck, W. (2006) 'A Fast Sequential Injection Analysis System for the Simultaneous Determination of Ammonia and Phosphate', *Microchimica Acta,* 154(1), pp. 31-38.

Frost, M. C. and Meyerhoff, M. E. (2015) 'Real-Time Monitoring of Critical Care Analytes in the Bloodstream with Chemical Sensors: Progress and Challenges', *Annual Review of Analytical Chemistry,* 8(1), pp. 171-192.

Fu, A. Y., Chou, H.-P., Spence, C., Arnold, F. H. and Quake, S. R. (2002) 'An Integrated Microfabricated Cell Sorter', *Analytical Chemistry,* 74(11), pp. 2451-2457.

Fukuba, T. and Fujii, T. (2021) 'Lab-on-a-chip technology for in situ combined observations in oceanography', *Lab on a Chip,* 21(1), pp. 55-74.

Fukuba, T., Noguchi, T., Okamura, K. and Fujii, T. (2018) 'Adenosine Triphosphate Measurement in Deep Sea Using a Microfluidic Device', *Micromachines,* 9(8), pp. 370.

Funk, W., Kerler, R., Boll, E. and Dammann, V. (1981) 'High-performance thin-layer chromatographic determination of fluorescence-labelled cortisol', *Journal of Chromatography A,* 217, pp. 349-355.

Gale, B. K., Jafek, A. R., Lambert, C. J., Goenner, B. L., Moghimifam, H., Nze, U. C. and Kamarapu, S. K. (2018) 'A Review of Current Methods in Microfluidic Device Fabrication and Future Commercialization Prospects', *Inventions,* 3(3), pp. 60.

Gao, R., Cheng, Z., deMello, A. J. and Choo, J. (2016) 'Wash-free magnetic immunoassay of the PSA cancer marker using SERS and droplet microfluidics', *Lab on a Chip,* 16(6), pp. 1022-1029.

Gao, R., Choi, N., Chang, S.-I., Kang, S. H., Song, J. M., Cho, S. I., Lim, D. W. and Choo, J. (2010) 'Highly sensitive trace analysis of paraquat using a surface-enhanced Raman scattering microdroplet sensor', *Analytica Chimica Acta,* 681(1), pp. 87-91.

Garstecki, P., Fuerstman, M. J., Stone, H. A. and Whitesides, G. M. (2006a) 'Formation of droplets and bubbles in a microfluidic T-junction-scaling and mechanism of break-up', *Lab Chip,* 6(3), pp. 437-46.

Garstecki, P., Fuerstman, M. J., Stone, H. A. and Whitesides, G. M. (2006b) 'Formation of droplets and bubbles in a microfluidic T-junction-scaling and mechanism of break-up', *Lab on a Chip,* 6(3), pp. 437-446.

Garstecki, P., Gitlin, I., DiLuzio, W., Whitesides, G. M., Kumacheva, E. and Stone, H. A. (2004) 'Formation of monodisperse bubbles in a microfluidic flow-focusing device', *Applied Physics Letters,* 85(13), pp. 2649-2651.

Garstecki, P., Stone, H. A. and Whitesides, G. M. (2005) 'Mechanism for Flow-Rate Controlled Breakup in Confined Geometries: A Route to Monodisperse Emulsions', *Physical Review Letters,* 94(16), pp. 164501.

Gatti, R., Antonelli, G., Prearo, M., Spinella, P., Cappellin, E. and De Palo, E. F. (2009) 'Cortisol assays and diagnostic laboratory procedures in human biological fluids', *Clinical Biochemistry,* 42(12), pp. 1205-1217.

Geißler, F., Achterberg, E. P., Beaton, A. D., Hopwood, M. J., Esposito, M., Mowlem, M. C., Connelly, D. P. and Wallace, D. (2021) 'Lab-on-chip analyser for the in situ determination of dissolved manganese in seawater', *Scientific Reports,* 11(1), pp. 2382.

Genfa, Z. and Dasgupta, P. K. (1989) 'Fluorometric measurement of aqueous ammonium ion in a flow injection system', *Analytical Chemistry,* 61(5), pp. 408-412.

Glawdel, T., Elbuken, C. and Ren, C. (2013) *Droplet Generation in Microfluidics.*

Gómez, A. M., Henao Carrillo, D. C. and Muñoz Velandia, O. M. (2017) 'Devices for continuous monitoring of glucose: update in technology', *Medical Devices (Auckland, N.Z.),* 10, pp. 215-224.

Gracie, K., Pang, S., Jones, G. M., Faulds, K., Braybrook, J. and Graham, D. (2017) 'Detection of cortisol in serum using quantitative resonance Raman spectroscopy', *Analytical Methods,* 9(10), pp. 1589-1594.

Grand, M. M., Clinton-Bailey, G. S., Beaton, A. D., Schaap, A. M., Johengen, T. H., Tamburri, M. N., Connelly, D. P., Mowlem, M. C. and Achterberg, E. P. (2017) 'A Lab-On-Chip Phosphate Analyzer for Long-term In Situ Monitoring at Fixed Observatories: Optimization and

Performance Evaluation in Estuarine and Oligotrophic Coastal Waters', *Frontiers in Marine Science,* 4(255).

Grieshaber, D., MacKenzie, R., Vörös, J. and Reimhult, E. (2008) 'Electrochemical Biosensors - Sensor Principles and Architectures', *Sensors (Basel, Switzerland),* 8(3), pp. 1400-1458.

Gu, H., Duits, M. H. G. and Mugele, F. (2011) 'Droplets Formation and Merging in Two-Phase Flow Microfluidics', *International Journal of Molecular Sciences,* 12(4), pp. 2572-2597.

Guckenberger, D. J., de Groot, T. E., Wan, A. M. D., Beebe, D. J. and Young, E. W. K. (2015) 'Micromilling: a method for ultra-rapid prototyping of plastic microfluidic devices', *Lab on a chip,* 15(11), pp. 2364-2378.

Guner, H., Ozgur, E., Kokturk, G., Celik, M., Esen, E., Topal, A. E., Ayas, S., Uludag, Y., Elbuken, C. and Dana, A. (2017) 'A smartphone based surface plasmon resonance imaging (SPRi) platform for on-site biodetection', *Sensors and Actuators B: Chemical,* 239, pp. 571-577.

Guo, M. T., Rotem, A., Heyman, J. A. and Weitz, D. A. (2012) 'Droplet microfluidics for high-throughput biological assays', *Lab on a Chip,* 12(12), pp. 2146-2155.

Hadwen, B., Broder, G. R., Morganti, D., Jacobs, A., Brown, C., Hector, J. R., Kubota, Y. and Morgan, H. (2012) 'Programmable large area digital microfluidic array with integrated droplet sensing for bioassays', *Lab on a Chip,* 12(18), pp. 3305-3313.

Han, Z., Li, W., Huang, Y. and Zheng, B. (2009) 'Measuring Rapid Enzymatic Kinetics by Electrochemical Method in Droplet-Based Microfluidic Devices with Pneumatic Valves', *Analytical Chemistry,* 81(14), pp. 5840-5845.

Hassan, S.-u., Morgan, H., Zhang, X. and Niu, X. (2015) 'Droplet Interfaced Parallel and Quantitative Microfluidic-Based Separations', *Analytical Chemistry,* 87(7), pp. 3895-3901.

Hassan, S.-u., Nightingale, A. M. and Niu, X. (2016) 'Continuous measurement of enzymatic kinetics in droplet flow for point-of-care monitoring', *Analyst,* 141(11), pp. 3266-3273.

Hassan, S.-u., Nightingale, M. A. and Niu, X. (2017) 'Optical Flow Cell for Measuring Size, Velocity and Composition of Flowing Droplets', *Micromachines,* 8(2).

Hatakeyama, T., Chen, D. L. and Ismagilov, R. F. (2006) 'Microgram-Scale Testing of Reaction Conditions in Solution Using Nanoliter Plugs in Microfluidics with Detection by MALDI-MS', *Journal of the American Chemical Society,* 128(8), pp. 2518-2519.

Heikenfeld, J., Jajack, A., Rogers, J., Gutruf, P., Tian, L., Pan, T., Li, R., Khine, M., Kim, J., Wang, J. and Kim, J. (2018) 'Wearable sensors: modalities, challenges, and prospects', *Lab on a Chip,* 18(2), pp. 217-248.

Hersini, K. J., Melgaard, L., Gazerani, P. and Petersen, L. J. (2014) 'Microdialysis of inflammatory mediators in the skin: a review', *Acta Derm Venereol,* 94(5), pp. 501-11.

Hosu, O., Ravalli, A., Lo Piccolo, G. M., Cristea, C., Sandulescu, R. and Marrazza, G. (2017) 'Smartphone-based immunosensor for CA125 detection', *Talanta,* 166, pp. 234-240.

Hsieh, A. T.-H., Pan, P. J.-H. and Lee, A. P. (2009) 'Rapid label-free DNA analysis in picoliter microfluidic droplets using FRET probes', *Microfluidics and Nanofluidics,* 6(3), pp. 391.

Huebner, A., Sharma, S., Srisa-Art, M., Hollfelder, F., Edel, J. B. and deMello, A. J. (2008) 'Microdroplets: A sea of applications?', *Lab on a Chip,* 8(8), pp. 1244-1254.

Jahn, I. J., Žukovskaja, O., Zheng, X. S., Weber, K., Bocklitz, T. W., Cialla-May, D. and Popp, J. (2017) 'Surface-enhanced Raman spectroscopy and microfluidic platforms: challenges, solutions and potential applications', *Analyst,* 142(7), pp. 1022-1047.

Jakiela, S., Kaminski, T. S., Cybulski, O., Weibel, D. B. and Garstecki, P. (2013) 'Bacterial Growth and Adaptation in Microdroplet Chemostats', *Angewandte Chemie International Edition,* 52(34), pp. 8908-8911.

Jannasch, H. W., Johnson, K. S. and Sakamoto, C. M. (1994) 'Submersible, Osmotically Pumped Analyzer for Continuous Determination of Nitrate in situ', *Analytical Chemistry,* 66(20), pp. 3352-3361.

Jin, S. H., Jeong, H.-H., Lee, B., Lee, S. S. and Lee, C.-S. (2015) 'A programmable microfluidic static droplet array for droplet generation, transportation, fusion, storage, and retrieval', *Lab on a Chip,* 15(18), pp. 3677-3686.

Jones, D. A., Parkin, M. C., Langemann, H., Landolt, H., Hopwood, S. E., Strong, A. J. and Boutelle, M. G. (2002) 'On-line monitoring in neurointensive care: Enzyme-based electrochemical assay for simultaneous, continuous monitoring of glucose and lactate from critical care patients', *Journal of Electroanalytical Chemistry,* 538-539, pp. 243-252.

Jung, S.-Y., Retterer, S. T. and Collier, C. P. (2010) 'On-demand generation of monodisperse femtolitre droplets by shape-induced shear', *Lab on a Chip,* 10(20), pp. 2688-2694.

Kabra, P. M., Tsai, L. L. and Marton, L. J. (1979) 'Improved liquid-chromatographic method for determination of serum cortisol', *Clinical Chemistry,* 25(7), pp. 1293-1296.

Kadlec, M. W., You, D., Liao, J. C. and Wong, P. K. (2014) 'A Cell Phone–Based Microphotometric System for Rapid Antimicrobial Susceptibility Testing', *Journal of Laboratory Automation,* 19(3), pp. 258-266.

Kaminski, T. S. and Garstecki, P. (2017) 'Controlled droplet microfluidic systems for multistep chemical and biological assays', *Chemical Society Reviews,* 46(20), pp. 6210-6226.

Kaushik, A., Vasudev, A., Arya, S. K., Pasha, S. K. and Bhansali, S. (2014) 'Recent advances in cortisol sensing technologies for point-of-care application', *Biosensors and Bioelectronics,* 53, pp. 499-512.

Khater, A., Mohammadi, M., Mohamad, A. and Nezhad, A. S. (2019) 'Dynamics of temperature-actuated droplets within microfluidics', *Scientific Reports,* 9(1), pp. 3832.

Kim, B. J. and Meng, E. (2015) 'Review of polymer MEMS micromachining', *Journal of Micromechanics and Microengineering,* 26(1), pp. 013001.

Kim, J., Imani, S., de Araujo, W. R., Warchall, J., Valdés-Ramírez, G., Paixão, T. R. L. C., Mercier, P. P. and Wang, J. (2015) 'Wearable salivary uric acid mouthguard biosensor with integrated wireless electronics', *Biosensors & bioelectronics,* 74, pp. 1061-1068.

Kiss, M. M., Ortoleva-Donnelly, L., Beer, N. R., Warner, J., Bailey, C. G., Colston, B. W., Rothberg, J. M., Link, D. R. and Leamon, J. H. (2008) 'High-Throughput Quantitative Polymerase Chain Reaction in Picoliter Droplets', *Analytical Chemistry,* 80(23), pp. 8975-8981.

Koh, A., Kang, D., Xue, Y., Lee, S., Pielak, R. M., Kim, J., Hwang, T., Min, S., Banks, A., Bastien, P., Manco, M. C., Wang, L., Ammann, K. R., Jang, K.-I., Won, P., Han, S., Ghaffari, R., Paik, U., Slepian, M. J., Balooch, G., Huang, Y. and Rogers, J. A. (2016) 'A Soft, Wearable Microfluidic Device for the Capture, Storage, and Colorimetric Sensing of Sweat', *Science translational medicine,* 8(366), pp. 366ra165-366ra165.

Koncki, R. (2007) 'Recent developments in potentiometric biosensors for biomedical analysis', *Analytica Chimica Acta,* 599(1), pp. 7-15.

Köster, S., Angilè, F. E., Duan, H., Agresti, J. J., Wintner, A., Schmitz, C., Rowat, A. C., Merten, C. A., Pisignano, D., Griffiths, A. D. and Weitz, D. A. (2008) 'Drop-based microfluidic devices for encapsulation of single cells', *Lab on a Chip,* 8(7), pp. 1110-1115.

Kovac, J. R. and Voldman, J. (2007) 'Intuitive, Image-Based Cell Sorting Using Optofluidic Cell Sorting', *Analytical Chemistry,* 79(24), pp. 9321-9330.

Lee, D. Y., Kim, E. and Choi, M. H. (2015) 'Technical and clinical aspects of cortisol as a biochemical marker of chronic stress', *BMB Reports,* 48(4), pp. 209-216.

Lee, G.-B., Chen, S.-H., Huang, G.-R., Sung, W.-C. and Lin, Y.-H. (2001) 'Microfabricated plastic chips by hot embossing methods and their applications for DNA separation and detection', *Sensors and Actuators B: Chemical,* 75(1), pp. 142-148.

Lee, Y.-S., Bhattacharjee, N. and Folch, A. (2018) '3D-printed Quake-style microvalves and micropumps', *Lab on a Chip,* 18(8), pp. 1207-1214.

Leland C. Clark, J., Wolf, R., Granger, D. and Taylor, Z. (1953) 'Continuous Recording of Blood Oxygen Tensions by Polarography', *Journal of Applied Physiology,* 6(3), pp. 189-193.

Lequin, R. M. (2005) 'Enzyme Immunoassay (EIA)/Enzyme-Linked Immunosorbent Assay (ELISA)', *Clinical Chemistry,* 51(12), pp. 2415.

Leung, K., Zahn, H., Leaver, T., Konwar, K. M., Hanson, N. W., Pagé, A. P., Lo, C.-C., Chain, P. S., Hallam, S. J. and Hansen, C. L. (2012) 'A programmable droplet-based microfluidic device applied to multiparameter analysis of single microbes and microbial communities', *Proceedings of the National Academy of Sciences,* 109(20), pp. 7665-7670.

Levine, A., Zagoory-Sharon, O., Feldman, R., Lewis, J. G. and Weller, A. (2007) 'Measuring cortisol in human psychobiological studies', *Physiology & Behavior,* 90(1), pp. 43-53.

Li, Q., Wang, F., Wang, Z. A., Yuan, D., Dai, M., Chen, J., Dai, J. and Hoering, K. A. (2013) 'Automated Spectrophotometric Analyzer for Rapid Single-Point Titration of Seawater Total Alkalinity', *Environmental Science & Technology,* 47(19), pp. 11139-11146.

Liau, A., Karnik, R., Majumdar, A. and Cate, J. H. D. (2005) 'Mixing Crowded Biological Solutions in Milliseconds', *Analytical Chemistry,* 77(23), pp. 7618-7625.

Lin, K., Zhu, Y., Zhang, Y. and Lin, H. (2019) 'Determination of ammonia nitrogen in natural waters: Recent advances and applications', *Trends in Environmental Analytical Chemistry,* 24, pp. e00073.

Link, D. R., Anna, S. L., Weitz, D. A. and Stone, H. A. (2004) 'Geometrically Mediated Breakup of Drops in Microfluidic Devices', *Physical Review Letters,* 92(5), pp. 054503.

Liu, F. W., Ding, S. T., Lin, E. C., Lu, Y. W. and Jang, J. S. R. (2017) 'Automated melting curve analysis in droplet microfluidics for single nucleotide polymorphisms (SNP) genotyping', *RSC Advances,* 7(8), pp. 4646-4655.

Liu, J., Enzelberger, M. and Quake, S. (2002) 'A nanoliter rotary device for polymerase chain reaction', *ELECTROPHORESIS,* 23(10), pp. 1531-1536.

Liu, K., Ding, H., Chen, Y. and Zhao, X.-Z. (2007) 'Droplet-based synthetic method using microflow focusing and droplet fusion', *Microfluidics and Nanofluidics,* 3(2), pp. 239-243.

Liu, W.-w. and Zhu, Y. (2020) '"Development and application of analytical detection techniques for droplet-based microfluidics"-A review', *Analytica Chimica Acta,* 1113, pp. 66-84.

Lorenz, R. M., Edgar, J. S., Jeffries, G. D. M. and Chiu, D. T. (2006) 'Microfluidic and Optical Systems for the On-Demand Generation and Manipulation of Single Femtoliter-Volume Aqueous Droplets', *Analytical Chemistry,* 78(18), pp. 6433-6439.

Luo, C., Yang, X., Fu, Q., Sun, M., Ouyang, Q., Chen, Y. and Ji, H. (2006) 'Picoliter-volume aqueous droplets in oil: Electrochemical detection and yeast cell electroporation', *ELECTROPHORESIS,* 27(10), pp. 1977-1983.

Ma, J., Li, P., Chen, Z., Lin, K., Chen, N., Jiang, Y., Chen, J., Huang, B. and Yuan, D. (2018) 'Development of an Integrated Syringe-Pump-Based Environmental-Water Analyzer (iSEA) and Application of It for Fully Automated Real-Time Determination of Ammonium in Fresh Water', *Analytical Chemistry,* 90(11), pp. 6431-6435.

Mai, T. D., Ferraro, D., Aboud, N., Renault, R., Serra, M., Tran, N. T., Viovy, J.-L., Smadja, C., Descroix, S. and Taverna, M. (2018) 'Single-step immunoassays and microfluidic droplet operation: Towards a versatile approach for detection of amyloid-β peptide-based biomarkers of Alzheimer's disease', *Sensors and Actuators B: Chemical,* 255, pp. 2126-2135.

Marcoux, P. R., Dupoy, M., Mathey, R., Novelli-Rousseau, A., Heran, V., Morales, S., Rivera, F., Joly, P. L., Moy, J.-P. and Mallard, F. (2011) 'Micro-confinement of bacteria into w/o emulsion droplets for rapid detection and enumeration', *Colloids and Surfaces A: Physicochemical and Engineering Aspects,* 377(1), pp. 54-62.

Mashaghi, S., Abbaspourrad, A., Weitz, D. A. and van Oijen, A. M. (2016) 'Droplet microfluidics: A tool for biology, chemistry and nanotechnology', *TrAC Trends in Analytical Chemistry,* 82, pp. 118-125.

Mata, A., Fleischman, A. J. and Roy, S. (2005) 'Characterization of Polydimethylsiloxane (PDMS) Properties for Biomedical Micro/Nanosystems', *Biomedical Microdevices,* 7(4), pp. 281-293.

Mazutis, L., Gilbert, J., Ung, W. L., Weitz, D. A., Griffiths, A. D. and Heyman, J. A. (2013) 'Single-cell analysis and sorting using droplet-based microfluidics', *Nature protocols,* 8(5), pp. 870-891.

McDonald, J. C., Duffy, D. C., Anderson, J. R., Chiu, D. T., Wu, H., Schueller, O. J. and Whitesides, G. M. (2000) 'Fabrication of microfluidic systems in poly(dimethylsiloxane)', *Electrophoresis,* 21(1), pp. 27-40.

McDonald, J. C. and Whitesides, G. M. (2002) 'Poly(dimethylsiloxane) as a Material for Fabricating Microfluidic Devices', *Accounts of Chemical Research,* 35(7), pp. 491-499.

Michelle L. Rogers, M. G. B. (2013) 'Real-Time Clinical Monitoring of Biomolecules', *Annual Review of Analytical Chemistry,* 6(1), pp. 427-453.

Millero, F. J. (2007) 'The Marine Inorganic Carbon Cycle', *Chemical Reviews,* 107(2), pp. 308-341.

Millero, F. J., Zhang, J.-Z., Lee, K. and Campbell, D. M. (1993) 'Titration alkalinity of seawater', *Marine Chemistry,* 44(2), pp. 153-165.

Mills, G. and Fones, G. (2012) 'A review of in situ methods and sensors for monitoring the marine environment', *Sensor Review,* 32(1), pp. 17-28.

Miralles, V., Huerre, A., Williams, H., Fournié, B. and Jullien, M.-C. (2015) 'A versatile technology for droplet-based microfluidics: thermomechanical actuation', *Lab on a Chip,* 15(9), pp. 2133-2139.

Moiseeva, E. V., Fletcher, A. A. and Harnett, C. K. (2011) 'Thin-film electrode based droplet detection for microfluidic systems', *Sensors and Actuators B: Chemical,* 155(1), pp. 408-414.

Moscone, D., Venema, K. and Korf, J. (1996) 'Ultrafiltrate sampling device for continuous monitoring', *Medical and Biological Engineering and Computing,* 34(4), pp. 290-294.

Mugele, F. and Baret, J.-C. (2005) 'Electrowetting: from basics to applications', *Journal of Physics: Condensed Matter,* 17(28), pp. R705-R774.

Mukerjee, E. V., Collins, S. D., Isseroff, R. R. and Smith, R. L. (2004) 'Microneedle array for transdermal biological fluid extraction and in situ analysis', *Sensors and Actuators A: Physical,* 114(2), pp. 267-275.

Nan, W., Fabienne, C., Regina, S., John, O., S., P. T., J., E. C., Christopher, A. and Yonggang, Z. (2011) 'Enzyme synthesis and activity assay in microfluidic droplets on a chip', *Engineering in Life Sciences,* 11(2), pp. 157-164.

Ng, A. H. C., Choi, K., Luoma, R. P., Robinson, J. M. and Wheeler, A. R. (2012) 'Digital Microfluidic Magnetic Separation for Particle-Based Immunoassays', *Analytical Chemistry,* 84(20), pp. 8805-8812.

Nguyen, N.-T., Ting, T.-H., Yap, Y.-F., Wong, T.-N., Chai, J. C.-K., Ong, W.-L., Zhou, J., Tan, S.-H. and Yobas, L. (2007) 'Thermally mediated droplet formation in microchannels', *Applied Physics Letters,* 91(8), pp. 084102.

Nightingale, A. M., Beaton, A. D. and Mowlem, M. C. (2015) 'Trends in microfluidic systems for in situ chemical analysis of natural waters', *Sensors and Actuators B: Chemical,* 221, pp. 1398-1405.

Nightingale, A. M., Evans, G. W. H., Xu, P., Kim, B. J., Hassan, S.-u. and Niu, X. (2017) 'Phased peristaltic micropumping for continuous sampling and hardcoded droplet generation', *Lab on a Chip,* 17(6), pp. 1149-1157.

Nightingale, A. M., Hassan, S.-u., Evans, G. W. H., Coleman, S. M. and Niu, X. (2018) 'Nitrate measurement in droplet flow: gas-mediated crosstalk and correction', *Lab on a Chip,* 18(13), pp. 1903-1913.

Nightingale, A. M., Hassan, S.-u., Makris, K., Bhuiyan, W. T., Harvey, T. J. and Niu, X. (2020) 'Easily fabricated monolithic fluoropolymer chips for sensitive long-term absorbance measurement in droplet microfluidics', *RSC Advances,* 10(51), pp. 30975-30981.

Nightingale, A. M., Hassan, S.-u., Warren, B. M., Makris, K., Evans, G. W. H., Papadopoulou, E., Coleman, S. and Niu, X. (2019a) 'A Droplet Microfluidic-Based Sensor for Simultaneous in Situ Monitoring of Nitrate and Nitrite in Natural Waters', *Environmental Science & Technology,* 53(16), pp. 9677-9685.

Nightingale, A. M., Leong, C. L., Burnish, R. A., Hassan, S.-u., Zhang, Y., Clough, G. F., Boutelle, M. G., Voegeli, D. and Niu, X. (2019b) 'Monitoring biomolecule concentrations in tissue using a wearable droplet microfluidic-based sensor', *Nature Communications,* 10(1), pp. 2741.

Niu, X., Gielen, F., Edel, J. B. and deMello, A. J. (2011) 'A microdroplet dilutor for high-throughput screening', *Nat Chem,* 3(6), pp. 437-42.

Niu, X., Gulati, S., Edel, J. B. and deMello, A. J. (2008) 'Pillar-induced droplet merging in microfluidic circuits', *Lab on a Chip,* 8(11), pp. 1837-1841.

Niu, X., Pereira, F., Edel, J. B. and de Mello, A. J. (2013) 'Droplet-Interfaced Microchip and Capillary Electrophoretic Separations', *Analytical Chemistry,* 85(18), pp. 8654-8660.

Niu, X., Zhang, M., Peng, S., Wen, W. and Sheng, P. (2007) 'Real-time detection, control, and sorting of microfluidic droplets', *Biomicrofluidics,* 1(4), pp. 44101-44101.

Ouimet, C. M., D'Amico, C. I. and Kennedy, R. T. (2017) 'Advances in capillary electrophoresis and the implications for drug discovery', *Expert opinion on drug discovery,* 12(2), pp. 213-224.

Pamme, N. (2006) 'Magnetism and microfluidics', *Lab on a Chip,* 6(1), pp. 24-38.

Pei, J., Li, Q., Lee, M. S., Valaskovic, G. A. and Kennedy, R. T. (2009) 'Analysis of Samples Stored as Individual Plugs in a Capillary by Electrospray Ionization Mass Spectrometry', *Analytical Chemistry,* 81(15), pp. 6558-6561.

Pereira, F., Niu, X. and deMello, A. J. (2013) 'A nano LC-MALDI mass spectrometry droplet interface for the analysis of complex protein samples', *PloS one,* 8(5), pp. e63087-e63087.

Pit, A. M., Duits, M. H. G. and Mugele, F. (2015) 'Droplet Manipulations in Two Phase Flow Microfluidics', *Micromachines,* 6(11), pp. 1768-1793.

Plant, J. N., Johnson, K. S., Needoba, J. A. and Coletti, L. J. (2009) 'NH4-Digiscan: an in situ and laboratory ammonium analyzer for estuarine, coastal, and shelf waters', *Limnology and Oceanography: Methods,* 7(2), pp. 144-156.

Postek, W., Kaminski, T. S. and Garstecki, P. (2017) 'A precise and accurate microfluidic droplet dilutor', *Analyst,* 142(16), pp. 2901-2911.

Price, C. P., St John, A. and Kricka, L. J. (2010) *Point-of-care testing.* Washington: AACC Press.

Price, D. A., Close, G. C. and Fielding, B. A. (1983) 'Age of appearance of circadian rhythm in salivary cortisol values in infancy', *Archives of Disease in Childhood,* 58(6), pp. 454.

Priest, C., Herminghaus, S. and Seemann, R. (2006) 'Controlled electrocoalescence in microfluidics: Targeting a single lamella', *Applied Physics Letters,* 89(13), pp. 134101.

Qiu, X.-c., Liu, G.-P. and Zhu, Y.-Q. (1987) 'Determination of water-soluble ammonium ion in soil by spectrophotometry', *Analyst,* 112(6), pp. 909-911.

Rajian, J. R., Fabiilli, M. L., Fowlkes, J. B., Carson, P. L. and Wang, X. (2011) 'Drug delivery monitoring by photoacoustic tomography with an ICG encapsulated double emulsion', *Optics Express,* 19(15), pp. 14335-14347.

Ren, K., Zhou, J. and Wu, H. (2013) 'Materials for Microfluidic Chip Fabrication', *Accounts of Chemical Research,* 46(11), pp. 2396-2406.

Rhie, W. and Higuchi, T. (2010) 'Design and fabrication of a screw-driven multi-channel peristaltic pump for portable microfluidic devices', *Journal of Micromechanics and Microengineering,* 20(8), pp. 085036.

Ronkainen, N. J., Halsall, H. B. and Heineman, W. R. (2010) 'Electrochemical biosensors', *Chemical Society Reviews,* 39(5), pp. 1747-1763.

Rose, S. and Nelson, J. (1955) 'A CONTINUOUS LONG-TERM INJECTOR', *Australian Journal of Experimental Biology and Medical Science,* 33(4), pp. 415-420.

Rushworth, C. M., Davies, J., Cabral, J. T., Dolan, P. R., Smith, J. M. and Vallance, C. (2012) 'Cavity-enhanced optical methods for online microfluidic analysis', *Chemical Physics Letters,* 554, pp. 1-14.

Russell, E., Koren, G., Rieder, M. and Van Uum, S. H. M. (2014) 'The Detection of Cortisol in Human Sweat: Implications for Measurement of Cortisol in Hair', *Therapeutic Drug Monitoring,* 36(1).

Sadik, O. A. and Van Emon, J. M. (1996) 'Applications of electrochemical immunosensors to environmental monitoring', *Biosensors and Bioelectronics,* 11(8), pp. i-x.

Sajid, M., Kawde, A.-N. and Daud, M. (2015) 'Designs, formats and applications of lateral flow assay: A literature review', *Journal of Saudi Chemical Society,* 19(6), pp. 689-705.

Samper, I. C., Gowers, S. A. N., Rogers, M. L., Murray, D.-S. R. K., Jewell, S. L., Pahl, C., Strong, A. J. and Boutelle, M. G. (2019) '3D printed microfluidic device for online detection of neurochemical changes with high temporal resolution in human brain microdialysate', *Lab on a Chip,* 19(11), pp. 2038-2048.

Searle, P. L. (1984) 'The berthelot or indophenol reaction and its use in the analytical chemistry of nitrogen. A review', *Analyst,* 109(5), pp. 549-568.

Seelmann, K., Aßmann, S. and Körtzinger, A. (2019) 'Characterization of a novel autonomous analyzer for seawater total alkalinity: Results from laboratory and field tests', *Limnology and Oceanography: Methods,* 17(10), pp. 515-532.

Sempionatto, J. R., Nakagawa, T., Pavinatto, A., Mensah, S. T., Imani, S., Mercier, P. and Wang, J. (2017) 'Eyeglasses based wireless electrolyte and metabolite sensor platform', *Lab on a Chip,* 17(10), pp. 1834-1842.

Shang, L., Cheng, Y. and Zhao, Y. (2017) 'Emerging Droplet Microfluidics', *Chemical Reviews,* 117(12), pp. 7964-8040.

Shimada, M., Takahashi, K., Ohkawa, T., Segawa, M. and Higurashi, M. (1995) 'Determination of Salivary Cortisol by ELISA and Its Application to the Assessment of the Circadian Rhythm in Children', *Hormone Research in Paediatrics,* 44(5), pp. 213-217.

Shippenberg, T. S. and Thompson, A. C. (2001) 'Overview of Microdialysis', *Current protocols in neuroscience / editorial board, Jacqueline N. Crawley ... [et al.],* CHAPTER, pp. Unit7.1-Unit7.1.

Shiu, P. P., Knopf, G. K., Ostojic, M. and Nikumb, S. (2008) 'Rapid fabrication of tooling for microfluidic devices via laser micromachining and hot embossing', *Journal of Micromechanics and Microengineering,* 18(2), pp. 025012.

Simon, M. and Lee, A. P. 'Chapter 2 Microfluidic Droplet Manipulations and Their Applications'.

Singh, M., Tong, Y., Webster, K., Cesewski, E., Haring, A. P., Laheri, S., Carswell, B., O'Brien, T. J., Aardema, C. H., Senger, R. S., Robertson, J. L. and Johnson, B. N. (2017) '3D printed conformal microfluidics for isolation and profiling of biomarkers from whole organs', *Lab on a Chip,* 17(15), pp. 2561-2571.

Smart, J.-W. M. a. W. (2004) 'LACTATE BIOSENSORS FOR CONTINUOUS MONITORING', *Frontiers in Bioscience,* 9, 3384-3391(September).

Song, H., Chen, D. L. and Ismagilov, R. F. (2006) 'Reactions in Droplets in Microfluidic Channels', *Angewandte Chemie International Edition,* 45(44), pp. 7336-7356.

Song, H. and Ismagilov, R. F. (2003) 'Millisecond Kinetics on a Microfluidic Chip Using Nanoliters of Reagents', *Journal of the American Chemical Society,* 125(47), pp. 14613-14619.

Song, H., Tice, J. D. and Ismagilov, R. F. (2003) 'A Microfluidic System for Controlling Reaction Networks in Time', *Angewandte Chemie International Edition,* 42(7), pp. 768-772.

Spaulding, R. S., DeGrandpre, M. D., Beck, J. C., Hart, R. D., Peterson, B., De Carlo, E. H., Drupp, P. S. and Hammar, T. R. (2014) 'Autonomous in Situ Measurements of Seawater Alkalinity', *Environmental Science & Technology,* 48(16), pp. 9573-9581.

Šraj, L. O. C., Almeida, M. I. G. S., Swearer, S. E., Kolev, S. D. and McKelvie, I. D. (2014) 'Analytical challenges and advantages of using flow-based methodologies for ammonia determination in estuarine and marine waters', *TrAC Trends in Analytical Chemistry,* 59, pp. 83-92.

Srigunapalan, S., Eydelnant, I. A., Simmons, C. A. and Wheeler, A. R. (2012) 'A digital microfluidic platform for primary cell culture and analysis', *Lab on a Chip,* 12(2), pp. 369-375.

St-Louis, P. (2000) 'Status of point-of-care testing: promise, realities, and possibilities', *Clinical Biochemistry,* 33(6), pp. 427-440.

St John, A. and Price, C. P. (2014) 'Existing and Emerging Technologies for Point-of-Care Testing', *The Clinical Biochemist Reviews,* 35(3), pp. 155-167.

Stan, C. A., Tang, S. K. and Whitesides, G. M. (2009) 'Independent control of drop size and velocity in microfluidic flow-focusing generators using variable temperature and flow rate', *Anal Chem,* 81(6), pp. 2399-402.

Author (2013)*: Water quality — Determination of selected parameters by discrete analysis systems — Part 1: Ammonium, nitrate, nitrite, chloride, orthophosphate, sulfate and silicate with photometric detection*: International Organization for Standardization.

Steinhubl, S. R., Muse, E. D. and Topol, E. J. (2015) 'The emerging field of mobile health', *Science translational medicine,* 7(283), pp. 283rv3-283rv3.

Steyer, D. J. and Kennedy, R. T. (2019) 'High-Throughput Nanoelectrospray Ionization-Mass Spectrometry Analysis of Microfluidic Droplet Samples', *Analytical Chemistry,* 91(10), pp. 6645-6651.

Stoytcheva, M. and Zlatev, R. (2014) 'Electrochemical Sensors for Environmental Analysis', in Kreysa, G., Ota, K.-i. & Savinell, R.F. (eds.) *Encyclopedia of Applied Electrochemistry*. New York, NY: Springer New York, pp. 613-616.

Su, W., Gao, X., Jiang, L. and Qin, J. (2015) 'Microfluidic platform towards point-of-care diagnostics in infectious diseases', *Journal of Chromatography A,* 1377, pp. 13-26.

Sun, K., Ramgir, N. and Bhansali, S. (2008) 'An immunoelectrochemical sensor for salivary cortisol measurement', *Sensors and Actuators B: Chemical,* 133(2), pp. 533-537.

Sung Kwon, C., Hyejin, M. and Chang-Jin, K. (2003) 'Creating, transporting, cutting, and merging liquid droplets by electrowetting-based actuation for digital microfluidic circuits', *Journal of Microelectromechanical Systems,* 12(1), pp. 70-80.

Svensson, C.-M., Shvydkiv, O., Dietrich, S., Mahler, L., Weber, T., Choudhary, M., Tovar, M., Figge, M. T. and Roth, M. (2019) 'Coding of Experimental Conditions in Microfluidic Droplet Assays Using Colored Beads and Machine Learning Supported Image Analysis', *Small,* 15(4), pp. 1802384.

Swinehart, D. F. (1962) 'The Beer-Lambert Law', *Journal of Chemical Education,* 39(7), pp. 333.

Tan, Y.-C., Fisher, J. S., Lee, A. I., Cristini, V. and Lee, A. P. (2004) 'Design of microfluidic channel geometries for the control of droplet volume, chemical concentration, and sorting', *Lab on a Chip,* 4(4), pp. 292-298.

Tan, Y.-C., Ho, Y. L. and Lee, A. P. (2007) 'Microfluidic sorting of droplets by size', *Microfluidics and Nanofluidics,* 4(4), pp. 343.

Tan, Y.-C. and Lee, A. P. (2005) 'Microfluidic separation of satellite droplets as the basis of a monodispersed micron and submicron emulsification system', *Lab on a Chip,* 5(10), pp. 1178-1183.

Teh, S.-Y., Lin, R., Hung, L.-H. and Lee, A. P. (2008) 'Droplet microfluidics', *Lab on a Chip,* 8(2), pp. 198-220.

Teste, B., Ali-Cherif, A., Viovy, J. L. and Malaquin, L. (2013) 'A low cost and high throughput magnetic bead-based immuno-agglutination assay in confined droplets', *Lab on a Chip,* 13(12), pp. 2344-2349.

Thorsen, T., Roberts, R. W., Arnold, F. H. and Quake, S. R. (2001) 'Dynamic Pattern Formation in a Vesicle-Generating Microfluidic Device', *Physical Review Letters,* 86(18), pp. 4163-4166.

Thouron, D., Vuillemin, R., Philippon, X., Lourenço, A., Provost, C., Cruzado, A. and Garçon, V. (2003) 'An Autonomous Nutrient Analyzer for Oceanic Long-Term in Situ Biogeochemical Monitoring', *Analytical Chemistry,* 75(11), pp. 2601-2609.

Tlili, C., Myung, N. V., Shetty, V. and Mulchandani, A. (2011) 'Label-free, chemiresistor immunosensor for stress biomarker cortisol in saliva', *Biosensors and Bioelectronics,* 26(11), pp. 4382-4386.

Tran, T. M., Lan, F., Thompson, C. S. and Abate, A. R. (2013) 'From tubes to drops: droplet-based microfluidics for ultrahigh-throughput biology', *Journal of Physics D: Applied Physics,* 46(11), pp. 114004.

Tresset, G. and Takeuchi, S. (2004) 'A Microfluidic Device for Electrofusion of Biological Vesicles', *Biomedical Microdevices,* 6(3), pp. 213-218.

Trivedi, V., Doshi, A., Kurup, G. K., Ereifej, E., Vandevord, P. J. and Basu, A. S. (2010) 'A modular approach for the generation, storage, mixing, and detection of droplet libraries for high throughput screening', *Lab on a Chip,* 10(18), pp. 2433-2442.

Unger, M. A., Chou, H. P., Thorsen, T., Scherer, A. and Quake, S. R. (2000) 'Monolithic microfabricated valves and pumps by multilayer soft lithography', *Science,* 288(5463), pp. 113-6.

Utada, A. S., Fernandez-Nieves, A., Stone, H. A. and Weitz, D. A. (2007) 'Dripping to Jetting Transitions in Coflowing Liquid Streams', *Physical Review Letters,* 99(9), pp. 094502.

Utada, A. S., Lorenceau, E., Link, D. R., Kaplan, P. D., Stone, H. A. and Weitz, D. A. (2005) 'Monodisperse Double Emulsions Generated from a Microcapillary Device', *Science,* 308(5721), pp. 537-541.

van Son, M., Schothorst, R. C. and den Boef, G. (1983) 'Determination of total ammoniacal introgen in water by flow injection analysis and a gas diffusion membrane', *Analytica Chimica Acta,* 153, pp. 271-275.

van Steijn, V., Kleijn, C. R. and Kreutzer, M. T. (2010) 'Predictive model for the size of bubbles and droplets created in microfluidic T-junctions', *Lab on a Chip,* 10(19), pp. 2513-2518.

Vashist, S. K. (2017) 'Point-of-Care Diagnostics: Recent Advances and Trends', *Biosensors,* 7(4), pp. 62.

Venugopal, M., Arya, S. K., Chornokur, G. and Bhansali, S. (2011) 'A realtime and continuous assessment of cortisol in ISF using electrochemical impedance spectroscopy', *Sensors and Actuators A: Physical,* 172(1), pp. 154-160.

Waheed, S., Cabot, J. M., Macdonald, N. P., Lewis, T., Guijt, R. M., Paull, B. and Breadmore, M. C. (2016) '3D printed microfluidic devices: enablers and barriers', *Lab on a Chip,* 16(11), pp. 1993-2013.

Walter, A., März, A., Schumacher, W., Rösch, P. and Popp, J. (2011) 'Towards a fast, high specific and reliable discrimination of bacteria on strain level by means of SERS in a microfluidic device', *Lab on a Chip,* 11(6), pp. 1013-1021.

Wan, Y., Su, Y., Zhu, X., Liu, G. and Fan, C. (2013) 'Development of electrochemical immunosensors towards point of care diagnostics', *Biosensors and Bioelectronics,* 47, pp. 1-11.

Wang, B. L., Ghaderi, A., Zhou, H., Agresti, J., Weitz, D. A., Fink, G. R. and Stephanopoulos, G. (2014) 'Microfluidic high-throughput culturing of single cells for selection based on extracellular metabolite production or consumption', *Nature Biotechnology,* 32, pp. 473.

Wang, C., Nguyen, N.-T. and Wong, T. N. (2007a) 'Optical measurement of flow field and concentration field inside a moving nanoliter droplet', *Sensors and Actuators A: Physical,* 133(2), pp. 317-322.

Wang, G., Lim, C., Chen, L., Chon, H., Choo, J., Hong, J. and deMello, A. J. (2009a) 'Surface-enhanced Raman scattering in nanoliter droplets: towards high-sensitivity detection of mercury (II) ions', *Analytical and Bioanalytical Chemistry,* 394(7), pp. 1827-1832.

Wang, J., Wang, J., Feng, L. and Lin, T. (2015a) 'Fluid mixing in droplet-based microfluidics with a serpentine microchannel', *RSC Advances,* 5(126), pp. 104138-104144.

Wang, R., Zhang, L., Gao, M., Wang, Q., Deng, Z. and Gui, L. (2019a) 'A Liquid-Metal-Based Dielectrophoretic Microdroplet Generator', *Micromachines,* 10(11), pp. 769.

Wang, W., Yang, C. and Li, C. M. (2009b) 'On-demand microfluidic droplet trapping and fusion for on-chip static droplet assays', *Lab on a Chip,* 9(11), pp. 1504-1506.

Wang, X., Yi, L., Mukhitov, N., Schrell, A. M., Dhumpa, R. and Roper, M. G. (2015b) 'Microfluidics-to-Mass Spectrometry: A review of coupling methods and applications', *Journal of chromatography. A,* 0, pp. 98-116.

Wang, Y.-C., Choi, M. H. and Han, J. (2004) 'Two-Dimensional Protein Separation with Advanced Sample and Buffer Isolation Using Microfluidic Valves', *Analytical Chemistry,* 76(15), pp. 4426-4431.

Wang, Y., Zhao, Y. and Cho, S. K. (2007b) 'Efficient in-droplet separation of magnetic particles for digital microfluidics', *Journal of Micromechanics and Microengineering,* 17, pp. 2148-2156.

Wang, Z. A., Moustahfid, H., Mueller, A. V., Michel, A. P. M., Mowlem, M., Glazer, B. T., Mooney, T. A., Michaels, W., McQuillan, J. S., Robidart, J. C., Churchill, J., Sourisseau, M., Daniel, A., Schaap, A., Monk, S., Friedman, K. and Brehmer, P. (2019b) 'Advancing Observation of Ocean Biogeochemistry, Biology, and Ecosystems With Cost-Effective in situ Sensing Technologies', *Frontiers in Marine Science,* 6(519).

Weeks, D. A. and Johnson, K. S. (1996) 'Solenoid Pumps for Flow Injection Analysis', *Analytical Chemistry,* 68(15), pp. 2717-2719.

Wettersten, N. and Maisel, A. (2015) 'Role of Cardiac Troponin Levels in Acute Heart Failure', *Cardiac Failure Review,* 1(2), pp. 102-106.

Whitesides, G. M. (2006) 'The origins and the future of microfluidics', *Nature,* 442, pp. 368.

Wild, D. (2013) *The immunoassay handbook.* Amsterdam: Elsevier.

Windmiller, J. R. and Wang, J. (2013) 'Wearable Electrochemical Sensors and Biosensors: A Review', *Electroanalysis,* 25(1), pp. 29-46.

Xi, H.-D., Zheng, H., Guo, W., Gañán-Calvo, A. M., Ai, Y., Tsao, C.-W., Zhou, J., Li, W., Huang, Y., Nguyen, N.-T. and Tan, S. H. (2017) 'Active droplet sorting in microfluidics: a review', *Lab on a Chip,* 17(5), pp. 751-771.

Xu, J. and Attinger, D. (2008) 'Drop on demand in a microfluidic chip', *Journal of Micromechanics and Microengineering,* 18(6), pp. 065020.

Xu, W., Sandford, R. C., Worsfold, P. J., Carlton, A. and Hanrahan, G. (2005) 'Flow Injection Techniques in Aquatic Environmental Analysis: Recent Applications and Technological Advances', *Critical Reviews in Analytical Chemistry,* 35(3), pp. 237-246.

Yang, T., Stavrakis, S. and deMello, A. (2017) 'A High-Sensitivity, Integrated Absorbance and Fluorescence Detection Scheme for Probing Picoliter-Volume Droplets in Segmented Flows', *Analytical Chemistry,* 89(23), pp. 12880-12887.

Yap, Y.-F., Tan, S.-H., Nguyen, N.-T., Murshed, S. M. S., Wong, T.-N. and Yobas, L. (2009) 'Thermally mediated control of liquid microdroplets at a bifurcation', *Journal of Physics D: Applied Physics,* 42(6), pp. 065503.

Yazdi, A. A., Popma, A., Wong, W., Nguyen, T., Pan, Y. and Xu, J. (2016) '3D printing: an emerging tool for novel microfluidics and lab-on-a-chip applications', *Microfluidics and Nanofluidics,* 20(3), pp. 50.

Yobas, L., Martens, S., Ong, W.-L. and Ranganathan, N. (2006) 'High-performance flow-focusing geometry for spontaneous generation of monodispersed droplets', *Lab on a Chip,* 6(8), pp. 1073-1079.

Yokokawa, R., Saika, T., Nakayama, T., Fujita, H. and Konishi, S. (2006) 'On-chip syringe pumps for picoliter-scale liquid manipulation', *Lab on a Chip,* 6(8), pp. 1062-1066.

Yu, J., Tao, D., Ng, E. X., Drum, C. L., Liu, A. Q. and Chen, C.-H. (2014) 'Real-time measurement of thrombin generation using continuous droplet microfluidics', *Biomicrofluidics,* 8(5), pp. 052108.

Zarei, M. (2017) 'Advances in point-of-care technologies for molecular diagnostics', *Biosensors and Bioelectronics,* 98, pp. 494-506.

Zeng, S., Li, B., Su, X. o., Qin, J. and Lin, B. (2009) 'Microvalve-actuated precise control of individual droplets in microfluidic devices', *Lab on a Chip,* 9(10), pp. 1340-1343.

Zeng, Y., Novak, R., Shuga, J., Smith, M. T. and Mathies, R. A. (2010) 'High-Performance Single Cell Genetic Analysis Using Microfluidic Emulsion Generator Arrays', *Analytical Chemistry,* 82(8), pp. 3183-3190.

Zhang, D. and Liu, Q. (2016) 'Biosensors and bioelectronics on smartphone for portable biochemical detection', *Biosensors and Bioelectronics,* 75, pp. 273-284.

Zhang, Y. and Jiang, H.-R. (2016) 'A review on continuous-flow microfluidic PCR in droplets: Advances, challenges and future', *Analytica Chimica Acta,* 914, pp. 7-16.

Zhao, Y., Liu, J., Chen, Z., Zhu, X. and Möller, M. (2018) 'Hybrid nanostructured particles via surfactant-free double miniemulsion polymerization', *Nature Communications,* 9(1), pp. 1918.

Zheng, B., Roach, L. S. and Ismagilov, R. F. (2003) 'Screening of Protein Crystallization Conditions on a Microfluidic Chip Using Nanoliter-Size Droplets', *Journal of the American Chemical Society,* 125(37), pp. 11170-11171.

Zhu, P. and Wang, L. (2017) 'Passive and active droplet generation with microfluidics: a review', *Lab on a Chip,* 17(1), pp. 34-75.

Zhu, Y. and Fang, Q. (2013) 'Analytical detection techniques for droplet microfluidics—A review', *Analytica Chimica Acta,* 787, pp. 24-35.

Appendix

Chapter 4

The graphical user interface (GUI) was developed by Brett Warren (SouthWestSensors Ltd) using Embarcadero C++ Builder. The GUI is used to access the ammonium sensor system via a USB data protocol. The GUI is used to view incoming sensor data as a time series. The GUI also allows the user to define and upload different parameters related to the ammonium sensor system. Figure 125 shows a screenshot of the GUI displaying raw light intensity data (in green) and a concentration profile of ammonium (orange) generated from the raw intensity data and some calibration points.

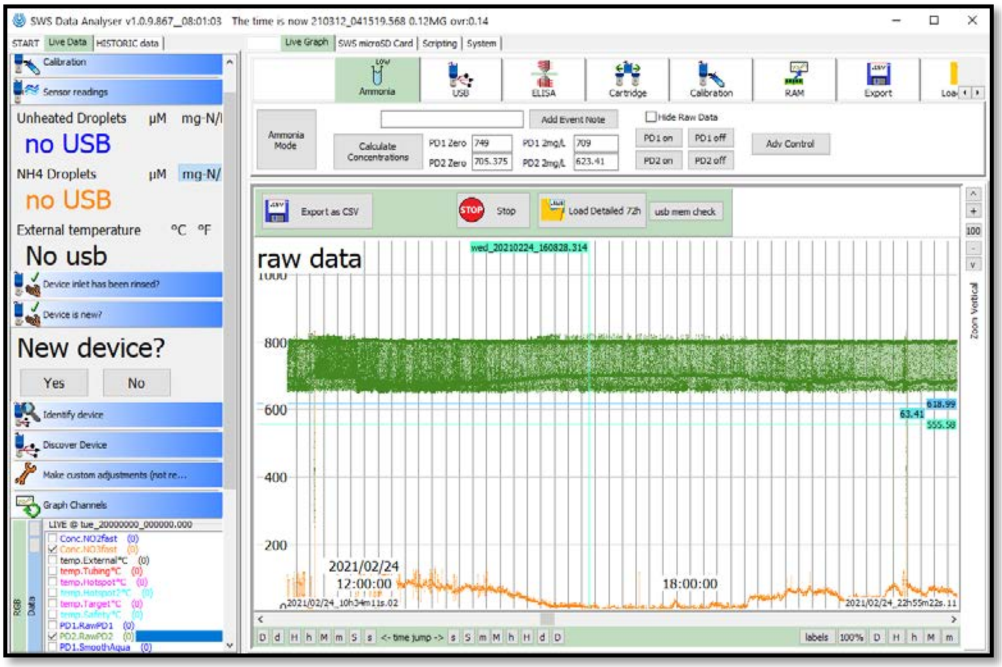

SWS Data Analyser v1.0.9.867_08:01:03 The time is now 210312_041519.568 0.12MG ovr:0.14

Unheated Droplets µM mg-N/l: no USB

NH4 Droplets µM mg-N/: no USB

External temperature °C °F: No usb

New device?

PD1 Zero 749

PD2 Zero 705.375

PD1 2mg/L 709

PD2 2mg/L 623.41

☐ Hide Raw Data

LIVE @ tue_20000000_000000.000

☐ Conc.NO2fast (0)
☑ Conc.NO3fast (0)
☐ temp.External°C (0)
☐ temp.Tubing°C (0)
☐ temp.Hotspot°C (0)
☐ temp.Hotspot2°C (0)
☐ temp.Target°C (0)
☐ temp.Safety°C (0)
☐ PD1.RawPD1 (0)
☑ PD2.RawPD2 (0)
☐ PD1.SmoothAqua (0)

__Figure 125.__ Screenshot of GUI displaying raw light intensity data (in green) and a concentration profile of ammonium (orange).

Chapter 5

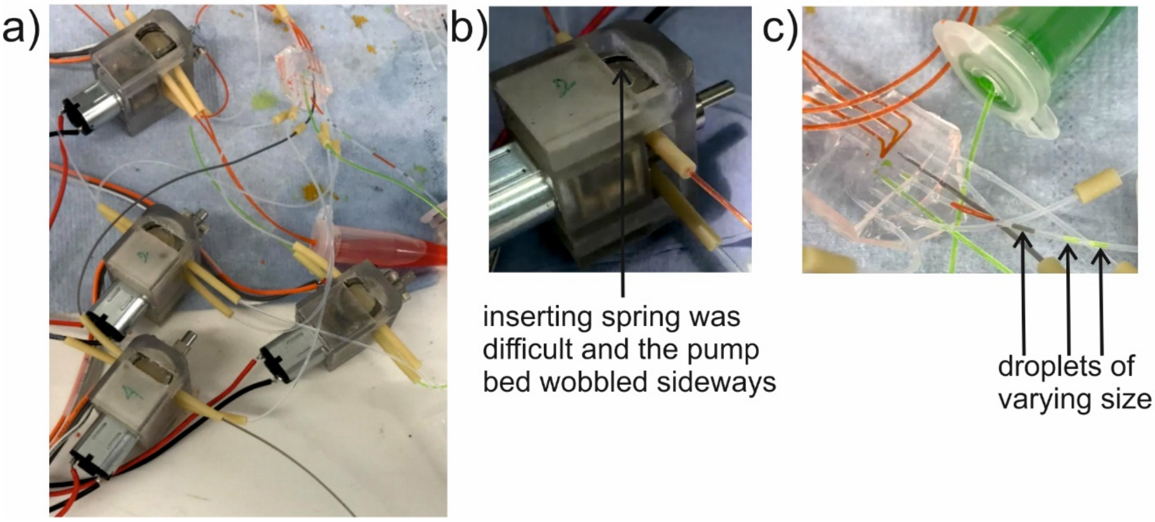

Figure 126. *Testing dual disc spring pump. (a) and (b) shows the fully assembled units with (b) zooming into the disk spring. (c) Irregular droplet formation.*

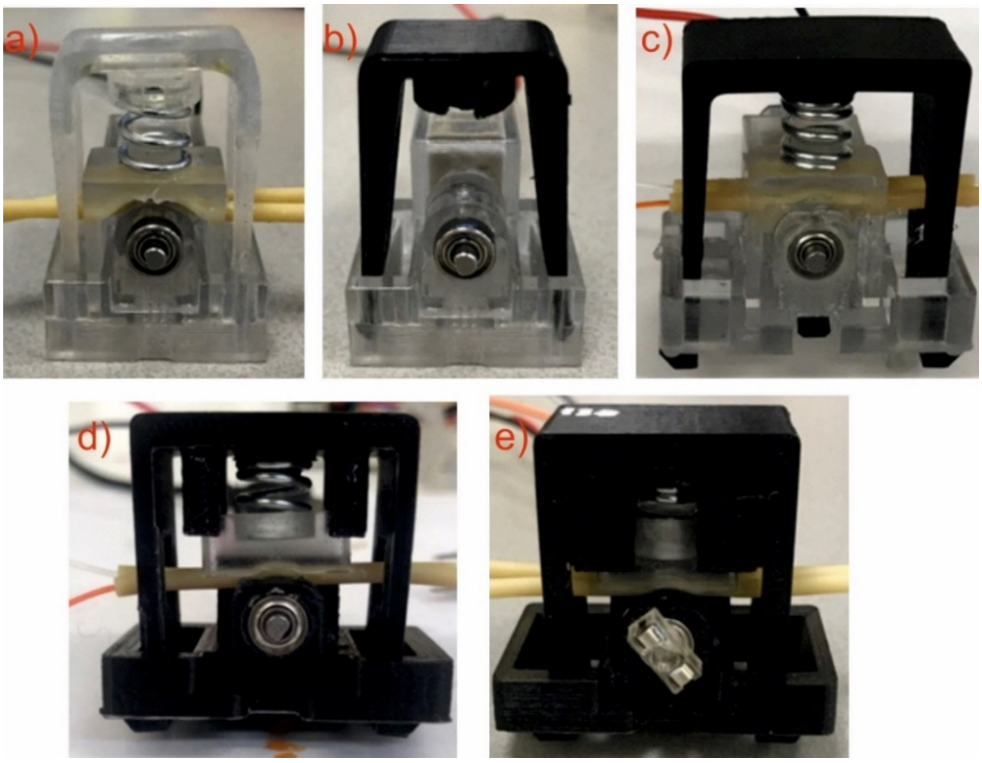

Figure 127. *Photographs of 3D printed assemblies of the single spring pump showing the evolution to the current working version.(a) Entire pump printed using 'VeroClear' material in glossy finish. (b) Replaced top cap in (a) using more flexible black PLA printed one. (c) Expanded the design to make it sturdier. (d) Modular pumpbed and top cap modified to adjust to the new pump bed design. (e) Final design with more restricted top cap to allow only vertical motion of the pump bed and also modified chassis for easier insertion of top.*

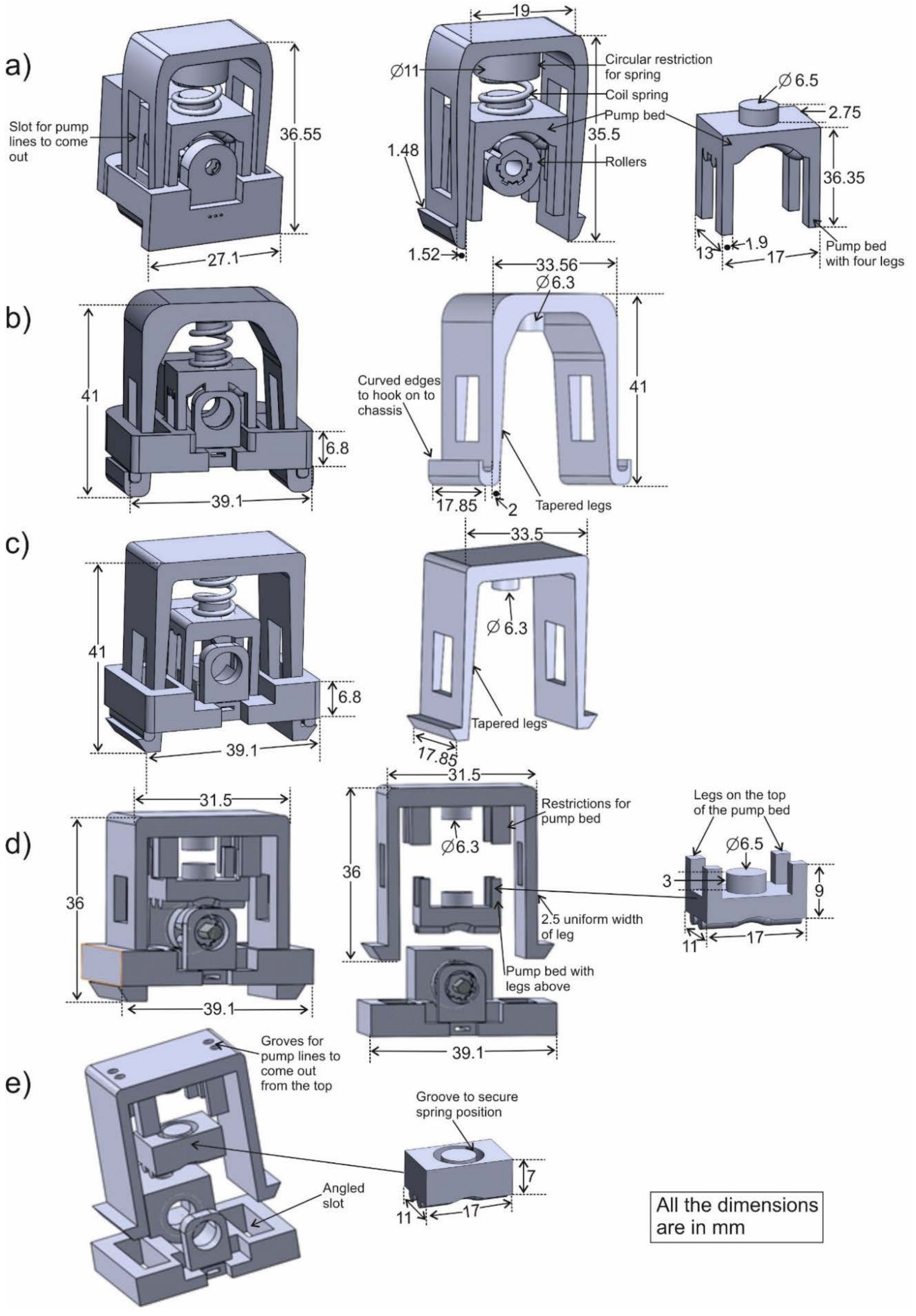

Figure 128. *SolidWorks drawings showing the evolution of single spring pump design indicating the changes in dimensions and highlighting the changes in key features.*

Figure 129 shows the transmitted light received by the photodetector, when droplets generated using the three two-line pump units, pass through the optical detector. The raw data trace is highly repeatable for each individual unit and almost the same through all three units.

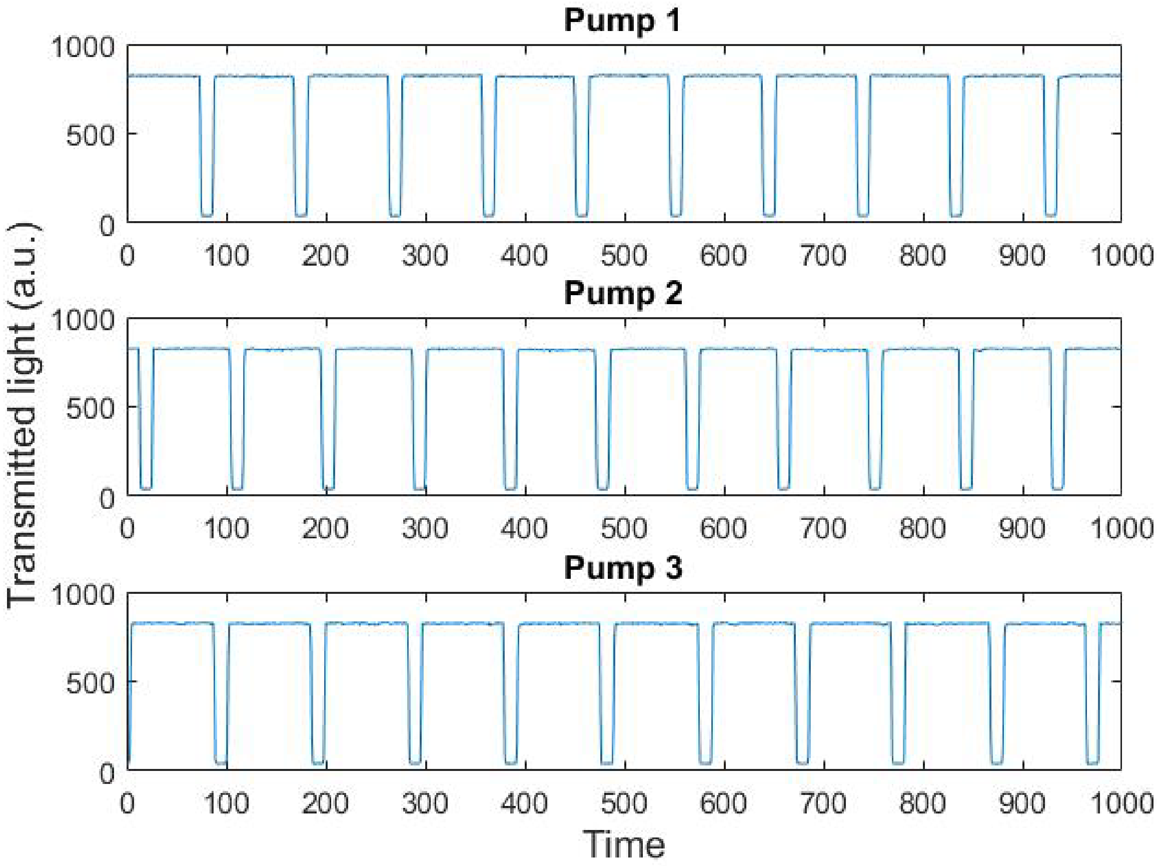

Figure 129. Transmitted light received by the photodetector when droplet generated using the three two-line pump units, pass through the flow cell.

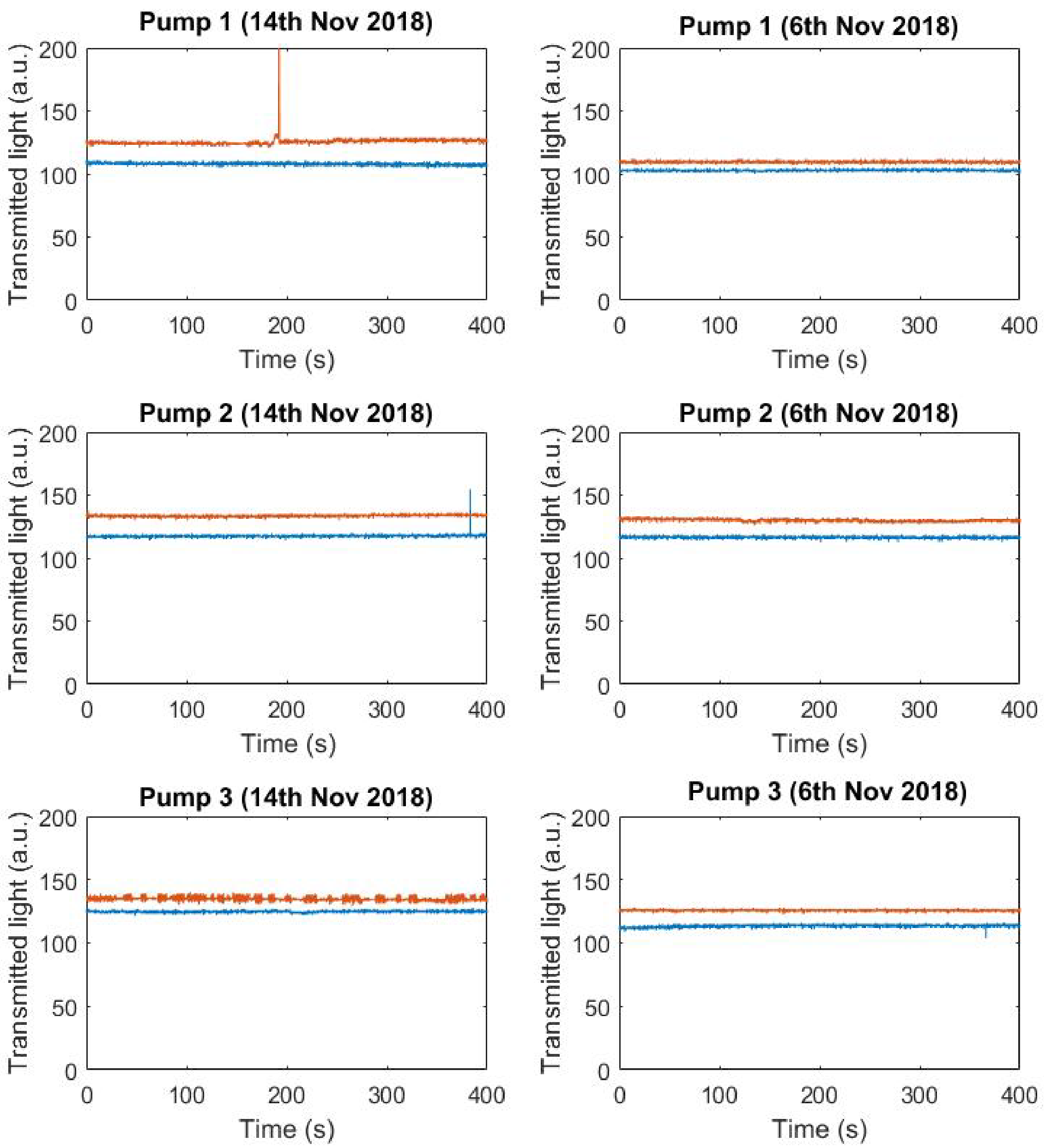

__Figure 130.__ Raw transmitted light intensity received by an optical detector, of continuous phase dye pumped through pump lines of two-line pump. The graphs show results for three pump units with the same experimental set up, tested on two separate days.

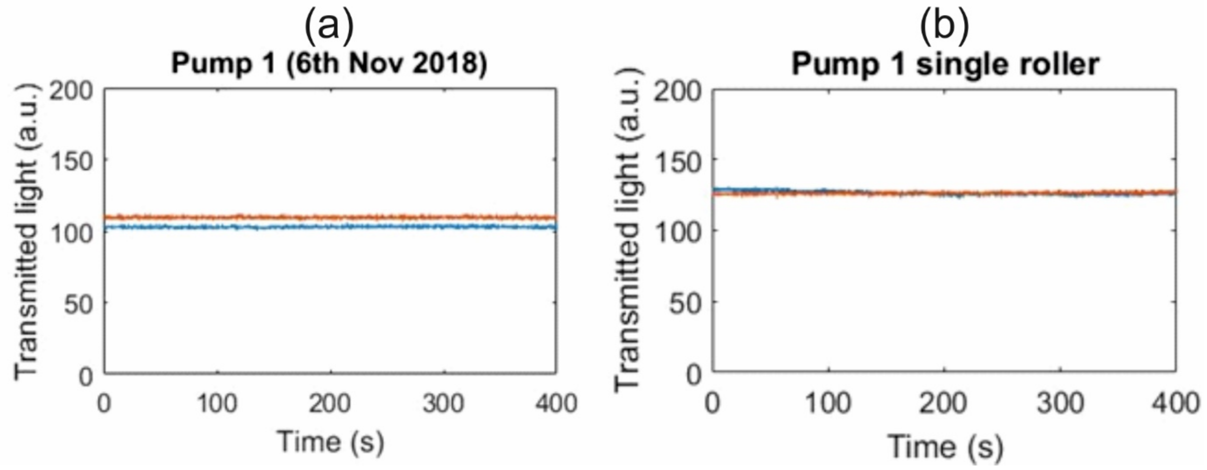

Figure 131. *Raw transmitted light intensity received by an optical detector, of continuous phase dye pumped through pump lines of two-line pump. (a) Data using out of phase rollers. (b) Data using single phase roller.*

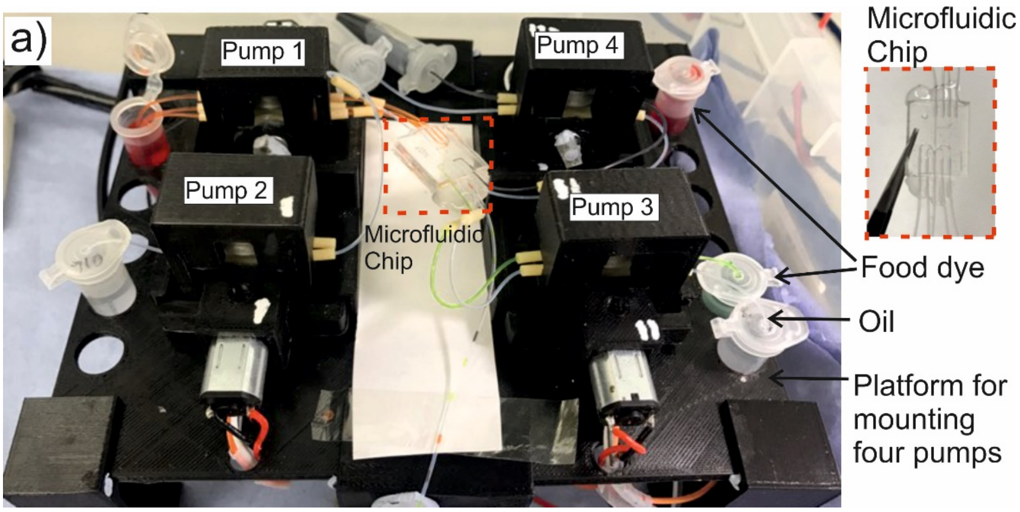

Figure 132. *First prototype of multiple pump platform displaying the fully assembled unit in operation.*

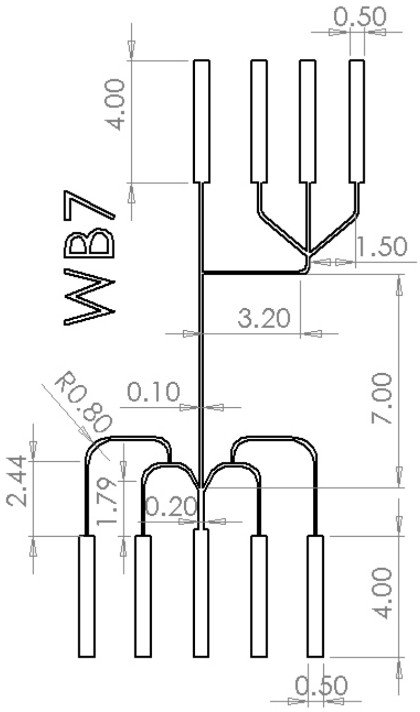

Figure 133. *SolidWorks sketch of PDMS junction chip (to be 3D printed) for multi-pump system for generating four droplet train for cortisol assay. The channel dimensions are 100 µm X 600 µm. The dimensions labelled on the sketch are in mm.*

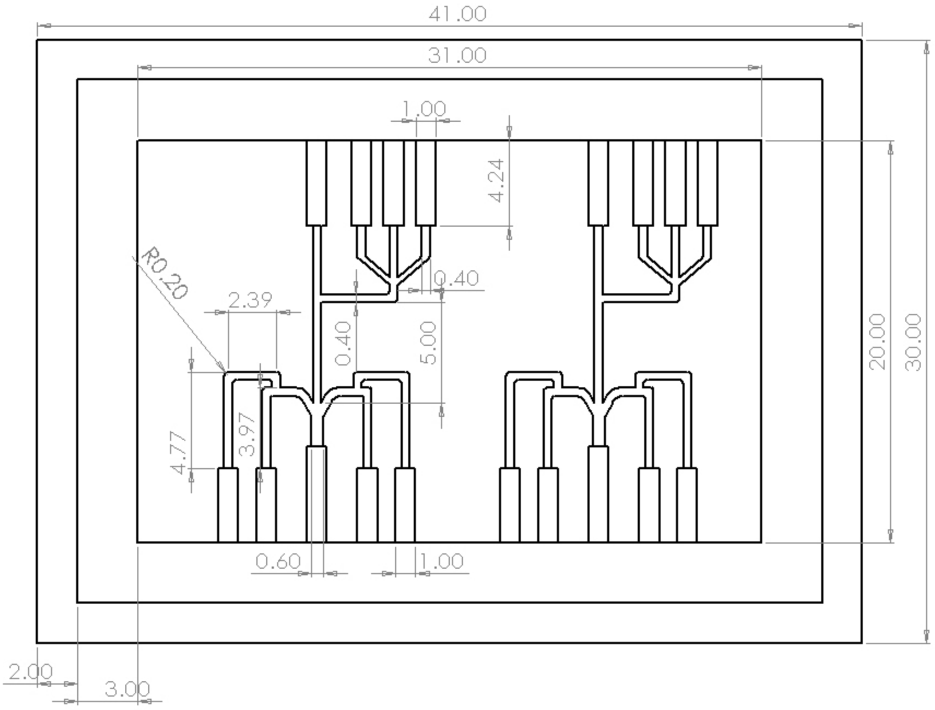

Figure 134. *Sketch of proto-mould (to be 3D printed in VeroClear) for cortisol assay Dyneon junction chip for multi-pump system. The channel dimensions are 400 µm X 450 µm. The dimensions labelled on the sketch are in mm.*

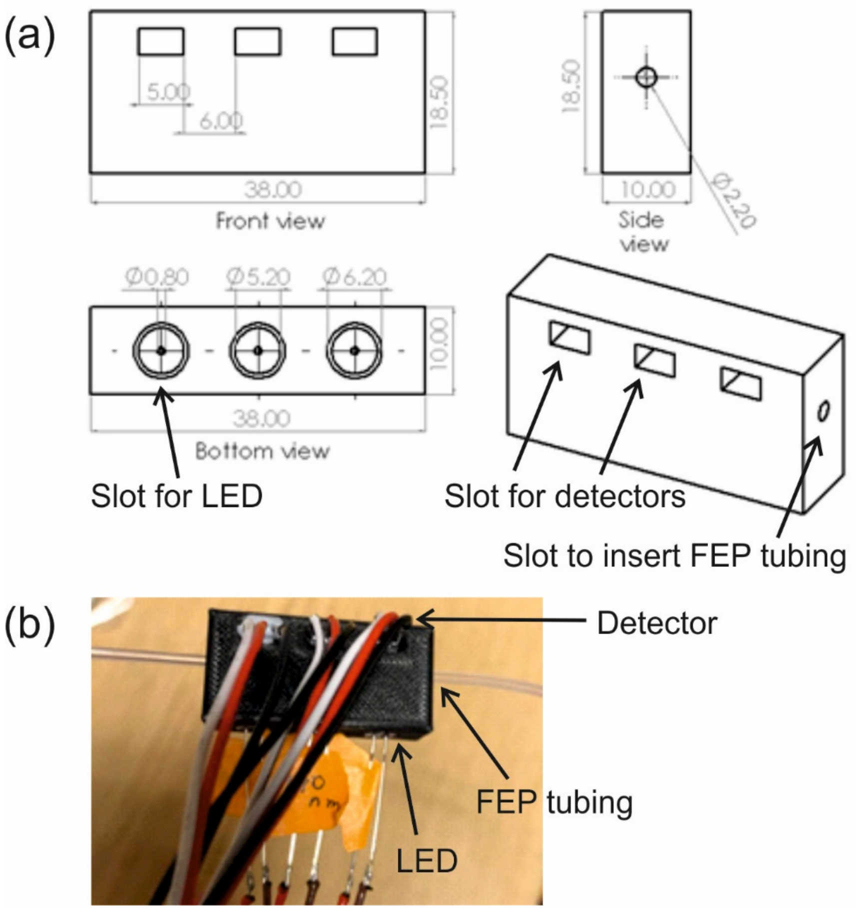

__Figure 135.__ 3D printed flow cell for measuring seawater total alkalinity. (a) Solidworks CAD models of multi LED flow cell. (b) Actual photograph of assembled flowcell.